Targeting lncRNAs in human cancer : insights into melanoma and clear cell renal cell carcinoma

Giovanni Gambi

UNIVERSITÉ DE STRASBOURG

ÉCOLE DOCTORALE DES SCIENCES DE LA VIE ET DE LA SANTÉ

Institut de Génétique et de Biologie Moléculaire et Cellulaire

THÈSE présentée par :

Giovanni GAMBI

soutenue le : **3 Mars 2021**

pour obtenir le grade de : **Docteur de l'université de Strasbourg**

Discipline : Sciences de la vie et de la Santé

Spécialité : Aspects moléculaires et cellulaires de la biologie

Targeting lncRNAs in human cancer: insights into melanoma and clear cell renal cell carcinoma

THÈSE dirigée par :

M. Davidson Irwin	Directeur de recherche CNRS, IGBMC, Illkirch

RAPPORTEURS :

Mme. Delmas Veronique	Directeur de recherche, Institut Curie, Paris
M. Goding Colin	PR PUPH, University of Oxford, Oxford

AUTRES MEMBRES DU JURY :

Mme. Lanfrancone Luisa	Directeur de recherche, Istituto Europeo di Oncologia, Milano
M. Metzger Daniel	Directeur de recherche CNRS, IGBMC, Illkirch

“Nothing in biology makes sense except in the light of evolution”

Teodosij Dobžanskij (1973)

ACKNOWLEDGMENTS

My scientific and professional journey started more than 10 years ago when my science high school teacher stressed the relevance of the quote in the previous page. I am grateful that my passion for biology could become my work and for this I thank my family that has always supported me at any level, at the university and during the graduate studies.

When I applied for the PhD programme in 2016 I was looking for a place to do research with a multidisciplinary approach. I stated in my cover letter: *"I seek to expand my knowledge of transcriptional end epigenetic regulation of gene expression, and of the cutting-edge technologies required to study them, in particular on a genome wide and proteomic scale*". After 4 years I feel fulfilled by the variety of methods I could learn about (from molecular to cellular biology, bioinformatics, proteomics, microscopy) and grateful for the mindset I gained to tackle scientific questions. For this, I thank my supervisor Irwin Davidson that welcomed me in his team, that guided my path, that discussed and supported my ideas.

Science is not made only of techniques and technologies, but also of people. Coming to a foreign country seemed a tough challenge at the beginning, but it was a decision that was worthwhile. I had the opportunity to live a different culture and working in an international environment has enriched my life. This would have not been possible without the luck of meeting amazing people, who I can define not only colleagues but friends. I hope we will strengthen our bond beyond this experience.

Finally, I am grateful I had a special person always on my side, that I knew I could rely on good and bad days. I hope this milestone I reached also thanks to your support will help us to build our life together.

ABBREVIATIONS

ASO	Antisense oligonucleotide
BCAA	Branched-chain amino acid
bDNA	Branched DNA
BRCA	Breast invasive carcinoma
CAGE	Cap analysis gene expression
CCLE	Cancer cell line encyclopedia
ccRCC	Clear cell renal carcinoma
ceRNA	competing endogenous RNA
ChIP	Chromatin Immunoprecipitation
ChIA-PET	Chromatin Interaction Analysis by Paired-End Tag
chRCC	Chromophobe renal carcinoma
CIMP	CpG island methylator phenotype
CLS	Capture long-read sequencing
CNV	Copy number variation
COAD	Colon adenocarcinoma
CT	Computed tomography
EMT	Epithelial to mesenchymal transition
GTEx	Gene tissue expression
HNSC	Head and Neck squamous cell carcinoma
KIRC	Kidney renal clear cell carcinoma
lincRNA	Long intergenic noncoding RNA
lncRNA	Long noncoding RNA
LUAD	Lung adenocarcinoma
LUSC	Lung squamous cell carcinoma

MRE	miRNA recognition element
MRI	Magnetic Resonance Imaging
ORF	Open reading frame
ORR	Overall response rate
OS	Overall survival
PDX	Patient derived xenotransplants
PFS	Progression-free survival
PRAD	Prostate adenocarcinoma
pRCC	Papillary renal carcinoma
qPCR	Quantitative PCR
RCC	Renal cell carcinoma
RNAseq	RNA sequencing
ROS	Reactive oxygen species
RTK	Receptor tyrosine kinase
RTKi	Receptor tyrosine kinase inhibitor
scRNAseq	Single cell RNAseq
SMT	Somatic mutation theory
TCA	Trycarboxylic acid
TCGA	The Cancer Genome Atlas
TE	Transposon element
TOFT	Tissue organization field theory
TSS	Transcription start site
XCI	X chromosome inactivation

TABLE OF CONTENTS

RÉSUMÉ EN FRANÇAIS

Le cancer est la deuxième cause de décès dans le monde, avec 9,6 millions de personnes qui mourront en 2018. Le mélanome et le carcinome rénal à cellules claires (CCRc) sont deux maladies agressives et malgré le développement de thérapies ciblées et d'immunothérapies, les patients diagnostiqués au stade métastatique ont toujours un mauvais pronostic. Il est donc urgent de trouver de nouvelles cibles pour les tests de diagnostic précoce et pour le traitement des formes métastatiques (American Cancer Society 2020). Les ARN non codants longs (LincRNA) sont des molécules d'ARN de plus de 200 bases qui ne codent pas pour une protéine mais participent aux fonctions cellulaires par différents mécanismes et dans divers compartiments cellulaires (Kopp and Mendell 2018). Compte tenu de leur grande spécificité tissulaire, de leur surexpression dans le cancer par rapport aux tissus normaux et de la possibilité de les cibler in vivo par l'administration d'oligonucléotides antisens (ASO), ils apparaissent aujourd'hui comme de nouvelles cibles thérapeutiques (Qian, Shi, and Luo 2020). En combinant des analyses de données publiques, l'inactivation et la surexpression in vitro ainsi que des études biochimiques, nous avons caractérisé un groupe de LincRNA qui sont essentiels pour la prolifération et la viabilité des cellules de mélanome et de ccRCC. Ces résultats fournissent des preuves solides de leur ciblage préclinique et à terme clinique.

Un réseau d'ARN longs non codants qui favorisent la prolifération et la survie des cellules de mélanome

Les facteurs de transcription MITF et SOX10 co-occupent environ 2000 éléments de régulation des gènes impliqués dans la réplication et la réparation de l'ADN et la mitose qui est à l'origine du phénotype prolifératif du mélanome. Avec d'autres facteurs de transcription

(tels que TFAP2A, PAX3), ils contrôlent un réseau de gènes qui caractérise les patients atteints mélanomes agressifs (Rambow et al. 2015). Parmi ces cibles, nous avons identifié de longs ARN non codants intergéniques (lincRNAs). Nous avons collaboré avec le groupe du Dr Chris Marine qui a caractérisé SAMMSON (Linc01212) en montrant que son expression était absolument spécifique au mélanome, sa régulation par SOX10 et son rôle essentiel dans les cellules du mélanome dans la coordination de la traduction nucléaire et cytoplasmique (Leucci et al, Nature 2016). Afin d'identifier et de caractériser d'autres LincRNA pertinents pour le mélanome, nous avons analysé les données de SOX10 et de MITF Chip-seq ainsi que le séquençage de l'ARN des cellules réduites au silence pour ces facteurs de transcription. Nous avons sélectionné 4 lincRNA (Linc00518, Linc00520, Linc00589, Linc02029) pour une étude plus approfondie en nous concentrant sur Linc00518 et Linc00520.

Des analyses approfondies des données publiques de séquençage de l'ARN ont montré que l'expression de ces lincRNAs est limitée aux mélanocytes de la peau dans les tissus adultes normaux et qu'elle est augmentée chez les patients atteints de mélanome. Cette découverte a été confirmée par une hybridation fluorescente in situ (FISH) utilisant le kit fluorescent multiplex RNAscope avec la coloration pour le MITF (comme marqueur mélanocytaire) et les lincRNAs. L'analyse de données RNA-seq de cellule unique (Tirosh et al. 2016) a mis en évidence une expression spécifiques des LincRNAs dans des cellules de mélanome et son absence dans les cellules T et B stromales, les macrophages, les cellules endothéliales et les fibroblastes. Les analyses des cohortes de mélanome TCGA ont également montré l'association entre leur expression et les caractéristiques cliniques de la maladie agressive.

Les données RNA-seq et ChIP-seq (Verfaillie et al. 2015; Tsoi et al. 2018) ont indiqué que chaque lincRNA était davantage exprimé dans les cellules MITF/SOX10 hautes (mélanocytaires) par rapport aux cellules MITF/SOX10 basses (mésenchymateuses). Il est

toutefois important de noter que Linc00518, mais pas Linc00520, était exprimé dans tous les types de cellules de mélanome, comme cela a également été vérifié sur un panel de lignées cellulaires par PCR quantitative et in vivo sur des données de RNA-seq provenant de PDX de mélanome (Rambow et al. 2018). Ce schéma d'expression unique est déterminé par un ensemble d'enhancers, comme le montre l'analyse des données Chip-seq des marques d'histones et des facteurs de transcription maîtres du mélanome (MITF, SOX10, TFAP2A, PAX3, FOSL2) de notre laboratoire et d'autres (Fontanals-Cirera et al. 2017). Nous nous sommes concentrés sur TFAP2A, car il est exprimé par toutes les sous-populations de mélanomes (Wouters et al. 2020) et se lie à de multiples éléments de régulation au niveau du locus Linc00518. L'inhibition de l'expression de TFAP2A par siRNA abaisse les niveaux de Linc00518 dans les cellules mélanocytaires (501mel) et mésenchymateuses (MM047).

Pour évaluer le rôle fonctionnel des LincRNAs, nous avons utilisé des oligonucléotides antisens (locked nucleic acid/LNA Gapmers, ASO) pour cibler leur expression dans les cellules de mélanome. L'inhibition de leur expression a diminué la prolifération cellulaire, comme l'ont montré le comptage des cellules et la coloration au violet de CellTrace, accompagnée de changements morphologiques et cytosquelettiques (coloration par immunofluorescence de la bêta-tubuline) et, surtout, d'une apoptose induite (Caspase 3 active, coloration à l'iodure d'Annexin-V/propidium par cytométrie de flux). Les résultats ont également été reproduits par interférence CRISPR en utilisant une protéine Cas9 (dCas9) morte fusionnée KAP1 et des ARN guides uniques (sgRNAs) ciblant les promoteurs de Linc00518 et Linc00520. Il est intéressant de noter que seul Linc00518 a affecté les cellules de mélanome mésenchymateuses, conformément à l'absence de Linc00520 dans ces cellules. Nous avons également testé l'effet du ciblage des combinaisons de Linc00518, Linc00520 et SAMMSON :

le ciblage de chaque combinaison a eu un effet synergique pro-apoptotique, mettant en évidence l'existence d'un réseau de LincRNA qui coopèrent pour promouvoir la prolifération et la survie des cellules de mélanome.

Nous avons décidé de caractériser le mécanisme d'action de Linc00518. Comme l'indiquent de multiples bases de données, Linc00518 est composé de 5 isoformes générés par épissage alternatif. L'analyse des données de paired end RNA-seq de lignées cellulaires de mélanomes et de lésions de patients a indiqué que les isoformes 1, 3 et 5 sont les plus exprimées et les plus régulées dans les mélanomes par rapport aux naevus acquis communs. Les analyses de la localisation subcellulaire de Linc00518 par FISH à l'aide de l'RNAscope sur des lignées cellulaires de mélanome ont montré sa présence dans le cytosol, à proximité de la membrane nucléaire. Nous avons confirmé la localisation cytosolique de Linc00518 par RT-qPCR sur des fractions d'ARN subcellulaire.

De nombreux lincRNA cytosoliques interagissent avec des protéines, régulant ainsi leur localisation, leur activité ou leur stabilité. Nous avons donc cherché à savoir si Linc00518 interagit avec des protéines en effectuant un pull down à l'aide de sondes oligonucléotidiques complémentaires biotinylées. Les complexes protéiques Linc00518 ont été purifiés à l'aide de billes magnétiques de streptavidine et les protéines éluées ont été soumises à une analyse par spectrométrie de masse. Nous avons trouvé 34 protéines enrichies dans les pulldowns de Linc00518 et avons décidé de nous concentrer sur la RAP2, une GTPase dont on a montré qu'elle régule plusieurs voies de signalisation (Machida et al. 2004; Di et al. 2015; Meng et al. 2018). Nous avons immunoprécipité RAP2 dans deux lignées cellulaires de mélanome (MM011, 501mel), en parallèle avec NONO et XRN2 en tant que témoins positifs et IgG normaux respectivement. Nous avons observé des interactions sélectives entre Linc00518 et RAP2, NEAT1-NONO et SAMMSON-XRN2 dans les deux lignées cellulaires. RAP2 est exprimé

sous la forme de trois paralogues différents (RAP2A/B/C) codés par 3 gènes distincts partageant environ 90% d'identité dans leurs séquences protéiques. Pour tester si Linc00518 a interagi spécifiquement avec l'un des paralogues, nous avons créé des lignées cellulaires inductibles exprimant chacune des protéines RAP2 marquées d'une séquence FLAG. Nous avons effectué des expériences d'immunoprécipitation en utilisant un anticorps anti-FLAG montrant que chacun des paralogues RAP2 s'associé à Linc00518. Nous avons ensuite testé si l'inhibition des paralogues de RAP2 induirait un changement phénotypique similaire à celui de Linc00518. Dans deux lignées cellulaires de mélanome (501mel, MM047), seul l'inhibition de RAP2C a réduit la prolifération et augmenté l'apoptose, comme pour le ciblage de Linc00518.

Nous avons cherché à savoir si Linc00518 et RAP2 partageaient la même localisation sous-cellulaire. Les signaux du lincRNA FISH ont été enrichis dans la région périnucléaire, nous avons donc émis l'hypothèse que Linc00518 et RAP2 pourraient être mitochondriaux. Pour le vérifier, nous avons procédé à une coloration immunofluorescente de RAP2 avec la protéine mitochondriale p32 dans deux lignées cellulaires de mélanome (501mel, MM117) et dans les deux cas, les signaux RAP2 et p32 se chevauchaient. Il est important de noter que cette co-localisation a été réduite après le l'inhibition de Linc00518, ce qui suggère qu'il régule la localisation mitochondriale de RAP2. Nous avons corroboré cette hypothèse en effectuant une purification mitochondriale suivie d'une extraction d'ARN et de protéines sur deux lignées cellulaires (501mel, MM011) qui ont été modifiées pour exprimer de manière Dox-inductible des shRNA spécifiques de Control ou de Linc00518. Dans les cellules knock down, des niveaux réduits de Linc00518 et de RAP2 ont été détectés dans des extraits de mitochondries purifiées. Ces résultats suggèrent que les deux molécules sont localisées dans les mitochondries et que Linc00518 influence la localisation mitochondriale de RAP2.

Compte tenu de la co-localisation de Linc00518 et de RAP2, nous avons demandé si leur inhibition affectait la fonction mitochondriale. L'immunofluorescence a montré une réduction de la coloration du Mitotracker CMXROS, mais aucun changement marquage de p32, ce qui suggère un effet sur la dépolarisation mais pas sur la masse mitochondriale. Nous l'avons confirmé par la coloration du Mitotracker CMXROS par cytométrie de flux, en réalisant une gating spécifique sur les cellules viables (Annexin V-/TOPRO-3-) pour exclure les effets confondants dus aux cellules apoptotiques. Le dysfonctionnement mitochondrial a également été mis en évidence par la mesure des niveaux de phosphorylation oxydative (OXPHOS) à l'aide du kit Seahorse Mitostress : l'inhibition de Linc00518 ou du RAP2C réduit le taux de consommation d'oxygène (OCR), en particulier la capacité respiratoire maximale (MRC) et la capacité de réserve.

Nous avons ensuite vérifié si la surexpression de Linc00518 pouvait stimuler la phosphorylation oxydative dans les cellules de mélanome. Nous avons créé des lignées cellulaires avec l'expression inductible par Dox de la GFP (comme témoin négatif) ou de chacune des isoformes de Linc00518. Nous avons réussi à surexprimer les isoformes 1, 2 et 3 et dans tous les cas, nous avons pu détecter une augmentation de la MRC et des capacités de réserve. Cet effet s'est accompagné d'une prolifération accrue dans les conditions d'adhérence et de suspension. Ces résultats suggèrent que la localisation mitochondriale de Linc00518 est pertinente pour la fonction mitochondriale.

Au cours des dernières années, le traitement du mélanome métastatique a été amélioré grâce à l'introduction de thérapies ciblées. Le Vemurafenib/PLX4032 cible spécifiquement la protéine oncogénique BRAF V600E pour inhiber la signalisation MAPK en aval. Les mélanomes traités par le Vemurafenib peuvent connaître une rémission, mais un pourcentage élevé de cas finit par rechuter et devenir résistant. Dans la première phase du

traitement, les cellules doivent s'adapter à l'inhibition de la voie glycolytique qui est normalement renforcée par la signalisation MAPK pour maintenir la demande énergétique. Il a été démontré que les cellules de mélanome réagissent en reprogrammant leur métabolisme pour augmenter la phosphorylation oxydative, à la fois par l'activité transcriptionnelle de PGC1alpha et l'inhibition de la protéine de fission mitochondriale DRP1 (Haq et al. 2013; Serasinghe et al. 2015). Étant donné leur influence sur la fonction mitochondriale et la phosphorylation oxydative, nous avons demandé si Linc00518 et RAP2C pouvaient contribuer au changement métabolique nécessaire pour que les cellules de mélanome s'adaptent au traitement par le Vemurafenib. Des analyses de données publiques sur les cellules traitées au vémurafénib ont indiqué une augmentation de l'expression de TFAP2A et de LINC00518 dans les premiers jours suivant le traitement. Nous avons confirmé ces observations par RT-qPCR sur d'autres lignées cellulaires de mélanome.

Nous avons ensuite traité les cellules de mélanome pendant trois jours avec du DMSO ou du Vemurafenib, les avons transfectées avec de l'ASO contrôle ou l'ASO ciblant Linc00518 ou siRAP2C et avons cultivé les cellules avec du vemurafenib ou du DMSO pendant trois jours supplémentaires. Nous avons mesuré l'OXPHOS avec l'instrument Seahorse et confirmé que le traitement au Vemurafenib augmentait l'OCR par rapport au contrôle DMSO. Cependant, les cellules traitées au Vemurafenib dans lesquelles Linc00518 ou RAP2C ont été inhibés n'étaient plus capables de maintenir l'augmentation de l'OCR. Cela suggère que Linc00518 et RAP2C sont nécessaires pour favoriser la phosphorylation oxydative nécessaire pour s'adapter à l'inhibition de la glycolyse.

Nous avons ensuite vérifié si l'inhibition de cette réponse adaptative pouvait entraîner une augmentation de l'apoptose. Nous avons traité les cellules avec du DMSO ou du Vemurafenib pendant 3 ou 6 jours, avec ou sans l'ASO pour Linc00518 ou siRAP2C, puis nous

avons effectué une analyse de la prolifération et de la survie par cytométrie de flux avec CellTrace et la caspase 3 active. Le Vemurafenib seul a induit une inhibition progressive de la prolifération, mais pas une augmentation significative de l'apoptose. L'inhibition de Linc00518 ou de RAP2C a induit une apoptose dans les cellules de contrôle DMSO, mais à un niveau significativement plus élevé dans les cellules traitées par Vemurafenib. Nous avons également testé si la surexpression de Linc00518 pouvait donner un avantage de croissance aux cellules de mélanome traitées par le Vemurafenib. Par rapport aux cellules GFP, les lignées cellulaires surexprimant les isoformes de Linc00518 ont montré une capacité de MRC et de réserve plus élevée lors du traitement au Vemurafenib et un taux de prolifération plus élevé dans le test de formation de mélanosphères. Ces résultats indiquent que Linc00518 et RAP2C favorisent l'adaptation des cellules de mélanome au Vemurafenib en augmentant la capacité d'OXPHOS. De plus, leur ciblage agit en synergie avec le Vemurafenib pour induire l'apoptose des cellules de mélanome.

MFI2-AS1 est un ARNc antisens qui favorise la prolifération et la survie des mélanomes et des carcinome reneaux à cellules claires

Le carcinome des cellules rénales (RCC) est une maladie courante et mortelle. Le RCC à cellules claires (ccRCC) est le sous-type le plus courant et représente la majorité des décès par cancer du rein, en raison de la prédominance de l'histologie des cellules claires dans les maladies métastatiques (83-88 %). Le RCC localisé peut être traité par néphrectomie partielle ou radicale, ablation ou surveillance active. Malgré la néphrectomie à visée curative, environ 30 % des patients atteints de RCC localisé finissent par développer des métastases qui nécessitent des thérapies systémiques et sont associées à une mortalité élevée (Hsieh et al. 2017). Des thérapies ciblées ont été mises au point, mais la réponse au traitement est variable et la plupart des patients finissent par progresser (Lee and Motzer 2017). Une nouvelle

génération d'agents d'immunothérapie sous la forme d'inhibiteurs du point de contrôle immunitaire des cellules T (anticorps contre le ligand 1/PDL1 de la protéine de mort cellulaire programmée ou la protéine de mort cellulaire programmée 1/PD1) est prometteuse, mais il est difficile de prédire la réponse et une grande partie des patients devient encore réfractaire au traitement (Escudier et al. 2019). Dans le but d'identifier de nouveaux biomarqueurs pour la prédiction de la récurrence de la maladie, nous avons analysé 351 ccRCC de l'Atlas TCGA et validé la classification de la récurrence basée sur l'expression des LncRNA dans une cohorte indépendante de 167 ccRCC localisés. Nous avons identifié le LncRNA MFI2-AS1 comme le meilleur candidat, montrant que son expression était associée à une survie sans maladie plus courte. Par rapport aux échantillons normaux, l'expression de MFI2-AS1 était augmentée dans les tissus tumoraux, et une expression plus élevée était associée à une dissémination métastatique. Ce résultat a également été validé dans une cohorte indépendante par une analyse PCR quantitative utilisant des sondes TaqMan (Filippot et al., Sci Rep 2017). MFI2AS1 est également fortement exprimé dans les mélanomes. Compte tenu des données ci-dessus, nous avons cherché à caractériser sa fonction moléculaire dans les cellules de ccRCC et de mélanome.

Tout d'abord, nous avons confirmé son expression in vivo par RNAscope sur des coupes de tumeurs de patients atteints de mélanome et de ccRCC. Dans les deux cas, nous avons détecté des molécules d'ARN spécifiques dans les cellules cancéreuses co-colorées avec les marqueurs MITF et PAX8 respectivement, mais pas dans le stroma. A l'inverse de Linc00518, MFI2AS1 était principalement nucléaire et plus fort chez un patient atteint de ccRCC porteur de métastases que chez un patient négatif.

Comme MFI2AS1 est prédit de comprendre 5 isoformes, nous avons vérifié si l'une d'entre elles ou toutes étaient exprimées. Nous avons trouvé 2 isoformes prédominantes

(appelées iso2 et iso5 à partir de maintenant) dans les données de paired-end RNA-seq de patients atteints de mélanome et de ccRCC et dans les lignées cellulaires. À l'aide d'amorces spécifiques, nous avons vérifié les niveaux de ces isoformes dans un panel de lignées cellulaires de mélanome et de ccRCC, confirmant une expression plus élevée des deux dans les cellules de mélanome. Nous avons également effectué des analyses RT-qPCR sur l'ARN extrait de différentes fractions subcellulaires (cytoplasmique, soluble dans le noyau et lié à la chromatine), constatant que l'iso5 est cytoplasmique et l'iso2 lié à la chromatine. Nous avons confirmé ce résultat en réalisant des expériences RNAscope sur des cellules de mélanome et de ccRCC.

Nous avons décidé de nous concentrer sur l'iso2 et avons effectué un pulldown en utilisant des sondes biotinylées couplées au séquençage à haut débit des molécules d'ADN précipitées avec l'ARN (Chirp-seq). Nous avons identifié des milliers de sites génomiques liés spécifiquement par MFI2AS1 par rapport au témoin négatif PCA3 ou au témoin positif NEAT1. Il est intéressant de noter que la majorité des sites liés par MFI2AS1 étaient associés au site d'initiation de la transcription (TSS). En comparant les pics Chirp avec Chip-seq pour différentes marques d'histones (H3K27ac, H3K4me3, H3K4me1) réalisées dans la même lignée cellulaire, nous avons confirmé une forte corrélation entre la liaison de MFI2AS1 et les promoteurs des gènes activement transcrits. Ces promoteurs sont principalement riches en GC, liés par des facteurs de transcription tels que GABPA, SP1, MYC, E2F1 et associés à des gènes importants pour les fonctions d'entretien (transcription, réparation de l'ADN, cycle cellulaire, signalisation intracellulaire, régulation du protéasome).

Nous avons ciblé l'expression de MFI2AS1 dans les cellules de mélanome et de ccRCC en utilisant des ASO et évalué les changements dans l'expression des gènes par RNA-seq. Globalement, nous avons constaté un bon chevauchement entre les gènes liés par le MFI2AS1

et ceux qui sont régulés par son inhibition, en particulier ceux associés aux ontologies géniques (GO) comme la transcription, la réparation de l'ADN, le cycle cellulaire et la signalisation intracellulaire. Cela a également été constaté en utilisant l'analyse GSEA avec une réduction du score pour les signatures MYC cibles, E2F cibles, réparation de l'ADN et transition du cycle cellulaire G2/M. Les analyses par cytométrie de flux des cellules knockdown ont montré une réduction de la prolifération telle qu'évaluée par la coloration Cell Trace Violet et une augmentation des cellules bloquées dans la phase G2/M par la coloration combinée Edu/TOPRO-3. Par Western Blot, nous avons également montré une augmentation des marqueurs de dommages à l'ADN. Dans l'ensemble, ces changements spectaculaires dans la physiologie cellulaire entraînent probablement l'apoptose que nous avons pu mesurer par cytométrie de flux pour la caspase 3 active. Ces effets étaient communs aux lignées cellulaires de mélanome et de ccRCC mais ne se sont pas produits dans les cellules HEKT négatives MFI2AS1 transfectées avec les ASO, confirmant ainsi leur spécificité. Ces expériences de renversement suggèrent que le MFI2AS1 affecte directement la transcription de ses gènes cibles impliqués dans les fonctions fondamentales des cellules cancéreuses.

Nous avons ensuite vérifié si la surexpression de MFI2AS1 pouvait donner un avantage prolifératif aux cellules HEKT où il n'est pas normalement exprimé. Par rapport aux cellules de contrôle GFP, les cellules surexprimant MFI2AS1 ont montré des taux de croissance plus élevés dans des conditions d'adhérence et de suspension. Par cytométrie de flux utilisant la coloration Cell Trace Violet, nous avons mis en évidence une augmentation progressive de la prolifération après 4 et 8 jours de surexpression. Nous avons vérifié le signal MFI2AS1 par RNAscope et avons constaté une augmentation des foyers nucléaires de molécules d'ARN similaires à celles endogènes que l'on trouve dans les cellules de mélanome et de ccRCC. Ces résultats suggèrent que la surexpression de MFI2AS1 pourrait avoir un effet de stimulation de

la croissance dans les cellules HEKT par un mécanisme nucléaire similaire à celui qui se produit dans les cellules de mélanome et de ccRCC.

Conclusions et perspectives

Nous fournissons des preuves de la pertinence fonctionnelle de deux lncRNA dans les cellules cancéreuses, Linc00518 et MFI2AS1. Bien qu'ils aient des localisations intra-cellulaires et des mécanismes d'action différents, les deux ARN partagent des caractéristiques intéressantes : leur expression est augmentée dans les cellules malignes par rapport aux tissus normaux, ils sont exprimés dans toutes les sous-populations de mélanomes et ils sont essentiels à la prolifération et à la survie des cellules cancéreuses. Ces caractéristiques en font des cibles intéressantes pour les études de preuve de concept (POC) in vivo afin de promouvoir l'exploitation clinique des ASO en tant qu'agents uniques, en combinaison ou en association avec d'autres thérapies anticancéreuses existantes. En collaboration avec l'organisation de transfert de technologie SATT, nous effectuons actuellement un criblage à haut débit pour identifier les ASO les plus efficaces ciblant Linc00518 en vue d'une validation préclinique supplémentaire sur des modèles de souris de xénogreffes dérivées de patients (PDX).

Parallèlement à l'application translationnelle de ces résultats, nous caractériserons davantage la fonction de ces lncRNA, afin de mieux comprendre leurs mécanismes d'action. Dans le cas de Linc00518, nous effectuerons des études protéomiques pour identifier les cibles en aval de RAP2, potentiellement une ou plusieurs protéines mitochondriales directement impliquées dans la phosphorylation oxydative ou importantes pour la biogenèse ou l'homéostasie mitochondriale, comme DRP1. Nous définirons l'interactome de RAP2 par immunoprécipitation suivie de spectrométrie de masse et le phospho-protéome des cellules knock down de RAP2, pour enfin identifier les protéines directement phosphorylées par cette GTPase. En cas de succès, ces données jetteraient la lumière sur une nouvelle voie de

régulation mitochondriale qui implique l'activité collaborative des protéines et des ARN non codants.

Dans le cas de MFI2AS1, nous essaierons de comprendre comment il affecte l'expression de ses gènes cibles : directement par sa liaison ou indirectement par l'organisation de la structure 3D de la chromatine. Il a été démontré, par exemple, que les mêmes classes de gènes hautement exprimés que nous avons trouvé ciblés par MFI2AS1 sont généralement transcrits dans des compartiments nucléaires distincts proches des para-speckles. Il est donc possible que cet lncRNA soit impliqué dans la stabilité ou la régulation de ces structures. Pour le vérifier, nous réaliserons des expériences de co-détection entre les signaux FISH et différents marqueurs des sous-compartiments nucléaires et par la purification de MFI2AS1 suivi de l'analyse par spectrométrie de masse de ses protéines partenaires. En cas de succès, ces expériences fourniraient des preuves d'un mécanisme de régulation des gènes qui est fondamental pour la prolifération et la survie des cellules cancéreuses.

Références

Di, Jiehui, Hui Huang, Debao Qu, Juangjuan Tang, Wenjia Cao, Zheng Lu, Qian Cheng, et al. 2015. "Rap2B Promotes Proliferation, Migration, and Invasion of Human Breast Cancer through Calcium-Related ERK1/2 Signaling Pathway." *Scientific Reports* 5 (December 2014): 1–11. https://doi.org/10.1038/srep12363.

Escudier, B., C. Porta, M. Schmidinger, N. Rioux-Leclercq, A. Bex, V. Khoo, V. Grünwald, S. Gillessen, and A. Horwich. 2019. "Renal Cell Carcinoma: ESMO Clinical Practice Guidelines for Diagnosis, Treatment and Follow-Up." *Annals of Oncology* 30 (5): 706–20. https://doi.org/10.1093/annonc/mdz056.

Fontanals-Cirera, Barbara, Dan Hasson, Chiara Vardabasso, Raffaella Di Micco, Praveen Agrawal, Asif Chowdhury, Madeleine Gantz, et al. 2017. "Harnessing BET Inhibitor Sensitivity Reveals AMIGO2 as a Melanoma Survival Gene." *Molecular Cell* 68 (4): 731-744.e9. https://doi.org/10.1016/j.molcel.2017.11.004.

Haq, Rizwan, Jonathan Shoag, Pedro Andreu-perez, Satoru Yokoyama, Hannah Edelman, Glenn C Rowe, Dennie T Frederick, et al. 2013. “Article Oncogenic BRAF Regulates Oxidative Metabolism via PGC1 a and MITF.” *Cancer Cell* 23 (3): 302–15. https://doi.org/10.1016/j.ccr.2013.02.003.

Hsieh, James J., Mark P. Purdue, Sabina Signoretti, Charles Swanton, Laurence Albiges, Manuela Schmidinger, Daniel Y. Heng, James Larkin, and Vincenzo Ficarra. 2017. “Renal Cell Carcinoma.” *Nature Reviews Disease Primers* 3: 1–19. https://doi.org/10.1038/nrdp.2017.9.

Kopp, Florian, and Joshua T. Mendell. 2018. “Functional Classification and Experimental Dissection of Long Noncoding RNAs.” *Cell* 172 (3): 393–407. https://doi.org/10.1016/j.cell.2018.01.011.

Lee, Chung-Han, and Robert J. Motzer. 2017. “The Evolution of Anti-Angiogenic Therapy for Kidney Cancer.” *Nature Reviews Nephrology* 13 (2): 69–70. https://doi.org/10.1038/nrneph.2016.194.

Machida, Noriko, Masato Umikawa, Kimiko Takei, Nariko Sakima, Bat Erdene Myagmar, Kiyohito Taira, Hiroshi Uezato, Yoshihide Ogawa, and Ken Ichi Kariya. 2004. “Mitogen-Activated Protein Kinase Kinase Kinase Kinase 4 as a Putative Effector of Rap2 to Activate the c-Jun N-Terminal Kinase.” *Journal of Biological Chemistry* 279 (16): 15711–14. https://doi.org/10.1074/jbc.C300542200.

Meng, Zhipeng, Yunjiang Qiu, Kimberly C. Lin, Aditya Kumar, Jesse K. Placone, Cao Fang, Kuei Chun Wang, et al. 2018. “RAP2 Mediates Mechanoresponses of the Hippo Pathway.” *Nature* 560 (7720): 655–60. https://doi.org/10.1038/s41586-018-0444-0.

Qian, Yuchen, Lei Shi, and Zhong Luo. 2020. “Long Non-Coding RNAs in Cancer: Implications for Diagnosis, Prognosis, and Therapy.” *Frontiers in Medicine* 7 (November): 1–8. https://doi.org/10.3389/fmed.2020.612393.

Rambow, Florian, Bastien Job, Valérie Petit, Franck Gesbert, Véronique Delmas, Hannah Seberg, Guillaume Meurice, et al. 2015. “New Functional Signatures for Understanding Melanoma Biology from Tumor Cell Lineage-Specific Analysis.” *Cell Reports* 13 (4): 840–53. https://doi.org/10.1016/j.celrep.2015.09.037.

Rambow, Florian, Aljosja Rogiers, Oskar Marin-Bejar, Sara Aibar, Julia Femel, Michael Dewaele, Panagiotis Karras, et al. 2018. “Toward Minimal Residual Disease-Directed Therapy in Melanoma.” *Cell* 174 (4): 843-855.e19. https://doi.org/10.1016/j.cell.2018.06.025.

Serasinghe, Madhavika N., Shira Y. Wieder, Thibaud T. Renault, Rana Elkholi, James J. Asciolla, Jonathon L. Yao, Omar Jabado, et al. 2015. “Mitochondrial Division Is Requisite to RAS-Induced Transformation and Targeted by Oncogenic MAPK Pathway Inhibitors.” *Molecular Cell* 57 (3): 521–36. https://doi.org/10.1016/j.molcel.2015.01.003.

Society, American Cancer. 2020. “Cancer Facts & Figures 2020.” *Atlanta: American Cancer Society*. https://doi.org/10.1038/s41598-018-28671-9.

Tirosh, Itay, Benjamin Izar, Sanjay M. Prakadan, Marc H. Wadsworth, Daniel Treacy, John J. Trombetta, Asaf Rotem, et al. 2016. “Dissecting the Multicellular Ecosystem of Metastatic Melanoma by Single-Cell RNA-Seq.” *Science* 352 (6282): 189–96. https://doi.org/10.1126/science.aad0501.

Tsoi, Jennifer, Lidia Robert, Kim Paraiso, Carlos Galvan, Katherine M. Sheu, Johnson Lay, Deborah J.L. Wong, et al. 2018. “Multi-Stage Differentiation Defines Melanoma Subtypes with Differential Vulnerability to Drug-Induced Iron-Dependent Oxidative Stress.” *Cancer Cell* 33 (5): 890-904.e5. https://doi.org/10.1016/j.ccell.2018.03.017.

Verfaillie, Annelien, Hana Imrichova, Zeynep Kalender Atak, Michael Dewaele, Florian Rambow, Gert Hulselmans, Valerie Christiaens, et al. 2015. “Decoding the Regulatory Landscape of Melanoma Reveals TEADS as Regulators of the Invasive Cell State.” *Nature Communications* 6: 1–16. https://doi.org/10.1038/ncomms7683.

Wouters, Jasper, Zeynep Kalender-Atak, Liesbeth Minnoye, Katina I Spanier, Maxime De Waegeneer, Carmen Bravo González-Blas, David Mauduit, et al. 2020. “Robust Gene Expression Programs Underlie Recurrent Cell States and Phenotype Switching in Melanoma.” *Nature Cell Biology* 22 (8): 986–98. https://doi.org/10.1038/s41556-020-0547-3.

PUBLICATIONS

- "Single-cell RNA sequencing reveals intratumoural heterogeneity in primary uveal melanomas and identifies HES6 as a driver of the metastatic disease" Pandiani C, Strub T, Nottet N, Cheli Y, **Gambi G**, Bille K, Husser, C, Dalmasso M, Beranger G, Lassalle S, Magnone V, Pedeutour, Irondelle M, Maschi C, Nahon-Esteve S, Martel A, Caujolle JP, Hofman P, LeBrigand K, Davidson I, Baillif S, Barbry P, Ballotti R, Bertolotto C, *Cell Death and Differentiation*, 2021
- "CHD4 regulates PADI1 and PADI3 expression linking pyruvate kinase M2 citrullination to glycolysis and proliferation." Coassolo S, Davidson G , Negroni L, **Gambi G**, Daujat S, Romier C, Davidson I. *Nature Communications*, 2021
- "Regulation of gene expression by chromatin remodellers Brg1 and Bptf in oncogenic Braf-driven mouse melanoma." Laurette P, Coassolo S, Davidson G, Michel I, **Gambi G**, Mengus G, Yao Q, Sohier P, Li M, Larue M, Davidson I, *Cell Death and Differentiation*, 2019
- "MITF-High and MITF-Low Cells and a Novel Subpopulation Expressing Genes of Both Cell States Contribute to Intra- and Intertumoural Heterogeneity of Primary Melanoma" Ennen M, Keime C, **Gambi G**, Kieny A, Coassolo S, Thibault-Carpentier C, Margerin-Schaller F, Davidson G, Vagne C, Lipsker D, Davidson I, *Clinical Cancer Research*, 2017

ORAL COMMUNICATIONS

- "MITF and SOX10 regulated Linc-RNAs essential for melanocyte and melanoma cell proliferation" Gambi G, Davidson G, Leucci E, Davidson I. *European Society for Pigment Cell Research (ESPCR) meeting 2019*, Bruxelles

INTRODUCTION

Within this study, we sought to identify and characterize lncRNAs with a relevant function in melanoma and clear cell renal carcinoma (ccRCC). Our aims were to describe new mechanisms of actions for these molecules and propose new targets for preclinical development. These two objectives are strongly interconnected as a better understanding of cancer biology is the foundation to develop better therapies for cancer patients. Our studies may provide a useful workflow to identify and characterize lncRNAs. Our strategy was to start from previously obtained data to set a list of candidates. The combination of expression studies, molecular and cell biology experiments allowed us to evaluate the in vitro and in vivo relevance of some of them.

We relied on high throughput RNA sequencing analyses and we confirmed them with independent techniques, in particular fluorescence in situ hybridization (FISH) and quantitative PCR (qPCR) on cell lines and patients' samples. To evaluate the role on cancer cells phenotype, we performed depletion and overexpression of our candidates and checked alterations in biological processes (proliferation, apoptosis, metabolism, cell cycle). Finally, we tried to dissect the molecular mechanisms behind the changes we noticed and we tackled the problem by isolating the lncRNAs to identify their protein partners or DNA binding sites. This last work package has been challenging but also rewarding in terms of innovative findings that we could propose. The next exciting steps will be in vivo preclinical experiments to demonstrate the therapeutic relevance of our targets and structural studies to dissect how they interact with their binding partners.

The description of this thesis work will be structured into five parts: a first section describing how lncRNAs have been historically identified, their characterizing molecular features and which tools we can use to study their functions; a second section about lncRNAs already described in cancer and the general aspects of our models, melanoma and ccRCC; the third section will focus on the work done on the lncRNA LINC00518 and its role in melanoma; the fourth one will describe the work about the lncRNA MFI2AS1 in both melanoma and ccRCC. The closing section will discuss both projects and future perspectives.

SECTION 1 - SEARCHING FOR LNCRNAS IN THE HUMAN GENOME

Despite the identification of the H19[1] and XIST[2] RNAs in the early 1990s, it was only during the genomic era of high throughput sequencing of DNA and RNA that we could fully appreciate the extent of lncRNAs transcription in human cells. The boost to investigate this class of RNAs came after the 2003 results of the International Human Genome Sequencing Consortium: an estimation of around 22,287 protein coding genes accounting for 1.2% of the euchromatic genome led the investigators to declare to the scientific community "*the need for reliable experimental and computational methods for comprehensive identification of non-coding RNAs*"[3]. In line with these findings, the FANTOM and RIKEN consortia analyses of mouse[4] and human[5] full-length cDNAs revealed that a significant part of the transcriptome (73% and 27% respectively) was lacking an apparent open-reading frame. Similar results were obtained from targeted chip-based analyses of chromosomes 21 and 22[6,7] between 2002 and 2004.

To uncover the significance of transcribed and non-transcribed noncoding regions, the National Human Genome Research Institute (NHGRI) launched in 2003 the ENCyclopedia Of DNA Elements (ENCODE) Project with the ambitious aim of comprehensively cataloging the structural and functional components of the genome of every human cell type and at all developmental stages[8]. This huge effort allowed a biochemical function to be assigned to around 80% of the genome and implemented the technological and computational methods that nowadays we are all familiar with[9,10]. Particularly relevant for the transcriptomic studies and the identification of lncRNAs have been all the RNA-centric methods: RNA-sequencing from different cell lines and multiple subcellular fractions; cap analysis of gene expression (CAGE) sequencing to define the 5' ends of RNAs; RNA-PET to capture full-length RNAs with

both a 5' cap and a polyA tail[10]; RNA Capture long seq (CLS) to target lncRNAs or unannotated loci and sequence the resulting full length cDNAs[11].

DEFINING NONCODARNIA

The huge amount of information obtained by the ENCODE project (especially regarding the exotic Noncodarnia world, as defined by John Rinn[12]) required an uniform system to annotate all the evidence-based gene features at high accuracy: the GENCODE initiative was thus established in 2003[13]. Version 7 was released in September 2012 and provided the most comprehensive set of genomic annotations up to that moment, with a systematic description of biotype and status at locus and transcript levels[14]. This reference gene set resulted from the combination of manual gene annotations from the Human and Vertebrate Analysis and Annotation (HAVANA) group and automatic gene annotations from Ensembl. Genes were classified into three groups: level 1 for those manually annotated and experimentally validated by RT-PCR-seq; level 2 for those manually annotated but lacking experimental validation; level 3 for those automatically annotated. The current reference publication was released in 2019[15] and it became the annotation of choice for many international consortia besides ENCODE, such as The Genotype-Tissue Expression (GTEx), the International Cancer Genome Consortium (ICGC), the 1000 Genomes Project, the Exome Aggregation Consortium (EXAC), the Genome Aggregation Database (gnomAD) and the Human Cell Atlas (HCA).

The GENCODE annotation defines 4 main biotypes[14]:

- **Protein-coding**, for genes characterized by a coding sequence (CDS) identical to an Entrez Gene registered cDNA (known status) or identical/homologous to a known cDNA not yet represented in Entrez Gene (novel status). Transcripts arising from a protein coding gene

locus can be also defined as NMD (if they contain a premature stop codon that leads to nonsense-mediated decay) or retained intron (if they contain an intronic sequence) [14].

- **Pseudogene**, for sequences derived from protein-coding genes that acquired disabling mutations (in-frame stop codons, frameshift indels, truncations or insertions) or that have no evident transcription. Pseudogenes can be further defined as processed (if derived from a retrotransposition event), unprocessed (if derived from a duplication event) or unitary (if derived from the lineage specific disruption of a protein-coding gene) [14].
- **Long noncoding RNA (lncRNA)**, for genes that do not contain an open reading frame (ORF) that can be unambiguously assigned as a CDS. These transcripts are further distinguished as antisense RNAs (transcribed from the opposite strand to a protein coding strand), lincRNAs (intergenic long noncoding RNAs), sense overlapping RNAs (when they contain a coding gene within an intron on the same strand), sense intronic RNAs (when the corresponding gene is contained within an intron of a coding gene but does not intersect any exons), processed transcript (when they do not fall in any other category) [14].
- **small noncoding RNA (sncRNA)**, which comprise microRNA (miRNA), small interfering RNAs (siRNA), small nucleolar RNAs (snoRNA), small nuclear RNA (snRNA), PIWI-interacting RNA (piRNA) and tRNA-derived small RNAs (tRFs)[14].

Although the most diffuse way to distinguish long and small ncRNAs relies on a 200 nucleotides threshold [16], the GENCODE annotation does not require lncRNA genes to be longer than this, but they must be free of secondary structures found in known sncRNAs. Nevertheless, very few annotated lncRNAs are shorter than 200nt.[15]

With the diffusion of RNA sequencing as a more affordable and feasible technique, individual labs out of big consortia could start performing transcriptomic studies and expand

the lncRNA genes annotation[17]. The possibility of identifying novel genes is not surprising since lncRNAs are often expressed in a spatial- or temporal restricted manner: this makes the sample of choice determinant for the analysis[18].

Researchers also exploited indirect strategies to discover lncRNA genes, relying on ChIP (chromatin immunoprecipitation) sequencing analyses of histone modifications[19]. Actively transcribed genes (identified by the presence of H3K4me3 at their promoters and H3K36me3 along the gene body) were filtered to remove known protein coding gene loci. This allowed the identification of around 1600 lncRNAs across four mouse cell types and among them, 100 were further functionally validated by different cell based assays[19].

The final result of all these efforts has been the emergence of several annotations in parallel with GENCODE, which differ for completeness (of transcripts length from start to end), comprehensiveness (of the number of genes that are included) and exhaustiveness (of the number of transcripts for each gene)[18]. In general, the first two parameters are anti-correlated and is difficult to have both high quality and size. The CLS FL annotation for instance, which relies on capture long-read sequencing technology, has the highest completeness (71%) but only 807 genes annotated[11]. The manually curated GENCODE and RefSeq have comparable profiles, with 15778 and 15791 lncRNA genes annotated with 13.5% and 11% completeness respectively[15,20]. MiTranscriptome was based on automatic annotation of short-read RNA-seq of 27 cancer types and provided 58548 lncRNA genes, but only 4.4% of them have complete transcript models[21]. The NONCODE collection, which integrates different manual literature searches and other annotations, has the largest genes size with 96308 human loci[22]. An issue of all these annotations is the poor overlap between them, even considering similar ones like GENCODE and RefSeq (around 40%). This points out the need for merging collections to

increase comprehensiveness, being careful to not include "artifacts" which characterize automated annotations[18].

The final goal would be to obtain a complete map of full-length lncRNAs expressed through the entire lifetime of an organism, such as *Homo Sapiens*. This challenging task may be tackled in the future by advances in long-read sequencing technologies (like PacBio[23] and Oxford Nanopore's MiniON[24]) coupled with RNA capture by oligonucleotides (RNA captureSeq), which can increase sequencing coverage by tens of fold[25]. This combination would allow to overcome the main limitations of short-read RNAseq: the inherent expression-dependent bias that constrains detection and resolution of low abundant RNAs (usually the top 1% of most expressed protein coding genes soaks around 40% of sequencing coverage[26]) and the lack of definition of long-range exon connectivity[27]. These issues are particularly relevant for lncRNAs, which tend to be expressed approximately one order of magnitude less than mRNAs[28] and globally display longer introns length[28]. RNA CLS already proved the possibility to discover novel transcripts or to correct previously mistaken annotations[11]. The regions to be targeted would be already known lncRNAs and suspect loci lying outside annotated exons, which could provide novel genes.

The power of this approach is exemplified by the targeted RNA-seq of chromosome 21 performed using the PacBio technology on K562 cells, brain, kidney and testis samples[29]. This analysis increased the coverage of chromosome 21 sequencing by 60-fold, showing that almost all the whole nonrepetitive regions harboured transcription. The number of noncoding multi-exonic isoforms was increased by 2.1-fold and incorporated previous partial annotations into single unified loci.

Another study compared RNA-seq and CaptureSeq capability to assemble and quantify lncRNAs and novel coding exons across 20 human tissues: the latter yielded on average a 2-3

log10 increase in signal, 20.6% more observed long noncoding exons and doubled the number of alternative splicing per locus from 1.8 to 3.6[30].

Sampling should also overcome the current limitation on European adult panel of organs or tumours and include tissues from embryos to aged adults[18]. Finally, most transcriptomic studies have been performed using oligo-dT based retrotranscription, making the knowledge on non-polyadenylated lncRNAs still limited.[31]

Nevertheless, compared to protein-coding genes it may be more difficult to define when the lncRNA population can be considered complete as we still do not have a reliable method to distinguish a priori biologically relevant transcripts from transcriptional noise. To avoid annotation research being doomed by pervasive transcription and unlimited combinatorial splicing, novel transcript discovery strategies should be monitored as a function of sequencing depth, so as to define when transcriptome complexity has been saturated[18,29].

MOLECULAR FEATURES OF LNCRNAS

LNCRNAS BIOGENESIS, SPLICING AND STABILITY

In parallel with the definition of lncRNAs collection, researchers tried to define their molecular features in comparison to messenger RNAs (mRNAs). The GENCODE v7 release in 2012 provided the first set of integrative analyses of transcriptome and epigenome data regarding lncRNAs[28]. Keeping in mind that this evaluation was only partially compared to the full spectrum of lncRNAs molecules, it was appreciated that the majority of them did not intersect with other protein-coding genes, making them intergenic (9518 out of 14880 annotated transcripts, 63.9%)[28]. Genic transcripts were covering exons (2411, 16%) or introns (2784, 18.7%) in a similar manner[28]. Analysis of CAGE data indicated that at comparable expression levels, lncRNAs had a similar number of annotated transcription start sites (TSS),

suggesting their capping at the 5'[28]. However they less frequently contained a polyadenylation site compared to protein-coding genes (39% vs 51%)[28].

Another difference seemed to be splicing regulation: although 98% of lncRNAs were spliced, 42% of them were characterized by only two exons (compared to 6% of protein coding genes) and while exons lengths of lncRNAs were comparable to those of protein-coding genes (median of 149bp vs 132bp), introns were almost twice longer (median of 2280bp vs 1602bp)[28]. lncRNA transcripts were therefore shorter on average (median of 592bp vs 2435bp). More than 25% of lncRNAs displayed alternative splicing with at least two isoforms per locus[28]. These results were similar to those obtained in a previous independent analysis, which indicated on average 2.9 exons and a mean transcript length of 1kbp for lncRNAs (vs. 10.7 exons and 2.9kb for protein-coding transcripts) and around 2.3 isoforms per locus[17].

However, these evaluations may have suffered from underestimation due to the discrepancy the low abundance of lncRNAs and sequencing coverage. When targeted single molecule RNAseq has been employed, even at saturation of sequencing depth it was still possible to detect new noncoding introns (while protein coding ones and exons in general reached a plateau), suggesting a broader variety of possible alternative splicing events compared to coding genes[29]. Calculation of a percent splice inclusion (PSI) score for each exon (as the ratio of reads that used the 5' and the 3' splice sites over the reads that skipped the exon out), indicated lower inclusion frequencies among noncoding exons than protein coding ones (55% vs 90.5%), again in line with a higher variability in splicing events[29]. These results highlight that standard RNAseq experiments may have not provided conclusive information regarding lncRNAs biogenesis and this apparent limitless diversity of noncoding RNAs may rely on the lack of ORF constraints.

In line with these findings, lncRNAs have been shown to have a higher intron retention rate compared to coding genes (17.3 times more) [32,33,34], in particular when they contain snoRNA sequences[16,28]. This effect is thought to depend on the absence of proximal RNA pol II phosphorylation at lncRNAs introns[33], to a smaller proportion of pyrimidines in the polypyrimidine tract (PPT), to a higher distance between the branch point and 3'splice sites and to a lower binding of the splicing factor U2AF65[34]. Nevertheless there are also lncRNAs which have conserved splice junctions, that are efficiently spliced (XIST, FIRRE, MIAT) and that require splicing to efficiently function[34].

Stability has also been suggested to differ between coding and lncRNAs. A first report exploiting microarrays (targeting around 7200 lncRNAs and 20000 protein coding genes on cells treated with actinomycin D over 32 hours), suggested on average a higher turnover of lncRNAs, although with a wide range of stabilities[35]. Metabolic labelling of RNA with 4-thiouridine (4SU) coupled with subcellular fractionation and RNA sequencing, provided a more comprehensive evaluation: on average, lncRNAs displayed a 3.4 and 9.6 higher rate of synthesis and degradation, respectively, compared to mRNAs, but again with a wide range of behaviour[33]. Indeed, it was possible to cluster protein coding and lncRNA genes together based on their metabolic profile and known functional lncRNAs were grouped with highly expressed coding genes[33]. Nevertheless the majority of lncRNAs were falling in the groups characterized by lower synthesis, higher degradation and higher nuclear retention[33].

This analysis of subcellular fractions also indicated a similar polyribosomal localisation of lncRNAs and protein coding genes, despite a general absence of actively translated ORFs in the former group[33]. The hypothesis that lncRNAs can code for proteins or small peptides is highly debated but in some cases proved to be true [36,37,38]. Annotation pipelines, like the GENCODE one, integrate prediction tools such as CPAT (Coding-Potential Assessment Tool,

evaluating intrinsic sequence properties), CPC (Coding Potential Calculator, checking similarities with other proteins), PhyloCSF (comparing evolutionarily conserved protein signatures) with mass spectrometry data, Uniprot and Pfam entries[28]. As part of the ENCODE project, a proteomic analysis of nine compartments from GM12878 and K562 cell lines identified 350 peptides out of total 79333 that matched the GENCODE lncRNA set, but only 12 loci had multiple in-frame peptides that could suggest a strong evidence of translation[39]. An improved proteogenomics pipeline has been introduced in 2016 and the re-analysis of 3 big datasets suggested 1400 novel protein coding genes, out of which only 8 fell in lncRNA loci[40]. Thus misannotation should be infrequent[41] and probably ribosome interaction is suggestive of translation but not sufficient: indeed contradictory conclusions have been taken from different ribosome profiling studies[42,43,44].

Ribosome fractionation experiments indicated that lncRNAs could be found from the free cytosolic to mono and polyribosomes pools, even if in small numbers and outcompeted by protein coding genes[45]. It is possible that besides some of these lncRNAs can be effectively translated, their binding results in no-sense mediated decay (NMD); alternatively, they could have a role in ribosomes regulation[45]. In any case, the verification of suspect coding potential cannot rely only on bioinformatics predictions, but requires careful experimental analyses[46].

REGULATED EXPRESSION OF LNCRNAS LOCI

As part of the ENCODE project, profiles of ChIPseq data of histone marks and transcription factors have been compared between lncRNAs and mRNAs[47]. It was initially shown that TSSs of the two groups had similar profiles for activation marks (H3K4me2, H3K4me3, H3K9ac, H3K27ac) with the presence of H3K4me3 at promoters and H3K36me3 across transcribed regions[28,19]. However, two peculiar classes of lncRNAs (enhancer

RNAs/eRNAs and promoter upstream transcripts/PROMPTs) are characterized by low levels of H3K4me3, high levels of H3K4me1 and H3K27ac and they lack H3K36me3 over the gene body[48].

Even if not polyadenylated and thus highly unstable, eRNAs have been shown to be transcribed from enhancers in a regulated manner (spatio/temporal or by specific stimuli)[49,50]. Still, it is controversial if they have a stand-alone function or they are just a by-product. They have been proposed to influence enhancer-promoter looping, RNA pol II loading and pausing or transcription factors trapping at genes that require high transcription levels[51].

PROMPTs are transcribed in sense or antisense fashion at promoter regions, they are unspliced and lack polyadenylation, which makes them highly unstable. Indeed, they become evident only after exosomes depletion[52]. As eRNAs they may result from promiscuous transcription events that are effectively recognized and discarded, but with a regulatory role (for instance, directional RNA production at bidirectional promoters or fine tuning of available transcription factors).[53]

Similar to protein coding genes, lncRNA expression levels positively correlate with those of H3K4me3 and H3K36me3 [54]. However, multiple RNA-seq and microarray studies on human cell lines and tissues, indicated global lower expression of lncRNAs compared to protein coding genes[17,28,33]. Another peculiarity of lncRNA genes seems to be their tissue-specificity and an enrichment in testis and brain samples, possibly pointing out a role in acquisition of specific traits [17,28].

However, this tissue specificity could also result from low sensitivity of the techniques used. A targeted analysis relying on custom microarray for around 10000 lncRNA transcripts indicated for all of them expression in at least two cell types and in all of them for 29%[28]. In

another study, it has been estimated that only 2.3% of lncRNAs are expressed in a tissue restricted manner and that 12% are expressed by all of them[55].

Despite the discrepancies between these studies, comparison of lncRNAs and protein-coding genes expressed in a similar range indicated higher tissue-specificity of the former group[17]. The reason behind this feature remains elusive, as lncRNA promoters are not more enriched for TATA box and Initiator motifs[56]. Massively parallel reporter assays (MPRA) suggested that eRNAs and lincRNAs may have a reduced number of transcription factors binding sites, which would limit their transcription in different cell types[56].

Analysis of hundreds of RNA-seq datasets across normal tissues of 16 studies has annotated 1184 lncRNAs as ubiquitously expressed (UE) and 2583 as tissue specific (TS)[55]. Examples of ubiquitously expressed lncRNAs are TUG1 or MALAT1[57]. UE lncRNAs are transcribed at high levels while TS at relatively low; at their promoters the former are bound by a higher number of transcription factors, have more frequently CpG islands and higher levels of active histone marks[55]. Each tissue has a variable number of TS lncRNAs, which does not depend on the total expressed amount[55]. Testis resulted again to have the highest number of TS and they may define a distinct class[55].

Validation of a lncRNA tissue-specificity requires additional validations, such as single molecule fluorescence in situ hybridization (FISH) on tissue samples combined with cell-type specific markers. In the future, the development of other technologies such as spatial transcriptomics and the extensive implementation of single cell RNA sequencing will boost the understanding of lncRNAs tissue-specific transcription, as demonstrated by some pioneering studies[58,59,60,61].

LNCRNAS ORIGINS AND CONSERVATION ACROSS SPECIES

Another debated aspect of lncRNAs is their poor conservation across species. A general conclusion is that, compared to protein coding genes, lncRNA exons but not promoter sequences are less conserved[19,28], suggesting lower sequence constraints but similar regulatory ones. Nevertheless, lncRNAs exons have higher conservation than introns or random intergenic sequences[62].

Again, there have been some discrepancies between studies, possibly due to differences in the lncRNAs analysed. With more inclusive and less-accurate annotations, the calculated mean conservation rate approaches that of non-transcribed intergenic regions[63]. On the other hand, analysis of 1898 manually curated loci (filtered for significant expression in humans) in nine tissues (colon, spleen, lung, testes, brain, kidney, liver, heart, skeletal muscle) across 6 placental mammals, identified orthologues for 98% of them in chimpanzee, 93% in rhesus, 73% in cow, 58% in mouse and 54% in rat[57]. Orthologous transcription was detected with lower percentages (80%, 63%, 38%, 38%, 35% in the same order as above) by analysing RNAseq data, indicating that sequence homology may not be sufficient to predict expression in other organisms[57].

Interestingly, tissue-specificity scores were significantly similar for lincRNAs orthologues and they were consistently expressed in the same tissues across species[57]. Unbiased clustering of lincRNAs across all tissues and species separated very well the tissues between each other. Together with the findings of higher promoters conservation, these results suggest that tissue specific expression may not be stochastic but regulated and maintained throughout evolution[57]. Ubiquitously expressed lncRNAs in humans such as MALAT1 and TUG1 were also ubiquitous in all the other species[57,55].

DNA sequence turnover is the easiest parameter to evaluate when genomes of closely related species are available, but it is not the only one. Some methods of scanning whole-

genome alignments such as EvoFold and RNAz allow prediction of sequences evolved to preserve RNA secondary structures[64]. This approach proved to be successful with small ncRNAs (snoRNAs, tRNAs, miRNAs) and allowed the identification of homologues of the Drosophila roX lncRNA [65]. Some functional human lncRNAs like MALAT1, NEAT1 and NORAD display regions whose structure evolved under selection constraints. However, on a genome wide basis these regions are very few and structure conservation without sequence alignability is rare[66].

In many cases lncRNAs are positionally conserved and their locus is found in the same relative orientation to orthologous protein-coding genes or other regions. In these cases exons conservation is poor, suggesting that functional sequences are too short to be detected or the act of transcription itself is under evolutionary constraints[67]. An example is the AIRN lncRNA locus that overlaps with the promoter of IGF2R[68].

Overall, we can divide lncRNAs in three groups: one characterized by conservation among species of the exon-intron structure and of multiple sequences (such as MIAT/GOMAFU, XIST, CYRANO, NEAT1, MALAT1, NORAD), but they constitute a minority[67]; a second in which the act of transcription and some RNA elements biased at the 5' are conserved (ONECUT); a third in which there are no similar sequences or structures across species, except for the promoter. The last group represents the majority and we can speculate a human specific function for these lncRNAs or that other lncRNAs evolved similar functions in other species[67]. Even for the first two groups, conservation may not underlie the same function in different species: loss of function experiments may not give the same phenotype in different models or the lncRNA in one species could not replace its orthologue. An example of discrepancy between species emerged from HOTAIR studies regarding regulation of HOXD cluster expression[69].

The fact that most vertebrate lncRNAs have no orthologues suggests that these genes frequently originated de novo due to different mechanisms. Protein coding genes evolve by duplication, but this seems infrequent for lncRNAs: intra-species similarities among lncRNAs are rare and unsupervised clustering retrieves families containing only two members or biased by genes with common repeats[28]. Three lncRNAs (XIST, JPX and FTX) originated from loss of coding potential of protein-coding genes due to mutations, transposable elements (TE) insertion and genomic rearrangement[70]. In other cases, integration of a TE containing a functional promoter (such as endogenous retroviruses) in close proximity with cryptic splicing and polyadenylation sites, drove transcription initiation at previously non-transcribed loci and generated new lncRNAs[71]. Indeed lncRNA sequences frequently overlap with at least one TE (80%) and around 25% of promoters and polyA signals are TE-derived[72]. Divergent transcription can also give rise to new transcripts in presence of concomitant mutations that stabilise cryptic splicing sites, for instance by favouring U1 binding[73].

lncRNAs that did not originate through these mechanisms probably arose from a favourable combination of mutations in cryptic promoters, splice sites and polyA signals in close proximity to enhancer regions. In any case de novo lncRNAs formation has probably been a frequent event in germ cells, which have an open chromatin environment, allowing for transcription and efficient selection of functional genes[66].

Other genomic changes are later responsible for increasing complexity of lncRNA loci and there is a mild correlation between evolutionary age and lncRNAs length: “young” lncRNAs (that are less 50 million years old) normally characterized by two-three exons and 1kbp length, while more ancient lncRNAs are longer, with more exons and transcript isoforms. For instance XIST is 17kb long and has 8 exons[2] and one isoform of ANRIL is 4kb long with 19 exons[74]. Additional exons may be introduced by TE insertions, which unlike for protein coding

genes may be not functional but not even deleterious, so weakly selected[72]. Alternatively, sequence duplication can induce formation of repeats, which increase the number of functional domains in the RNA (for instance binding sites with a partner) and so they are positively maintained[75]. This ‘‘copy-paste’’ model may explain how lncRNA genes are capable of acquiring new functions over short evolutionary timescales.

FIGURE 1 - LNCRNAS ORIGINS, IDENTIFICATION AND MOLECULAR FEATURES

A. lncRNAs originate thanks to genetic events that abolish coding potential or start transcription from previously untranscribed regions. Further insertions or mutations can increase their complexity. On the side is represented a model of primate specific lncRNAs emergence thanks to transposons insertions. **B.** lncRNAs have been annotated in a manual manner combining ESTs and cDNAs sequences with 5' and 3' data obtained by CAGE and 3P-seq, respectively. Short read sequencing technologies allowed a genome wide discovery of lncRNA genes: reads are either first mapped to the genome and then assembled into transcripts (genome-guided assembly), or first assembled into transcripts (de novo assembly) and then mapped to the genome. Long read sequencing technologies start to be more frequently employed, allowing a more faithful definition of transcript models. Both manual and automatic annotations are checked by bioinformatic algorithms or against proteomic databases entries for the presence of known or putative open reading frames. **C.** lncRNAs can be transcribed in two main ways, overlapping the sequences of another gene (genic) or from an independent promoter (intergenic). eRNAs and PROMPTs are two peculiar classes of RNAs transcribed at enhancers and promoters, respectively. **D.** mRNAs, lncRNAs, eRNAs and PROMPTs differ for some molecular features, especially at the post-transcriptional processing and stability level.

GIVING FUNCTIONAL SIGNIFICANCE TO ANNOTATIONS

The results of the ENCODE and FANTOM projects, the discovery of unstable RNAs such as PROMPTs and eRNAs, the binding of RNA Pol II to intergenic regions or heterochromatin domains[76], diffused the idea in the 2000s that this pervasive transcription had to be functional. In support of this idea, the percentage of the noncoding transcriptome tends to increase in higher order organisms[77], but opponents pointed out the low phylogenetic conservation and low abundance of these transcripts. Indeed, the majority of cellular RNA by mass is represented by rRNAs (80-90%), tRNAs (10-15%), mRNAs (3-7%): other small nuclear RNAs and lncRNAs constitute a minority (around 0.65% and 0.03-0.2%)[78]. Although XIST is present in 0.1-2 thousands copies, all other lncRNAs together result in 3-50 thousands copies[78]. According to ENCODE, less than 1000 lncRNAs are present at more than one copy per cell in the human cell lines analysed[79].

Low abundance may be due to the fact that inappropriate transcription is counteracted by rapid degradation. Indeed some noncoding RNA classes become apparent only after exosome inhibition[52]. RNA polymerase has a low but existing probability to start transcription on any accessible DNA sequence, either on loosed heterochromatin or from still nucleosome packed regions[80]. Unless the RNA is too deleterious, natural selection can do nothing to prevent pervasive transcription, meaning that a basal level of spurious RNA is expected. This consideration should act as an alarm towards an hyper-adaptationistic belief that any transcribed DNA is functional.[78]

Still, a ncRNA may have a very restricted expression pattern or a function that does not require it to be present in high quantity (for instance a cis-regulation near its site of transcription). Rapid degradation may constitute an advantageous way for the cells to respond

quickly to environmental changes, with ncRNAs being produced, functioning and getting degraded very rapidly [81]. As previously stated, in some instances the act of transcription itself has a function, allowing a favourable chromatin remodelling or interfering with transcription of neighbouring loci[68]. In these cases, transcription per se would represent the mechanistic factor and RNAs a by-product, whose abundance may become irrelevant.

The best way to approach "functionalisation" of lncRNAs probably stands in the middle, keeping in mind that low expression does not mean "junk" and that an RNA may not be functional by virtue of its mere existence. A rigorous approach is required, according to which a lncRNA has to be considered non-functional unless further elements could prove the opposite[78]. These features can be a sufficiently high levels of expression (because it poses a significant energetic cost for the cells), a medium-high degree of conservation (which would reflect evolutionary constraints) and experimental evidences proving a role in some biological processes[78].

Looking at some updated statistics regarding lncRNA research, it is evident that despite the high rate of publications over the last years[82], there is still a big gap between the number of annotated genes and those that have been functionally characterized (140356 vs 1867)[83]. This discrepancy may derive from the diffused emphasis on descriptive studies, which aimed at annotating new genes or associating their expression with cancer signatures or genome-wide association studies (GWAS), without providing mechanistic evidence[82]. Another bias affecting the field is the focus on gene expression related mechanisms, such as transcriptional regulation (397 associated lncRNAs), competing endogenous RNAs/ceRNAs (182), splicing regulation (19), translational control (17), RNA interference (3). Involvement in other processes, such as metabolism or signalling, still represents an exception[83].

UNDERSTANDING LNCRNAS FUNCTIONS FROM THEIR LOCALISATION

A useful way to classify lncRNAs is based on their localisation. This feature, once considered to be irrelevant, appears to be non- random for the majority of transcripts[84]. Unlike protein coding genes, lncRNAs are not translated so they will frequently rely on proximity to convey their function[2]. In this perspective studying subcellular localisation becomes a crucial step to elucidate their mechanisms of action.

It was initially reported that lncRNAs had a significant enrichment in chromatin and nuclear RNA fractions compared to protein coding genes[28], but other reports indicated only a modest difference[33,45,85]. A comprehensive analysis of publications provided a curated qualitative and quantitative information for more than 11000 lncRNA transcripts from 9494 genes and three main species (human, mouse, fruit fly)[86]. Overall 28% of them were found to be nuclear, 16% cytoplasmic and 55% both nuclear and cytoplasmic. Focusing on human data, 32% of lncRNAs were nuclear, 12% cytoplasmic and 54% present in both fractions. While intronic and antisense transcripts displayed only 0.7% and 9.7% cytoplasmic localisation, 25.2% of lincRNAs were characterized by it, suggesting a more variable targeting[86].

Subcellular localisation studies have been performed with two main approaches: oligonucleotide hybridization coupled to imaging (in situ hybridization/ISH) and biochemical fractionation coupled to RNA quantification. The former approach allows detection of single RNA molecules and relies on fluorescent labelling of multiple fluorescent oligonucleotides (single molecule fluorescent ISH/smFISH) [87] or indirect labelling of non-fluorescent probes which carry a common extra sequence called readout[88]. An example is the branched DNA system developed by ACD (RNAscope protocol): RNA molecules are targeted by contiguous pairs of probes; binding of both is required for hybridization of a pre-amplifier (Amp oligo), which is further bound by several HRP-conjugated amplifiers; final step is tyramide signal

amplification (TSA)[89]. Compared to traditional smFISH, this approach relies on common reagents for signal amplification (allowing more flexibility and reduced costs for probes design), it can be automated and it can be combined with protein immunofluorescence[90]. Through informatic analysis of microscopy images it is possible to obtain an absolute quantification of targets and their positional information (subcellular compartment; diffused signal or concentrated in foci). The drawbacks of smFISH are the limited throughput and the difficulty to target RNAs with short sequences or many repeats[91].

Biochemical fractionation of compartments or organelles coupled with quantitative PCR (for single genes analyses) or RNA sequencing (for genome wide analyses/also known as CeFra-seq) overcomes the throughput issue of smFISH[92]. However this method is restricted by the availability of reliable protocols, which should minimize contaminations between fractions (for instance cytoplasmic RNAs bound to the nuclear membrane or nuclear RNAs released during mitosis)[91]. Moreover, quantification can be expressed only in a relative fashion (as a ratio between the target signal and the total RNA mass of the compartment) which can be biased by the relative amount of RNA in the compartments considered: for instance, cellular cytoplasm tends to contain several times more RNA molecules than the nucleus and this amount may vary between cells or cell types. A new approach called ALEC (absolute localisation estimation from CeFra-seq) allows absolute quantification to be inferred from matched CeFra-seq and whole cell RNAseq data[93].

New technologies have been introduced to improve smFISH and fractionation methods. APEX-RIP exploits a gene fusion to target the APEX enzyme (engineered ascorbate peroxidase) to a specific subcellular compartment (for instance nucleoli, nuclear pore, nuclear lamina, ER lumen, ER membrane, cytosol, outer mitochondrial membrane, mitochondrial matrix) and induce the biotinylation of proteins in close proximity. After protein-RNA

crosslinking, biotinylated proteins can be isolated using streptavidin and the purified RNA sequenced, allowing the mapping of thousands of RNA at the same time[94,95]. This approach is advantageous if fractions are difficult to isolate, but requires prior knowledge of the marker-protein to be fused with APEX.

Fluorescent in situ RNA-sequencing (FISSEQ) tried to overcome the low throughput of smFISH while maintaining positional information: RNAs are crosslinked to nearby proteins, reverse transcribed in situ using random primers and modified nucleotides, which allow a second crosslinking reaction of cDNAs to cellular structures; cDNAs are then circularized and amplified by rolling circle reaction, de-crosslinked and sequenced in situ using SOLiD platform[96]. The current limitations of this technique are the lower read coverage compared to standard RNA-seq and the requirement of customized instrumentation.

Two techniques relying on sequencing of barcoded RNA molecules providde information about subnuclear structures and their spatial relationships without the need of fractionation or oligonucleotides hybridization: RNA proximity sequencing[97] and split-pool recognition of interactions by tag extension (SPRITE)[98]. Both approaches highlighted how transcription in the nucleus does not occur randomly, but in RNA-dense areas such as the nuclear speckles. To specifically identify RNAs bound to these structures or other chromatin sites, Chromatin Associated RNA sequencing (ChAR-seq) has been employed on Drosophila cells: following RNA-DNA crosslinking, RNA molecules are retrotranscribed using an adeylated bridge oligo containing a DpnII restriction site; after DpnII digestion of cDNAs and genomic DNA, molecules in close proximity are ligated and sequenced; this method allows to identify RNAs involved in cis and trans transcriptional activities[99].

LncRNAs positional analysis requires also to understand how these molecules are retained in the nucleus or targeted to other compartments. Unlike proteins (which rely on

nuclear localisation or other kinds of signal peptides[100]), evidences for lncRNA targeting motifs are still preliminary: for instance, an AGCCC stretch in the BORG lncRNA[101] or the 156bp local repeating RNA domain (RDD) present in FIRRE are suggested to promote their nuclear localisation[75].

A massively parallel RNA assay (MPRNA) has been employed to discover RNA motifs capable of nuclear targeting: 11696 barcoded oligos tiling 38 human lncRNAs have been fused to a cytosolic localised reporter transcript (a noncoding frameshifted variant of Sox2 called fsSox2) and transfected; fractionation and sequencing of barcodes allowed to identify motifs that enriched sfSox2 in the nuclear fraction over the total population[102].

Another screening of 109-mer fragments from 37 human lncRNAs fused to a GFP mRNA reporter also provided motifs that regulate nuclear/cytoplasmic localisation: C-rich motifs derived from antisense Alu repeats can recruit hnRNPK and promote nuclear targeting[103].

Similar sequences may exist also for targeting towards other organelles, relying on RNA-protein or RNA-RNA interactions. An interesting example is the mitochondrial targeting of the RMRP lncRNA: nuclear export is dependent on CRM1 (chromosome region maintainance 1) after binding to the HuR (human antigen R) protein; once in the mitochondria, the lncRNA is accumulated in the matrix by GRSF1 (G-rich RNA sequence binding factor 1)[104].

Nuclear export may depend on RNA maturation like for mRNAs: proteins from the transcription export complex (TREX) and nuclear RNA export factor 1 (NXF1) recognize components of the 5'Cap, exon-junctions and other processing factors to promote the transport through the pore. Many lncRNAs are capped, spliced and polyadenylated, making plausible the dependence on TREX[105]. Interestingly nuclear lncRNAs show reduced binding to NFX1 proteins compared to cytosolic ones[106].

LNCRNAS ACTING IN THE NUCLEUS

The first and most studied lncRNA-related nuclear process is the X-chromosome inactivation (XCI) mediated by XIST [2,107]. Its investigation constituted a main driver for the development of methods to study lncRNAs and the pulldown of XIST by biotinylated oligonucleotides coupled with DNA sequencing or mass spectrometry has been performed by different labs[108,109,110,111,112,113].

The term "RNA pulldown" actually encompasses a family of methods which differ for design of capture oligonucleotides and crosslinking conditions. For example, in CHART (Capture hybridization analysis of RNA targets)[114] cells are formaldehyde crosslinked, sonicated and lysates incubated with a minimal set of biotin tagged DNA oligonucleotides (C-oligos) of 20-mer. These are designed against accessible regions on the basis of an RNAseH sensitivity assay. Following RNA isolation by streptavidin pulldown, interacting DNA and protein molecules can be analysed by high-throughput sequencing or mass spectrometry, respectively. This protocol has been employed not only for XIST[109], but also roX2[114], NEAT1 and MALAT1[115].

CHIRP (Chromatin Isolation by RNA Purification) has a very similar protocol and differs only in the probes design, which tiles all transcript length avoiding repetitive regions[108,111]. This approach saves performing the time consuming RNAseH assay and does not require a priori knowledge of the lncRNA domains. This protocol has been performed for XIST[108,111], TERC[108], HOTAIR[108], 7SK[116], FOXC1 eRNA[117].

In RAP (RNA affinity purification)[112,118] oligonucleotides also tile the whole transcript but they are 120 and not 20-mer long, thus decreasing off-target binding. Cells are not crosslinked by formaldehyde but by UV exposure, which should more specifically fix direct RNA-protein interactions and not indirect ones[119]. RAP was used for XIST[112] and FIRRE[120].

Analysis of proteins eluted after these pulldown methods can be performed by non-quantitative or quantitative mass spectrometry (MS) approaches[121]. In the first case, purified proteins from the sample of interest and the negative control are separated on a gel and only specific bands are identified by MS; alternatively, both total proteomes are analysed in duplicate or triplicate and only proteins enriched in the specific pulldown are considered[111].

Following a quantitative method, cells are metabolically labelled to tag proteins differently in the control and specific pulldowns; after shotgun MS, isotopes of the proteins from the 2 samples are compared to identify specific interactors[112]. Normally most abundant RNA binding proteins, such as hnRNPs, are quantitively similar in both samples, while specific interactors are less present in the negative control[121]. The choice of the method depends on the pulldown strategy: in the absence of crosslinking reagents, denaturing purification strategy and less stringent washing steps, it may be preferable a quantitative analysis[121].

Validation of pulldown-MS should involve the immunoprecipitation of the candidate partners and analysis for the presence of the RNA of interest by quantitative PCR or RNAseq. Several protocols have been developed, which involve UV crosslinking (Crosslinking and immunoprecipitation/CLIP) or not (RNA immunoprecipitation/RIP). The native approach is easier and preserves complexes in physiological conditions, but it may bring down RNAs that come from indirect interactions[122]. Regarding high-throughput DNA sequencing of chromatin sites pulled down after CHART/CHIRP or RAP, bioinformatic pipelines similar to ChIP experiments are commonly used[115].

RNA and protein-centric experiments have shown how nuclear lncRNAs can mediate a wide variety of functions, affecting a large number of genes or acting at more local level. In the first group we can list lncRNAs that affect chromosomes architecture and interactions (XIST[123], FIRRE[120]), that regulate RNA polymerase I and II activity (Alu[124], 7SK[125], SLERT[126]) or

the assembly of nuclear bodies (NEAT1[127], MALAT1[128]): they are usually expressed at moderate levels and have a trans-activity. Other lncRNAs regulate smaller sets of genes in cis or trans-acting fashion by establishing chromatin loops (CCAT1-L[129], Kcnq1ot1[130]), by recruiting chromatin remodelers or histone modifying enzymes (MHRT[131], lncPRESS1[132], HOTAIR[133], HOTTIP[134]), by forming R loops (TERRA[135], Khps1[136], VIM-AS1[137]), by interacting with transcription factors (Lethe[138]) or by the mere fact of being transcribed (Airn[68], Uph[139], PVT1[140]). Finally, some lncRNAs regulate transcription unrelated processes, such as telomeres extension (TERC[141]), genome stability (NORAD[142]) and DNA replication (CONCR[143]). New mechanisms of action are continuously proposed [144,145,146], so only some reference examples will be described in detail.

LncRNA- mediated chromatin regulation

XCI has been studied for almost 30 years and represents the most well understood lncRNA regulated biological process[123]. XIST presents several features that characterize also other lncRNAs, so it constitues a good model to describe them and make comparisons.

XIST is a 15kb lncRNA which together with other genes (NAP1L2, CDX4, CHIC1, TSIX, JPX, FTX, XCPT, RNF12) forms the X inactivation center (Xic)[147]. Once it is upregulated from one of the two X chromosomes in female cells, it accumulates in cis- at around 2000 copies per cell, driving a multistep process that ultimately silences more than 1000 genes. Only some of them (known as escapees) and the Xic itself (which remains outside the XIST domain) are not repressed[147].

Discrete regions of XIST called A-F repeats mediate its functions: the A element is necessary for gene silencing and it interacts with SPEN (also known as SHARP, SMRT/HDAC-1 associated repressor protein), WTAP (Wilms tumour 1-associated protein) and RBM15 (RNA-

binding motif protein 15) [123]; repeats C, E and probably F mediate XIST interaction with the X chromosome via the CIZ1 (Cip1-interacting zing finger protein 1) and hnRNPU/SAFA proteins[123]; repeats B and C promote recruitment of the Polycomb repressive complex 1 (PRC1) via hnRNPK[123].

The mechanism of initial accumulation of XIST is not completely understood but it does not depend on a specific RNA/DNA interaction, as autosomes expressing XIST can also be coated by it[148]. It may be mediated by the two nuclear matrix proteins SAFA and CIZ1, which are necessary but not sufficient for XIST localisation[149].

Once targeted, interaction with SHARP and the SMRT co-repressor complex results in HDAC3 mediated histone deacetylation and rapid gene silencing[112]. Deacetylation is one of the earliest events and its followed by the recruitment of PRC2 via SHARP and hnRNPK, which promotes deposition of the repressive mark H3K27me3 on histones and the consolidation of silencing[150].These findings highlight the modular nature of XIST and how it can act as a scaffold to interact with protein complexes and bring them together.

Interaction with chromatin regulators is common also to other lncRNAs: they can recruit chromatin histone modifiers, DNA methyltransferase 1 (DNMT1) or chromatin remodelers (such as SWI/SNF); they can act as co-activators of transcription factors or compete allosterically with other proteins (as decoys); in some cases they coordinate the functions of multiple protein complexes[146]. An example is HOTAIR (HOX transcript antisense RNA), which by interactions with LSD1-CoREST-REST and PRC2 complexes coordinates removal of H3Kme2 and deposition of H3K27me3 to silence HOXD expression[133]. The lncRNA Kcnq1ot1 associates with PRC2 and G9a promoting deposition of H3K27me3 and H3K9me3 and repression of the genes of the Kcnq1 imprinting domain[151]. Interaction with PRC2 has actually been shown to involve all RNAs in the cell, raising concerns about its specificity or its nature

of being direct or indirect[152]. lncRNAs are also involved in gene activation, such as HOTTIP (HOXA transcript at the distal tip), whose interaction with WDR5 promotes H3K4me3 deposition at promoters across the HOXA gene cluster[134].

Other lncRNAs characterised by repeated recognition sequences can engage multivalent protein interactions: FIRRE has 12 repeated exons generated by duplication that interact with SAFA proteins, similarly to XIST; this allows the formation of a network of genomic sites that get close to each other[120].

lncRNAs do not only participate in the recruitment of chromatin regulators but can also prevent their activity. Two examples are MHRT (which sequesters BRG1 and balances its activity to avoid heart hyperthrophy[131]) and lncPRESS1 (which decoys SIRT6 deacetylase activity at pluripotency gene promoters to activate their transcription[132]).

Finally, lncRNAs can also interact with proteins involved in large-scale chromosome remodelling: XIST has been shown to interact with the lamin B receptor (LBR), a transmembrane protein at the inner nuclear membrane that interacts with lamin B and anchors chromatin to the nuclear lamina; XIST can thus reposition the inactivated X close to this region and this is thought to stabilize the XIC process[113].

A key question that emerged is: how these lncRNAs can find their targets on the genome? Three options have been proposed:

- they act at their site of transcription, where RNA polymerase tethers the lncRNA; examples are NEAT1 (which co-transcriptionally gets recognized by paraspeckles proteins and triggers the nucleation of these nuclear bodies[153]) and those lncRNAs that exert their function through their act of transcription (such as Airn[68])

- they interact with DNA via hybridization and triplex mediated base-pairing; this is typical of some antisense lncRNAs, which form R-loops close to their site of transcription and then recruit transcription co-factors to the promoter. For instance, Khps1 is transcribed antisense to SPHK1 and after R-loop formation it recruits p300 to the locus, thus increasing chromatin accessibility, E2F1 binding and SPHK1 expression[136]
- they interact with proteins with DNA binding activity; roX (RNA on X chromosome) mediates X chromosome inactivation in Drosophila and it is targeted by interaction with CLAMP (chromatin-linked adaptor for MSL proteins), which recognizes around 150 binding sites on the X chromosome[154].

lncRNAs can exploit either one or more of these mechanisms, but they are often not sufficient to explain their behaviour: for instance XIST and FIRRE are tethered to chromatin via SAFA proteins, but these can localise also to other sites in the genome[155]. So, how can XIST specifically inactivate only one X chromosome? 3D proximity could be a key factor for selective activity: as indicated by highest interaction frequencies on Hi-C maps, once transcribed, XIST associates with those sites that are close to it, not necessarily in linear space[110]. Remarkably, forced expression of XIST at the HPRT locus induced a similar effect and associated with genes characterized by high contact frequency with HPRT. Thus the pre-existing X chromosome conformation is the main factor that drives the nucleation of XIC[110].

How XIST can then spread to the rest of the chromosome is still not understood, but it may involve multiple cycles of XIST diffusion from its transcription site and change of chromatin architecture: initial transcription increases XIST local concentration (seeding); the lncRNA acts as a scaffold, forming a complex with protein partners (XIST+SHARP+hnRNPK) and gets recruited to chromatin (XIST+SAFA); then it induces heterochromatin modifications

(histone deacetylation and H3K27me3) and progressively repositions the X chromosome to a new nuclear region (thanks to LBR interaction); as XIST continues to be transcribed it can iteratively repeat this process until completed[155]. This model of seeding, scaffolding and downstream modifications may characterize other lncRNAs.

3D proximity highlights that, unlike proteins, lncRNAs can immediately exert their function after their transcription. Moreover, the high concentration at their locus explains how low abundance transcripts can reliably identify their targets. Expression levels may be an intrinsic feature that controls the extent to which lncRNAs spread and control nearby genes: for instance, Kcnq1ot1 can silence the expression of several neighbouring genes[130], while the lower expressed HOTTIP activates only the HOXA genes[134].

Another advantage of spatial proximity is the possibility to act in trans in an inter-chromosomal and not only intra-chromosomal manner: this is exemplified by FIRRE (which can engage genes from its chromosome and others from the 2, 17 and 15)[120], CISTR-ACT (encoded on chromosome 12 but acting on the 17 gene SOX9)[156] and HOTAIR[108] (transcribed from the HOXC locus and acting on the HOXD one[157]).

LncRNAs and nuclear bodies

LncRNAs interactions with proteins and DNA enable also the formation of dynamic spatial compartments in the nucleus. While XIST and FIRRE create compartments that organize chromatin, other lncRNAs nucleate and maintain nuclear bodies (NBs), microscopically visible non-membrane bound structures in the nucleoplasm[158]. Unlike protein aggregates (such as amyloid plaques) NBs can be broken down and constantly exchange RNAs and proteins with the nucleoplasm pool. Several kinds have been identified (nucleoli, Cajal bodies, PML bodies, nuclear speckles, paraspeckles, PcG bodies) and it is possible that additional structures still

need to be characterized[158]. Different functions have been proposed (genome organization and maintenance; RNAs processing; retention of proteins and RNAs; response to stress; maturation of multi-factor complexes) but their physiological role is still debated[158].

Paraspeckles biogenesis constitutes an interesting example of how proximity influences formation of cellular structures. It relies on the seeding role of NEAT1 (nuclear paraspeckle assembly transcript 1) which recruits a specific set of proteins and increases their local concentration. Thanks to their low complexity domains, these proteins oligomerize resulting in a liquid-liquid phase separation from the nucleoplasm[159].

First described in 2002[160], over the years more than 40 different protein components have been identified. Despite differences in size and number, paraspeckles have been found in most cell types (except embryonic stem cells and induced pluripotent stem cells[161]) and tissues, with higher abundance in murine luteal cells and at the tip of gut epithelium. Indeed, despite being not essential for normal development in mice, NEAT1 knock out decreases fertility due to defects in corpus luteum and mammary glands[162].

Super resolution microscopy and biochemical studies[163,164] showed that despite their liquid-like state, paraspeckles are subdivided into a shell and core regions, which contain specific proteins and parts of NEAT1: in the former, the 5' and 3' ends of NEAT1 (which acquires a "bent" conformation) interact with TDP43[159]; in the core the rest of NEAT1 sequence interacts with the NONO, SFPQ, PSPC1 and FUS proteins (plus accessory ones), while RBM14 and BRG1 are present in patches[159].

NEAT1 transcription gives rise to the architectural mono-exonic transcript of 23kb (NEAT1_2) with a triplex helix at the 3', and a shorter form of 3.7kb (NEAT1_1) with unclear function[165]. NEAT1_1 depends on an early polyadenylation site that cleaves the nascent transcript, unless the HNRNPK protein prevents this event[166]. In the absence of early

termination, NEAT1_2 is co-transcriptionally bound by SFPQ and NONO[163]. These RNA-protein interactions trigger NONO and SFPQ oligomerisation along the RNA thanks to intrinsically disordered regions of their coiled coil domains, creating bundles that stabilise the otherwise unstable NEAT1_2. These bundles are then fused into a mature paraspeckle by FUS, again thanks to prion-like low complexity domains[159]. The number and length of paraspeckles is directly proportional to NEAT1_2 production[167].

No distinct catalytic activity has been detected in paraspeckles and the two molecular mechanisms that have been proposed are RNA or proteins sequestration. It has been shown that double stranded RNA species containing inverted repeat motifs can be sequestered by NONO and SFPQ, reducing their translation rate[168]. Increased NEAT1 expression and paraspeckles formation in situations of stress (such as viral infections) have been shown to reduce nucleoplasm availability of SFPQ, reducing its repressive activity on IL-8 and the immune-responsive genes RIG-I and DDX60[169,167]. Other paraspeckles proteins may be regulated similarly to SFPQ so further investigations need to be performed. In addition, the biological role of paraspeckles may emerge in other cellular stress contexts and this may explain the absence of dramatic effects of NEAT1 knock out mice in untreated setting[162].

It is possible that paraspeckles act on their targets in close proximity to chromatin sites: analysis of NEAT1 DNA binding sites performed by CHART-seq, indicated an enrichment at the transcription start and termination sites (TSS, TTS) of expressed genes[114]. The binding profile was nicely overlapping with the one obtained from the paraspeckle protein PSF ChIP-seq data. These results suggest a role for NEAT1 in regulation of transcription, but did not provide a mechanistic explanation or which would be the functional role.

In the same study it has been also performed the CHART-seq for MALAT1, an 8kbp lncRNA transcribed 53kbp far from NEAT1. Similarly to NEAT1, MALAT1 was shown to bind

expressed genes, with an overlap with the gene body histone modification H3K36me3 and enrichment at the TTS but not the TSS[114]. These results were confirmed in an independent RAP-DNAseq experiment[118]. Authors also sequenced the RNAs eluted with MALAT1 and showed how it interacts co-transcriptionally (but indirectly) with nascent pre-mRNAs, especially multi-exonic ones that undergo alternative splicing. These results are in line with the proposed role of MALAT1 on regulating serine/arginine (SR) splicing factors activity and alternative splicing at nuclear speckles (NSs)[128].

These nuclear bodies are dispersed in the human interphase nucleus (normally 20-50/nucleus) and connected by fine fibrils to form a cluster. They are slightly denser than the nucleoplasm and characterized by higher protein concentration: low-complexity regions of their components allow multivalent interactions and phase separation over the surrounding homogenous solution[170]. Multi-colour structured illumination microscopy (SIM) experiments showed that MALAT1 localises at the periphery of NSs (with splicing factors being more internal)[171] and several NSs components such as RNPS1, SRm160 and IBP160 are required for this targeting[172]. However, unlike NEAT1 for paraspeckles, MALAT1 is not required for NSs formation, assembly or maintenance and knock out mice do not experience changes in their structure[173]. Its role seems to regulate distribution and phosphorylation of splicing factors and its knockdown alters alternative splicing[128].

How it exerts its function is not clear, but it may act as a scaffold to promote protein-protein, protein-RNA or protein-DNA interactions, repositioning active genes at the periphery of nuclear speckles[174]. These putative interactors may explain how it can contact thousands of actively transcribed genes even at large distance from its locus. Its high abundance (around 3000 copies per cell)[175] and stability may allow it to diffuse and find sites for which it has high affinity.

Nuclear compartmentalisation regulated by lncRNAs is probably still far from being completely understood. Nevertheless, either controlled by RNA-protein interactions that mediate chromatin spatial constraints or the formation of liquid-like nuclear bodies, it provides an efficient, quick and dynamic level of gene expression control. Relying on diffusion-based processes rather than active ATP consumption, it represents an energetically favourable system and it allows to simultaneously target multiple genes[174].

Similar to linear operons in bacteria, lncRNA-mediated gene networks allow efficient expression of genes assembled together to regulate a shared function: this is the case of the FIRRE-dependent structures, which promote activation of genes involved in energy metabolism and/or adipogenesis[120]. It is possible that these nuclear organizational centres occur in a cell-type specific manner, in line with the finding that lncRNAs are highly tissue-specific[155] and with the results of RADICL-seq experiments[176].

The putative existence of lncRNA-dependent nuclear structures is in line with the model of transcription factories. As evidenced by Hi-C and Pol2 ChIA-PET studies[177,178], genes from the same or different chromosomes tend to interact between each other with a frequency proportional to their expression levels, so that highly expressed genes are brought in close proximity to concentrate the transcriptional machinery and increase its efficiency. SPRITE[98] experiments have confirmed that transcription does not happen with spatial randomness and that highly expressed genes tend to accumulate around nuclear speckles, while silent regions are partitioned towards the nucleolus. It would be interesting to know if this mechanism is regulated by lncRNA-protein interactions inducing this peculiar chromosomal architecture or by potentially uncharacterized nuclear bodies.

LNCRNAS ACTING IN THE CYTOSOL

The investigation of cytosolic lncRNAs is less advanced than the nuclear ones. Most reports support a role in regulation of mRNAs stability or translation, but there are also examples of lncRNAs modulating protein localisation, post-translation modifications and downstream activities[179]. A frequently proposed mechanism of action is upregulation of a transcript expression by competing for miRNAs that would otherwise downregulate it. This competing endogenous RNA (ceRNA) hypothesis seems to characterise two classes in particular: pseudogene-derived transcripts and circular RNAs (circRNAs)[180].

In the first case, these RNAs share the miRNA binding sites with their parent coding gene. A well know example is PTENP1, which is homologous to PTEN but with a mutation that prevents its translation. It shares targets sites for miR-17, 21, 214, 19 and 26 and simultaneous inhibition of all of them increases expression of both PTEN and PTENP1, with a decrease of cells clonogenic capacity[181].

circRNAs typically derive from a backsplicing event, meaning that the splice donor site of one exon is ligated to the splice acceptor site on an upstream one. This results in a circular transcript with increased stability compared to a linear one, since no free ends are available for exonuclease digestion[182]. An example of circRNA sponging a miRNA is Sry, which contains 16 binding sites for miR-138 and co-precipitates with Argonaute 2 (AGO2)[183]. circRNAs are not degraded after miRNA binding so they were proposed as attractive ceRNAs; however a genome wide analysis suggested that only few of them contained more than ten binding site for an individual miRNA[182] and they did not enrich after AGO2 immunoprecipitation by iCLIP[184]. Therefore, effective miRNA sponging by circRNA may be unusual.

lncRNAs have been also reported to act as ceRNAs, showing for instance a role in embryonic stem cells[185] and muscle cells differentiation[186]. In these reports, lincRNA-RoR and

linc-MD1 sponged miRNAs that regulate the expression of transcription factors (OCT4, NANOG and SOX2 in the first case, MAML1 and MEF2C in the latter), exemplifying the concept of pathway divergence: miRNA competition by lowly expressed lncRNAs can have an broad effect thanks to changes in transcription factors that regulate multiple downstream targets.

Nevertheless, despite these attractive examples, the model of ceRNA as a general mechanism has been controversial. It has been shown that controlled in vivo expression of a transcript competing for miR-122 (highly expressed in the liver) at physiological levels (5100 copies) did not affect the miRNA levels, expression of its targets and downstream physiological responses[187]. The reason could be the huge discrepancy between the 5100 copies of target and the predicted 150000 miR-122 binding sites. In line with this, mathematical models predict that effective sponging occurs only when miRNA and target levels are near equimolar[188]. This finding has two implications:

- individual ceRNAs may have a limited potential to influence stability of other transcripts, unless targeting a lowly expressed miRNA. However it has been shown that low expressed miRNAs have normally little regulatory capacity, so their change would not be particularly meaningful[189]
- at steady state levels most lncRNAs are expressed at very low levels, making hard for them to be effective sponges. In this view mRNAs should have a stronger influence on miRNA competition. PTEN for instance has been shown to compete for miRNA binding with other coding genes, such as CNOT6L, VAPA, VCAN and ZEB2[190]

The hype on lncRNAs as ceRNAs has been probably driven by the ease of defining a function for poorly characterized transcripts. The result of many reports diffused in the last years[83] may suffer from limitations in the experimental methods: since they relied on

overexpression systems (of target or miRNA) it becomes difficult to interpret these results in a physiological setting and they may overestimate the potential activity of the ceRNA[180].

A second mechanism for lncRNAs to influence stability of mRNAs is by recruiting factors that can degrade them, such as Staufen 1 (STAU1). This protein recognizes double stranded RNA molecules (such as a 19 bp stem loop present in the ARF1 mRNA) and induces decay (STAU1-mediated messenger RNA decay or SMD) in a similar manner to non-sense mediated decay/NMD[191]. It has been shown that imperfect base pairing between an Alu element in an mRNA and another in a lncRNA can trigger SMD. These lncRNAs were defined as half-STAU1-binding site RNAs (1/2-sbsRNAs) and they can regulate SMD of some targets[192].

lncRNAs binding to proteins involved in mRNA decay can also induce the opposite effect if they act as decoys. For instance, NORAD (noncoding RNA activated by DNA damage) interacts with PUMILIO1 and PUMILIO2 (PUM1/2) proteins in the cytoplasm, preventing their binding to the PUMILIO responsive elements (PREs) present at the 3'UTR of target mRNAs[193]. Once recognized, the PRE would stimulate their deadenylation and decapping, thus reducing stability and translation; NORAD contains around 15-17 PREs and its decoy activity protects mRNAs coding for proteins involved in genome stability[194].

Some cytoplasmic lncRNAs also regulate translation rate of mRNA targets. An interesting example is the Uchl1 antisense RNA, which overlaps at the 5' of the Uchl1 gene (ubiquitin carboxy-terminal hydrolase L1). The antisense RNA is normally nuclear, but under mTORC1 inhibition by rapamycin, it translocates to the cytosol, where its pairing with Uchl1 mRNA favours its translation, despite rapamycin blocks CAP-dependent translation. It has been proposed as a mechanism to maintain synthesis of pro-survival proteins in situations of stress[195]. On the other hand, the lincRNA-p21 (a transcript expressed between the CDKN1A and SFSR3 genes) associates via Rck with JUNB1 and CTNNB1 mRNAs and reduces their

translation rate. This inhibitory activity is buffered by the HuR protein, which recruits AGO2 to the lincRNA and promotes its degradation. It is not clear the mechanism of lincRNA-p21 effect on translation but it may involve ribosome drop-off following its association[196].

Another example is lncMyoD, which is expressed next to the MyoD gene: upon muscle cells differentiation, MyoD gets upregulated and increases lncMyoD as well, which interacts with the IGF2-mRNA-binding protein 2/IGFBP2. This has a decoy effect for translation of proliferative genes (such as NRAS and MYC) and allows cell cycle exit and muscle cells differentiation[197].

All together these findings highlight the relevance of lncRNAs not only on transcriptional but also post-transcriptional processes and translation. It is possible that this role is even more extensive than currently known and it will be relevant to better define how these lncRNA-protein and lncRNA-ribosome interactions take place.

Nevertheless, these are not the only cytoplasmic mechanisms of action that have been characterized and it is emerging also an influence on signalling pathways via regulation of proteins post-translational modifications. For instance, in dendritic cells lnc-DC promotes STAT3 phosphorylation on tyrosine 705 by binding and inhibiting the SHP1 phosphatase[198]; in breast cancer cells, NKILA (NF-Kb interacting lncRNA) interacts and prevents phosphorylation of IkB, which otherwise would inhibit NFKB nuclear translocation and transcriptional activity[199]. These findings should constitute a stimulus to perform new RNA-pulldown experiments on cytoplasmic lncRNA to unveil similar mechanisms of action.

Finally, as lncRNAs have been shown localise to specific subnuclear areas, it is conceivable a regulated targeting also to discrete organelles in the cytoplasm. An interesting approach to map lncRNAs across specific subcellular areas could be APEX-seq, as previously described. Using this technique, it was found that while some RNAs localised as previously

reported (such as XIST at the nuclear lamina or IARS2 at the outer mitochondrial memberane/OMM), 31 noncoding RNAs unexpectedly enriched at the endoplasmic reticulum membrane/ERM[95].

Some reports also suggest mitochondrial import of nuclear encoded lncRNAs[200]. One of them is the previously cited RMRP, which is transported in two steps by CRM1 and GRSF1. Its loss-of-function reduces oxygen consumption rate and mitochondrial DNA replication, but the underlying mechanism is unknown[104].

This work interestingly suggested a lncRNA mitochondrial import mechanism based on protein interaction which could characterize also other transcripts. For instance, the 5S ribosomal RNA binds to the rhodanese protein and exploits its mitochondrial import signal to translocate into the matrix[201]. 5S and other cytosolic RNAs (RNAse P, MRP) are imported by the polynucleotide phosphorylase (PNPASE), a 3'-5' exoribonuclease and polyA polymerase localised in the mitochondrial intermembrane space[202]. This interaction is dependent on a stem-loop structure, which may be present also on other RNAs.

Some lncRNAs are also encoded by the mitochondrial genome[203]. One of them is called SncmtRNA, a 2.4 kb transcript composed by 815 nucleotides of inverted repeats fused to the 16S ribosomal RNA sequence. Although is function is not understood, it has been shown to be highly expressed in proliferative cells. On the other hand, two antisense transcripts to sncmtRNA (ASncmtRNA-1 and ASncmtRNA-2) are expressed in normal cells and downregulated in tumour ones. All of them can be found in the nucleus, suggesting a retrograde movement[204]. Another chimeric transcript derived from the 5'end of COX2 and the 3'end of CYTB named LIPCAR (long intergenic RNA predicting CARdiac remodeling) was found upregulated in patients with chronic heart failure, but no functional link with the disease has been suggested[205]. Three other lncRNAs (lncND5, lncND6, lncCyb) form intermolecular

duplexes with their complementary RNAs (ND5, ND6 and Cytb) and they may have a role in their stabilisation or expression[203]. It is evident that research about mitochondrial lncRNAs is still at its infancy. It requires additional information to confirm sufficient expression in these organelles, how the RNAs are imported and if they regulate some aspects of mitochondrial function (biogenesis, fission, fusion or oxidative phosphorylation).

FIGURE 2 - FUNCTIONAL STUDY OF LNCRNAS

A. The understanding of lncRNAs mechanisms of action requires an integrated approach involving biochemical and genomic techniques. A starting point is the subcellular localisation analysis, which can guide the decision of downstream methods to follow. For instance, a nuclear lncRNA would be likely involved in gene expression regulation, making the identification of its potential chromatin binding sites or RNA/protein partners very useful. Positional information influences the method of pulldown (total vs enrichment of a subcellular fraction) and can rely on fractionation or FISH experiments. Results of RNA-centric techniques should be corroborated by complementary studies, such as RNA-immunoprecipitation for RNA-protein interactions or transcriptomic/chromosome conformation analyses for RNA-chromatin or RNA-RNA relationships. **B.** These techniques opened a window on the lncRNAs regulated cellular processes in the nucleus and cytosol. Nuclear lncRNAs have been shown to regulate gene expression by acting on chromatin (at local or broad level), on transcription activation/repression or on nuclear bodies biogenesis. lncRNAs can also have non transcriptional related roles (stability of telomeres, mitosis). When exported to the cytosol they can regulate mRNAs stability and translation, post-translational modifications of signalling molecules, or mitochondrial function. **C.** Super resolution microscopy and phase-separation studies unveiled the molecular structure of nuclear bodies such as nuclear speckles and paraspeckles, and may aid to characterize other subcellular structures regulated by lncRNAs.

PERSPECTIVES ON LNCRNAS RESEARCH

In the last 10 years the technological progress to study lncRNAs has developed exponentially[206]. Despite the need to improve annotations and the definition of the lncRNAome, it is time to focus the efforts on biochemical and structural studies, which have already demonstrated the power to unveil unexpected molecular and cellular biological processes[122,207]. So far 3 main criteria have been exploited to select functional lncRNAs: sufficient expression levels, sequence or structure conservation and proof of controlled expression (from analysis of chromatin marks and transcription factors at regulatory regions; presence of 5'cap, polyA, splicing maturation). All strategies that are more adapted for protein coding genes. The development of genome wide functional screens based on CRISPR technology may provide a useful tool[208], but they are dependent on the cell line used, meaning that the specific set of lncRNAs expressed may bias the possibility of finding interesting targets. In addition, the readout assay has to be carefully designed to be meaningful.

The case-by-case approach, although with low throughput, probably represent the most informative one: focusing on a small set of lncRNAs (identified by genomic or protein-centric approaches) allows detailed information to be gained regarding subcellular localisation, biological relevance of the RNA molecule and the eventual RNA, DNA or protein partners. Gathering all these pieces of information, coupled with loss and gain of function experiments, allows the definition of downstream molecular events and the related biological function.

An aspect at still an embryonal stage is the study of lncRNAs 3D structures, how they affect interaction with DNA or proteins and if it they are organized in domains[207]. Some bioinformatic tools have been proposed to predict secondary structures from the RNA sequence[64], but this revolution has to rely on biochemical methods [65,209–212]. The possibility to identify specific residues responsible for interactions would open a whole new field for

targeting RNA and protein functions with small molecules, without the need to degrade the RNA transcript itself.

SECTION 2 - LNCRNAS IN CANCER

Cancer is the second leading cause of death and constitutes a major public health problem worldwide. Although during the period 2013-2017 the overall cancer death rate decreased by 1.5% on average per year, incidence rates have flattened among males and slightly increased among females[213]. Major progress has been made in the last 30 years, considering the 29% decrease of cancer deaths per 100 000 people from 1991 (215) to 2017 (152), but this change has been relied on public campaigns against tobacco smoking[214]. In addition to a better education about major cancer risks factors (cigarette smoking, excessive alcohol use, obesity), increased number of people underwent population-based screening and new therapeutic options have been introduced (genome-targeted therapies and immunotherapy in particular). Nevertheless, endpoints for breast and colorectal cancer screening in the US during the 2007-2017 period were not met overall[215] and advanced treatments still have limited access for patients or their success rates is restricted by resistance emergence[216]. Decreasing cancer rates and improving patient outcomes will thus derive from a combined effort on making screenings and treatments more accessible, educating people about cancer risks factors and developing more effective and sustainable diagnostic tests and therapeutics.

The possibility to sequence the human genome has revolutionized our general understanding of the genetic code and gave the possibility to better characterizes diseases such as cancer. The combination of next-generation sequencing (NGS) and advanced

computational data analysis allowed to identify cancer driver genes, to better understand the biological basis of different cancer types and to discover genomic biomarkers of drug response and resistance. These advances ultimately led to the possibility of developing targeted small molecules and antibody base therapies against cancer dependencies and guide clinical decision making in a personalized manner[217].

A major effort to define the molecular features of major cancer types has been represented by The Cancer Genome Atlas (TCGA) project, launched in 2006 by the NIH to integrate research from different disciplines and multiple institutions. Over 14 years, the TCGA generated 2.5 petabytes of publicly available genomic, epigenomic, transcriptomic and proteomic data (together with their corresponding clinical information) on over 20 000 cancer and matched normal samples across 33 cancer types[218].

This collection has been the foundation of several studies trying to derive translational utility of these data[219, 220], focusing not only on protein coding genes. The study of cancer related non-coding RNAs was prompted by the results of the ENCODE project and by the appreciation that recurrent somatic[221] or copy-number alterations[222] occur also in noncoding regions. Although micro-RNAs have been the first noncoding RNAs to be investigated[223], lncRNAs also exhibit interesting features for cancer research:

- several of them sustain carcinogenic functions with cancer specific expression, two important features for therapeutic targeting[224]
- their characterisation as biomarkers would allow the development of non-invasive diagnostic methods (for instance relying on body fluid samples[225])

On the other hand, cancer cells represent an ideal in vitro model to perform demanding biochemical RNA-centric experiments, such as RNA pulldowns[122].

A first analysis of TCGA data about lncRNAs expression across 13 cancer types with a total of 5037 samples, detected 32.5% of GENCODE annotated lncRNAs[226]. Focusing on 7 normal-tumour matched types (BRCA, COAD, HNSC, KIRC, LUAD, LUSC, PRAD), 15% and 11.8% of lncRNAs were up- and down-regulated in cancer, respectively. 60% of these altered RNAs were cancer-specific and the others shared by at least two cancers. Only 5 genes (0.22%) were deregulated in all 7 types, compared to 2.47% of protein-coding genes, suggesting more cancer-specific alterations[226].

Unsupervised clustering of lncRNAs was able to separate normal from tumour samples and tumour samples of different types. In line with this, lncRNAs showed higher specificity scores[17] across TCGA samples and CCLE (Cancer Cell Line Encyclopedia) cell lines compared to pseudogenes and protein coding genes. lncRNA expression may thus be used to characterize tumours with unknown origins[226]. Similar conclusions were driven by other TCGA analyses, which provided signatures of lncRNAs for each cancer type able to distinguish cancer from healthy samples[227].

The LncRNA Spatial Atlas (lncSpA) database gathers expression data from various sources (GTEx, HBM2.0, HPA, FANTOM5, TCGA) and constitutes a valuable resource to evaluate lncRNA expression across normal and cancer tissues[228]. It discriminates lncRNAs as tissue specific (when expressed only in a particular tissue), tissue enriched (when expressed 5-fold more in a particular tissue compared to all the others) or tissue enhanced (when expressed 5-fold more in one tissue compared to the average of all the others together). It also defined 399 differentially expressed lncRNAs in normal vs tumour samples, while 267 associated with worse patients survival[229].

Besides expression changes, lncRNA genes have been found to be altered also at the genomic level in cancer. Across 13 cancer types from TCGA, 13.16% and 13.53% of lncRNAs

were characterized by high-frequency (more than 25% of specimens) gain and loss, respectively. For 36.27% of them there was a positive correlation with the expression level, indicating copy number variations as a mechanism of lncRNAs deregulation in cancer[226]. This phenomenon has been confirmed by other reports[230,231].

Epigenetic alterations can be further responsible for deregulated lncRNA expression in cancer. Analysis of DNA methylation at CpG islands across TCGA samples showed that while protein coding genes promoters were predominantly hypermethylated (in accordance with the CpG islands hypermethylation phenotype/CIMP[232]), lncRNA promoters were equally hypo- and hypermethylated (for instance 504 and 639 genes for BRCA, respectively) compared to normal samples[233]. Combining DNA methylation and expression data showed a significant negative correlation between the two and allowed to identify 1006 epigenetically activated (EA) and 1117 silenced (ES) lncRNAs. Some of the EA lncRNAs were significantly correlated with poor survival in at least 1 cancer type, and the opposite was true for ES ones[233].

Interestingly, two EA lncRNAs (SNHG12, MINCR) showed expression in multiple cancer types: both of them are relevant for cancer cells proliferation and regulated by the transcription factor MYC[234,235], which is known to promote tumour progression at different levels[236,237]. Among the targets of MYC there are protein coding genes (involved in cell cycle, DNA repair, glycolysis, etc) but also lncRNAs[238–240]. Similar to SNHG12 and MINCR, these lncRNAs promote cell proliferation, suggesting they constitute downstream effectors of the MYC-dependent program. Interestingly, some lncRNAs can also regulate MYC activity, such as EPIC1[233], PCAT1, CCAT1, and CCAT2[224]. Since MYC targeting by small molecules has so far proven to be challenging[241], inhibition of these lncRNAs could represent an alternative strategy.

FUNCTIONS OF CANCER RELEVANT LNCRNAS

A longstanding dominant view of carcinogenesis has been that tumours are initiated at single cell level by mutagens (somatic mutation theory or SMT). The premise of this reductionist and genetic deterministic approach is that normal cells reside in a state of quiescence and their proliferation is controlled by growth factors (external influence) or oncogenes (intrinsic influence)[242]. DNA mutations can induce the loss of this control by increasing the activity of oncogenes or inhibiting the one of tumour suppressors, and result in clonal expansion. Further alterations are then responsible for the metastatic spread[242]. In this perspective several lncRNAs can be considered as oncogenes (H19[243], HOTAIR[244], LUNAR1[245], MALAT1[246], THOR[247]) or tumour suppressors (GAS5[248], NORAD[249]).

However the SMT fails to explain some exceptions to its premises, such as mutated oncogenes and aneuploidy in normal tissues, absence of mutations in some tumours and spontaneous regressions[242]. It has been extended with elements of the tissue organization field theory (TOFT), which states that cells are in a default proliferative and invasive state, constrained by other tissue elements: alterations in the interactions between stroma and parenchyma result in neoplasm formation and metastasis[242].

The revision of the initial reductionist view led to define a group of features that characterise tumours, combining intrinsic cancer cell features with others related to the microenvironment. They are called the hallmarks of cancer[250,251] and comprise: sustaining proliferative signalling; evading growth suppressors; activating invasion and metastasis; enabling replicative immortality; inducing angiogenesis; resisting cell death[250]; avoiding immune destruction; tumour-promoting inflammation; genome instability; deregulating cellular energetics[251]. Cancer relevant lncRNAs have been shown to participate in all of these

hallmarks[224,249,252,253], exploiting mechanisms of action already described in the physiological context (protein complexes scaffold; recruitment of chromatin modifying enzymes; post-transcriptional and translational regulation; decoy for RNA binding proteins; signalling regulators). The discussion will focus on lncRNAs involved in cell division, DNA repair and metabolism of cancer cells.

lncRNAs involved in cell division and DNA repair

In normal tissues, mitogenic signals trigger intracellular cascades that result in cell division. This ensures the homeostasis of tissues cell number, architecture and functionality. Cancer cells circumvent the dependence on mitogens via different mechanisms: autocrine or paracrine release of growth factors; increased membrane expression of their receptors; constitutive activation of intracellular signalling pathway components[251]. The latter effect can rely on altered activity of intermediate cascade proteins (kinases, small GTPases) or the ultimate effectors, that is transcription factors[250].

lncRNAs have been shown to sustain the expression or activities of MYC or E2F1, which are relevant to express genes involved in cell division and survival[254,255]. MYC resides in the 8q24.21 region, which is gained in many human cancers[256] and comprises also the PVT1, CCDC26 and GSDMC genes. In the breast cancer MMTVneu mouse model, single copy gain of human MYC or the PVT1, CCDC26 and GSDMC trio does not impact on tumour development, but the gain of whole region reduces tumour latency[257]. This cooperative relationship relies on the fact that PVT1 prevents MYC degradation by reducing its phosphorylation on tyrosine 58. In human cancer PVT1 co-amplifies with MYC (97.3% of tumours with 8q24 gains) and its reduction impairs proliferation and clonogenic capacity[257].

MYC protein levels are also regulated by LINC01638 (which prevents SHOP-mediated ubiquitination)[258], GHET1[259] and THOR[247] (which by stabilizing IGF2BP1 interaction with the MYC mRNA promote its translation). lncRNAs can also increase transcription of the MYC gene: CCAT1-L regulates a CTCT-dependent chromatin loop that is important for MYC transcription[129], while CCAT2 enhances the activity of TCFL2[260]. On the other hand, PCAT1 sponges miR-34 and protects MYC mRNA from degradation[261]. Interestingly, PCAT1, CCAT1-L and CCAT2 are also part of the 8qp24.21 regions, suggesting that MYC gets co-amplified with genes that can stimulate its expression.

Other lncRNAs influence MYC transcriptional activity: EPIC1 interacts with MYC and somehow boost the expression of its target genes[233]; similarly PCGEM1 promotes MYC chromatin recruitment and transcription of genes involved in metabolic pathways[262]; MINCR has been suggested to have the same role but it was not demonstrated to interact directly with MYC[234]. Interestingly, MINCR and PCGEM1 are MYC-targets, suggesting the existence of a positive feedback loop.

lncRNAs can also act as coactivators of the E2F1 transcription factor: LINC00337 was shown to do so in pancreatic ductal adenocarcinoma cells[263], while ERINA in breast cancer[264], suggesting that different lncRNAs can mediate the same function in different tumour types. One of the oncogenic mechanisms proposed for H19[265] is to sponge miR-29-3p from E2F1 mRNA in clear cell carcinoma cells[266].

Other lncRNAs promote cell division by acting directly on genes involved in this process. LAST interacts with CNBP (a nucleic acid-binding protein) to stabilize cyclin D1 (CCND1) mRNA, allowing its translation and the transition from G1 to S phase[267]. Interestingly, LAST and CCND1 are transcribed on chromosome 11, on the same strand and 1.8Mb apart in a MYC-dependent manner, suggesting to be co-regulated and acting in close proximity once

expressed[267]. CCND1, along with other targets, was shown also to be indirectly induced by CASC11, another MYC-dependent lncRNA: its effects relies on interaction with hnRNP-K and stabilisation of beta-catenin mRNA[268].

Other lncRNAs sustain uncontrolled proliferation by inhibiting growth suppressors. HOTAIR[269], MYClo-1[239], and DANCR[270] repress CDKN1A/p21, which inhibits CDK2 and G1 to S phase transition. HOTAIR represses CDKN1A by targeting EZH2[269] to its locus; MYClo-1 interacts with the ELAVL1/HuR protein[271] and may stabilize its binding to the CDKN1A promoter[239]; the mechanism underlying DANCR effect in human B lymphoma was not clarified[270], but in gastric cancer it was suggested to target EZH2 to repress lncRNA-LET[272]. Similarly to MYClo-1, MYClo-2 was shown to target hnRNPK to CDKN1B/p27 (a CDK2, CDK4 inhibitor) and repress its expression[239]. p27 levels are also dampened by UCA1[273] and TRMP[274], which interact and sequester two proteins that promote its translation (hnRNP I and PTBP1, respectively).

Another interesting example is the CDKN2B antisense RNA, also known as ANRIL[275]. This gene of 126 kb and 19-21 exons, completely overlaps with CDKN2B (which encodes for p15, a CDK4/6 inhibitor) and it transcribed in a divergent fashion to CDKN2A (this encodes for p14 and p16, which modulate p53 and inhibit CDK4/6, respectively). ANRIL is a nuclear lncRNA[85] and it was shown to interact with the PRC1 component CBX7 to recruit the complex on CDKN2A and promote H3K27me3 dependent silencing[276]. At CDKN2B it recruits PRC2 via SUZ12[277]. Thus, ANRIL should act in proximity to its locus. Nevertheless, it was shown to recruits PRC1 and 2 also to distant genes, probably by recognition of Alu motifs, which are present both in ANRIL and at the promoters of his targets[278].

Interestingly, ANRIL is induced by E2F1 upon during ATM-dependent DNA damage response: while p53 activation arrests cell cycle, E2F1 increases ANRIL to repress INK4 family

members and alleviate p53 and pRb signalling to avoid senescence. In this way at the end of the repair process, the cell can re-enter in the cell cycle[279]. It is possible that cancer cells have hijacked this evolutionary mechanism to exploit ANRIL non-genetic repression of the INK4 locus, sustain proliferation and avoid senescence. Indeed other oncogenes can also promote ANRIL expression in cancer cells (MYC[280], SOX2[281], SP1[282]).

In a similar manner, upon DNA damage induction by neocarzinostatin (NCS), ATM promotes via NFKB the expression of the lncRNA-JADE, which activates the nearby gene JADE1[283]. This protein, together with HBO1, catalyses H4 acetylation at K5, K8 and K12, which similarly to gamma H2Ax, are recognized by Mdc1 to repair double strand breaks. lncRNA-JADE is upregulated in a percentage of breast cancer patients and its knockdown suppresses tumour growth, suggesting a beneficial role on DNA repair[283].

These examples indicate the relevance of lncRNAs in avoiding apoptosis and senescence in cancer cells experiencing DNA damage, a relevant feature given their high genome instability[251]. Other lncRNAs actively participate in DNA repair, especially in double strand breaks. Like lncRNA-JADE, DDSR1 is induced by NFKB upon ATM activation: it interacts with and targets proteins involved in homology repair; its knockdown impairs this process, reducing cells proliferation and increasing sensitivity to PARP inhibitors[284].

LINP1 was found to be highly expressed in triple negative breast cancer cells and relevant for double strand breaks repair by non-homologous end joining (NHEJ): it is expressed downstream EGF signalling and upon DNA damage it interacts with Ku80, acting as a scaffold for the formation of the Ku80-DNA-PKcs (DNA dependent protein kinase catalytic subunit) complex[285]. This activity increases the efficiency of NHEJ and protects cancer cells from external stress: indeed inhibition of LINP1 was shown to increase sensitivity to irradiation[285].

A p53-regulated lncRNA named GUARDIN also helps to preserve genome integrity: binding BRCA1 and BARD1 proteins via distinct structural regions, it acts as a scaffold that stabilizes their interaction; GUARDIN knock down at steady state or upon genotoxic stress (doxorubicin treatment) reduces BRCA1 levels and homology repair efficiency, finally triggering apoptosis[286]. These results suggest a potential strategy of co-targeting lncRNAs with DNA damage inducing agents or PARP inhibitors.

Several reports have also evidenced an intricate network of lncRNAs regulating p53 activity. This protein has been defined the "guardian of the genome"[287], being a central sensor of genomic stress or abnormalities: DNA damage, nucleotides depletion, suboptimal glucose or oxygen levels induce its activation and transcription of its targets, which stop cell division until the problem is resolved. If the damage is irreparable, cells undergo PUMA and NOXA mediated apoptosis[288]. Given its determinant role in cells fate, p53 activity is tightly regulated and frequently lost in cancer cells, so that they can sustain genomic instability without undergoing senescence or apoptosis.

Some lncRNAs are regulators of p53 through different mechanisms. In some instances, they are also its targets, and establish positive and negative feedback loops. Regulation of p53 activity occurs directly at the transcriptional or post-transcriptional levels or indirectly on its target genes.

CTCF has been shown to be involved in p53 increase upon DNA damage. This effect involves the Wrap53 gene, which is transcribed in an antisense divergent fashion at the 5' of p53[289]. Despite being a protein coding gene, what's relevant for p53 is its non-coding function: once transcribed, this RNA binds to CTCF, favours its stabilisation and p53 transcription. Similar to p53, knock down of Wrap53 impairs DNA damage response, despite its coded protein is not involved in it[289]. CTCF has two RNA-binding zing finger domains whose deletion

disrupt its dimerization, genome binding and chromatin loops formation, suggesting that proximal binding of RNAs may constitute a diffuse mechanism beside the p53 locus[290].

p53 expression and activity can be affected at the translation level or by post-translation modifications. The Ror lncRNA has been shown to interact with the cytoplasmic and phosphorylated form of hnRNP I, an RNA binding protein that binds to p53 IRES at the 5'UTR and represses its translation[291]. MALAT1 has also been proposed as a negative regulator: it interacts with the DBC1 protein, which mediates sequestration of the SIRT1 deacetylase; the reduction of free SIRT1 induces a deacetylation of p53 which negatively impacts on its stability and transcriptional activity[292]. The lncRNA PURPL also acts as a decoy and dampens p53 stabilization: it interacts and sequesters the MYBBP1A complex, which is important for p53 tetramerization[293]. Since p53 is primed to many of its targets before its activation (to induce a quick response)[294], targeting these inhibitory lncRNAs may constitute an interesting strategy in p53 wild type tumours: its basal activity could be increased and impair cancer cells proliferation or induce cell death.

Other lncRNAs have a positive effect on p53 activity. MEG3 is an imprinted gene that reduces levels of MDM2, the p53 partner that mediates its degradation[295]. Consequently, MEG3 overexpression was associated with p53-dependent increased transcription of p21[296]. Not surprisingly, MEG3 loss is a common phenomenon in many tumours[297]. The DINO lncRNA also increases p53 protein stability and transcriptional activity, although the underlying mechanism of action is not clear[298].

Ror, PURPL and DINO are themselves targets of p53, implying they are involved in negative and positive feedback loops. Since they can exert their function right after transcription and in proximity to p53, they provide a very quick and specific level of regulation. DINO is of further interest because is transcribed divergent to the CDKN1A gene and close to

other two p53 dependent lncRNAs: PANDA (2.5 kb far) and lincRNA-p21(10 kb far). The former inhibits the expression of pro-apoptotic genes by sequestering the transcription factor NF-YA[299] (and indeed was found to be highly expressed in osteosarcoma cells[300]); the latter interacts with hnRNPK and co-represses with p53 its targets, thanks to an unknown chromatin targeting mechanism. Its overexpression in lung adenocarcinoma cells increases apoptosis and reduces proliferation in presence or absence of doxorubicin[301]. In line with these findings, it is downregulated in several tumours[302].

This locus shows how complex p53 regulation can be, with one lncRNA (DINO) that upon its transcription can stimulate p53 to further express p21 and two regulatory lncRNAs that balance its response in a positive (lincRNA-p21) and negative (PANDA) manner. The whole response is further controlled by other lncRNAs, such as APTR[303] and FAL1[230] that can repress CDKN1A expression by recruiting PRC2 and PRC1, respectively.

There is also a link between p53 activity and NEAT1. Several reports indicated that p53 activation by different stimuli (irradiation, doxorubicin, reactive oxygen species, hydroxyurea, adryamicin) or Nutilin-3a (a small molecule that inhibits MDM2 interaction) promotes NEAT1_2 expression and paraspeckles formation[304–307]. This phenomenon is particularly relevant during early steps of carcinogenesis or in cancer cells experiencing replication stress (for instance induced by chemotherapy): NEAT1_2 deficiency seems to reduce the cells capability to deal with double strand breaks induced by replication fork collapse, resulting in accumulation of DNA damage and ultimately apoptosis[305]. Paraspeckles may act by sequestration of proteins involved in replication forks firing or those of the DBHS family (SFPQ, NONO, PSPC1), which once displaced from chromatin would allow DNA reparation[305].

Paraspeckles increase upon Nutilin-3a or hydroxyurea treatment may depend on reduction of Integrator components. This complex is responsible for termination of NEAT1

transcription at the shorter form and when it gets reduced cells experience a switch from NEAT1_1 to the longer NEAT1_2[165]. Interestingly ovarian and epithelial cancer patients with low INTS10 levels show lower response to chemotherapy, possibly due to increased paraspeckles formation[165]. The same relationship with chemotherapy characterizes NEAT1 high patients[305]. This pathway may constitute a mechanism of stress adaptation therapeutically targetable, by combining NEAT1 inhibition with DNA damaging agents (doxorubicin, platinum compounds) or replication stress inducers (PARP inhibitors)[305,308].

All together these findings provide a very interesting network of functional relationships between lncRNAs and p53 that evolved to regulate its response in a quick and tight manner. Similar to protein-coding components of the p53 pathway, lncRNAs are altered or exploited by cancer cells to evade growth suppression in presence of genomic instability. In addition, they collaborate in repair of DNA damage induced by oncogenesis, as exemplified by NEAT1, DDRS1 and LINP1.

LNCRNAS SUSTAINING METABOLIC DEMANDS

Cancer cells chronic and uncontrolled proliferation rate requires the reprogramming of metabolic processes. These changes allow to improve cellular fitness during tumourigenesis, especially under stressful conditions[309]. The main reprogrammed activities are energy production, macromolecules biosynthesis and redox balance. They are so common among different tumour types that they were added to the first set of cancer hallmarks[251].

Reprogramming means that a conventional metabolic process is enhanced or suppressed compared to benign tissues as a consequence of mutations or other factors. The archetype is the Warburg effect or aerobic glycolysis, which was defined from the observation in 1920s by Otto Warburg that cancer cells constitutively uptake and use glucose to produce

lactate regardless of oxygen availability[310]. This effect has then been documented in many tumour types and exploited to non-invasively detect solid lesions using positron emission tomography (PET) with a radiolabelled analogue of glucose (^{18}F-fluorodeoxyglucose, FDG) as a reporter[311].

Despite Warburg's observation being correct, it led to the widely diffused misconception that cancer cells rely only on glycolysis as their major source of ATP[312,313]. The switch to glycolysis from the more energetically efficient mitochondrial oxidative phosphorylation (approximately 18 times more in ATP production from one glucose molecule) was proposed to help in sustaining nucleotide biosynthesis via the pentose phosphate pathway and to reduce the production of ROS species[314]. However, metabolic flux studies using ^{13}C-glucose administration coupled with nuclear magnetic resonance (NMR) of downstream metabolites, demonstrated that the majority of cancer cells produce energy via glucose oxidation[315,316]: analysis of isotope enrichment showed that human non-small cell lung tumours metabolise glucose through glycolysis and the tricarboxylic acid (TCA) cycle concurrently, with metabolic activity of both pathways higher than the adjacent lung tissue.

These results were corroborated by analysis of single cell RNA sequencing of melanoma and squamous cell carcinoma of head and neck (HNSCC) samples, which provided an indirect estimation of active metabolic processes. Gene ontology analysis indicated in both tumour types higher metabolic activity compared to normal cells and a positive correlation between glycolytic and mitochondrial activity, indicating they are not mutually exclusive[317]. Moreover, oxidative phosphorylation constituted the major source of intra- and intertumoural variance, suggesting that it may be responsible for adaptation to environmental factors. Interestingly these conclusions were in discrepancy with bulk RNAseq analysis of normal and

malignant samples or cancer cell lines, suggesting that bulk or in vitro measurements may underestimate the differences present in vivo[317].

Cancer cells seem to support anabolism, catabolism and redox balance downstream from a common set of pathways, which have been found to be frequently enhanced by genetic or epigenetic alterations. One of them is the PI3K-Akt-mTOR axis, which promotes increased glycolytic flux and fatty acid biosynthesis via activation of the transcription factors HIF1-alpha and SREBP[318]. Similarly, MYC is frequently upregulated due to chromosomal translocations, amplifications or single nucleotide polymorphisms and some of its targets include glucose transporters, enzymes involved in glycolysis, fatty acid synthesis, glutaminolysis and mitochondrial metabolism[319]. Oncogenes like KRAS can co-opt both PI3K and MYC pathways.

In addition, to adapt to low oxygen levels (hypoxia) caused by the lower rate of neo-angiogenesis compared to tumour growth, cells rely on HIF-1 stabilisation and the induction of genes increasing the glycolytic flux[320]. Some tumour are characterized by constitutive HIF-1 activity also in normoxic conditions (pseudohypoxia) thanks to hyperactivation of mTORC1 or loss of VHL, which would promote its degradation[321].

HIF-1 is a heterodimer of HIF-1 alpha and beta: the latter is a constitutively expressed subunit, the former is oxygen-responsive. Under normoxic conditions, it is hydroxylated on proline residues 402 and/or 564 by proline hydroxyldomain (PHD) proteins and then recognized by VHL, which ubiquitinates and targets it to the proteasome[321]. In the absence of oxygen, PHD is inhibited, HIF-1alpha accumulates and together with the beta subunit drives transcription at hypoxia response element (HREs)-containing genes[322,323]. Among them there is lincRNA-p21, previously described as a p53-induced lncRNA[301]. Its knockdown dampened glycolysis stimulation upon hypoxia induction and reduced HIF-1 transcriptional activity, suggesting a role in its regulation: lincRNA-p21 was found to interact with HIF-1 alpha and

VHL, thus inhibiting their association and the subsequent ubiquitination[324]. However, lincRNA-p21 overexpression under normoxic conditions was not sufficient to increase HIF1-alpha levels, suggesting to be involved in the positive feedback loop that sustains HIF-1 alpha activity only after hypoxia induction.

Unlike the study performed on mouse cells showing its repressive activity thanks to hnRNPK interaction[301], these experiments indicated a cytoplasmic localisation of lincRNA-p21[324], similarly to another report that suggested a role in translation inhibition[196]. In this case, lincRNA-p21 knockdown decreased growth of xenografts in vivo, suggesting a tumour promoting rather than suppressive effect. This discrepancy may rely on differences between the human and mouse genes and it indicates a possible dual nature (nuclear/cytoplasmic) of this lncRNA.

HIF-1 alpha is regulated by another lncRNA in triple-negative breast cancer cells: LINK-A[325]. It has two different stem loops interacting with the BRK and LRRK2 kinases. Upon HB-EGF stimulation, LINK-A participates in the downstream signalling cascade, facilitating BRK recruitment at the EGFR-GPNMB receptor. BRK phosphorylates HIF-1alpha on tyrosine 565 while LRKK2 on serine 797 and these modifications inhibit proline 564 hydroxylation and proteasomal degradation. Stabilisation of HIF-1 alpha in normoxic conditions has the pro-tumourigenic effect of stimulating glycolysis: LINK-A depletion affects growth in vitro and in vivo and its RNA levels (together with phosphorylation of GPNMB, BRK and HIF-1 alpha) are positively correlated with poor prognosis of breast cancer patients[325]. This study interestingly shows a lncRNA acting as a scaffold for the efficient transduction of a growth factor signalling pathway.

During tumour growth cells experience different metabolic states. At the beginning they are in a nutrient-replete condition and they rely on oxygen, glucose and glutamine to

sustain glycolysis and mitochondrial respiration[309]. When tumour size increases, cells located near the vasculature will not be much affected, but the distant ones will have diminished accessibility to nutrients and oxygen. They may start to rely on alternative sources, such as oxidation of fatty acids and BCAAs or macromolecules degradation after autophagy induction or macropinocytosis[309]. These catabolic pathways are triggered by the AMP kinase (AMPK), which is activated when ATP levels diminish: the rise of ADP activates adenylate kinase, which converts two ADP molecules into adenosine 5'monophosphate (AMP) and ATP as a salvage mechanism; AMP activates AMPK, which phosphorylates mTORC1 and ACC (to inhibit protein and fatty acids synthesis respectively) and ULK1 to promote autophagy[326].

Despite it evolved as a mechanism to adapt to nutrient deprivation, chronic AMPK activation would counteract tumour development and indeed members of this pathway are frequently inactivated in cancer cells[327]. The lncRNA NBR2 has been proposed as a positive regulator of AMPK and consistently it was shown to be downregulated in breast and renal cancer patients, associating with better overall survival and reduced tumour growth in vivo[328]. Mechanistically, NBR2 is increased upon energy stress downstream AMPK and interacts with it, potentiating its inhibitory effect on mTORC1 and ACC. Like other lncRNAs previously described, NBR2 establishes a positive feedback loop that sustains AMPK activity especially on the long period. Interestingly NBR2 is transcribed in a divergent fashion 218bp apart from BRCA1 and the two suppressor genes are frequently co-deleted in breast and ovarian cancer patients[329].

Cancer cell proliferation does not require only ATP production but also synthesis of proteins, lipids and nucleic acids. Fatty acids require acetyl-CoA and NADPH as starting blocks and cells obtain them from glucose metabolism, glutamine, acetate (the last two especially during hypoxia) and the pentose phosphate pathway[309]. For amino acids and nucleotides, cells

acquire simple nutrients (sugars, essential amino acids, etc.) from the extracellular space, process them through the pentose phosphate pathway and the TCA cycle into smaller intermediates and re-assemble them in amino acids and nucleotides[309]. Protein synthesis is the most energy demanding process in the cell and it is very tightly regulated, from rRNA biogenesis in the nucleoli to ribosome recycling[330].

lncRNAs can influence translation of their targets, as previously described, but also regulate rRNAs biogenesis in the nucleoli. These nuclear bodies assemble by phase separation of its components thanks to interaction of proteins containing intrinsic disordered domains (such as fibrillarin, nucleolin and nucleophosmin) with noncoding RNAs (rRNAs and Alu-related B1 RNAs)[331]. They are divided into three parts: the fibrillar center (FC), where ribosomal DNA is transcribed by polymerase I giving rise to the 45S RNA; the dense fibrillar component (DFC), where the 45S is cleaved into the mature transcripts (18S, 5.8S and 28S); the granular component (GC), where the ribosomes are assembled between rRNAs and ribosomal proteins[332].

Nucleoli assemble around chromosomal nucleolar organising regions (NORs) that contain repeated copies (more than 400) of rRNA genes distributed across 5 chromosomes. Only some of these regions are active, but their transcription can be increased to sustain proliferation (nucleolar hypertrophy). The regulation of this process is hijacked by cancer cells to boost ribosomes biogenesis and protein synthesis[333]. Indeed BHM-21, a RNA polymerase I inhibitor, has potent anti-cancer properties[334].

DDX21 is a DEAD-box RNA helicase that forms ring-shaped structures around polymerase I in the nucleoli: the result of this interaction is to control pol I activity and restrain rRNAs transcription. SLERT is a 694 bp sno-lncRNA derived from an exon skipping event at the human TBRG4 locus: it is characterized by 2 snoRNAs separated by an internal sequence[126].

The snoRNAs are responsible for SLERT targeting to the nucleoli, while the internal sequence for DDX21 binding: this results into an allosteric change that induces a more open structure and reduced inhibition of pol I. SLERT binding is thus a mechanism to increase rRNAs biogenesis: indeed its knockdown/overexpression, reduce/increase clonogenic capacity and in vivo growth, respectively[126].

A similar example of anabolic reprogramming in cancer cells is provided by SAMMSON, a lncRNA expressed in very restricted manner in melanoma cells. SAMMSON was found to interact with three major regulators of ribosome biogenesis in the nucleus and cytoplasm: XRN2, CARF and p32. XRN2 is a 5' to 3' exoribonuclease that degrades the spacer fragments of rRNAs, ensuring proper maturation of the 5.8S and 28S RNAs[335]; p32/C1QBP is a mitochondrial protein that interacts with RNAse H1 to produce the 12S and 16S mitochondrial rRNAs[336]; CARF exerts a negative effect on XRN2 activity and rRNAs maturation, by keeping the protein outside the nucleoli[337]. In melanoma cells SAMMSON creates aberrant complexes by sequestering CARF with p32 in the mitochondria and reducing its inhibitory effect on XRN2, which accumulates in the nucleoli[338]. XRN2 and p32 coordinated increased activity boost both nuclear and mitochondrial rRNA biogenesis, avoiding the proteotoxic stress that would be generated by an unbalanced increase of only one of the two[338]. This anabolic mechanism has a proliferative effect on cells overexpressing SAMMSON together with an oncogene, making SAMMSON expression advantageous upon increased protein synthesis demand[338]. Moreover, by sustaining mitochondrial biogenesis upon glycolysis inhibition by BRAF targeting, it helps melanoma cells to adapt to a situation of energetic demand. These results highlights the potential therapeutic relevance of targeting this lncRNA as single agents or in combination with BRAF inhibitors, as both strategies showed potent pro-apoptotic effects[231].

All together these results indicate the importance of lncRNAs in regulating metabolic processes, a role that has been demonstrated also outside the cancer context[339]. Further investigations about nucleolar and cytoplasmic lncRNAs will for sure unveil other mechanisms of action linked with energy production and protein synthesis.

FIGURE 3 - LNCRNAS ROLES IN CANCER PROGRESSION

A. lncRNAs have been shown to be involved in all the cancer hallmarks. In bold are indicated genes described in the text. Picture adapted from [251]. **B.** Transcription factors like MYC and p53 promote the transcription of lncRNAs and are themselves regulated by lncRNAs. When the two conditions co-exist, positive and negative feedback loops are established, with eventually cancer sustaining functions.

OUR MODELS OF STUDY: MELANOMA AND CLEAR CELL RENAL CARCINOMA

The description presented so far should have highlighted relevance in cancer, both from a biological and a potential therapeutic point of view. lncRNA investigation can reveal unexpected cellular and molecular mechanisms of action and provide interesting targets for cancer treatment. In our team, we decided to investigate lncRNAs function in two cancer types: melanoma and clear cell renal cell carcinoma (ccRCC), for which the main pathological, clinical and molecular features will be summarized.

MELANOMA PATHOLOGY AND GENETIC ALTERATIONS

Melanoma is a cancer of the skin, accounting for only 1% of all cases in this tissue but for the vast majority of deaths (with a 6.8% estimated lethality in 2020 in the US)[214]. It more frequently arises in non-Hispanic white people and the overall incidence has increased over the past 30 years[214]. New treatments improved patients' outcomes with a 7% reduction of the death rate from 2013 to 2017[214].

Melanoma is highly curable when detected at its early stage and treated by surgical removal of the lesion, the surrounding tissues and sometimes the sentinel lymph node[214]. While five-year survival rate is 99% for local disease, this percentage drops to 65% and 25% for regional (when the tumour spread into surrounding organs or tissues) and distant (when

the tumour spread to remote parts of the body from the primary site) diseases, respectively[214]. This highlights the need for improved clinical management of metastatic patients.

Melanoma lesions arise from melanocytes, the neural crest derived, pigment-producing cells that during development colonize different parts of the body: skin, eyes and to a lower extent other organs[340]. 4-5% of primary melanomas are non-cutaneous (ocular; mucosal; oral; rectal; vulvar; vaginal; nasal), but they will not be described in detail[341].

In the human epidermis there are around 1500 melanocytes/mm^2 and they represent a minor population that divides less than twice per year[342]. Their function is to produce the melanin pigment and provide it to neighbouring keratinocytes, which transport it to the nucleus to protect the genome from UV-radiation induced DNA damage[343]. The stimulus for melanin production comes from the keratinocytes themselves: upon UV-induced DNA damage and in a p-53 dependent manner, they produce and secrete the alpha-melanocyte stimulating hormone (alphaMSH), which binds to the melanocortin 1 receptor (MC1R) on melanocytes and stimulates melanin production, which is finally secreted via the melanosomes[344].

Cutaneous melanoma neoplasms can be classified based on their anatomic site and the relative degree of sun exposure, with subtypes characterized by different age onset and tumourigenic processes. In Caucasians, the majority of lesions arise on hair follicles bearing skin exposed to UV radiation (chronically sun damaged/CSD): these melanomas typically originate in the elderly (more than 55 years) on the head, neck and dorsal surfaces of distal extremities[341]. They are characterized by high mutational load and associate with NF1, NRAS, BRAF(nonV600E) or KIT mutations[345]. Precursor benign lesions are typically not found.

Non-CSD melanomas typically involve intermittently sun-exposed regions, such as the trunk and proximal extremities. They manifest in younger individuals (less than 55 years old)

and are commonly associated with lower mutation burden and predominance of the BRAFV600E mutation[346]. They are more frequently detected with a nevus remnant[347]: nevi are benign proliferations of melanocytes that normally arise in the first two decades of life. Although they have a low likelihood to progress to melanomas, they contribute to a considerable proportion of cases due to their high prevalence[346]. For this reason, together with reduction of intense UV radiation exposure, it is recommended to perform periodic skin examination to evaluate emergence of new lesions or changes in the appearance of older ones[214]. Evaluation of warning signs according to the ABCDE rule (Asymmetry, Border irregularity, Color not uniform, Diameter larger than 6mm) can help to distinguish benign nevi from dysplastic ones or melanomas in situ[348].

The increase in melanocytes proliferation that gives rise to nevi is thought to initiate from a mutation in the BRAF gene that changes Valine 600 to Glutamate (V600E)[349 350]. Due to BRAF oncogene induced senescence[351,352], cells will undergo only a limited number of divisions and normally nevi do not change in size for many years, finally involuting and disappearing around 50 years of age[353].

It is debated if intermediate lesions (also called dysplastic nevi), characterized by overlapping benign and malignant features, represent an evolution of nevi towards malignancy[354]. This hypothesis is in contrast with the finding that dysplastic nevi present also NRAS mutations, which are infrequent in common nevi[349 350]. Some families with germline variants in CDKN2A, CDK4, TERT or POT1, are characterized by multiple dysplastic nevi, which probably arise de novo once melanocytes acquire an activating mutation[346]. Despite their occasional positivity for proliferation markers, the risk of progression to melanoma is very low[355].

Melanoma in situ (MIS) is an early form of primary melanoma in which the malignant cells are still confined to the epidermis. It can present with a pagetoid (normally associated with BRAFV600E and non-CSD lesions) or lentiginous (CSD lesions) pattern. In the former case, it arises from precursor lesions or de novo; in the latter typically de novo[356]. Emergence of MIS is associated with TERT mutations (single nucleotide polymorphisms at his promoter or amplifications) that increase its expression and allow to overcome the replicative senescence barrier[350]. Due to this temporal evolution, these alterations are defined as secondary to the primary MAPK ones.

Transformed cells may remain confined to the epidermis for years before eventually invade the dermis or the submucosa, suggesting the requirement for additional alterations: cells may need to overcome the microenvironment dependency or escape from immune surveillance[346]. A frequent mutation of invasive lesions is bi-allelic loss of CDKN2A; other alterations involve cell cycle genes (CDK4, CCND1, RB1, PPP6C) and members of SWI/SNF chromatin remodelling complex (ARID2, ARID1A, SMARCA4, PBRM1)[349,350]. Although most invasive melanomas evolve from an in situ lesion, the nodular type appears suddenly without any apparent precursor: it is probably caused by a rapid succession of mutations or from a melanocyte harbouring secondary and tertiary lesions that acquired a proliferation inducing mutation[357]. Compared to precursor lesions, invasive ones show no increase of point mutations but have higher number of copy number alterations[349]. Other late alterations involve p53[358], PTEN[359] and PIK3CA[350].

Melanoma invasiveness defines disease staging: at stage I or II, melanoma cells disseminate via vascular and lymphatic routes without developing macroscopic lesions in distant sites; stage III is declared when metastatic deposits are detected in regional lymph nodes; at stage IV they are found in distant organs (such as lung and brain)[346].

THE MAPK PATHWAY AND THE DEVELOPMENT OF TARGET THERAPY

The study of melanocytic lesions progression has highlighted over the years the central role of the MAPK pathway. Through sequential activation of kinase modules, this pathway translates mitogenic information of growth factors into gene expression changes that promote proliferation, survival, differentiation and migration depending on the cellular context[360]. Mitogens binding to their receptor triggers an activation cascade started by a small g-protein (Ras) and then sequentially propagated by MAPKKK (Raf, Tpl2), MAPKK (MEK1 and 2) and MAPK kinases (ERK1 and 2)[361].

The Ras-Raf node represents a very sensitive point of regulation and indeed these proteins are mutated with high frequency in several cancers[362]. Activating KRAS and NRAS mutations invariably occur on codons 12, 13 or 61 and prevent GTP hydrolysis, thus reducing detachment with the target Raf and resulting in its continuous activation in the absence of upstream stimuli[363]. The importance of RAS in different tumours pushed the development of therapeutic inhibitors (Farnesyl Transferase Inhibitors/FTIs) which however gave disappointing results in the clinic[364].

Ras binds to the N-terminal regulatory domain of RAF (Ras-binding domain/RBD) and promotes its recruitment and activation at the plasma membrane[365]. Three isoforms exist (A/B/C-Raf) with BRAF being more frequently mutated in cancer and associated with oncogenesis: the reason behind seems a lower threshold of activation sufficient to stimulate its serine/threonine kinase activity[366]. Over the 45 BRAF identified mutations, V600E accounts for around 90% of cases: this amino acid change abrogates the interaction between the glycine-rich loop and the activation segment that suppresses the kinase activity[367].

Activated BRAF interacts via the C-terminus with MEK1 and 2 and phosphorylates their serine 217 and 221, respectively; these dual-specificity kinases then phosphorylate ERK1 and

2 on threonine 202 and tyrosine 204[365]. While the proximal MAPK pathway components are restricted in phosphorylation targets, ERK1/2 activation results in a wide variety of effects: the majority of direct targets reside in the cytoplasm (such as cytoskeletal and adherent junctions components involved in cell detachment and motility), while indirect effects rely mostly on nuclear activation of transcription factors, such as c-Fos, c-Myc and c-Jun[368,369]. Numerous studies highlighted the role of the ERK/MAPK pathway in melanoma cells proliferation, survival, invasion, tumour hypoxia and angiogenesis[370].

Analysis of patients' mutations in MAPK pathway components indicates alterations of BRAF in 56% of non-CSD and 50% of CSD cases and of NRAS in 15% and 30%, respectively[369]. MEK1 mutations occur in 6% of cases overall, often associated with BRAF or NRAS mutations. ERK mutations are infrequent (ERK1 1%, ERK2 never detected)[369]. The mutational estimations gathered from separate studies are in line with the TCGA whole exome sequencing (WES) results on 318 melanoma patients (58 primary, 262 metastatic), among which 52% harboured BRAF activating mutations (mostly on V600-87%), 28% NRAS activating mutations (mostly on Q61-88%) and 14% NF1 loss of function (a small GTPase known to downregulate RAS activity) [371]. 14% of patients lacked any of these 3 kinds of alterations and were defined as triple wild-type: these samples had significantly more copy-number segments enriched for amplifications of known oncogenes (KIT, PDGFRA, KDR, CDK4, CCND1). Integrating mutation, copy-number and methylation data, it emerged that the RAS-MAPK-AKT pathway, cell cycle genes and p53 were altered in 91%, 69% and 19% of cases, respectively[371].

The development of therapeutic agents targeting MAPK pathway components in melanoma initially focused on RAF (Sorafenib)[372] and MEK (Selumetinib[373] and PD0325901[374]), but gave low response rates. Subsequent BRAF inhibitors and new MEK inhibitors provided more sustainable effects and improved clinical results[375].

Type I BRAF inhibitors (Vemurafenib, Dabrafenib, Encorafenib) occupy the ATP binding pocket and stabilize the kinase in its active conformation; type II inhibitors (Sorafenib, LY3009120, Lifirafenib) stabilize the kinase in its inactive conformation[376]. Vemurafenib interacts with BRAF V600E/D/R mutants and it has been approved for treatment of BRAF-mutant metastatic melanoma by FDA in 2011 based on the results of the BRIM-3 trial[377]. Despite more than 50% response rate and the improved overall survival compared with Dacarbazine (13.2 vs 9.7 months) [377], only 5% of patients experience complete response and the of them progresses within 5-7 months[375]. Dabrafenib inhibits BRAF V600E/K/D and was approved in 2013 on the basis of the BREAK-3 trial, with similar clinical results obtained with Vemurafenib[378].

The short term efficacy of these drugs relies on rapid emergence of resistance due to genetic, epigenetic or transcriptomic changes, which in most cases induce reactivation of the MAPK pathway[379]. This observation posed the basis to combine BRAF inhibitor with molecules targeting downstream pathway members, in particular MEK. The second rationale to develop MEK inhibitors was the treatment of non BRAF mutant patients[369].

Trametinib acts as an allosteric MEK1/2 inhibitor and binds close to the ATP binding pocket, thus competing with it[380]. As single agent, Trametinib improved overall survival compared to paclitaxel (METRIC-trial[381]) but its major use is in combination with Dabrafenib: the COMBI-D[382] and COMBI-V[383] trials indicated improved clinical responses and reduced toxicity compared to Dabrafenib and Vemurafenib monotherapies, respectively. This combination treatment has been approved in 2014 and was followed by approval of Vemurafenib+Cobimetinib (a MEK1/2 inhibitor; co-BRIM trial[384]) in 2015 and the Encorafenib +Binimetinib (a non-ATP competitive MEK1/2 inhibitor) co-treatment in 2018 (COLUMBUS trial[385]). Although there does not seem to be a difference in the efficacy of these 3

combinations, Encorafenib+Binimetinib seems to have the best toxicity profile. Binimetinib is also considered the best MEK inhibitor for NRAS mutant melanoma[386].

CURRENT MELANOMA CLINICAL MANAGEMENT

In parallel with target therapies, immunotherapy also provided major improvements in the treatment of metastatic melanoma: the administration of non-specific immunomodulatory cytokines (such as IL2, type I interferons) or molecules blocking signals inhibiting T cell activation (anti-PD1/PDL1/CTLA4 antibodies), aims at enhancing patient's anti-tumour immune response[387]. Treatment with anti-CTLA4 monoclonal antibody (Ipilimumab) proved better overall survival compared to the placebo in the EORTC trial, but associated with some long-lasting adverse reactions (colitis and endocrinopathies)[388]. Adjuvant anti-PD1 (Nivolumab) showed significant benefit for stage III and IV melanoma compared with Ipilimumab and fewer adverse events[389]. Combination of nivolumab plus ipilimumab also showed very promising clinical activity, though with increased toxicity[390]. Ongoing trials are also evaluating the benefit of combining target- and immunotherapy[391].

Current clinical management of stage I/II melanoma patients envisages wide local excision (WLE) of primary tumours with safety margins without adjuvant treatment. Decision making for stage III/IV patients after resection depend on mutation status and safety of treatments: for wild type melanoma immunotherapy is the only choice and the first line for NRAS mutant patients (MEK inhibition second-line); for BRAF mutant patients, if immunotherapy is not safe, target therapy is preferred as first line and the treatments can be subsequently inverted in second line. Despite the progresses in treatment of stage IV disease, the majority of patients has poor prognosis and inclusion in clinical trials remains the priority for most of them[392].

MELANOMA HETEROGENEITY AT THE ROOT OF THERAPY RESISTANCE

Compared to other human cancer, melanoma is characterized by the highest mutation rate (16.8 mutations/Mb)[371], which is a valuable source of intra- and inter-tumoural heterogeneity. This represents a critical problem for clinical management and may explain the high degree of primary[360] and secondary[393] resistance events to targeted therapy appreciated in patients.

It has been suggested that increased levels of MAP3K8/COT[394], CCND1 amplifications[395] and loss of NF1[396], PTEN[397], RB1[397], CDKN2A[395] could confer intrinsic resistance to MAPK inhibition. Secondary resistance occurs after an initial therapeutic response and it is characterized by the persistence of a resistant sub-population of cells that causes the relapse[393]: among the alterations there are NRAS or KRAS activating mutations[398,379], increased CRAF levels[399], alternatively spliced BRAF (lacking exons 4-8)[400], MEK1/2[401] and ERK1/2[402] mutations, stimulation of PDGFR[403], IGF1R[404], EGFR[405] downstream signalling, AKT1/3 mutations[406]. The goal of elucidating intrinsic and acquired resistance mechanisms is to improve treatment efficacy and increase the complete response rate. For this reason a lot of effort has been devoted to this task in the last years[398,407,408].

However, genetic heterogeneity alone does not always explain melanoma progression or resistance emergence: for instance, comparative analyses of matched primary and metastatic lesions did not identify mutations restricted to the latter[409] and insensitivity to BRAF inhibition can emerge in the absence of genetic alterations[410]. This suggests that gene expression changes also play a role and for this reason they have been extensively analysed[411–413].

Since initial studies using microarrays, it seemed evident a relationship between melanoma cells phenotype and gene expression: samples could be clustered into distinct

groups based on gene signatures and their proliferative and invasive capacities[414–417]. Mutual exclusive expression of few markers were sufficient to define the two phenotypes: the "proliferative" by MITF and SOX10; the "invasive" by TGFbeta and AXL[415,417].

MITF has been initially identified and characterized as a master regulator of pigmentation in mice and humans[418,419] and then emerged to be important also for melanoma cells proliferation and survival[420]. It is a bHLH-LZ (basic domain helix-loop-helix leucine zipper) transcription factor of the MiT subfamily and its targets are involved in a variety of cellular processes (DNA repair, survival, cell division, pigmentation)[421].

Its inhibition in melanoma cells induces cell cycle arrest[422,423], but intriguingly its overexpression associates with a similar phenotype[424]. This discrepancy was reconciled by the rheostat model, suggesting that melanoma MITF-low/invasive cells undergo cell-division arrest due to increased p27 levels; MITF intermediate levels promote proliferation, while MITF-high cells experience differentiation related G1-arrest and reduced invasiveness[425].

The central role of MITF prompted to evaluate its regulators to identify other factors involved in the proliferative and invasive phenotypes: on one hand, SOX10[426] and PAX3[427] were described as positive promoters of its expression, while BRN2[428] and GLI2[429,430] as negative ones. Accordingly, the former were added among the transcription factors promoting the proliferative phenotype, while the latter the invasive one.

Analysis of the MITF interactome by tandem affinity-MS[431] and genome binding by ChIP sequencing experiments[423], further clarified its partners and recruitment to target genes in melanoma. MITF was found to interact with a PBAF complex containing BRG1 and CHD7 and to recruit it at active genes promoters and enhancers, cooperating with other transcription factors (SOX10, TFAP2A, YY1) at the latter[431]. In line with this, BRG1 was also shown to impact on melanoma cells proliferation, similarly to MITF and SOX10[432]. The

relevance of these three proteins in regulating melanoma proliferation and survival has been confirmed by RNA sequencing analyses of melanoma cells knocked down for them[423,431]. RNA sequencing studies on melanoma short term cultures also extended the initial microarray studies regarding proliferative and invasive gene signatures: they validated previous results of MITF-SOX10 proliferative targets (68-99% of overlap) and the invasive ones (65-69% of overlap), further suggesting a role of AP-1 and TEAD factors in governing the latter[433].

The existence of these two melanoma states suggested that tumour progression and metastasis formation would derive from a sequential transitions between the proliferative and invasive phenotypes, in a process resembling epithelial to mesenchymal transition (EMT)[434]. Since melanocytes have no epithelial origin, it was inappropriate to associate EMT with melanoma and so the phenotype switching term was adopted[434]. Although the transition from the invasive to the proliferative state has been rarely documented[435], several stress conditions were shown to dedifferentiate melanoma cells and downregulate MITF expression (hypoxia, low glucose and amino acid starvation, inflammatory signalling)[412].

Interestingly, this de-differentiation has been associated with the emergence of resistance to target-[410,436,437] and immunotherapy[438]. In addition, melanoma MITF low/AXL high cells were shown to be intrinsically resistant to MAPK inhibition[439] and this prompted to combine BRAF/MEK inhibitors with the anti-AXL monoclonal antibody (AXL-107-MMAE): this approach evidenced a synergistic effect of the drugs, suggesting the possibility of targeting distinct melanoma populations in vivo[440]. An alternative proposed approach was to push invasive melanoma cells towards a more differentiated and proliferative phenotype via methotrexate (MTX)-dependent MITF induction, making the cells sensitive to the tyrosinase-processed antifolate prodrug 3-O-(3,4,5-trimethoxybenzoyl)-(-)-epicatechin (TMECG; a DHFR inhibitor)[441].

Despite the contribution of the rheostat-phenotype switching model to the understanding of melanoma molecular complexity, in the last years new findings evidenced the need to expand its conclusions. The main driver was the appreciation that melanoma cells could display both invasive and proliferative markers at the same time on cell lines[442] and in vivo[443].

Transcriptomic analyses of a panel of 53 melanoma cell lines succeeded in defining 4 different subpopulations: two MITF-low ones (distinguished by expression of SOX9 in cluster 1 and SOX10 in cluster 2), the melanocytic/differentiated MITF-high cluster 4, and the intermediate state between them, defined as cluster 3 (these cells express MITF but also neural crest like markers)[410]. The existence of intermediate phenotypes was confirmed by additional scRNAseq data on a different cohort of short term cultures and allowed a comprehensive characterisation of the gene-regulatory networks underlying each state[444].

The evidence of intermediate states relies not only on transcriptomic studies: for instance, cells grown in spheroids were shown to display proliferative and invasive properties at the same time[445]. Glutamine limitation normally induces an invasive phenotype via phosphorylation of eIF2alpha: this mechanism aims to limit translation, increase motility to search for nutrients and arrest cell division; induction of eIF2alpha phosphorylation (by inhibition of its phosphatase) in nutrient-rich conditions (defined as pseudostarvation) is able to increase invasiveness without proliferation reduction[446].

The characterisation of melanoma states did not involve only cell lines as emerged from scRNAseq studies on PDX (patient derived xenotransplants)[411]. These latest findings allowed a general consensus to be reached about melanoma states and the MITF rheostat model has been updated[411]. Proliferative cells with intermediate MITF levels express lineage identity genes and they can be defined as “melanocytic”; under stress situations or drug

treatment they may change their phenotype lowering the expression of metabolic genes and acquiring a "starved" MITF-intermediate phenotype (marked by CD36 expression); progressive de-differentiation would lead to reduction of MITF towards the "neural crest-like state" (characterized by SOX10 expression and neural markers such as NGFR and AQP1) and/or to a final "undifferentiated" state, in which lineage markers and SOX10 are lost. On the opposite side, MITF-intermediate cells may acquire a "hyper-differentiated" phenotype ($MITF_{high}$, $SOX10_{low}$) with increased pigmentation genes expression and reduced proliferation[412]. In this perspective, the terms invasive and proliferative become obsolete, as multiple state can present invasive (undifferentiated, neural-crest, starved) and proliferative (starved, melanocytic) behaviours.

It must be highlighted though that in the PDX analysed, these states did not contribute equally to tumours composition and some cells did not fit any category: at the beginning of the experiment (t0) cells were found to be principally melanocytic (60%) or in an uncharacterized cycling state (20%); upon MAPK inhibition (t1-2) most of them underwent a switch towards the starved phenotype (60%), while a minority downregulated MITF acquiring the neural-crest (15%) and undifferentiated (3%) phenotypes; upon relapse (t4), the majority of cells displayed again an MITF-intermediate/high phenotype[411]. In addition, another population characterized by expression of innate immunity genes has been proposed, but its contribution has not been investigated in detail.

These findings raise the question if the MITF low states significantly contribute to minimal residual disease and relapse or the switch towards the starved phenotype is sufficient to explain resistance emergence. Of course, the results of this PDX study do not allow a general conclusion to be reached, but it remains to be clarified how the cells transition from a state to another and if they really constitute distinct entities.

Undifferentiated and hyper-differentiated cells may represent unstable outliers that would ultimately revert to the bulk MITF-intermediate population cell state[447] and melanoma cells may actually be characterized by a "fluid" state shaped by environmental cues (stromal cells interactions, oxygen and nutrient availability) or external factors (drug treatments). Following a TOFT perspective[242], the default cellular state would be to both proliferate and migrate and stochastically other phenotypes may be selected to sustain the cellular fitness when the situation mutates. Further in-vivo experiments of lineage tracing and fate-mapping, coupled with functional characterisation of the different populations at steady state and upon therapy will improve our knowledge regarding melanoma phenotypes and their dynamic changes.

Still, this model represents a useful means to evaluate if uncharacterized genes are expressed in a restricted or broad manner among cells characterized by different transcriptional programs. Identification of therapeutic targets expressed in a pan-melanoma manner may be very useful to hit the spectrum of melanoma cells in the broadest way and maybe reduce the risk of minimal residual disease. For instance, the lncRNA SAMMSON has been shown to be expressed by all melanoma cell lines irrespective of mutational status or MITF/SOX10 expression and to be relevant for their survival[231]. Identifying similar genes and eventually co-target them could be an alternative to combinations of drugs towards each of the different melanoma states (such as AXL-107-MMAE and TMECG) [412].

FIGURE 4 - MELANOMA PROGRESSION AND INTRATUMOURAL HETEROGENEITY

A. Melanoma lesions can arise de novo or evolving from pre-neoplastic ones, with different ontogeny trajectories depending on chronic sun damage (CSD). Dotted lines indicate more infrequent evolutionary events. Histological pictures were taken from [346]. **B.** Patients lesions are characterized by intratumoural heterogeneity both at the genetic and epigenetic levels. Microarray and RNA sequencing experiments underlined the existence of different states, which can be broadly distinguished on the basis of MITF and SOX10 expression levels. Each phenotype is characterized by transcriptomic and phenotypical features and transitions between them can be induced by environmental cues (such as starvation) or drug exposure (such as MAPK inhibitors).

ADAPTIVE RESPONSE TO MAPK PATHWAY INHIBITION

The study of melanoma states over the course of MAPK inhibition highlighted the existence of non-genetic adaptive mechanisms[412]. Similarly to other stresses (hypoxia, nutrient starvation) drug exposure induces an innate response that allows to adapt and resist (also known as induced drug-tolerant state)[448]. The relevance of gene expression changes during this process is underlined by the co-operative effects of MAPK inhibition together with the one of transcription (in particular at super-enhancer regulated genes) mediated by CDK7[449] or BET inhibitors[450].

Upon MAPK inhibition, sensitive cells undergo a progressive series of transcriptional changes derived by reduced activity of ERK1/2 on his pleiotropic direct and indirect targets. A central node is represented by the network of transcription factors regulating MITF, which is balanced to grant sufficient “proliferative” levels but not excessive to induce differentiation

and G1 arrest[421]. The MAPK pathway exerts both a negative regulation on MITF (by repressing its activators SOX10[426] and PAX3[427]) and a positive one by sustaining BRN2[451]: ERK phosphorylates SOX10 on threonine 240 and 244, preventing the activating sumoylation at lysine 55; BRAF and MEK stimulate expression of the SKI transcriptional co-repressor, which acts on PAX3[452,453]; mutated BRAF sustains BRN2, which promotes PAX3[454] and MITF expression[451]. BRN2 is further stimulated by WNT/beta-catenin signaling[428], which can also directly promote MITF transcription[455] and inhibit GSK3 (responsible for MITF nuclear export mediated by phosphorylation of serines 73 and 69[456]). FGF2 mediated STAT3 activation has also been shown to promote PAX3 expression[457].

Increased expression and activity of MITF promotes pro-survival genes (such as BCL2A1[458]), melanocytic ones (indeed some cell lines experience a transient increase of pigmentation[410,437,459]) and importantly PGC1alpha, which transcribes genes involved in mitochondria biogenesis[460]. This latter step is fundamental to balance the metabolic stress and reduction of ATP production induced by MAPK inhibition, because ERK1/2 normally sustains the pro-glycolytic MYC and HIF-1alpha activities[319,461]. ERK1/2 also normally reduces mitochondrial respiration by phosphorylating DRP1 on serine 616, promoting its activity and mitochondrial fission[462]: upon MAPK inhibition, DRP1 is less phosphorylated and mitochondria get more elongated, increasing the rate of oxidative phosphorylation. The combined effect of increased activity of PGC1alpha and mitochondria remodelling is fundamental to preserving ATP production upon glycolysis inhibition[463].

SOX10 de-repression has also the effect of increasing the levels of the FOXD3 transcription factor[464], responsible for increased expression of ERBB3 on the surface and activation of its downstream signalling by NRG1 towards AKT[465]. Other receptor tyrosine kinases (RTKs) are important to activate pro-survival signalling and get upregulated thanks to

RUNX2[466] and JUN[467]: the resulting increase of EGFR, IGF1R, PDGFR, AXL and other receptors promotes downstream activation of PI3K-AKT-mTOR, JNK, PKC[466,467]. EGFR and AKT (together with E2F targets and MYC) are also induced by YAP/TAZ, which translocate to the nucleus following actin remodelling induced by BRAF inhibition[468]. Activation of PI3K-AKT-mTOR is essential to sustain protein synthesis by phosphorylating the eIF4F complex[469] and promoting the expression of the enzymes responsible for wobble uridine 34 of tRNAs, which increases translation of HIF1alpha and the related pro-glycolytic effects[470]. Indeed, resistant cells are characterized by persistent formation of the eIF4F complex and increased expression of the U34 enzymes[469,470].

Overall these findings suggest that the adaptive response to MAPK inhibition is very articulated at multiple levels (transcriptional and not). The earliest events (between 1-3 days of treatment) are direct consequences of ERK inhibition and involve the release of the inhibitory effects on SOX10[464] and PAX3[452], the increased expression and nuclear retention of MITF[452,454] and the reduced recruitment of DRP1 to mitochondria[462]. MITF induction increases PGC1alpha and mitochondrial biogenesis[460]: this quick response allows the cells to avoid a metabolic crisis associated with glycolysis inhibition[461] and the induction of apoptosis[463]. Subsequently (in a variable number of days) more indirect effects take place, such as FOXD3, RUNX2 and JUN dependent remodelling of surface RTKs[465–467], which stimulate pro-survival signalling[437]. In particular, PI3K-AKT-mTOR is responsible to sustain protein translation[469] and recovery of HIF1alpha expression[470], and re-establish glycolysis.

Cells that succeed in activating this stress response and tolerate initial MAPK inhibition, upon continuous drug treatment will progressively change their phenotype due to the establishment of feedback loops (unless they acquire secondary resistance via a genetic alteration[410]). The result can be de-differentiation[410], increased expression of AXL[439], GLI2[471]

and JUN[472], restored glycolysis, activated JNK signaling[437], increased invasive capacity and SREBP1 activity (which stimulates lipogenesis and protects from oxidative stress[473]).

This phenotype change resembles the one induced by glucose or amino acids depletion, which via ATF4 promote MITF downregulation, reduced proliferation and increased invasinveness[446]. However, since resistant cells should not suffer from lack of nutrients, they can continue to proliferate, in a state of pseudostarvation (similar to the effect of Salubrinal treatment[446]).

Strategies to counteract resistance emergence and increase efficacy of MAPK inhibition can focus on components of the early stress response: in line with this idea, their targeting showed synergistic effects with BRAF and MAPK inhibitors. Examples are Nelfinavir[452] or the STAT3 inhibitor WP1066[457] (which suppress PAX3 induction), Lapatinib (which inhibits ERBB3 activation[465]), Gamitrinib (which inhibits HSP90 and mitochondrial savage biogenesis[474]) or JNKIn8 (which inhibits JNK signaling[472]). Failure of this approach would then need drugs able to sensitize resistant cells to apoptosis by targeting their acquired vulnerabilities (such as the dependence on PI3K-AKT-mTOR signalling[467] or GLI2[471]) or their markers (such as AXL[440]).

FIGURE 5 - ERK RELATED TRANSCRIPTION FACTORS NETWORK AND CHANGES UPON MAPK INHBITION

ERK1/2 have a pleiotropic range of targets, which promote melanoma cells proliferation and survival. Upon MAPK inhibition by BRAFi or MEKi, melanoma cells undergo an adaptive response to avoid apoptosis, which initially involves the release of mitochondrial fission stimulation by DRP1 and the increased activity of PGC1alpha. This stimulates oxidative phosphorylation (oxphos) and saves from energetic deficiency induced by glycolysis reduction. Later events promote the increased expression of receptor tyrosine kinases (RTKs) and the activation of proliferative and survival signalling factors. Biological process or transcription factors inhibited or stimulated upon MAPK inhibition are coloured in blue/green, respectively.

ccRCC: PATHOLOGY, TREATMENT AND GENOMIC FEATURES

The majority of kidney cancers are renal cell carcinomas (RCC), while renal pelvis and Wilms tumours together represent 6% of all cases[214]. RCC can present in a heterogenous manner, with different subtypes characterized by a combination of histopathological and genetic features. The three main ones are clear-cell RCC (ccRCC, around 75% of cases), papillary RCC (pRCC, around 15% of cases) and chromophobe RCC (chRCC, around 5% of cases); other minor subtypes (with each less than 1% of incidence) include MiT family translocation RCCs/tRCCs, collecting ducts RCC, medullary RCC, clear cell papillary RCC, acquired cystic disease-associated RCC, tubulocystic RCC, mucinous tubular and spindle RCC, succinate dehydrogenase-deficient RCC, hereditary leiomyomatosis, RCC-associated RCC and oncocytoma; tumours not fitting any of these subtypes are defined unclassified RCCs (uRCCs)[475].

Around 70 000 people are diagnosed each year with RCC and 15 000 will eventually die[214] in the US. The incidence has increased after the 1970s, but mostly due to the diffusion of non-invasive radiological techniques: indeed, nowadays the majority of cases are detected by incidental findings rather than paraneoplastic syndromes. In the 2007-2016 period the raise of incidence has been quite stable (only +0.5% for men)[214]. Two third of cases are diagnosed with a localized disease and have a 5-year relative survival rate of 75%, which however drops to 70 and 12% for regional and distant metastatic disease, respectively[214]. The median age of patients is 64 years in the US[214] and younger subjects (less that 46 years) frequently harbour an hereditary kidney cancer syndrome (3-5% of all RCCs) with mutations in one of 11 involved genes (BAP1, FLCN, FH, MET, PTEN, SDHB, SDHC, SDHD, TSC1, TSC2 and VHL)[476].

Non-invasive imaging allows definition of tumour size, the extent of invasion outside the kidney, regional lymph node involvement and the presence of distant metastasis. This information is the basis for disease staging: at stage I/II the tumour is wholly localized in the kidney; at stage III it extends into major veins or adrenal glands within Gerota's fascia or regional lymph nodes; at stage IV tumour invasion goes beyond the Gerota's fascia, eventually to distant organs[475]. ccRCC can spread via lymphatic or blood vessels and colonize lung, bone, liver, brain, pancreas, adrenal gland, parathyroid and thyroid glands, muscle, skin and soft tissue[477], with liver metastases associated with poorer prognosis[478]. Synchronous metastases are detected before surgery and characterize 30% of patients; metachronous metastases arise between 3 months and as late as 30 years after primary surgery in up to 50% of cases. In both instances, they can be solitary, in limited number and locations (between 3 and 5; defined as oligometastases) or multiple in number and sites[479].

Staging guides treatment decisions. Stage I/II patients suitable for surgery normally undergo partial (tumour removal with preservation of healthy parenchyma) or radical (whole kidney removal) nephrectomy; the former is mandatory in patients with one kidney, while the latter in cases with multiple small renal tumours or that extend into the vasculature[480]. Aged patients or those with comorbidities normally undergo ablative therapy (cryotherapy, radiotherapy) or just active surveillance of tumour growth (computed tomography/CT or magnetic resonance imaging/MRI every three months the first year; every 6 months the second one, and annually thereafter).[480] For stage III patients radical nephrectomy is recommended (if possible) with involved lymph nodes removal; adjuvant therapy with Sunitinib or Sorafenib after surgery did not show disease-free survival benefits[481]. Thus, systemic therapies with target inhibitors or immunotherapy are normally administered only to stage IV patients or stage III with inoperable disease[480]. Solitary and oligometastases can

be treated by surgery or ablative therapy, while widespread diffusion may require a combination of metastases resection and systemic therapy[482].

A renal core biopsy or specimens from the partial or radical nephrectomy allow to perform the histopathological confirmation of the malignancy. Some lesions may present a combination of features from different subtypes, but normally samples can be easily classified[475]. ccRCC cells predominantly have a clear cytoplasm with a solid, trabecular, tubular or cystic growth pattern; pRCC cells are small, with scarce cytoplasm with basophilic (type 1) or eosinophilic (type 2) staining pattern; chRCC cells have a pale or eosinophilic granular cytoplasm due to abundant cytoplasmic vesicles and grow as large solid sheets[483]. However, the presence of clear cells or papillary structures are not exclusive features of ccRCC and pRCC, respectively[484]. In addition, sarcomatoid cells of high-grade malignancy can be found in all RCC types[485].

Each RCC subtype has been characterized at the molecular level, with a key contribution by the TCGA project. It provided DNA, RNA and protein analyses from approximately 400 ccRCC cases (TCGA KIRC)[486], 161 pRCCs (TCGA KIRP)[487] and 66 chRCCs (TCGA KICH)[488] with their corresponding healthy kidney tissues. After the publication of the single studies, a pan RCC cancer analysis has been performed to compare the three subtypes against each other, resulting in a total of 843 cases (additional samples have been added to the original datasets)[489]. This comprehensive study highlighted how RCC should not be treated as a uniform disease and provided a framework for the search of new targets which could be directed across all patients for common alterations or in a subtype specific manner[490].

In ccRCCs, the most frequent alteration (approximately 90% of cases) is VHL loss by genetic (point mutations, insertions, indels, chromosome 3p25 loss) or epigenetic (promoter DNA methylation) mechanisms[486]. In normoxic conditions, VHL mediates HIF1alpha and

HIF2alpha proteasomal degradation via targeting to the E3 ligase complex[322]. Its loss induces aberrant accumulation of HIF proteins, which promote uncontrolled transcription of genes involved in angiogenesis and glycolysis, despite sufficient oxygen levels (pseudohypoxia): accordingly ccRCC tumours are highly vascular and rich in glycogens[491]. Inactivating mutations in other VHL complex components (TCEB1, CUL2) are mutually exclusive with those in VHL[489].

VHL loss alone is not sufficient to develop ccRCC (as evidenced also in mice models[492]) and additional genetic or epigenetic alterations are required, such as inactivating mutations of PBRM1 (29-41% of cases), SETD2 (8-12%), BAP1 (6-10%) or KDM5C (4-7%)[475]. Activating mutations of the PI3K-AKT-mTOR pathway (involving PTEN, mTOR, PIK3CA), loss of CDKN2A and TP53 mutations are also frequent (16.2, 16.2 and 2.6%, respectively)[486]. As PRBM1, SETD2 and BAP1 reside at 3p21 and VHL at 3p25, a single copy loss of 3p causes their haploinsufficiency[486]. 67% and 45% of cases are also characterized by gain of chromosome arm 5q (which contains 60 genes, including the SQSTM1 oncogene) and loss of chromosome 14q (which includes HIF1A), respectively[486]. Other significantly mutated genes have lower mutation rates but belong to the same pathway, such as the Hippo (3.9% of cases) and NRF2/ARE pathways (3.2%), the SWI/SNF complex (47.1%), histone methyltransferases (23.8%), the PI3K/AKT pathway (16.2%), histone demethylases (13%), the BAP1/ASXL1 histone de-ubiquitinase complex (12.1%) and histone acetyltransferases (4.8%)[489]. Nevertheless, only TP53, BAP1, CDKN2A inactivating alterations are associated with poorer survival[489].

Like other cancers, DNA hypermethylation of CpG islands of tumour suppressors characterises also ccRCC: for instance, promoter hypermethylation of VHL constitutes a second hit in combination with 3p loss, leading to loss of heterozigosity[493]. Among TCGA patients, those characterized by increased DNA methylation (37.3% of cases) have higher-stage disease and poorer survival[486]. Interestingly, DNA hypermethylation correlates with

SETD2 mutation[489]: this functional relationship has been reproduced also in vitro by inactivating SETD2[494], suggesting a relationship between H3K36me3 deposition and DNA methylation. Additional non-TCGA studies indicated poorer survival of patients harbouring SFRP1 and DKK1 promoter hypermethylation[495].

These genetic and epigenetic alterations ultimately result in deregulated transcriptomes in ccRCC cells. This level of inter-tumoural heterogeneity has been initially appreciated by microarray studies, which allowed to define two distinct subgroups of patients, with ccA ones having improved survival compared to ccB[496]. ccA tumours were characterized by higher expression of genes involved in hypoxia, angiogenesis, fatty acid metabolism and organic acid metabolism, while ccB for epithelial to mesenchymal transition (EMT), cell cycle and wound healing[496].

Subsequently, RNA sequencing data of the TCGA project allowed for a genome wide unsupervised clustering of ccRCC patients, with 4 different subsets being identified (m1-4) and ccA overlapping with m1 and ccB genes distributed in m2 and m3 (m4 may account for unclassified samples of the previous study)[486]. Pathway analysis for each cluster was not performed, but correlation analysis between patient outcome and protein, RNA and DNA methylation levels, indicated worse survival in patients with reduced AMPK and Krebs cycle activities and upregulation of genes involved in the pentose phosphate pathway, glutamine transport and fatty acid production[486].

These results suggested a metabolic shift in ccRCC cells, which has been further characterized at the transcriptomic[489] and metabolomic[491] levels. Global comparison of RCC TCGA samples, indicated low expression of Krebs cycle and electron transport chain components in ccRCC compared to pRCC and chRCC; ccRCCs displayed higher expression of glycolytic genes and suppressors of the pyruvate dehydrogenase complex[489]. These results are

in line with the metabolic reprogramming induced by HIF1, which promotes expression of HK1, LDHA and PDK1[497].

Metabolomic profiling of 138 ccRCC tumour/normal pairs confirmed some of these findings and extended them. First, it indicated tumour abundance of carbohydrates (such as maltotriose, maltose, fructose-1-phosphate and glucose-6-phosphate/G6P) with consistent increase of glycolysis metabolites (glucose, G6P, fructose-6-phosphate/F6P); increased levels of G6P and F6P correlated with 6-phosphoglucoronate/6PG, an intermediate of the pentose phosphate pathway which boosts nucleotide biosynthesis[491]. Among TCA cycle metabolites, citrate, cis-aconitate and succinate showed increased levels, while fumarate and malate were reduced[491]. Citrate can produce cytosolic acetyl-coA and sustain fatty acid synthesis; reduced levels of fumarate and malate together with increase in succinate suggest a decrease oxidative phosphorylation[491]. Interestingly, high-glutathione and high-dipeptide levels correlated with worse disease stage and risk of recurrence, while the RNA levels of the enzymes involved in their metabolism did not show this relationship: this highlights the importance of integrating proteomic and transcriptomic studies to not miss potential interesting clinical features[491].

In line with the task of integrating data from different platforms, some groups tried to combine genomic and proteomic data. For example, the cluster of clusters analysis (COCA) has been performed using the TCGA data of DNA copy number, DNA methylation, mRNA, miRNA and protein levels of KIRC/KIRP/KICH cases and allowed to separate RCC tumours into 9 subtypes[498]. Of the three ccRCC subtypes, CCe.2 patients had the best survival outcome, CC-e.1 ones were intermediate and CC-e.3 associated with the poorest one. The CC-e.3 signature correlated with the previously described ccB expression pattern (higher expression of cell-cycle and hypoxia related genes and markers of EMT), while m1 and m3 overlapped with CC-e.2 and CC-e.3 respectively, and CC-e.1 with m2 and m4[498].

More recently, the Clinical Proteomics Tumour Analysis Consortium (CPTAC) performed a proteogenomic characterization of 110 treatment naïve ccRCCs and paired normal adjacent tissues[499]. After cryopulverization, each tissue was subject to genomic, transcriptomic and proteomic analyses. Several TCGA findings were confirmed, such as: the profile of somatic mutations; the increased protein levels of genes involved in EMT, hypoxia, glycolysis; the downregulation of TCA cycle and oxphos enzymes; the activation of the MAPK/ERK and AKT-mTOR pathways downstream to EGFR/VEGF[499].

In addition, whole genome sequencing (WGS) of the same tumours, revealed a group of high-grade lesions characterized by genomic instability and extensive copy number variations across all chromosomes. 3p loss was the most frequent event (93%), followed by 5q gain (54%), 14q loss (42%), chromosome 7 gain (34%) and chromosome 9 loss (21%). Translocations were present in 61% of cases, predominantly involving the 3p and 5q. This t(3:5) was mutually exclusive with a novel rearrangement (t(3:2)) and it has been suggested to be an early event in some patients due to chromothripsis[500].

These copy number variations were associated with changes in some signalling pathways: loss of chromosome 3p was linked to the HIF1 mediated metabolic reprogramming; 5q gain to increased mTORC1 and MYC signalling; 7p gain with increased protein translation and EMT; 9p loss (which includes CDKN2A) with increased translation, mTOR and MYC signaling[499].

DEVELOPMENT OF TARGETED THERAPY FOR CCRCC

The hallmark event of ccRCC is the stabilization of HIF1 due to VHL inactivation. As pointed out, this leads to a global cellular reprogramming similar to the adaptive response to hypoxia, even if in the presence of normal oxygen levels. Part of this response involves the

increase in angiogenesis, that is the spreading of new blood-vessels[501]: this physiological process is exploited by tumour cells to increase their oxygen and nutrients supply and it has been recognized as an hallmark of cancer[251].

ccRCC and VHL disease (the familial autosomal dominant syndrome characterized by germline VHL mutations[502]) are characterized by highly vascular tumours and this finding constituted the rationale to target angiogenesis in ccRCC by dampening its signaling[503]. This goal can be achieved by reducing the levels of the VEGF pro-angiogenic factor (using the anti-VEGF antibody Bevacizumab) or interfering with the activation of its receptor tyrosine kinase (VEGFR) using small molecule inhibitors (Axitinib, Pazopanib, Sorafenib, Sunitinib)[321]. The identification of additional proangiogenic factors secreted by stromal components led to the development of agents targeting other RTKs, such as MET (Cabozantinib) and FGFR (Lenvatinib)[504].

The introduction of the anti-angiogenic therapy constituted a new hope for advanced ccRCC patients, since treatment options were limited to cytokines (interferon, IL2), which had a durable response rate of only 7-8% and high toxicity[505]. The TARGET phase III trial indicated increased progression-free survival (PFS) and overall survival (OS) of Sorafenib and led to its approval by FDA in 2005[506]. In 2007, Sunitinib also showed better responses compared to interferon alpha and thus was approved[507].

Pazopanib is a second generation receptor tyrosine kinase inhibitor (RTKi) that was compared to Sunitinib as first-line therapy during the COMPARZ trial, showing similar PFS but slight better overall response rates (ORRs) (31% vs 25%): this led to his approval in 2009[508]. Another second-generation inhibitor (Axitinib) was compared to Sorafenib in the AXIS trial, demonstrating significantly longer PFS as second line treatment[509]; however it showed inferior results as first line option compared to Sunitinib and Pazopanib[510].

The development of RTK inhibitors was accompanied by the introduction of other approaches. Bevacizumab is a human recombinant monoclonal antibody that binds and neutralizes VEGF-A. Its efficacy in combination with interferon-alpha was tested in the AVOREN trial, that indicated longer PFS and ORR in patients receiving the two drugs compared to interferon alone[511]. Another deregulated pathway in ccRCC is the PI3K-AKT-mTOR axis, which thanks to mTOR promotes HIF1 translation together with other pro-tumorigenic effect[512]. The mTORC inhibitor Temsirolimus demonstrated better clinical responses compared to interferon and it was approved in 2007[513]. Everolimus showed clinical efficacy during the RECORD1 trial in patients progressing after Sorafenib or Sunitinib treatment and it was approved as second line option in 2009[514]. Overall, Sunitinib, Pazopanib and Bevacizumab+IFN-alpha are approved as first line options, while Axitinib as second line; mTOR inhibitors can be used as second-line or as first line in patients with poor risk status[475].

These drugs allowed a great improvement of patients outcome, with a median increase of survival of about 30 months compared to cytokine therapy; nevertheless, the majority of patients ultimately undergo relapse[515]. New RTK inhibitors have been introduced in 2016 (Lenvatinib[516], Cabozantinib[517]) after showing improved clinical outcomes compared to mTOR monotherapy inhibition. Immunotherapy using Nivolumab has been tested as second line treatment in patients failing therapy with Sunitinib and Pazopanib and showed an overall survival benefit compared to Everolimus (despite limited response rate of 25%)[518]. The combination of Nivolumab+Ipilimumab has then been tested as first line option taking Sunitinib as a control, and provided better overall survival and response rates[519]. Similarly to melanoma, immunotherapy and target therapy combination is currently under testing, together with the development of new therapeutic approaches[520]. The IMmotion151 trial

showed a better PFS of the combination Atezolizumab (anti-PDL1) plus Bevacizumab versus Sunitinib and longer-term follow-up will establish a survival benefit[521].

A more precise patients stratification would also allow to improve treatment outcome, allowing a more rational choice of systemic drugs as mono- or combination therapy and in which sequence. Several clinical normograms have been developed to select treatment and the two most common are the one of the Memorial Sloan Kettering Cancer Center (MSKCC) and the international Metastatic Renal Cell Carcinoma Database Consortium (IMDC)[522]. Similarly, other models are used to predict risk of recurrence: the UCLA Integrated Scoring System (UISS) and the Leibovich score[523]. They incorporate several clinical and laboratory parameters, but genomic data have not been integrated.

Some attempts have been made to characterize patients' lesions on the basis of gene expression data: ClearCode34 is a 34 genes panel used to classify cases into the low-risk ccA and high-risk ccB groups, which showed superior prognostic power compared to UISS[524]; another 16 genes panel has been associated with recurrence following surgery in stage I-III patients on a cohort of 626 patients[525]; BAP1 and PBRM1 mutations have been associated with high- and low-risk of recurrence, respectively[526]. Despite their attractive prognostic value, these scores are not readily available for clinical use, due to the costs, the expertise needed and some discrepancies between the panels[523].

Recently, gene expression analysis of 823 baseline tumours out of the 915 patients enrolled in the IMmotion151 trial allowed to cluster patients into 7 groups, broadly divided into the "angiogenic" and "proliferative" categories[527]: the former (Clusters 1, 2, 3 and 7) were characterized by higher expression of VEGF related genes, while the latter (Clusters 4, 5, 6) by MYC, E2F targets and genes involved in anabolic processes. While cluster 1 and 2 responded with no difference in PFS to Atezolimumab+Bevacizumab or sunitinib (likely due to the

presence of anti-angiogenic drugs in both arms), cluster 4 and 5 patients responded better to the combination therapy[527]. These results suggest the usefulness of biomarkers development for clinical decisions.

FIGURE 6 - RENAL CARCINOMA SUBTYPES AND MAIN DEREGULATED SIGNALLING PATHWAYS IN CCRCC

A. Renal carcinomas can present with different histological features (pictures taken from [490]). Each subtype is characterized by different survival outcomes[489]. CIMP stands for CpG island methylator phenotype. **B.** ccRCC cells communicate with endothelial ones to promote neo-angiogenesis, which is necessary to sustain the supply of oxygen and nutrients. Thanks to VHL loss and activating mutations in the PI3K-Akt-mTOR pathway, the transcription factor HIF-1 promotes the expression of genes involved in glycolysis and angiogenesis, even in the presence of oxygen in the extracellular space (pseudohypoxia). VEGF and other growth factors activate endothelial and other stromal cells, which then aid tumour growth in a paracrine manner. Given the relevance of this interplay, several inhibitors have been developed, targeting VEGFR and other receptor tyrosine kinases, VEGF or mTOR. The inhibitory effects of TSC1/2 on mTOR and VHL on HIF-1 are frequently lost due to genetic alterations.

ANALYSES OF CCRCC INTRA AND INTERTUMOURAL HETEROGENEITY

Some aspects of ccRCC clinical management still suffer for limited efficacy or lack of predictive tools. Despite around 70% of patients have localized disease and can be cured by local resection alone, 30-35% of patients after surgery can develop metachronous distant metastases even after decades[528]. Parameters such as tumour size, grade[529], the presence of vascular or fat invasion[530] and sarcomatoid differentiation[531], are correlated with risk of relapse but they have a low predictive value. In addition, 20% of patients with multiple metastases undergoing surgery and adjuvant therapy progress as early as 1 month, sometimes even failing to receive systemic drugs due to rapid progression[482]. These issues highlight the

need for biomarkers to identify patients harbouring occult metastases and for therapeutic strategies to overcome resistance.

TCGA and other studies provided a huge improvement in the understanding of the molecular features of ccRCC, but they are biased by their single-biopsy nature: multi-region exome sequencing and copy number analyses of 10 ccRCCs samples (with 79 different areas considered) indicated a more extensive level of heterogeneity than previously thought[532,533]. First, only a small number of alterations were clonal (such as VHL mutation and 3p loss) and additional mutations in driver genes occurred in distinct subclonal regions of the primary tumours[533]. This behaviour is in line with a tree (or trunk-branch) model in which the ubiquitous events form the trunk, while heterogenous mutations arising with spatial and temporal variance constitute the branches[534].

Second, the frequency of known mutations and somatic copy number was higher compared to those obtained from TCGA analyses (for instance 40% vs 21% for BAP1, 40% vs 5% for TP53, which are known markers of poorer survival)[533]. This suggests that single biopsies may be limited in capturing intratumoural heterogeneity and that sequencing coverage may be insufficient to reliably detect subclones that are rare in one area but common in other parts[534]. It has been estimated that at least three regions should be sequenced to detect aberrations in driver genes such as VHL, PBRM1, SETD2 or BAP1 with 90% confidence[535]. However, this prediction may not be valid for less frequent but still therapeutically targetable driver genes (such as MTOR).

To expand these findings, the TRACERx (Tracking Renal Cell Cancer Evolution through therapy) Renal program was launched in July 2012, enrolling 320 patients undergoing nephrectomy. Main objectives were to improve data quality by reducing sampling biases and to identify metastasis seeding clones by comparison with the matched primary tumours.

Indeed large scale simultaneous analyses of matched primary and metastatic tumours are still limited[536].

Initial reports from about 100 primary tumours (for which 38 had metastatic counterparts) indicated that the pattern of intratumoural heterogeneity could influence evolution and progression to metastasis. Rapid progression (occurring at multiple sites within 6 months after surgery) was observed in patients with primary multiple clonal driver mutations or with clonal/subclonal BAP1 mutations; attenuated progression (single site within 6 months) was characterized by clonal PBRM1 mutations with a subsequent subclonal mutation of SETD2 or PI3K pathway genes[500]. Compared to primary lesions, metastatic sites displayed lower clonal variance and fewer driver mutations (with only 5.4% arising de novo), suggesting an evolutionary bottlenecking phenomenon[537]. This finding underpins the role of nephrectomy in reducing the source of diversity and minimizing the risk of future metastasis. A potent driver of metastasis and mortality risk was 9p loss, while 14q loss showed only a trend towards significance: interestingly both CNVs were subclonal, suggesting that they could have been lost by single biopsy approaches[537].

This analysis also allowed the appreciation of distinct modes of metastatic dissemination. In patients with primary tumours with low intratumoural heterogeneity but high chromosomal complexity, metastatic competence was acquired early, leading to rapid invasion of distant sites, relapse and poor response to systemic therapy: these cases must have occult metastases already at the time of diagnosis or surgery and improving their outcome represent a clinical challenge[537]. On the other hand, in patients bearing primary tumours with high intratumoural heterogeneity but lower chromosomal complexity, metastatic competence was acquired as the result of gradual accumulation of mutations,

normally involving PBRM1. These patients initially display solitary or oligometastases, with marked latency to widespread dissemination[537].

Altogether these data provide useful insights for more rationalized clinical decisions relying on molecular profiling: for instance, patients with a high risk pattern could undergo a more aggressive treatment; alternatively, the decision of which systemic therapy to administer could rely on the driver mutations present in multiple metastatic biopsies, and targeting common alterations would induce the most efficacious effect[490]. Nevertheless, routinely performing multi-region analyses to define the patient molecular profile constitute a technical challenge at the moment.

Intratumoural heterogeneity of ccRCC tumours has been interrogated also at the transcriptomic level by scRNAseq[538]. Compared to melanoma[539,540], the investigation of ccRCC is still limited to three tumours being analysed[538]. However, some initial insights have been provided regarding the ontogeny from proximal tubule cells and characterization of stromal and immune cell populations[541]. Further studies may extend the knowledge regarding ccRCC intratumoural heterogeneity, suggesting even non-genetic mechanisms driving metastasis or therapy resistance.

HOW MELANOMA AND CCRCC COULD BENEFIT FROM LNCRNA RESEARCH

Up to date, there are no reports indicating lncRNA genes as mutational drivers of melanoma or ccRCC. Nevertheless, there are several examples of lncRNAs whose expression is deregulated and that exert a tumorigenic function[542,543]. Those with a restricted expression to cancer cells could potentially be exploited for diagnostic or therapeutic purposes.

Alternatively, association with prognostic value, prediction of metastatic dissemination and risk of recurrence, would make them interesting biomarkers.

Therapeutic targeting of lncRNAs falls into the broader objective of targeting RNAs to treat human diseases[544]. Despite the drug discovery process has been traditionally protein-centric, modulating RNAs stability, activity or translation could potentially open a wide array of possibilities and expand the number of druggable targets. Of particular interest would be mRNAs of proteins that are difficult to hit using conventional methods, and non-coding RNAs[545].

The attractiveness is increased by the consideration that targeting by Watson-Crick hybridization is in principle better understood, more predictable and much more specific than binding of a small molecule[546]. Lead compounds can be screened more rapidly using high-content assays and in principle allow for personalized approaches against patient-specific sequences[547]. In this view, it has been striking the case of Milasen manufacturing, a splice-modulating antisense oligonucleotide specifically designed to treat a rare, fatal neurodegenerative disease (neuronal ceroid lipofuscinosis 7/CLN7) identified in a 6 years old girl[548]: in 18 months from the diagnosis, the mutation has been characterized and an ASO against the splice defect screened and validated in vitro; after toxicology studies in rats, the ASO was administered in the patient and prevented potentially lethal seizures[548]. Despite being an exceptional case, Milasen demonstrates the high potential of these drugs.

So far only 10 RNA-targeting drugs have been approved by the FDA, but many other are under preclinical or clinical development, with a trend towards growth[547]. Two classes of RNA therapeutics have been developed (siRNAs and antisense oligonucleotides/ASOs) and the latter will be discussed in detail.

ANTISENSE OLIGONUCLEOTIDE-BASED THERAPY

ASOs are chemically synthesized single strand DNA oligonucleotides of 12-30 bases, designed to bind an RNA and inhibit it by RNAse H1 dependent degradation or steric blocking. The former mechanism relies on the formation of an RNA (target)-DNA (ASO) duplex recognized by RNAseH1, which then degrades the RNA molecule; steric blocking can prevent or enhance translation, compete for other protein binding or modulate splicing[546]. To date, three RNAseH1 dependent (Fomivirsen, Mipomersen, Inotersen) and three splice-switching ASOs (Eteplirsen, Golodirsen, Nusinersen) have been approved by the FDA[547].

ASOs are chemically modified at the backbone and nucleosides level to protect them from nucleases and to pass the plasma membrane without the need of vectorization. Their chemistry influences also the mechanism of action[546]. Over the years, new modifications have been introduced and this led to different generations of ASOs.

In the first one, an atom of Sulphur or a methyl or amine group substituted one of the non-bridging oxygen atoms in the phosphodiester bond, thus generating phosphorothioates (PS), methyl-phosphonates, and phosphoramidates ASOs, respectively[549]. The PS-backbone has been the most diffused and allowed an increase ASOs nucleases resistance (changing the half-life from minutes to days), binding to plasma proteins (such as albumin; thus reducing renal clearance) and scavenger receptors (such as the sabilins STAB1 and 2; thus increasing cellular internalisation).[547].

Second generation ASOs experienced addition of alkyl groups (methyl, methoxyethyl) to the 2' position of the ribose, thus introducing the 2'-OME and 2'-MOE classes, respectively. These modifications reduced toxicity and increased nuclease resistance and target affinity[549].

The last generation of ASOs comprises a large number of modifications. The most common ones are: introduction of a methylene bridge between the 2'-oxygen to the 4'-carbon

of the ribose (locked nucleic acid configuration or LNA); replacement of the ribose with a morpholine moiety and of the phosphodiestere bond by a phosphorodiamidate one (phosphorodiamidate morpholino oligomers or PPMO); replacement of the ribose-phosphate backbone by a polyamide one consisting of repeats of N-(2-aminothyl) glycine units (peptide nucleic acids or PNAs)[549]. LNAs enhance nuclease stability and target affinity[550], while PPMO and PNA reduce the charge of the ASO and increase plasma protein binding[551]. Second and third generation modifications do not allow recruitment of RNAseH1, so to restore the degradative function it is necessary to insert a stretch of unmodified/PS nucleotides between the modified ones: this results in the "gapmer" configuration[552].

Unlike siRNAs, PS-ASOs can be delivered in vitro and in vivo even in the absence of lipids or other types of nanoformulations. The free uptake of "naked" oligonucleotides (also defined as gymnosis[553]) is normally mediated at the plasma membrane by interaction with protein receptors that mediate clathrin-dependent or caveolin-dependent internalization. STAB1 and 2 and other proteins have been shown to interact with ASOs, while other receptors can recognize bioconjugates added to them[554]. Among these there are lipids (such as cholesterol, which may facilitate lipoproteins interaction), peptides, antibodies, aptamers and sugars. The last group includes an example of success, N-acetylgalactosamine (GalNAc): it was shown to bind to the asialoglyco-protein receptor 1 (ASGR1 or ASPGR) which is highly expressed by hepatocytes and promotes endocytic uptake; in the endosome the acidic pH reduces GalNAc-ASGR1 interaction and the subsequent GalNac enzymatic degradation frees the ASO[555]. This conjugation offers a liver-specific and efficient means of targeting, which increased ASOs potency by 7-fold in the mouse and around 30-fold in humans, allowing a reduction in dose administered from 200-300 mg to 4-5mg per week. This makes a substantial improvement in terms of costs and potential toxicity[556].

Interestingly, it has been shown that the physiological state of the cells can influence PS-ASOs internalization: for instance, rapidly growing cells (such as malignant, keratinocytes or B/T-cells stimulated with mitogens) have increased rates of uptake[554]. A lot of effort is dedicated to clarify ASOs productive internalization pathways in order to exploit them.

Once internalized, ASOs need to escape from the endosomes or liposomes to reach their targets. Although the mechanism behind this is not well clarified, the ANXA2[557] and TCP1beta[558] proteins have been proposed to facilitate ASOs trafficking from early to late endosomes and their subsequent release. After that, PS-ASOs normally accumulate in cytoplasmic or nuclear foci and interact with proteins that influence their localization or function, depending on the 2' substitutes, the number of PS residues and their sequence[554].

Transfection-mediated ASO delivery promotes initially accumulation in P-bodies (between 30 and 60 minutes) and then in PS-bodies (thanks to the activity of TCP1beta[558]) which enrich in the nucleus and can then shuttle back to the cytosol (possibly in a RAN dependent manner[559]). The increase in nuclear signal requires 1-2.5 hours and relies also on ASOs retention in paraspeckles (due to interaction with NONO, PSF and PSPC1[560]); on the other hand, nucleoli are normally devoid[561]. PS bodies re-form after mitosis, distribute in daughter cells and buffer the amount of ASOs available in the nucleoplasm[561]. Overall, the ASO intracellular ASO distribution after transfection is very efficient and can lead to 80% target RNA reduction already in 3 hours[560].

Since free uptake relies on endosomal trafficking, ASOs remain mostly cytoplasmic (even if inhibition of nuclear RNAs has been reported) and target inhibition requires more time (80% reduction in 14 hours)[558].

ASO-protein interactions are critical because they do not only influence ASOs intracellular distribution, but also the activity: for instance, paraspeckles proteins compete

with RNAseH1 for RNA-DNA duplexes binding and hamper the degradation process[557]. A proteomic evaluation of ASOs interactors has been performed by pulldown of biotinylated gapmers with the same sequence but different 2' modifications: interestingly, the eluted proteins generally differed, with the more hydrophobic 2' sites (2'-fluoro or constrained 2'-O-ethyl) characterized by a more promiscuous profile; on the other extreme, 2'MOE tended to bind to less proteins and with reduced avidity[557]. A modified NanoBRET assay further allowed the quantification of dissociation constants between proteins and ASOs and indicated up to 1000-fold differences based on 2' modification (with similar sequence) or sequence (with same chemistry)[562].

These data highlight the importance for sequence and chemical modifications for ASOs delivery, uptake, interaction with proteins and activity. A better understanding of the intracellular mechanisms will allow a more rationalized design according to the desired effect and the localization of the RNA target, improving efficiency and specificity.

A comprehensive knowledge on how ASOs can interact with proteins in a sequence and chemistry dependent manner, could also provide predictive models for on- and off-target effects, very useful for lead development. Current strategies mostly rely on sequence based bioinformatic analyses that estimate sensitivity and specificity, but have limited power. The result is that broad screenings of thousands or hundreds of ASO need to be performed, followed by subsequent phases of optimization (focusing on hotspot regions that show significant effect on the target). In vitro results need then to be translated in vivo, which could pose a problem if the ASO (despite its efficiency) is poorly distributed or internalized. Improvement of pharmacokinetic and dynamic requires a second phase of development with testing alternative chemistries or gapmer configurations[563]. The possibility to better predict

the life cycle of candidate ASOs would allow an easier and less expensive development process.

At body level, effective delivery of ASOs still represents a challenge. Once systemically injected, they need to resist nuclease degradation, avoid clearance in the kidney or by the reticuloendothelial system, evade non-productive binding by plasma proteins and cross the capillary endothelium to reach the target tissue[547]. Since distribution depends on blood flow, high perfused organs are those that mostly accumulate ASOs (liver, kidney, fat, bone marrow, spleen)[564]. Liver is further facilitated by the discontinuous nature of the sinusoidal epithelium and the high presence of scavenger receptors on hepatocytes[547].

To date, the majority of ASOs are thus administered locally (eye, spinal cord) or to the liver. The eye has been the target of the first commercialized ASO in 1998: Fomivirsen was developed to degrade the immediate early-2 mRNA of the CMV virus, which causes retinitis in immunodeficient patients. Despite therapy efficacy, it was withdrawn in 2000s due to localized adverse events[565].

Intrathecal injection for treatment of central nervous system (CNS) diseases is mandatory because ASOs cannot pass the blood-brain barrier, but it demonstrated a safe profile and favourable distribution: avoiding renal clearance, ASO concentration can remain sustained for long, allowing over weeks periods between injections[566]. In addition to Milasen, another ASO (Nusinersen) successfully improved the treatment of a CNS disease, the spinal muscular atrophy (SMA) [567]. It is an autosomal recessive pathology characterized by loss of motor neurons: in type 1, the progression is so severe that induces infant death (and it is the most common genetic cause of it); type 2 patients survive but become paralyzed over the years[568]. The defect resides in the SMN1 protein loss due to inactivating mutations; despite the SMN2 paralog could rescue the defect, its transcript is normally spliced in a way that could

only produce a truncated protein, because of the exclusion of exon 7. Nusinersen acts as a steric blocker and binds the intronic splicing silencer sequence N1 (ISS-N1), promoting exon 7 inclusion and SMN2 protein stabilisation[569]. Clinically, it increased the survival of SMA1 patients and improved the motor capacities also of SMA2 ones: the results have been so remarkable to early terminate the phase 3 studies[567].

There are also examples of ASOs developed for oncologic treatment but the systemic extrahepatic administration still constitutes a big challenge. For this reason and efficacy failures, none of these compounds obtained market authorization. Still, several ASOs are currently undergoing clinical trials[547]. Danvatirsen (or AZD9150, IONOS-STAT3-2.5) is an RNAseH1 dependent ASO targeting STAT3, a transcription factor with oncogenic function in many tumours[570]. It demonstrated preclinically efficacy in lymphoma and lung cancer models[571]; during the phase 1 clinical trial on diffuse large B-cell lymphoma (DLBCL), it proved to be well tolerated and efficacious in a subset of patients[572]. Apatorsen (OGX-427) promotes degradation of the chaperone Hsp27, which is very highly expressed in some cancers and associated with poor prognosis[573]. Preliminary results of a phase II clinical trial on metastatic urothelial carcinoma patients combining the ASO with docetaxel showed improved clinical benefit compared to monotherapy[574].

Other ASOs have demonstrated preclinical efficacy and are of particular interest. In melanoma, for instance, in addition to the already described SAMMSON lncRNA (whose targeting ASO reduced tumour progression in PDX models[231]), the TYRP1 (Tyrosinase-related protein 1) mRNA showed an interesting potentially targetable non-coding function: its 3'UTR contains three non-canonical miRNA recognition elements (MREs) that sponge the miR-16 miRNA away from RAB17, a protein with a pro-tumourigenic function in melanoma. ASOs

binding to the TYRP1 MREs (and acting as target-site blockers/TSB), freed miR-16, reduced RAB17 levels and hampered PDX tumour growth[575].

Despite at its infancy, the usage of ASOs for cancer therapy may strongly develop in the future, as demonstrated by huge investments by leading companies in the field, such as Ionis Pharmaceuticals (www.ionispharma.com/ionis-innovation/pipeline/, 2020).

FIGURE 7 - ANTISENSE OLIGONUCLEOTIDES MODIFICATIONS AND LNA-GAPMERS MECHANISM OF TARGET DEGRADATION

A. Over the years, the basic DNA chemistry of antisense oligonucleotides (ASO) has been progressively modified to increase their stability and target affinity. Some modifications involved to the backbone of the ASO (1st gen), while other the nucleoside (2nd/3rd gen). **B.** Since RNAseH1 cannot interact with the DNA-RNA duplex in the presence of the LNA modification, the ASO configuration is changed to have LNA modified nucleotides separated by unmodified ones (GapmeR).

LNCRNAS AS CANCER BIOMARKERS

Regarding their role as biomarkers, many lncRNAs have been proposed to predict the presence of malignant cells (diagnostic biomarker) or patient outcome (prognostic biomarker)[576]. Some of them are dysregulated in multiple cancers (such as MALAT1, H19, PVT1, HOTAIR), while others in a more restricted manner[577]. However, a cancer specific alteration cannot directly translate into usage as biomarker, but requires the development of an assay, the assessment of its clinical validity and utility compared to existing methods, the relative costs and the ease of integration in the healthcare[578].

To date, the only lncRNA analysed in clinical practice and whose test is approved[579], is PCA3 for prostate cancer. This lncRNA was identified in 1999 as being overexpressed in virtually all prostate carcinoma specimens compared to normal prostate tissue[580]. This finding was the rationale to exploit it for cancer detection in patients at risk, since the other available biomarker (PSA measured in blood) had poor specificity and resulted in a large number of unnecessary biopsies and overtreatments[581]. The development of an assay to measure PCA3

and PSA RNA levels from urine samples and the definition of the PCA3 score (ratio PCA3/PSA), demonstrated a better performance for predicting biopsy outcome compared to serum PSA[582]. However it showed a lower sensitivity and unlike PSA, did not correlate with prostate volume or Gleason score[583].

The possibility to exploit lncRNAs as non-invasive biomarkers using liquid biopsies like PCA3 is very attractive, but requires candidates to be expressed at sufficient levels and to be released outside the cells by vesicles (such as exosomes or microvesicles) or as free RNA[576]. Stability in the extracellular space constitutes a challenge for RNAs due to alkaline pH, heavy metal ions, RNA hydrolyzing enzymes: only the association with proteins, lipoproteins and extracellular vesicles can increase a predicted half-life of 15 seconds to minutes and hours[584]. Thus, altered tumour expression may not be sufficient to suggest the clinical utility of a candidate, but requires to verify its stability in body fluids. MALAT-1 may represent an attractive example because it is well expressed and detectable in the blood[585] and urine[586] of breast and prostate cancer patients, respectively. On the other hand, some RNAs are intrinsically more stable, such as circRNAs (that lack the free ends targeted by exoribonucleases) and they gained interest for body fluids detection[182].

In addition, implementation of lncRNAs testing from liquid biopsies would require tackling a series of technical issues regarding the pre- and analytical steps, which are probably the root of the lack of reproducibility between some studies[578]. It would be necessary to define standardized protocols for: samples storage, RNA extraction (column based or not) and quantification (Nanodrop spectrophotometer is usually not sufficiently sensitive); the assay (qPCR or more sensitive derived methods such as digital PCR and droplet digital PCR) and the normalization methods (choice of internal controls that ensure data quality and minimize

variance)[587]. The development of lab-on-a-chip devices may solve all these issues, allowing integrated purification and analysis of samples with minimal manipulation[588].

The alternative choice for detection of potentially relevant lncRNAs in patients would be to rely on biopsies, but this is not always possible (such as in the case of difficult to reach tumours). Moreover, it means losing the opportunity to search for occult metastases or residual of disease that may give a relapse[589].

Nevertheless, analysis of lesions biopsies based on lncRNA expression could provide useful information, such as the discrimination between a benign and a malignant lesion. As previously stated, this is a relevant issue for melanocytic lesions, which sometimes are difficult to classify even by expert dermathologists[346]. A molecular test that has been developed exploits an adhesive patch that once applied to a suspect melanocytic lesion, allows the purification of the RNA from the detached cells and its analysis by qPCR[590] for the expression of PRAME (Preferentially Expressed Antigen in Melanoma) and the lncRNA LINC00518: this test showed a 91% sensitivity and 69% specificity for the discrimination of non- and melanoma lesions and may provide a useful tool for doubtful cases[591].

It has also been previously stressed how frequently ccRCC patients treated by nephrectomy for localized disease ultimately develop metastases, which may have been occult at the time of surgery[475]. Actual clinical management based on the UISS and Leibovich scores could be improved, exploiting for instance molecular testing of lncRNAs. A filtering strategy has been applied to identify lncRNAs associated with recurrence risk, overlapping a group of lncRNAs expressed in localized TCGA KIRC samples and associated with lower disease free and overall survival, with a group of lncRNAs significantly overexpressed in tumour versus normal kidney: the result of this analysis has been a set of 5 candidates, among which MFI2-AS1 has been taken for lowest expression in normal kidney and consistency across all survival

endpoints[592]. In an independent cohort, MFI2AS1 expression has been evaluated by qPCR, discriminating patients as expressing and not: the former group was associated with shorter disease-free survival and MFI2AS1 expression status improved the prediction of recurrence defined by patients Leibovich score. These results suggest that testing this lncRNA expression may improve ccRCC patients stratification and influence the clinical decisions[592].

REFERENCES

1. Dees, E. C., Ingram, R. S. & Tilghman, S. M. The product of the H19 gene may function as an RNA. *Mol. Cell. Biol.* **10**, 28–36 (1990).
2. Brockdorff, N. *et al.* The product of the mouse Xist gene is a 15 kb inactive X-specific transcript containing no conserved ORF and located in the nucleus. *Cell* **71**, 515–526 (1992).
3. F.S. Collins, E.S. Lander, J. Rogers, et al. International Human Genome Sequencing Consortium,Finishing the euchromatic sequence of the human genome. *Nature* **431**, 931–945 (2004).
4. Team, T. F. C. and the R. G. E. R. G. P. I. & I. Analysis of the mouse transcriptome based on functional annotation of 60,770 full-length cDNAs. *Nature* 563–573 (2002).
5. Ota, T. *et al.* Complete sequencing and characterization of 21,243 full-length human cDNAs. *Nat. Genet.* **36**, 40–45 (2004).
6. Kapranov, P. *et al.* Large-scale transcriptional activity in chromosomes 21 and 22. *Science.* **296**, 916–919 (2002).
7. Rinn, J. L. *et al.* The transcriptional activity of human chromosome 22. *Genes Dev.* **17**, 529–540 (2003).
8. Feingold, E. A. *et al.* The ENCODE (ENCyclopedia of DNA Elements) Project. *Science.* **306**, 636–640 (2004).
9. Birney, E. *et al.* Identification and analysis of functional elements in 1% of the human genome by the ENCODE pilot project. *Nature* **447**, 799–816 (2007).
10. Dunham, I. *et al.* An integrated encyclopedia of DNA elements in the human genome. *Nature* **489**, 57–74 (2012).
11. Lagarde, J. *et al.* High-throughput annotation of full-length long noncoding RNAs with capture long-read sequencing. *Nat. Genet.* **49**, 1731–1740 (2017).
12. Perkel, J. M. Visiting 'Noncodarnia'. *Biotechniques* **54**, 301–304 (2013).
13. Harrow, J. *et al.* GENCODE: producing a reference annotation for ENCODE. *Genome Biol.* **7 Suppl 1**, 1–9 (2006).
14. Harrow, J. *et al.* GENCODE: The reference human genome annotation for the ENCODE project. *Genome Res.* **22**, 1760–1774 (2012).
15. Frankish, A. *et al.* GENCODE reference annotation for the human and mouse genomes. *Nucleic Acids Res.* **47**, D766–D773 (2019).

16. Kapranov, P. *et al.* RNA maps reveal new RNA classes and a possible function for pervasive transcription. *Science.* **316**, 1484–1488 (2007).
17. Cabili, M. *et al.* Integrative annotation of human large intergenic noncoding RNAs reveals global properties and specific subclasses. *Genes Dev.* **25**, 1915–1927 (2011).
18. Uszczynska-Ratajczak, B., Lagarde, J., Frankish, A., Guigó, R. & Johnson, R. Towards a complete map of the human long non-coding RNA transcriptome. *Nat. Rev. Genet.* **19**, 535–548 (2018).
19. Guttman, M. *et al.* Chromatin signature reveals over a thousand highly conserved large non-coding RNAs in mammals. *Nature* **458**, 223–227 (2009).
20. O'Leary, N. A. *et al.* Reference sequence (RefSeq) database at NCBI: Current status, taxonomic expansion, and functional annotation. *Nucleic Acids Res.* **44**, D733–D745 (2016).
21. Iyer, M. K. *et al.* The landscape of long noncoding RNAs in the human transcriptome. *Nat. Genet.* **47**, 199–208 (2015).
22. Fang, S. *et al.* NONCODEV5: A comprehensive annotation database for long non-coding RNAs. *Nucleic Acids Res.* **46**, D308–D314 (2018).
23. Sharon, D., Tilgner, H., Grubert, F. & Snyder, M. A single-molecule long-read survey of the human transcriptome. *Nat. Biotechnol.* **31**, 1009–1014 (2013).
24. Garalde, D. R. *et al.* Highly parallel direct RNA sequencing on an array of nanopores. *Nat. Methods* **15**, 201–206 (2018).
25. Mercer, T. R. *et al.* Targeted RNA sequencing reveals the deep complexity of the human transcriptome. *Nat. Biotechnol.* **30**, 99–104 (2012).
26. Jiang, L. *et al.* Synthetic spike-in standards for RNA-seq experiments. *Genome Res.* **21**, 1543–1551 (2011).
27. Deveson, I. W., Hardwick, S. A., Mercer, T. R. & Mattick, J. S. The Dimensions, Dynamics, and Relevance of the Mammalian Noncoding Transcriptome. *Trends Genet.* **33**, 464–478 (2017).
28. Derrien, T. *et al.* The GENCODE v7 catalog of human long noncoding RNAs: Analysis of their gene structure, evolution, and expression. *Genome Res.* **22**, 1775–1789 (2012).
29. Deveson, I. W. *et al.* Universal Alternative Splicing of Noncoding Exons. *Cell Syst.* **6**, 245-255.e5 (2018).
30. Clark, M. B. *et al.* Quantitative gene profiling of long noncoding RNAs with targeted RNA sequencing. *Nat. Methods* **12**, 339–342 (2015).
31. Yang, L., Duff, M. O., Graveley, B. R., Carmichael, G. G. & Chen, L. L. Genomewide characterization of non-polyadenylated RNAs. *Genome Biol.* **12**, 1–14 (2011).
32. Tilgner, H. *et al.* Deep sequencing of subcellular RNA fractions shows splicing to be predominantly co-transcriptional in the human genome but inefficient for lncRNAs. *Genome Res.* **22**, 1616–1625 (2012).
33. Mukherjee, N. *et al.* Integrative classification of human coding and noncoding genes through RNA metabolism profiles. *Nat. Struct. Mol. Biol.* **24**, 86–96 (2017).
34. Melé, M. *et al.* Chromatin environment, transcriptional regulation, and splicing distinguish lincRNAs and mRNAs. *Genome Res.* **27**, 27–37 (2017).
35. Clark, M. B. *et al.* Genome-wide analysis of long noncoding RNA stability. *Genome Res.* **1262**, 305–320 (2012).
36. Nelson, B. R. *et al.* A peptide encoded by a transcript annotated as long noncoding RNA enhances SERCA activity in muscle. *Science.* **351**, (2016).
37. Anderson, D. M. *et al.* A micropeptide encoded by a putative long noncoding RNA

regulates muscle performance. *Cell* **160**, 595–606 (2015).
38. Matsumoto, A. *et al.* MTORC1 and muscle regeneration are regulated by the LINC00961-encoded SPAR polypeptide. *Nature* **541**, 228–232 (2017).
39. Bánfai, B. *et al.* Long noncoding RNAs are rarely translated in two human cell lines. *Genome Res.* **22**, 1646–1657 (2012).
40. Wright, J. C. *et al.* Improving GENCODE reference gene annotation using a high-stringency proteogenomics workflow. *Nat. Commun.* **7**, (2016).
41. Verheggen, K. *et al.* Noncoding after All: Biases in Proteomics Data Do Not Explain Observed Absence of lncRNA Translation Products. *J. Proteome Res.* **16**, 2508–2515 (2017).
42. Ingolia, N. T., Lareau, L. F. & Weissman, J. S. Ribosome profiling of mouse embryonic stem cells reveals the complexity and dynamics of mammalian proteomes. *Cell* **147**, 789–802 (2011).
43. Guttman, M., Russell, P., Ingolia, N. T., Weissman, J. S. & Lander, E. S. Ribosome profiling provides evidence that large noncoding RNAs do not encode proteins. *Cell* **154**, 240–251 (2013).
44. Ji, Z., Song, R., Regev, A. & Struhl, K. Many lncRNAs, 5'UTRs, and pseudogenes are translated and some are likely to express functional proteins. *Elife* **4**, 1–21 (2015).
45. Van Heesch, S. *et al.* Extensive localization of long noncoding RNAs to the cytosol and mono- and polyribosomal complexes. *Genome Biol.* **15**, 1–12 (2014).
46. Housman, G. & Ulitsky, I. Methods for distinguishing between protein-coding and long noncoding RNAs and the elusive biological purpose of translation of long noncoding RNAs. *Biochim. Biophys. Acta - Gene Regul. Mech.* **1859**, 31–40 (2016).
47. Ernst, J. *et al.* Mapping and analysis of chromatin state dynamics in nine human cell types. *Nature* **473**, 43–49 (2011).
48. Marques, A. C. *et al.* Chromatin signatures at transcriptional start sites separate two equally populated yet distinct classes of intergenic long noncoding RNAs. *Genome Biol.* **14**, (2013).
49. Kim, T. K. *et al.* Widespread transcription at neuronal activity-regulated enhancers. *Nature* **465**, 182–187 (2010).
50. de Santa, F. *et al.* A large fraction of extragenic RNA Pol II transcription sites overlap enhancers. *PLoS Biol.* **8**, (2010).
51. Li, W., Notani, D. & Rosenfeld, M. G. Enhancers as non-coding RNA transcription units: Recent insights and future perspectives. *Nat. Rev. Genet.* **17**, 207–223 (2016).
52. Preker, P. *et al.* RNA Exosome Depletion Reveals Transcription Upstream of Active Human Promoters. *Science.* 1851–1854 (2008).
53. Preker, P. *et al.* PROMoter uPstream Transcripts share characteristics with mRNAs and are produced upstream of all three major types of mammalian promoters. *Nucleic Acids Res.* **39**, 7179–7193 (2011).
54. Sati, S., Ghosh, S., Jain, V., Scaria, V. & Sengupta, S. Genome-wide analysis reveals distinct patterns of epigenetic features in long non-coding RNA loci. *Nucleic Acids Res.* **40**, 10018–10031 (2012).
55. Jiang, C. *et al.* Identifying and functionally characterizing tissue-specific and ubiquitously expressed human lncRNAs. *Oncotarget* **7**, 7120–7133 (2016).
56. Mattioli, K. *et al.* High-throughput functional analysis of lncRNA core promoters elucidates rules governing tissue-specificity. *Genome Res.* 344–355 (2019) doi:10.1101/482232.

57. Washietl, S., Kellis, M. & Garber, M. Evolutionary dynamics and tissue specificity of human long noncoding RNAs in six mammals. *Genome Res.* **24**, 616–628 (2014).
58. Liu, S. J. *et al.* Single-cell analysis of long non-coding RNAs in the developing human neocortex. *Genome Biol.* **17**, 1–17 (2016).
59. Zhang, X., Wang, Z., Poon, M. & Yang, J. Spatial-temporal transcriptional dynamics of long non-coding RNAs in human brain. *Human Molecular Genetics* **26**, 3202–3211 (2017).
60. Zhou, J. *et al.* Combined Single-Cell Profiling of lncRNAs and Functional Screening Reveals that H19 Is Pivotal for Embryonic Hematopoietic Stem Cell Development Article Combined Single-Cell Profiling of lncRNAs and Functional Screening Reveals that H19 Is Pivotal for Emb. *Stem Cell* **24**, 285-298.e5 (2019).
61. Xia, C., Fan, J., Emanuel, G., Hao, J. & Zhuang, X. Spatial transcriptome profiling by MERFISH reveals subcellular RNA compartmentalization and cell cycle-dependent gene expression. *Proceedings of the National Academy of Sciences of the United States of America* **116**, (2019).
62. Necsulea, A. *et al.* The evolution of lncRNA repertoires and expression patterns in tetrapods. *Nature* **505**, 635–640 (2014).
63. Managadze, D., Rogozin, I. B., Chernikova, D., Shabalina, S. A. & Koonin, E. V. Negative correlation between expression level and evolutionary rate of long intergenic noncoding RNAs. *Genome Biol. Evol.* **3**, 1390–1404 (2011).
64. Gorodkin, J. *et al.* De novo prediction of structured RNAs from genomic sequences. *Trends Biotechnol.* **28**, 9–19 (2010).
65. Quinn, J. J. *et al.* Rapid evolutionary turnover underlies conserved lncRNA-genome interactions. *Genes Dev.* **30**, 191–207 (2016).
66. Ulitsky, I. Evolution to the rescue: Using comparative genomics to understand long non-coding RNAs. *Nat. Rev. Genet.* **17**, 601–614 (2016).
67. Hezroni, H. *et al.* Principles of Long Noncoding RNA Evolution Derived from Direct Comparison of Transcriptomes in 17 Species. *Cell Rep.* **11**, 1110–1122 (2015).
68. Latos, P. A. *et al.* Airn transcriptional overlap, but not its lncRNA products, induces imprinted Igf2r silencing. *Science.* **338**, 1469–1472 (2012).
69. Schorderet, P. & Duboule, D. Structural and functional differences in the long non-coding RNA hotair in mouse and human. *PLoS Genet.* **7**, 1–10 (2011).
70. Duret, L., Chureau, C., Samain, S., Weissanbach, J. & Avner, P. The Xist RNA gene evolved in eutherians by pseudogenization of a protein-coding gene. *Science.* **312**, 1653–1655 (2006).
71. Cordaux, R. & Batzer, M. A. The impact of retrotransposons on human genome evolution. *Nat. Rev. Genet.* **10**, 691–703 (2009).
72. Kapusta, A. *et al.* Transposable Elements Are Major Contributors to the Origin, Diversification, and Regulation of Vertebrate Long Noncoding RNAs. *PLoS Genet.* **9**, (2013).
73. Wu, X. & Sharp, P. A. Divergent transcription: A driving force for new gene origination? *Cell* **155**, 990 (2013).
74. Kong, Y., Hsieh, C. H. & Alonso, L. C. ANRIL: A lncRNA at the CDKN2A/B locus with roles in cancer and metabolic disease. *Front. Endocrinol. (Lausanne).* **9**, 1–13 (2018).
75. Hacisuleyman, E., Shukla, C. J., Weiner, C. L. & Rinn, J. L. Function and evolution of local repeats in the Firre locus. *Nat. Commun.* **7**, (2016).
76. Steinmetz, E. J. *et al.* Genome-Wide Distribution of Yeast RNA Polymerase II and Its

Control by Sen1 Helicase. *Mol. Cell* **24**, 735–746 (2006).
77. Kapusta, A. & Feschotte, C. Volatile evolution of long noncoding RNA repertoires: Mechanisms and biological implications. *Trends Genet.* **30**, 439–452 (2014).
78. Palazzo, A. F. & Lee, E. S. Non-coding RNA: What is functional and what is junk? *Front. Genet.* **5**, 1–11 (2015).
79. Djebali, S. *et al.* Landscape of transcription in human cells. *Nature* **489**, 101–108 (2012).
80. Moazed, D. Small RNAs in transcriptional gene silencing and genome defence. *Nature* **457**, 413–420 (2009).
81. Dinger, M. E., Amaral, P. P., Mercer, T. R. & Mattick, J. S. Pervasive transcription of the eukaryotic genome: Functional indices and conceptual implications. *Briefings Funct. Genomics Proteomics* **8**, 407–423 (2009).
82. Miao, Y. *et al.* Trends of long noncoding RNA research from 2007 to 2016: A bibliometric analysis. *Oncotarget* **8**, 83114–83127 (2017).
83. Ma, L. *et al.* Lncbook: A curated knowledgebase of human long non-coding rnas. *Nucleic Acids Res.* **47**, D128–D134 (2019).
84. Wilk, R., Hu, J., Blotsky, D. & Krause, H. M. Diverse and pervasive subcellular distributions for both coding and long noncoding RNAs. *Genes Dev.* **30**, 594–609 (2016).
85. Cabili, M. N. *et al.* Localization and abundance analysis of human lncRNAs at single-cell and single-molecule resolution. *Genome Biol.* **16**, 1–16 (2015).
86. Wen, X. *et al.* LncSLdb: A resource for long non-coding RNA subcellular localization. *Database* **2018**, 1–6 (2018).
87. Femino, A. M., Fay, F. S., Fogarty, K. & Singer, R. H. Visualization of single RNA transcripts in situ. *Science.* **280**, 585–590 (1998).
88. Pichon, X., Lagha, M., Mueller, F. & Bertrand, E. A Growing Toolbox to Image Gene Expression in Single Cells: Sensitive Approaches for Demanding Challenges. *Mol. Cell* **71**, 468–480 (2018).
89. Chan, S. *et al.* A method for manual and automated multiplex RNAscope in situ hybridization and immunocytochemistry on cytospin samples. *PLoS One* **13**, (2018).
90. Kann, A. P. & Krauss, R. S. Multiplexed RNAscope and immunofluorescence on whole-mount skeletal myofibers and their associated stem cells. *Development.* **146**, (2019).
91. Carlevaro-Fita, J. & Johnson, R. Global Positioning System: Understanding Long Noncoding RNAs through Subcellular Localization. *Mol. Cell* **73**, 869–883 (2019).
92. Taliaferro, J. M., Wang, E. T. & Burge, C. B. Genomic analysis of RNA localization. *RNA Biol.* **11**, 1040–1050 (2014).
93. Mas-Ponte, D. *et al.* LncATLAS database for subcellular localisation of long noncoding RNAs. *RNA* 1080–1087 (2017) doi:10.1101/116335.
94. Kaewsapsak, P., Shechner, D. M., Mallard, W., Rinn, J. L. & Ting, A. Y. Live-cell mapping of organelle-associated RNAs via proximity biotinylation combined with protein-RNA crosslinking. *Elife* **6**, 1–31 (2017).
95. Fazal, F. M. *et al.* Atlas of Subcellular RNA Localization Revealed by APEX-Seq. *Cell* **178**, 473-490.e26 (2019).
96. Lee, J. H. *et al.* Highly multiplexed subcellular RNA sequencing in situ. *Science.* **343**, 1360–1363 (2014).
97. Morf, J. *et al.* RNA proximity sequencing reveals the spatial organization of the transcriptome in the nucleus. *Nat. Biotechnol.* **37**, 793–802 (2019).
98. Quinodoz, S. A. *et al.* Higher-Order Inter-chromosomal Hubs Shape 3D Genome Organization in the Nucleus. *Cell* **174**, 744-757.e24 (2018).

99. Bell, J. C. *et al.* Chromatin-associated RNA sequencing (ChAR-seq) maps genome-wide RNA-to-DNA contacts. *Elife* **7**, 1–28 (2018).
100. Chen, Y., Shanmugam, S. K. & Dalbey, R. E. The Principles of Protein Targeting and Transport Across Cell Membranes. *Protein J.* **38**, 236–248 (2019).
101. Zhang, B. *et al.* A Novel RNA Motif Mediates the Strict Nuclear Localization of a Long Noncoding RNA. *Mol. Cell. Biol.* **34**, 2318–2329 (2014).
102. Shukla, C. J. *et al.* High-throughput identification of RNA nuclear enrichment sequences . *EMBO J.* **37**, 1–11 (2018).
103. Lubelsky, Y. & Ulitsky, I. Sequences enriched in Alu repeats drive nuclear localization of long RNAs in human cells. *Nature* **555**, 107–111 (2018).
104. Noh, J. H. *et al.* HuR and GRSF1 modulate the nuclear export and mitochondrial localization of the lncRNA RMRP. *Genes Dev.* **30**, 1224–1239 (2016).
105. Köhler, A. & Hurt, E. Exporting RNA from the nucleus to the cytoplasm. *Nat. Rev. Mol. Cell Biol.* **8**, 761–773 (2007).
106. Viphakone, N. *et al.* Co-transcriptional Loading of RNA Export Factors Shapes the Human Transcriptome. *Mol. Cell* **75**, 310-323.e8 (2019).
107. Brown, C. J. *et al.* The human XIST gene: Analysis of a 17 kb inactive X-specific RNA that contains conserved repeats and is highly localized within the nucleus. *Cell* **71**, 527–542 (1992).
108. Chu, C., Qu, K., Zhong, F. L., Artandi, S. E. & Chang, H. Y. Genomic Maps of Long Noncoding RNA Occupancy Reveal Principles of RNA-Chromatin Interactions. *Mol. Cell* **44**, 667–678 (2011).
109. Simon, M. D. *et al.* High-resolution Xist binding maps reveal two-step spreading during X-chromosome inactivation. *Nature* **504**, 465–469 (2013).
110. Engreitz, J. M. *et al.* The Xist lncRNA exploits three-dimensional genome architecture to spread across the X chromosome. *Science.* **341**, 1–9 (2013).
111. Chu, C. *et al.* Systematic discovery of Xist RNA binding proteins. *Cell* **161**, 404–416 (2015).
112. McHugh, C. A. *et al.* The Xist lncRNA interacts directly with SHARP to silence transcription through HDAC3. *Nature* **521**, 232–236 (2015).
113. Chen, C. K., Chow, A., Lai, M. & Guttman, M. Xist recruits the X chromosome to the nuclear lamina to enable chromosome-wide silencing. *Science.* **356**, 1–9 (2017).
114. Simon, M. D. *et al.* The genomic binding sites of a noncoding RNA. *Proc. Natl. Acad. Sci. U. S. A.* **108**, 20497–20502 (2011).
115. West, J. A. *et al.* The Long Noncoding RNAs NEAT1 and MALAT1 Bind Active Chromatin Sites. *Mol. Cell* **55**, 791–802 (2014).
116. Liu, W. *et al.* Brd4 and JMJD6-associated anti-pause enhancers in regulation of transcriptional pause release. *Cell* **155**, 1581–1595 (2013).
117. Li, W. *et al.* Functional roles of enhancer RNAs for oestrogen-dependent transcriptional activation. *Nature* **498**, 516–520 (2013).
118. Engreitz, J. M. *et al.* RNA-RNA interactions enable specific targeting of noncoding RNAs to nascent pre-mRNAs and chromatin sites. *Cell* **159**, 188–199 (2014).
119. Spiniello, M. *et al.* HyPR-MS for multiplexed discovery of MALAT1, NEAT1 and NORAD lncRNA protein interactomes. *J Proteome Res* 1–17 (2018).
120. Hacisuleyman, E. *et al.* Topological organization of multichromosomal regions by the long intergenic noncoding RNA Firre. *Nat. Struct. Mol. Biol.* **21**, 198–206 (2014).
121. McHugh, C. A., Russell, P. & Guttman, M. Methods for comprehensive experimental

identification of RNA-protein interactions. *Genome Biol.* **15**, 1–10 (2014).
122. Barra, J. & Leucci, E. Probing long non-coding RNA-protein interactions. *Front. Mol. Biosci.* **4**, 1–10 (2017).
123. Loda, A. & Heard, E. Xist RNA in action: Past, present, and future. *PLoS Genet.* **15**, 1–17 (2019).
124. Mariner, P. D. *et al.* Human Alu RNA Is a Modular Transacting Repressor of mRNA Transcription during Heat Shock. *Mol. Cell* **29**, 499–509 (2008).
125. Calo, E. *et al.* RNA helicase DDX21 coordinates transcription and ribosomal RNA processing. *Nature* **518**, 249–253 (2015).
126. Xing, Y. H. *et al.* SLERT Regulates DDX21 Rings Associated with Pol I Transcription. *Cell* **169**, 664-678.e16 (2017).
127. Clemson, C. M. *et al.* An Architectural Role for a Nuclear Noncoding RNA: NEAT1 RNA Is Essential for the Structure of Paraspeckles. *Mol. Cell* **33**, 717–726 (2009).
128. Tripathi, V. *et al.* The nuclear-retained noncoding RNA MALAT1 regulates alternative splicing by modulating SR splicing factor phosphorylation. *Mol. Cell* **39**, 925–938 (2010).
129. Xiang, J. F. *et al.* Human colorectal cancer-specific CCAT1-L lncRNA regulates long-range chromatin interactions at the MYC locus. *Cell Res.* **24**, 513–531 (2014).
130. Zhang, H. *et al.* Long noncoding RNA-mediated intrachromosomal interactions promote imprinting at the Kcnq1 locus. *J. Cell Biol.* **204**, 61–75 (2014).
131. Han, P. *et al.* A long noncoding RNA protects the heart from pathological hypertrophy. *Nature* **514**, 102–106 (2014).
132. Jain, A. K. *et al.* LncPRESS1 Is a p53-Regulated LncRNA that Safeguards Pluripotency by Disrupting SIRT6-Mediated De-acetylation of Histone H3K56. *Mol. Cell* **64**, 967–981 (2016).
133. Tsai, M. *et al.* Long Noncoding RNA as Modular Scaffold of Histone Modification Complexes. *Science.* **329**, 689–693 (2010).
134. Wang, K. C. *et al.* A long noncoding RNA maintains active chromatin to coordinate homeotic gene expression. *Nature* **472**, 120–126 (2011).
135. Graf, M. *et al.* Telomere Length Determines TERRA and R-Loop Regulation through the Cell Cycle. *Cell* **170**, 72-85.e14 (2017).
136. Postepska-Igielska, A. *et al.* LncRNA Khps1 Regulates Expression of the Proto-oncogene SPHK1 via Triplex-Mediated Changes in Chromatin Structure. *Mol. Cell* **60**, 626–636 (2015).
137. Boque-Sastre, R. *et al.* Head-to-head antisense transcription and R-loop formation promotes transcriptional activation. *Proc. Natl. Acad. Sci. U. S. A.* **112**, 5785–5790 (2015).
138. Rapicavoli, N. A. *et al.* A mammalian pseudogene lncRNA at the interface of inflammation and antiinflammatory therapeutics. *Elife* **2013**, 1–16 (2013).
139. Anderson, K. M. *et al.* Transcription of the non-coding RNA upperhand controls Hand2 expression and heart development. *Nature* **539**, 433–436 (2016).
140. Cho, S. W. *et al.* Promoter of lncRNA Gene PVT1 Is a Tumor-Suppressor DNA Boundary Element. *Cell* **173**, 1398-1412.e22 (2018).
141. Leeper, T. C. & Varani, G. The structure of an enzyme-activating fragment of human telomerase RNA. *Rna* **11**, 394–403 (2005).
142. Munschauer, M. *et al.* The NORAD lncRNA assembles a topoisomerase complex critical for genome stability. *Nature* **561**, 132–136 (2018).
143. Marchese, F. P. *et al.* A Long Noncoding RNA Regulates Sister Chromatid Cohesion. *Mol.*

Cell **63**, 397–407 (2016).
144. Yao, R., Wang, Y. & Chen, L. Cellular functions of long noncoding RNAs. *Nat. Cell Biol.* **21**, (2019).
145. Khosraviani, N., Ostrowski, L. A. & Mekhail, K. Roles for Non-coding RNAs in Spatial Genome Organization. *Frontiers in Cell and Developmental Biology* vol. 7 1–16 (2019).
146. Sun, Q., Hao, Q. & Prasanth, K. V. Nuclear Long Noncoding RNAs: Key Regulators of Gene Expression. *Trends Genet.* **34**, 142–157 (2018).
147. Galupa, R. & Heard, E. X-chromosome inactivation: A crossroads between chromosome architecture and gene regulation. *Annu. Rev. Genet.* **52**, 535–566 (2018).
148. Okamoto, I. *et al.* Evidence for de novo imprinted X-chromosome inactivation independent of meiotic inactivation in mice. *Nature* **438**, 369–373 (2005).
149. Sunwoo, H., Colognori, D., Froberg, J. E., Jeon, Y. & Lee, J. T. Repeat E anchors Xist RNA to the inactive X chromosomal compartment through CDKN1A-interacting protein (CIZ1). *Proc. Natl. Acad. Sci. U. S. A.* **114**, 10654–10659 (2017).
150. Kalantry, S. *et al.* The Polycomb group protein Eed protects the inactive X-chromosome from differentiation-induced reactivation. *Nat. Cell Biol.* **8**, 195–202 (2006).
151. Mohammad, F. *et al.* Kcnq1ot1/Lit1 Noncoding RNA Mediates Transcriptional Silencing by Targeting to the Perinucleolar Region. *Mol. Cell. Biol.* **28**, 3713–3728 (2008).
152. Davidovich, C., Zheng, L., Goodrich, K. J. & Cech, T. R. Promiscuous RNA binding by Polycomb repressive complex 2. *Nat. Struct. Mol. Biol.* **20**, 1250–1257 (2013).
153. Mao, Y. S., Sunwoo, H., Zhang, B. & Spector, D. L. Direct visualization of the co-transcriptional assembly of a nuclear body by noncoding RNAs. *Nat. Cell Biol.* **13**, 95–101 (2011).
154. Meller, V. H. *et al.* Ordered assembly of roX RNAs into MSL complexes on the dosage-compensated X chromosome in Drosophila. *Curr. Biol.* **10**, 136–143 (2000).
155. Quinodoz, S. & Guttman, M. Long noncoding RNAs: An emerging link between gene regulation and nuclear organization. *Trends in Cell Biology* vol. 24 651–663 (2014).
156. Maass, P. G. *et al.* A misplaced lncRNA causes brachydactyly in humans. *J. Clin. Invest.* **122**, 3990–4002 (2012).
157. Denholtz, M. *et al.* Long-range chromatin contacts in embryonic stem cells reveal a role for pluripotency factors and polycomb proteins in genome organization. *Cell Stem Cell* **13**, 602–616 (2013).
158. Staněk, D. & Fox, A. Nuclear bodies: news insights into structure and function. *Curr. Opin. Cell Biol.* **46**, 94–101 (2017).
159. Fox, A. H., Nakagawa, S., Hirose, T. & Bond, C. S. Paraspeckles: Where Long Noncoding RNA Meets Phase Separation. *Trends Biochem. Sci.* **43**, 124–135 (2018).
160. Fox, A. H. *et al.* Paraspeckles: a novel nuclear domain. *Curr. Biol.* **12**, 13–25 (2002).
161. Chen, L. L. & Carmichael, G. G. Altered Nuclear Retention of mRNAs Containing Inverted Repeats in Human Embryonic Stem Cells: Functional Role of a Nuclear Noncoding RNA. *Mol. Cell* **35**, 467–478 (2009).
162. Nakagawa, S., Naganuma, T., Shioi, G. & Hirose, T. Paraspeckles are subpopulation-specific nuclear bodies that are not essential in mice. *J. Cell Biol.* **193**, 31–39 (2011).
163. West, J. A. *et al.* Structural, super-resolution microscopy analysis of paraspeckle nuclear body organization. *J. Cell Biol.* **214**, 817–830 (2016).
164. Yamazaki, T. *et al.* Functional Domains of NEAT1 Architectural lncRNA Induce Paraspeckle Assembly through Phase Separation. *Mol. Cell* **70**, 1038-1053.e7 (2018).
165. Barra, J. *et al.* Integrator restrains paraspeckles assembly by promoting isoform

switching of the lncRNA NEAT1. *Sci. Adv.* **6**, 1–17 (2020).
166. Naganuma, T. *et al.* Alternative 3'-end processing of long noncoding RNA initiates construction of nuclear paraspeckles. *EMBO J.* **31**, 4020–4034 (2012).
167. Hirose, T. *et al.* NEAT1 long noncoding RNA regulates transcription via protein sequestration within subnuclear bodies. *Mol. Biol. Cell* **25**, 169–183 (2014).
168. Prasanth, K. V. *et al.* Regulating gene expression through RNA nuclear retention. *Cell* **123**, 249–263 (2005).
169. Imamura, K. *et al.* Long Noncoding RNA NEAT1-Dependent SFPQ Relocation from Promoter Region to Paraspeckle Mediates IL8 Expression upon Immune Stimuli. *Mol. Cell* **53**, 393–406 (2014).
170. Galganski, L., Urbanek, M. O. & Krzyzosiak, W. J. Nuclear speckles: Molecular organization, biological function and role in disease. *Nucleic Acids Res.* **45**, 10350–10368 (2017).
171. Fei, J. *et al.* Quantitative analysis of multilayer organization of proteins and RNA in nuclear speckles at super resolution. *J. Cell Sci.* **130**, 4180–4192 (2017).
172. R., M. *et al.* Identification of cis- and trans-acting factors involved in the localization of MALAT-1 noncoding RNA to nuclear speckles. *Rna* **18**, 738–751 (2012).
173. Nakagawa, S. *et al.* Malat1 is not an essential component of nuclear speckles in mice. *Rna* **18**, 1487–1499 (2012).
174. Engreitz, J. M., Ollikainen, N. & Guttman, M. Long non-coding RNAs: Spatial amplifiers that control nuclear structure and gene expression. *Nature Reviews Molecular Cell Biology* vol. 17 756–770 (2016).
175. Dodd, D. W., Gagnon, K. T. & Corey, D. R. Digital quantitation of potential therapeutic target RNAs. *Nucleic Acid Ther.* **23**, 188–194 (2013).
176. Bonetti, A. *et al.* RADICL-seq identifies general and cell type–specific principles of genome-wide RNA-chromatin interactions. *Nat. Commun.* **11**, 1–14 (2020).
177. Rao, S. S. P. *et al.* A 3D map of the human genome at kilobase resolution reveals principles of chromatin looping. *Cell* **159**, 1665–1680 (2014).
178. Li, G. *et al.* Extensive promoter-centered chromatin interactions provide a topological basis for transcription regulation. *Cell* **148**, 84–98 (2012).
179. Noh, J. H., Kim, K. M., McClusky, W. G., Abdelmohsen, K. & Gorospe, M. Cytoplasmic functions of long noncoding RNAs. *Wiley Interdisciplinary Reviews: RNA* vol. 9 1–15 (2018).
180. Thomson, D. W. & Dinger, M. E. Endogenous microRNA sponges: Evidence and controversy. *Nat. Rev. Genet.* **17**, 272–283 (2016).
181. Poliseno, L. *et al.* A coding-independent function of gene and pseudogene mRNAs regulates tumour biology. *Nature* **465**, 1033–1038 (2010).
182. Jeck, W. R. & Sharpless, N. E. Detecting and characterizing circular RNAs. *Nat. Biotechnol.* **32**, 453–461 (2014).
183. Hansen, T. B. *et al.* Natural RNA circles function as efficient microRNA sponges. *Nature* **495**, 384–388 (2013).
184. Bosson, A. D., Zamudio, J. R. & Sharp, P. A. Endogenous miRNA and target concentrations determine susceptibility to potential ceRNA competition. *Mol. Cell* **56**, 347–359 (2014).
185. Wang, Y. *et al.* Endogenous miRNA Sponge lincRNA-RoR Regulates Oct4, Nanog, and Sox2 in Human Embryonic Stem Cell Self-Renewal. *Dev. Cell* **25**, 69–80 (2013).
186. Cesana, M. *et al.* A long noncoding RNA controls muscle differentiation by functioning

as a competing endogenous RNA. *Cell* **147**, 358–369 (2011).
187. Broderick, J. A. & Zamore, P. D. Competitive Endogenous RNAs Cannot Alter MicroRNA Function InVivo. *Mol. Cell* **54**, 711–713 (2014).
188. Bosia, C., Pagnani, A. & Zecchina, R. Modelling Competing Endogenous RNA Networks. *PLoS One* **8**, (2013).
189. Brown, B. D. *et al.* Endogenous microRNA can be broadly exploited to regulate transgene expression according to tissue, lineage and differentiation state. *Nat. Biotechnol.* **25**, 1457–1467 (2007).
190. Tay, Y. *et al.* Coding-independent regulation of the tumor suppressor PTEN by competing endogenous mRNAs. *Cell* **147**, 344–357 (2011).
191. Kim, Y. K., Furic, L., DesGroseillers, L. & Maquat, L. E. Mammalian Staufen1 recruits Upf1 to specific mRNA 3'UTRs so as to elicit mRNA decay. *Cell* **120**, 195–208 (2005).
192. Gong, C. & Maquat, L. E. LncRNAs transactivate STAU1-mediated mRNA decay by duplexing with 39 UTRs via Alu eleme. *Nature* **470**, 284–290 (2011).
193. Miller, M. A. & Olivas, W. M. Roles of Puf proteins in mRNA degradation and translation. *Wiley Interdiscip. Rev. RNA* **2**, 471–492 (2011).
194. Lee, S. *et al.* Noncoding RNA NORAD Regulates Genomic Stability by Sequestering PUMILIO Proteins. *Cell* **164**, 69–80 (2016).
195. Carrieri, C. *et al.* Long non-coding antisense RNA controls Uchl1 translation through an embedded SINEB2 repeat. *Nature* **491**, 454–457 (2012).
196. Yoon, J. H. *et al.* LincRNA-p21 Suppresses Target mRNA Translation. *Mol. Cell* **47**, 648–655 (2012).
197. Gong, C. *et al.* A Long Non-coding RNA, LncMyoD, Regulates Skeletal Muscle Differentiation by Blocking IMP2-Mediated mRNA Translation. *Dev. Cell* **34**, 181–191 (2015).
198. Wang, P. *et al.* The STAT3-binding long noncoding RNA lnc-DC controls human dendritic cell differentiation. *Science.* **344**, 310–313 (2014).
199. Liu, B. *et al.* A Cytoplasmic NF-κB Interacting Long Noncoding RNA Blocks IκB Phosphorylation and Suppresses Breast Cancer Metastasis. *Cancer Cell* **27**, 370–381 (2015).
200. Mercer, T. R. *et al.* The human mitochondrial transcriptome. *Cell* **146**, 645–658 (2011).
201. Smirnov, A., Entelis, N., Martin, R. P. & Tarassov, I. Biological significance of 5s rRNA import into human mitochondria: Role of ribosomal protein MRP-L18. *Genes Dev.* **25**, 1289–1305 (2011).
202. Wang, G. *et al.* PNPASE regulates RNA import into mitochondria. *Cell* **142**, 456–467 (2010).
203. Rackham, O. *et al.* Long noncoding RNAs are generated from the mitochondrial genome and regulated by nuclear-encoded proteins. *Rna* **17**, 2085–2093 (2011).
204. Burzio, V. A. *et al.* Expression of a family of noncoding mitochondrial RNAs distinguishes normal from cancer cells. *Proc. Natl. Acad. Sci. U. S. A.* **106**, 9430–9434 (2009).
205. Kumarswamy, R. *et al.* Circulating long noncoding RNA, LIPCAR, predicts survival in patients with heart failure. *Circ. Res.* **114**, 1569–1575 (2014).
206. Kopp, F. & Mendell, J. T. Functional Classification and Experimental Dissection of Long Noncoding RNAs. *Cell* **172**, 393–407 (2018).
207. Chu, C., Spitale, R. C. & Chang, H. Y. Technologies to probe functions and mechanisms of long noncoding RNAs. *Nat. Struct. Mol. Biol.* **22**, 29–35 (2015).
208. Liu, S. J. *et al.* CRISPRi-based genome-scale identification of functional long noncoding

RNA loci in human cells. *Science.* **355**, (2017).
209. Quinn, J. J. *et al.* Revealing long noncoding RNA architecture and functions using domain-specific chromatin isolation by RNA purification. *Nat. Biotechnol.* **32**, 933–940 (2014).
210. Quinn, J. J. & Chang, H. Y. *In situ dissection of RNA functional subunits by domain-specific chromatin isolation by RNA purification (dChIRP)*. *Methods in Molecular Biology* vol. 1262 (2015).
211. Spitale, R. C. *et al.* Structural imprints in vivo decode RNA regulatory mechanisms. *Nature* **519**, 486–490 (2015).
212. Liu, F., Somarowthu, S. & Pyle, A. M. Visualizing the secondary and tertiary architectural domains of lncRNA RepA. *Nat. Chem. Biol.* **13**, 282–289 (2017).
213. Henley, S. J. *et al.* Annual report to the nation on the status of cancer, part I: National cancer statistics. *Cancer* **126**, 2225–2249 (2020).
214. Society, A. C. Cancer Facts & Figures 2020. *Atlanta: American Cancer Society* (2020) doi:10.1038/s41598-018-28671-9.
215. Henley, S. J. *et al.* Annual report to the nation on the status of cancer, part II: Progress toward Healthy People 2020 objectives for 4 common cancers. *Cancer* **126**, 2250–2266 (2020).
216. Seebacher, N. A., Stacy, A. E., Porter, G. M. & Merlot, A. M. Clinical development of targeted and immune based anti-cancer therapies. *Journal of Experimental and Clinical Cancer Research.* **38**, 1-39 (2019).
217. Berger, M. F. & Mardis, E. R. The emerging clinical relevance of genomics in cancer medicine. *Nat. Rev. Clin. Oncol.* **15**, 353–365 (2018).
218. Blum, A., Wang, P. & Zenklusen, J. C. SnapShot: TCGA-Analysed Tumors. *Cell* **173**, 530 (2018).
219. Hoadley, K. A. *et al.* Multiplatform analysis of 12 cancer types reveals molecular classification within and across tissues of origin. *Cell* **158**, 929–944 (2014).
220. Liu, J. *et al.* An Integrated TCGA Pan-Cancer Clinical Data Resource to Drive High-Quality Survival Outcome Analytics. *Cell* **173**, 400-416.e11 (2018).
221. Maurano, M. T. *et al.* Systematic localization of common disease-associated variation in regulatory DNA. *Science.* **337**, 1190–1195 (2012).
222. Beroukhim, R. *et al.* The landscape of somatic copy-number alteration across human cancers. *Nature* **463**, 899–905 (2010).
223. Iorio, M. V. & Croce, C. M. MicroRNA dysregulation in cancer: Diagnostics, monitoring and therapeutics. A comprehensive review. *EMBO Mol. Med.* **4**, 143–159 (2012).
224. Arun, G., Diermeier, S. D. & Spector, D. L. Therapeutic Targeting of Long Non-Coding RNAs in Cancer. *Trends in Molecular Medicine* vol. 24 257–277 (2018).
225. Qi, P., Zhou, X. yan & Du, X. Circulating long non-coding RNAs in cancer: Current status and future perspectives. *Mol. Cancer* **15**, 1–11 (2016).
226. Yan, X. *et al.* Comprehensive Genomic Characterization of Long Non-coding RNAs across Human Cancers. *Cancer Cell* **28**, 529–540 (2015).
227. Iyer, M. K. *et al.* The landscape of long noncoding RNAs in the human transcriptome. *Nat. Genet.* **47**, 199–208 (2015).
228. Bolha, L., Ravnik-Glavač, M. & Glavač, D. Long Noncoding RNAs as Biomarkers in Cancer. *Dis. Markers* **2017**, (2017).
229. Lv, D. *et al.* LncSpA: LncRNA Spatial Atlas of Expression across Normal and Cancer Tissues. *Cancer Res.* **80**, 2067–2071 (2020).

230. Hu, X. *et al.* A Functional Genomic Approach Identifies FAL1 as an Oncogenic Long Noncoding RNA that Associates with BMI1 and Represses p21 Expression in Cancer. *Cancer Cell* **26**, 344–357 (2014).
231. Leucci, E. *et al.* Melanoma addiction to the long non-coding RNA SAMMSON. *Nature* **531**, 518–522 (2016).
232. Esteller, M., Corn, P. G., Baylin, S. B. & Herman, J. G. A gene hypermethylation profile of human cancer. *Cancer Res.* **61**, 3225–3229 (2001).
233. Wang, Z. *et al.* lncRNA Epigenetic Landscape Analysis Identifies EPIC1 as an Oncogenic lncRNA that Interacts with MYC and Promotes Cell-Cycle Progression in Cancer. *Cancer Cell* **33**, 706-720.e9 (2018).
234. Doose, G. *et al.* MINCR is a MYC-induced lncRNA able to modulate MYC's transcriptional network in Burkitt lymphoma cells. *Proc. Natl. Acad. Sci. U. S. A.* **112**, E5261–E5270 (2015).
235. Ruan, W., Wang, P., Feng, S., Xue, Y. & Li, Y. Long non-coding RNA small nucleolar RNA host gene 12 (SNHG12) promotes cell proliferation and migration by upregulating angiomotin gene expression in human osteosarcoma cells. *Tumor Biol.* **37**, 4065–4073 (2016).
236. Gabay, Meital, Yulin Li, and D. F. MYC Activation Is a Hallmark of Cancer Initiation and Maintenance. **36**, 186–194 (2009).
237. Schaub, F. X. *et al.* Pan-cancer Alterations of the MYC Oncogene and Its Proximal Network across the Cancer Genome Atlas. *Cell Syst.* **6**, 282-300.e2 (2018).
238. Hart, J. R., Roberts, T. C., Weinberg, M. S., Morris, K. V & Vogt, P. K. MYC regulates the non-coding transcriptome. *Oncotarget* **5**, 12543–12554 (2014).
239. Kim, T. *et al.* Role of MYC-Regulated long noncoding RNAs in cell cycle regulation and tumorigenesis. *J. Natl. Cancer Inst.* **107**, 1–11 (2015).
240. Raffeiner, P. *et al.* An MXD1-derived repressor peptide identifies noncoding mediators of MYC-driven cell proliferation. *Proc. Natl. Acad. Sci. U. S. A.* **117**, 6571–6579 (2020).
241. Villanueva, M. T. Long path to MYC inhibition approaches clinical trials. *Nat. Rev. Drug Discov.* **18**, 2019 (2019).
242. Sonnenschein, C. & Soto, A. M. Over a century of cancer research: Inconvenient truths and promising leads. *PLoS Biol.* **18**, 1–12 (2020).
243. Berteaux, N. *et al.* H19 mRNA-like noncoding RNA promotes breast cancer cell proliferation through positive control by E2F1. *J. Biol. Chem.* **280**, 29625–29636 (2005).
244. Gupta, R. A. *et al.* Long non-coding RNA HOTAIR reprograms chromatin state to promote cancer metastasis. *Nature* **464**, 1071–1076 (2010).
245. Trimarchi, T. *et al.* Genome-wide mapping and characterization of notch-regulated long noncoding RNAs in acute leukemia. *Cell* **158**, 593–606 (2014).
246. Gutschner, T., Hämmerle, M. & Diederichs, S. MALAT1 - A paradigm for long noncoding RNA function in cancer. *J. Mol. Med.* **91**, 791–801 (2013).
247. Hosono, Y. *et al.* Oncogenic Role of THOR, a Conserved Cancer/Testis Long Non-coding RNA. *Cell* **171**, 1559-1572.e20 (2017).
248. Hu, G., Lou, Z. & Gupta, M. The long non-coding RNA GAS5 cooperates with the eukaryotic translation initiation factor 4E to regulate c-Myc translation. *PLoS One* **9**, (2014).
249. Garcia, L. *et al.* lncRNAs in Hallmarks of Cancer and Clinical Applications. *Non-Coding RNAs* (2020) doi:10.5772/intechopen.88903.
250. Hanahan, D. & Weinberg, R. A. The Hallmarks of Cancer. *Cell* **100**, 57–70 (2000).

251. Hanahan, D. & Weinberg, R. A. Hallmarks of cancer: The next generation. *Cell* **144**, 646–674 (2011).
252. Aprile, M., Katopodi, V., Leucci, E. & Costa, V. Lncrnas in cancer: From garbage to junk. *Cancers (Basel).* **12**, 1–32 (2020).
253. Schmitt, A. M. & Chang, H. Y. Long Noncoding RNAs in Cancer Pathways. *Cancer Cell* **29**, 452–463 (2016).
254. Dang, C. V. MYC on the path to cancer. *Cell* **149**, 22–35 (2012).
255. Chen, H. Z., Tsai, S. Y. & Leone, G. Emerging roles of E2Fs in cancer: An exit from cell cycle control. *Nat. Rev. Cancer* **9**, 785–797 (2009).
256. Sato, K. *et al.* Clinical significance of alterations of chromosome 8 in high-grade, advanced, nonmetastatic prostate carcinoma. *J. Natl. Cancer Inst.* **91**, 1574–1580 (1999).
257. Tseng, Y. Y. *et al.* PVT1 dependence in cancer with MYC copy-number increase. *Nature* **512**, 82–86 (2014).
258. Luo, L. *et al.* LINC01638 lncRNA activates MTDH-Twist1 signaling by preventing SPOP-mediated c-Myc degradation in triple-negative breast cancer. *Oncogene* **37**, 6166–6179 (2018).
259. Yang, F. *et al.* Long non-coding RNA GHET1 promotes gastric carcinoma cell proliferation by increasing c-Myc mRNA stability. *FEBS J.* **281**, 802–813 (2014).
260. Ling, H. *et al.* CCAT2, a novel noncoding RNA mapping to 8q24, underlies metastatic progression and chromosomal instability in colon cancer. *Genome Res.* **23**, 1446–1461 (2013).
261. Prensner, J. R. *et al.* The Long Non-Coding RNA PCAT-1 Promotes Prostate Cancer Cell Proliferation through cMyc. *Neoplasia (United States)* **16**, 900–908 (2014).
262. Hung, C. L. *et al.* A long noncoding RNA connects c-Myc to tumor metabolism. *Proc. Natl. Acad. Sci. U. S. A.* **111**, 18697–18702 (2014).
263. Wang, H. *et al.* Long noncoding RNA Linc00337 functions as an E2F1 co-activator and promotes cell proliferation in pancreatic ductal adenocarcinoma. *J. Exp. Clin. Cancer Res.* **39**, 1–14 (2020).
264. Fang, Z. *et al.* ERINA Is an Estrogen-Responsive LncRNA That Drives Breast Cancer through the E2F1/RB1 Pathway. *Cancer Res.* **80**, 4399–4413 (2020).
265. Ghafouri-Fard, S., Esmaeili, M. & Taheri, M. H19 lncRNA: Roles in tumorigenesis. *Biomed. Pharmacother.* **123**, (2020).
266. He, H., Wang, N., Yi, X., Tang, C. & Wang, D. Long non-coding RNA H19 regulates E2F1 expression by competitively sponging endogenous miR-29a-3p in clear cell renal cell carcinoma. *Cell Biosci.* **7**, 1–12 (2017).
267. Cao, L., Zhang, P., Li, J. & Wu, M. Last, a c-Myc-inducible long noncoding RNA, cooperates with CNBP to promote CCND1 MRNA stability in human cells. *Elife* **6**, 1–28 (2017).
268. Zhang, Z. *et al.* Long non-coding RNA CASC11 interacts with hnRNP-K and activates the WNT/β-catenin pathway to promote growth and metastasis in colorectal cancer. *Cancer Lett.* **376**, 62–73 (2016).
269. Liu, Z. *et al.* The Long Noncoding RNA HOTAIR Contributes to Cisplatin Resistance of Human Lung Adenocarcinoma Cells via downregualtion of p21WAF1/CIP1 Expression. *PLoS One* **8**, 1–15 (2013).
270. Lu, Y. *et al.* MYC targeted long noncoding RNA DANCR promotes cancer in part by reducing p21 levels. *Cancer Res.* **78**, 64–74 (2018).

271. Wang, J. *et al.* Multiple functions of the RNA-binding protein HuR in cancer progression, treatment responses and prognosis. *Int. J. Mol. Sci.* **14**, 10015–10041 (2013).
272. Mao, Z. *et al.* LncRNA DANCR promotes migration and invasion through suppression of lncRNA-LET in gastric cancer cells. *Biosci. Rep.* **37**, (2017).
273. Huang, J. *et al.* Long non-coding RNA UCA1 promotes breast tumor growth by suppression of p27 (Kip1). *Cell Death Dis.* **5**, e1008–e1008 (2014).
274. Yang, Y. *et al.* TRMP, a p53-inducible long noncoding RNA, regulates G1/S cell cycle progression by modulating IRES-dependent p27 translation. *Cell Death Dis.* **9**, (2018).
275. Pasmant, E. *et al.* Characterization of a germ-line deletion, including the entire INK4/ARF locus, in a melanoma-neural system tumor family: Identification of ANRIL, an antisense noncoding RNA whose expression coclusters with ARF. *Cancer Res.* **67**, 3963–3969 (2007).
276. Yap, K. L. *et al.* Molecular Interplay of the Noncoding RNA ANRIL and Methylated Histone H3 Lysine 27 by Polycomb CBX7 in Transcriptional Silencing of INK4a. *Mol. Cell* **38**, 662–674 (2010).
277. Kotake, Y. *et al.* Long non-coding RNA ANRIL is required for the PRC2 recruitment to and silencing of p15 INK4B tumor suppressor gene. *Oncogene* **30**, 1956–1962 (2011).
278. Holdt, L. M. *et al.* Alu Elements in ANRIL Non-Coding RNA at Chromosome 9p21 Modulate Atherogenic Cell Functions through Trans-Regulation of Gene Networks. *PLoS Genet.* **9**, 1–12 (2013).
279. Wan, G. *et al.* Long non-coding RNA ANRIL (CDKN2B-AS) is induced by the ATM-E2F1 signaling pathway. *Cell. Signal.* **25**, 1086–1095 (2013).
280. Lu, Y. *et al.* Long noncoding RNA ANRIL could be transactivated by c-Myc and promote tumor progression of non-small-cell lung cancer. *Onco. Targets. Ther.* **9**, 3077–3084 (2016).
281. Wu, J. H., Tang, J. M., Li, J. & Li, X. W. Upregulation of SOX2-activated lncRNA ANRIL promotes nasopharyngeal carcinoma cell growth. *Sci. Rep.* **8**, 1–8 (2018).
282. Huang, M. De *et al.* Long non-coding RNA ANRIL is upregulated in hepatocellular carcinoma and regulates cell apoptosis by epigenetic silencing of KLF2. *J. Hematol. Oncol.* **8**, 1–14 (2015).
283. Wan, G. *et al.* A novel non-coding RNA lncRNA-JADE connects DNA damage signalling to histone H4 acetylation. *EMBO J.* **32**, 2833–2847 (2013).
284. Sharma, V. *et al.* A BRCA 1-interacting lnc RNA regulates homologous recombination . *EMBO Rep.* **16**, 1520–1534 (2015).
285. Zhang, Y. *et al.* Long noncoding RNA LINP1 regulates repair of DNA double-strand breaks in triple-negative breast cancer. *Nat. Struct. Mol. Biol.* **23**, 522–530 (2016).
286. Hu, W. L. *et al.* GUARDIN is a p53-responsive long non-coding RNA that is essential for genomic stability. *Nat. Cell Biol.* **20**, 492–502 (2018).
287. Lane, D. P. P53, Guardian of the Genome. *Nature* vol. 358 15–16 (1992).
288. Levine, A. J. P53: 800 Million Years of Evolution and 40 Years of Discovery. *Nat. Rev. Cancer* **20**, 471–480 (2020).
289. Saldaña-Meyer, R. *et al.* CTCF regulates the human p53 gene through direct interaction with its natural antisense transcript, Wrap53. *Genes Dev.* **28**, 723–734 (2014).
290. Saldaña-Meyer, R. *et al.* RNA Interactions Are Essential for CTCF-Mediated Genome Organization. *Mol. Cell* **76**, 412-422.e5 (2019).
291. Zhang, A. *et al.* The human long non-coding RNA-RoR is a p53 repressor in response to DNA damage. *Cell Res.* **23**, 340–350 (2013).

292. Chen, R. *et al.* Quantitative proteomics reveals that long non-coding RNA MALAT1 interacts with DBC1 to regulate p53 acetylation. *Nucleic Acids Res.* **45**, 9947–9959 (2017).
293. Li, X. L. *et al.* Long Noncoding RNA PURPL Suppresses Basal p53 Levels and Promotes Tumorigenicity in Colorectal Cancer. *Cell Rep.* **20**, 2408–2423 (2017).
294. Allen, M. A. *et al.* Global analysis of p53-regulated transcription identifies its direct targets and unexpected regulatory mechanisms. *Elife* **3**, 1–29 (2014).
295. Ashcroft, M. & Vousden, K. H. Regulation of p53 stability. *Oncogene* **18**, 7637–7643 (1999).
296. Zhou, Y. *et al.* Activation of p53 by MEG3 non-coding RNA. *J. Biol. Chem.* **282**, 24731–24742 (2007).
297. Zhou, Y., Zhang, X. & Klibanski, A. MEG3 noncoding RNA: A tumor suppressor. *J. Mol. Endocrinol.* **48**, 45–53 (2012).
298. Schmitt, A. M. *et al.* An inducible long noncoding RNA amplifies DNA damage signaling. *Nat. Genet.* **48**, 1370–1376 (2016).
299. Hung, T. *et al.* Extensive and coordinated transcription of noncoding RNAs within cell-cycle promoters. *Nat. Genet.* **43**, 621–629 (2011).
300. Kotake, Y. *et al.* Long noncoding RNA PANDA positively regulates proliferation of osteosarcoma cells. *Anticancer Res.* **37**, 81–86 (2017).
301. Huarte, M. *et al.* A large intergenic noncoding RNA induced by p53 mediates global gene repression in the p53 response. *Cell* **142**, 409–419 (2010).
302. Chen, S. *et al.* LincRNa-p21: function and mechanism in cancer. *Med. Oncol.* **34**, (2017).
303. Negishi, M. *et al.* A new lncRNA, APTR, associates with and represses the CDKN1A/p21 promoter by recruiting polycomb proteins. *PLoS One* **9**, (2014).
304. Blume, C. J. *et al.* P53-dependent non-coding RNA networks in chronic lymphocytic leukemia. *Leukemia* **29**, 2015–2023 (2015).
305. Adriaens, C. *et al.* P53 induces formation of NEAT1 lncRNA-containing paraspeckles that modulate replication stress response and chemosensitivity. *Nat. Med.* **22**, 861–868 (2016).
306. Mello, S. S. *et al.* Neat1 is a p53-inducible lincRNA essential for transformation suppression. *Genes Dev.* **31**, 1095–1108 (2017).
307. Idogawa, M., Ohashi, T., Sasaki, Y., Nakase, H. & Tokino, T. Long non-coding RNA NEAT1 is a transcriptional target of p53 and modulates p53-induced transactivation and tumor-suppressor function. *Int. J. Cancer* **140**, 2785–2791 (2017).
308. Shin, V. Y. *et al.* Long non-coding RNA NEAT1 confers oncogenic role in triple-negative breast cancer through modulating chemoresistance and cancer stemness. *Cell Death Dis.* **10**, (2019).
309. De Berardinis, R. J. & Chandel, N. S. Fundamentals of cancer metabolism. *Sci. Adv.* **2**, (2016).
310. Koppenol, W. H., Bounds, P. L. & Dang, C. V. Otto Warburg's contributions to current concepts of cancer metabolism. *Nat. Rev. Cancer* **11**, 325–337 (2011).
311. Almuhaideb, A., Papathanasiou, N. & Bomanji, J. 18F-FDG PET/CT imaging in oncology. *Ann. Saudi Med.* **31**, 3–13 (2011).
312. Weinhouse, S., Warburg, O., Burk, D. & Schade, A. L. On Respiratory Impairment in Cancer Cells. *Science.* **124**, 267–272 (1956).
313. Zu, X. L. & Guppy, M. Cancer metabolism: Facts, fantasy, and fiction. *Biochem. Biophys. Res. Commun.* **313**, 459–465 (2004).

314. Jose, C., Bellance, N. & Rossignol, R. Choosing between glycolysis and oxidative phosphorylation: A tumor's dilemma? *Biochim. Biophys. Acta - Bioenerg.* **1807**, 552–561 (2011).
315. Fan, T. W. M. *et al.* Altered regulation of metabolic pathways in human lung cancer discerned by 13C stable isotope-resolved metabolomics (SIRM). *Mol. Cancer* **8**, 1–19 (2009).
316. Hensley, C. T. *et al.* Metabolic Heterogeneity in Human Lung Tumors. *Cell* **164**, 681–694 (2016).
317. Xiao, Z., Dai, Z. & Locasale, J. W. Metabolic landscape of the tumor microenvironment at single cell resolution. *Nat. Commun.* **10**, 3763 (2019).
318. Dibble, C. C. & Manning, B. D. Signal integration by mTORC1 coordinates nutrient input with biosynthetic output. *Nat. Cell Biol.* **15**, 555–564 (2013).
319. Stine, Z. E., Walton, Z. E., Altman, B. J., Hsieh, A. L. & Dang, C. V. MYC, Metabolism, and Cancer. *Cancer Discov.* **5**, 1024–1039 (2015).
320. Nakazawa, M. S., Keith, B. & Simon, M. C. Oxygen availability and metabolic adaptations. *Nat. Rev. Cancer* **16**, 663–673 (2016).
321. Chappell, J. C., Payne, L. B. & Kimryn Rathmell, W. Hypoxia, angiogenesis, and metabolism in the hereditary kidney cancers. *Journal of Clinical Investigation* vol. 129 442–451 (2019).
322. Maxwell, P. H. *et al.* The tumour suppressor protein VHL targets hypoxia-inducible factors for oxygen-dependent proteolysis. *Nature* **399**, 271–275 (1999).
323. Maxwell, P. H., Pugh, C. W. & Ratcliffe, P. J. Activation of the HIF pathway in cancer. *Curr. Opin. Genet. Dev.* **11**, 293–299 (2001).
324. Yang, F., Zhang, H., Mei, Y. & Wu, M. Reciprocal Regulation of HIF-1α and LincRNA-p21 Modulates the Warburg Effect. *Mol. Cell* **53**, 88–100 (2014).
325. Lin, A. *et al.* The LINK-A lncRNA activates normoxic HIF1α signalling in triple-negative breast cancer. *Nat. Cell Biol.* **18**, 213–224 (2016).
326. Hardie, D. G., Schaffer, B. E. & Brunet, A. AMPK: An Energy-Sensing Pathway with Multiple Inputs and Outputs. *Trends Cell Biol.* **26**, 190–201 (2016).
327. Shackelford, D. B. & Shaw, R. J. The LKB1-AMPK pathway: Metabolism and growth control in tumour suppression. *Nat. Rev. Cancer* **9**, 563–575 (2009).
328. Liu, X. *et al.* LncRNA NBR2 engages a metabolic checkpoint by regulating AMPK under energy stress. *Nat. Cell Biol.* **18**, 431–442 (2016).
329. Gad, S. *et al.* Characterisation of a 161 kb deletion extending from the NBR1 to the BRCA1 genes in a French breast-ovarian cancer family. *Hum. Mutat.* **21**, 654 (2003).
330. Robichaud, N., Sonenberg, N., Ruggero, D. & Schneider, R. J. Translational control in cancer. *Cold Spring Harb. Perspect. Biol.* **11**, (2019).
331. Caudron-Herger, M. *et al.* Alu element-containing RNA s maintain nucleolar structure and function. *EMBO J.* **34**, 2758–2774 (2015).
332. Feric, M. *et al.* Coexisting Liquid Phases Underlie Nucleolar Subcompartments. *Cell* **165**, 1686–1697 (2016).
333. Nguyen, L. X. T., Raval, A., Garcia, J. S. & Mitchell, B. S. Regulation of Ribosomal Gene Expression in Cancer. *J. Cell. Physiol.* **230**, 1181–1188 (2015).
334. Peltonen, K. *et al.* A targeting modality for destruction of RNA polymerase I that possesses anticancer activity. *Cancer Cell* **25**, 77–90 (2014).
335. Miki, T. S. & Großhans, H. The multifunctional RNase XRN2. *Biochem. Soc. Trans.* **41**, 825–830 (2013).

336. Wu, H., Sun, H., Liang, X., Lima, W. F. & Crooke, S. T. Human RNase H1 Is Associated with Protein P32 and Is Involved in Mitochondrial Pre-rRNA Processing. *PLoS One* **8**, (2013).
337. Sato, S. *et al.* Collaborator of alternative reading frame protein (CARF) regulates early processing of pre-ribosomal RNA by retaining XRN2 (5'-3' exoribonuclease) in the nucleoplasm. *Nucleic Acids Res.* **43**, 10397–10410 (2015).
338. Vendramin, R. *et al.* SAMMSON fosters cancer cell fitness by concertedly enhancing mitochondrial and cytosolic translation. *Nat. Struct. Mol. Biol.* **25**, 1035–1046 (2018).
339. Zhao, X. Y. & Lin, J. D. Long Noncoding RNAs: A New Regulatory Code in Metabolic Control. *Trends Biochem. Sci.* **40**, 586–596 (2015).
340. Mort, R. L., Jackson, I. J. & Patton, E. E. The melanocyte lineage in development and disease. *Development* **142**, 1387–1387 (2015).
341. Bastian, B. C. *The molecular pathology of melanoma: An integrated taxonomy of melanocytic neoplasia*. *Annual Review of Pathology: Mechanisms of Disease* vol. 9 (2014).
342. Jimbow, K., Roth, S. I., Fitzpatrick, T. B. & Szabo, G. Mitotic activity in non-neoplastic melanocytes in vivo as determined by histochemical, autoradiographic, and electron microscope studies. *J. Cell Biol.* **66**, 663–670 (1975).
343. Kaidbey, K. H., Agin, P. P., Sayre, R. M. & Kligman, A. M. Photoprotection by melanin—a comparison of black and Caucasian skin. *J. Am. Acad. Dermatol.* **1**, 249–260 (1979).
344. Ando, H. *et al.* Melanosomes are transferred from melanocytes to keratinocytes through the processes of packaging, release, uptake, and dispersion. *J. Invest. Dermatol.* **132**, 1222–1229 (2012).
345. Sanna, A. *et al.* Tumor genetic heterogeneity analysis of chronic sun-damaged melanoma. *Pigment Cell Melanoma Res.* **33**, 480–489 (2020).
346. Shain, A. H. & Bastian, B. C. From melanocytes to melanomas. *Nat. Rev. Cancer* **16**, 345–358 (2016).
347. Purdue, M. P. *et al.* Etiologic and other factors predicting nevus-associated cutaneous malignant melanoma. *Cancer Epidemiol. Biomarkers Prev.* **14**, 2015–2022 (2005).
348. Schadendorf, D. *et al.* Melanoma. *Nat. Rev. Dis. Prim.* **1**, 1–20 (2015).
349. Shain, A. H. *et al.* The Genetic Evolution of Melanoma from Precursor Lesions. *N. Engl. J. Med.* **373**, 1926–1936 (2015).
350. Shain, A. H. *et al.* Genomic and Transcriptomic Analysis Reveals Incremental Disruption of Key Signaling Pathways during Melanoma Evolution. *Cancer Cell* **34**, 45-55.e4 (2018).
351. Michaloglou, C. *et al.* BRAFE600-associated senescence-like cell cycle arrest of human naevi. *Nature* **436**, 720–724 (2005).
352. Vredeveld, L. C. W. *et al.* Abrogation of BRAFV600E-induced senescence by PI3K pathway activation contributes to melanomagenesis. *Genes Dev.* **26**, 1055–1069 (2012).
353. Mackie, R. M., English, J., Aitchison, T. C., Fitzsimons, C. P. & Wilson, P. The number and distribution of benign pigmented moles (melanocytic naevi) in a healthy British population. *Br. J. Dermatol.* **113**, 167–174 (1985).
354. Duffy, K. & Grossman, D. The dysplastic nevus: From historical perspective to management in the modern era: Part I. Historical, histologic, and clinical aspects. *J. Am. Acad. Dermatol.* **67**, 1.e1-1.e16 (2012).
355. Tucker, M. A. *et al.* A natural history of melanomas and dysplastic nevi: An atlas of lesions in melanoma-prone families. *Cancer* **94**, 3192–3209 (2002).

356. Shitara, D. *et al.* Nevus-associated melanomas: Clinicopathologic features. *Am. J. Clin. Pathol.* **142**, 485–491 (2014).
357. Shain, A. H. & Bastian, B. C. The Genetic Evolution of Melanoma. *N. Engl. J. Med.* **374**, 991–993 (2016).
358. Hodis, E. *et al.* A landscape of driver mutations in melanoma. *Cell* **150**, 251–263 (2012).
359. Birck, A., Ahrenkiel, V., Zeuthen, J., Hou-Jensen, K. & Guldberg, P. Mutation and Allelic Loss of the PTEN/MMAC1 gene in Primary and Metastatic Melanoma Biopsies. *J. Invest. Dermatol.* **114**, 277–280 (2000).
360. Amaral, T. *et al.* The mitogen-activated protein kinase pathway in melanoma part I – Activation and primary resistance mechanisms to BRAF inhibition. *Eur. J. Cancer* **73**, 85–92 (2017).
361. Dhillon, A. S., Hagan, S., Rath, O. & Kolch, W. MAP kinase signalling pathways in cancer. *Oncogene* **26**, 3279–3290 (2007).
362. Sebolt-Leopold, J. S. & Herrera, R. Targeting the mitogen-activated protein kinase cascade to treat cancer. *Nat. Rev. Cancer* **4**, 937–947 (2004).
363. Downward, J. Targeting RAS signalling pathways in cancer therapy. *Nat. Rev. Cancer* **3**, 11–22 (2003).
364. Caponigro, F., Casale, M. & Bryce, J. Farnesyl transferase inhibitors in clinical development. *Expert Opin. Investig. Drugs* **12**, 943–954 (2003).
365. Guo, Y. *et al.* ERK/MAPK signalling pathway and tumorigenesis (Review). *Exp. Ther. Med.* 1997–2007 (2020) doi:10.3892/etm.2020.8454.
366. Wellbrock, C., Karasarides, M. & Marais, R. The RAF proteins take centre stage. *Nat. Rev. Mol. Cell Biol.* **5**, 875–885 (2004).
367. Davies, H. *et al.* Mutations of the BRAF gene in human cancer. *Nature* **417**, 949–954 (2002).
368. Ünal, E. B., Uhlitz, F. & Blüthgen, N. A compendium of ERK targets. *FEBS Lett.* **591**, 2607–2615 (2017).
369. Savoia, P., Fava, P., Casoni, F. & Cremona, O. Targeting the ERK signaling pathway in melanoma. *Int. J. Mol. Sci.* **20**, 1–37 (2019).
370. Wellbrock, C. & Arozarena, I. The complexity of the ERK/MAP-kinase pathway and the treatment of melanoma skin cancer. *Front. Cell Dev. Biol.* **4**, 1–9 (2016).
371. Akbani, R. *et al.* Genomic Classification of Cutaneous Melanoma. *Cell* **161**, 1681–1696 (2015).
372. Eisen, T. *et al.* Sorafenib in advanced melanoma: a Phase II randomised discontinuation trial analysis. *Br. J. Cancer* **95**, 581–586 (2006).
373. Kirkwood, J. M. *et al.* Phase II, open-label, randomized trial of the MEK1/2 inhibitor selumetinib as monotherapy versus temozolomide in patients with advanced melanoma. *Clin. cancer Res. an Off. J. Am. Assoc. Cancer Res.* **18**, 555–567 (2012).
374. LoRusso, P. M. *et al.* Phase I pharmacokinetic and pharmacodynamic study of the oral MAPK/ERK kinase inhibitor PD-0325901 in patients with advanced cancers. *Clin. cancer Res. an Off. J. Am. Assoc. Cancer Res.* **16**, 1924–1937 (2010).
375. McArthur, G. A. & Ribas, A. Targeting oncogenic drivers and the immune system in melanoma. *J. Clin. Oncol.* **31**, 499–506 (2013).
376. Liu, Y. & Gray, N. S. Rational design of inhibitors that bind to inactive kinase conformations. *Nat. Chem. Biol.* **2**, 358–364 (2006).
377. Chapman, P. B. *et al.* Improved Survival with Vemurafenib in Melanoma with BRAF V600E Mutation. *N. Engl. J. Med.* **364**, 2507–2516 (2011).

378. Hauschild, A. *et al.* Dabrafenib in BRAF-mutated metastatic melanoma: A multicentre, open-label, phase 3 randomised controlled trial. *Lancet* **380**, 358–365 (2012).
379. Johnson, D. B. *et al.* Acquired BRAF inhibitor resistance: A multicenter meta-analysis of the spectrum and frequencies, clinical behaviour, and phenotypic associations of resistance mechanisms. *Eur. J. Cancer* **51**, 2792–2799 (2015).
380. Roskoski, R. Targeting oncogenic Raf protein-serine/threonine kinases in human cancers. *Pharmacol. Res.* **135**, 239–258 (2018).
381. Flaherty, K. T. *et al.* Improved Survival with MEK Inhibition in BRAF-Mutated Melanoma. *N. Engl. J. Med.* **367**, 107–114 (2012).
382. Long, G. V. *et al.* Combined BRAF and MEK Inhibition versus BRAF Inhibition Alone in Melanoma. *N. Engl. J. Med.* **371**, 1877–1888 (2014).
383. Robert, C. *et al.* Improved Overall Survival in Melanoma with Combined Dabrafenib and Trametinib. *N. Engl. J. Med.* **372**, 30–39 (2015).
384. Larkin, J. *et al.* Combined Vemurafenib and Cobimetinib in BRAF -Mutated Melanoma. *N. Engl. J. Med.* **371**, 1867–1876 (2014).
385. Dummer, R. *et al.* Encorafenib plus binimetinib versus vemurafenib or encorafenib in patients with BRAF-mutant melanoma (COLUMBUS): a multicentre, open-label, randomised phase 3 trial. *Lancet Oncol.* **19**, 603–615 (2018).
386. Queirolo, P. & Spagnolo, F. Binimetinib for the treatment of NRAS-mutant melanoma. *Expert Rev. Anticancer Ther.* **17**, 985–990 (2017).
387. Ratterman, M., Hallmeyer, S. & Richards, J. Sequencing of New and Old Therapies for Metastatic Melanoma. *Curr. Treat. Options Oncol.* **17**, 1–9 (2016).
388. Eggermont, A. M. M. *et al.* Adjuvant ipilimumab versus placebo after complete resection of high-risk stage III melanoma (EORTC 18071): A randomised, double-blind, phase 3 trial. *Lancet Oncol.* **16**, 522–530 (2015).
389. Weber, J. S. *et al.* Adjuvant therapy with nivolumab (NIVO) versus ipilimumab (IPI) after complete resection of stage III/IV melanoma: Updated results from a phase III trial (CheckMate 238). *J. Clin. Oncol.* **36**, 9502 (2018).
390. Zimmer, L. *et al.* Adjuvant nivolumab plus ipilimumab or nivolumab monotherapy versus placebo in patients with resected stage IV melanoma with no evidence of disease (IMMUNED): a randomised, double-blind, placebo-controlled, phase 2 trial. *Lancet (London, England)* **395**, 1558–1568 (2020).
391. Yu, C. *et al.* Combination of immunotherapy with targeted therapy: Theory and practice in metastatic melanoma. *Front. Immunol.* **10**, (2019).
392. Michielin, O., Van Akkooi, A. C. J., Ascierto, P. A., Dummer, R. & Keilholz, U. Cutaneous melanoma: ESMO Clinical Practice Guidelines for diagnosis, treatment and follow-up. *Ann. Oncol.* **30**, 1884–1901 (2019).
393. Amaral, T. *et al.* MAPK pathway in melanoma part II—secondary and adaptive resistance mechanisms to BRAF inhibition. *Eur. J. Cancer* **73**, 93–101 (2017).
394. Johannessen, C. M. *et al.* COT drives resistance to RAF inhibition through MAP kinase pathway reactivation. *Nature* **468**, 968–972 (2010).
395. Nathanson, K. L. *et al.* Tumor genetic analyses of patients with metastatic melanoma treated with the BRAF inhibitor dabrafenib (GSK2118436). *Clin. Cancer Res.* **19**, 4868–4878 (2013).
396. Nissan, M. H. *et al.* Loss of NF1 in Cutaneous Melanoma Is Associated with RAS Activation and MEK Dependence. *Cancer Res.* **74**, 2340–2350 (2014).
397. Xing, F. *et al.* Concurrent loss of the PTEN and RB1 tumor suppressors attenuates RAF

dependence in melanomas harboring V600E BRAF. *Oncogene* **31**, 446–457 (2012).
398. Nazarian, R. *et al.* Melanomas acquire resistance to B-RAF(V600E) inhibition by RTK or N-RAS upregulation. *Nature* **468**, 973–977 (2010).
399. Montagut, C. *et al.* Elevated CRAF as a potential mechanism of acquired resistance to BRAF inhibition in melanoma. *Cancer Res.* **68**, 4853–4861 (2008).
400. Poulikakos, P. I. *et al.* RAF inhibitor resistance is mediated by dimerization of aberrantly spliced BRAF(V600E). *Nature* **480**, 387–390 (2011).
401. Trunzer, K. *et al.* Pharmacodynamic effects and mechanisms of resistance to vemurafenib in patients with metastatic melanoma. *J. Clin. Oncol. Off. J. Am. Soc. Clin. Oncol.* **31**, 1767–1774 (2013).
402. Goetz, E. M., Ghandi, M., Treacy, D. J., Wagle, N. & Garraway, L. A. ERK mutations confer resistance to mitogen-activated protein kinase pathway inhibitors. *Cancer Res.* **74**, 7079–7089 (2014).
403. Shi, H., Kong, X., Ribas, A. & Lo, R. S. Combinatorial treatments that overcome PDGFRβ-driven resistance of melanoma cells to V600EB-RAF inhibition. *Cancer Res.* **71**, 5067–5074 (2011).
404. Villanueva, J. *et al.* Acquired Resistance to BRAF Inhibitors Mediated by a RAF Kinase Switch in Melanoma Can Be Overcome by Cotargeting MEK and IGF-1R/PI3K. *Cancer Cell* **18**, 683–695 (2010).
405. Girotti, M. R. & Marais, R. Deja Vu: EGF receptors drive resistance to BRAF inhibitors. *Cancer Discov.* **3**, 487–490 (2013).
406. Shao, Y. & Aplin, A. E. Akt3-mediated resistance to apoptosis in B-RAF-targeted melanoma cells. *Cancer Res.* **70**, 6670–6681 (2010).
407. Shi, H. *et al.* Acquired resistance and clonal evolution in melanoma during BRAF inhibitor therapy. *Cancer Discov.* **4**, (2014).
408. Hugo, W. *et al.* Non-genomic and Immune Evolution of Melanoma Acquiring MAPKi Resistance. *Cell* **162**, 1271–1285 (2015).
409. Turajlic, S. *et al.* Whole genome sequencing of matched primary and metastatic acral melanomas. *Genome Res.* **22**, 196–207 (2012).
410. Tsoi, J. *et al.* Multi-stage Differentiation Defines Melanoma Subtypes with Differential Vulnerability to Drug-Induced Iron-Dependent Oxidative Stress. *Cancer Cell* **33**, 890-904.e5 (2018).
411. Rambow, F. *et al.* Toward Minimal Residual Disease-Directed Therapy in Melanoma. *Cell* **174**, 843-855.e19 (2018).
412. Rambow, F., Marine, J. C. & Goding, C. R. Melanoma plasticity and phenotypic diversity: Therapeutic barriers and opportunities. *Genes and Development*. **33** 1295–1318 (2019).
413. Arozarena, I. & Wellbrock, C. Phenotype plasticity as enabler of melanoma progression and therapy resistance. *Nat. Rev. Cancer* **19**, 377–391 (2019).
414. Bittner, M. *et al.* Molecular classification of cutaneous malignant melanoma by gene expression profiling. *Nature* **406**, 536–540 (2000).
415. Hoek, K. S. *et al.* Metastatic potential of melanomas defined by specific gene expression profiles with no BRAF signature. *Pigment Cell Res.* **19**, 290–302 (2006).
416. Hoek, K. S. *et al.* In vivo switching of human melanoma cells between proliferative and invasive states. *Cancer Res.* **68**, 650–656 (2008).
417. Widmer, D. S. *et al.* Systematic classification of melanoma cells by phenotype-specific gene expression mapping. *Pigment Cell Melanoma Res.* **25**, 343–353 (2012).
418. Tachibana, M. *et al.* Cochlear disorder associated with melanocyte anomaly in mice

with a transgenic insertional mutation. *Mol. Cell. Neurosci.* **3**, 433–445 (1992).
419. Steingrímsson, E. *et al.* Molecular basis of mouse microphthalmia (mi) mutations helps explain their developmental and phenotypic consequences. *Nat. Genet.* **8**, 256–263 (1994).
420. Garraway, L. A. *et al.* Integrative genomic analyses identify MITF as a lineage survival oncogene amplified in malignant melanoma. *Nature* **436**, 117–122 (2005).
421. Goding, C. R. & Arnheiter, H. MITF — the first 25 years. *Genes Dev.* 1–25 (2019) doi:10.1101/gad.324657.119.ness.
422. Widlund, H. R. *et al.* β-Catenin–induced melanoma growth requires the downstream target Microphthalmia-associated transcription factor. *J. Cell Biol.* **158**, 1079–1087 (2002).
423. Strub, T. *et al.* Essential role of microphthalmia transcription factor for DNA replication, mitosis and genomic stability in melanoma. *Oncogene* **30**, 2319–2332 (2011).
424. Carreira, S. *et al.* Mitf cooperates with Rb1 and activates p21Cip1 expression to regulate cell cycle progression. *Nature* **433**, 764–769 (2005).
425. Carreira, S. *et al.* Mitf regulation of Dia1 controls melanoma proliferation and invasiveness. *Genes Dev.* **20**, 3426–3439 (2006).
426. Huber, W. E. *et al.* A tissue-restricted cAMP transcriptional response: SOX10 modulates alpha-melanocyte-stimulating hormone-triggered expression of microphthalmia-associated transcription factor in melanocytes. *J. Biol. Chem.* **278**, 45224–45230 (2003).
427. Lang, D. *et al.* Pax3 functions at a nodal point in melanocyte stem cell differentiation. *Nature* **433**, 884–887 (2005).
428. Goodall, J. *et al.* Brn-2 Expression Controls Melanoma Proliferation and Is Directly Regulated by β-Catenin. *Mol. Cell. Biol.* **24**, 2915–2922 (2004).
429. Alexaki, V. I. *et al.* GLI2-mediated melanoma invasion and metastasis. *J. Natl. Cancer Inst.* **102**, 1148–1159 (2010).
430. Javelaud, D. *et al.* GLI2 and M-MITF transcription factors control exclusive gene expression programs and inversely regulate invasion in human melanoma cells. *Pigment Cell Melanoma Res.* **24**, 932–943 (2011).
431. Laurette, P. *et al.* Transcription factor MITF and remodeller BRG1 define chromatin organisation at regulatory elements in melanoma cells. *Elife* **2015**, 1–40 (2015).
432. Cronin, J. C. *et al.* SOX10 ablation arrests cell cycle, induces senescence, and suppresses melanomagenesis. *Cancer Res.* **73**, 5709–5718 (2013).
433. Verfaillie, A. *et al.* Decoding the regulatory landscape of melanoma reveals TEADS as regulators of the invasive cell state. *Nat. Commun.* **6**, 1–16 (2015).
434. Hoek, K. S. & Goding, C. R. Cancer stem cells versus phenotype-switching in melanoma. *Pigment Cell Melanoma Res.* **23**, 746–759 (2010).
435. Kim, I. S. *et al.* Microenvironment-derived factors driving metastatic plasticity in melanoma. *Nat. Commun.* **8**, (2017).
436. Konieczkowski, D. J. *et al.* A melanoma cell state distinction influences sensitivity to MAPK pathway inhibitors. *Cancer Discov.* **4**, 816–827 (2014).
437. Su, Y. *et al.* Single-cell analysis resolves the cell state transition and signaling dynamics associated with melanoma drug-induced resistance. *Proc. Natl. Acad. Sci. U. S. A.* **114**, 13679–13684 (2017).
438. Mehta, A. *et al.* Immunotherapy resistance by inflammation-induced dedifferentiation. *Cancer Discov.* **8**, 935–943 (2018).
439. Müller, J. *et al.* Low MITF/AXL ratio predicts early resistance to multiple targeted drugs

in melanoma. *Nat. Commun.* **5**, (2014).
440. Boshuizen, J. *et al.* Cooperative targeting of melanoma heterogeneity with an AXL antibody-drug conjugate and BRAF/MEK inhibitors. *Nat. Med.* **24**, 203–212 (2018).
441. Sáez-Ayala, M. *et al.* Directed Phenotype Switching as an Effective Antimelanoma Strategy. *Cancer Cell* **24**, 105–119 (2013).
442. Ennen, M. *et al.* Single-cell gene expression signatures reveal melanoma cell heterogeneity. *Oncogene* **34**, 3251–3263 (2015).
443. Ennen, M. *et al.* MITF-high and MITF-low cells and a novel subpopulation expressing genes of both cell states contribute to intra- and intertumoral heterogeneity of primary melanoma. *Clin. Cancer Res.* **23**, 7097–7107 (2017).
444. Wouters, J. *et al.* Robust gene expression programs underlie recurrent cell states and phenotype switching in melanoma. *Nat. Cell Biol.* **22**, 986–998 (2020).
445. Haass, N. K. *et al.* Real-time cell cycle imaging during melanoma growth, invasion, and drug response. *Pigment Cell Melanoma Res.* **27**, 764–776 (2014).
446. Falletta, P. *et al.* Translation reprogramming is an evolutionarily conserved driver of phenotypic plasticity and therapeutic resistance in melanoma. *Genes Dev.* **31**, 18–33 (2017).
447. Bai, X., Fisher, D. E. & Flaherty, K. T. Cell-state dynamics and therapeutic resistance in melanoma from the perspective of MITF and IFNγ pathways. *Nature Reviews Clinical Oncology* vol. 16 549–562 (2019).
448. Menon, D. R. *et al.* A stress-induced early innate response causes multidrug tolerance in melanoma. *Oncogene* **34**, 4448–4459 (2015).
449. Rusan, M. *et al.* Suppression of adaptive responses to targeted cancer therapy by transcriptional repression. *Cancer Discovery*. **8**, 59-73 (2018).
450. Echevarría-Vargas, I. M. *et al.* Co-targeting BET and MEK as salvage therapy for MAPK and checkpoint inhibitor-resistant melanoma . *EMBO Mol. Med.* **10**, 1–15 (2018).
451. Wellbrock, C. *et al.* Oncogenic BRAF regulates melanoma proliferation through the lineage specific factor MITF. *PLoS One* **3**, (2008).
452. Smith, M. P. *et al.* Inhibiting Drivers of Non-mutational Drug Tolerance Is a Salvage Strategy for Targeted Melanoma Therapy. *Cancer Cell* **29**, 270–284 (2016).
453. Yang, G. *et al.* Inhibition of PAX3 by TGF-β Modulates Melanocyte Viability. *Mol. Cell* **32**, 554–563 (2008).
454. Smith, M. P. *et al.* A PAX3/BRN2 rheostat controls the dynamics of BRAF mediated MITF regulation in MITFhigh/AXLlow melanoma. *Pigment Cell Melanoma Res.* **32**, 280–291 (2019).
455. Takeda, K. *et al.* Induction of melanocyte-specific microphthalmia-associated transcription factor by Wnt-3a. *J. Biol. Chem.* **275**, 14013–14016 (2000).
456. Ngeow, K. C. *et al.* BRAF/MAPK and GSK3 signaling converges to control MITF nuclear export. *Proc. Natl. Acad. Sci. U. S. A.* **115**, E8668–E8677 (2018).
457. Liu, F. *et al.* Stat3-targeted therapies overcome the acquired resistance to vemurafenib in melanomas. *J. Invest. Dermatol.* **133**, 2041–2049 (2013).
458. Haq, R. *et al.* BCL2A1 is a lineage-specific antiapoptotic melanoma oncogene that confers resistance to BRAF inhibition. *Proc. Natl. Acad. Sci. U. S. A.* **110**, 4321–4326 (2013).
459. Fufa, T. D. *et al.* MEK inhibition remodels the active chromatin landscape and induces SOX10 genomic recruitment in BRAF(V600E) mutant melanoma cells. *Epigenetics and Chromatin* **12**, 1–18 (2019).

460. Haq, R. *et al.* Article Oncogenic BRAF Regulates Oxidative Metabolism via PGC1 a and MITF. *Cancer Cell* **23**, 302–315 (2013).
461. Parmenter, T. J. *et al.* Response of BRAF -Mutant Melanoma to BRAF Inhibition Is Mediated by a Network of Transcriptional Regulators of Glycolysis. *Cancer Discovery.* **4**, 423-433 (2014).
462. Serasinghe, M. N. *et al.* Mitochondrial division is requisite to RAS-induced transformation and targeted by oncogenic MAPK pathway inhibitors. *Mol. Cell* **57**, 521–536 (2015).
463. Li, J. *et al.* Mitochondrial elongation-mediated glucose metabolism reprogramming is essential for tumour cell survival during energy stress. *Oncogene* **36**, 4901–4912 (2017).
464. Han, S. *et al.* ERK-mediated phosphorylation regulates SOX10 sumoylation and targets expression in mutant BRAF melanoma. *Nat. Commun.* **9**, 1–14 (2018).
465. Abel, E. V. *et al.* Melanoma adapts to RAF/MEK inhibitors through FOXD3-mediated upregulation of ERBB3. *J. Clin. Invest.* **123**, 2155–2168 (2013).
466. Boregowda, R. K. *et al.* The transcription factor RUNX2 regulates receptor tyrosine kinase expression in melanoma. *Oncotarget* **7**, 29689–29707 (2016).
467. Titz, B. *et al.* JUN dependency in distinct early and late BRAF inhibition adaptation states of melanoma. *Cell Discov.* **2**, (2016).
468. Kim, M. H. *et al.* Actin remodeling confers BRAF inhibitor resistance to melanoma cells through YAP/TAZ activation. *EMBO J.* **35**, 462–478 (2016).
469. Boussemart, L. *et al.* eIF4F is a nexus of resistance to anti-BRAF and anti-MEK cancer therapies. *Nature* **513**, 105–109 (2014).
470. Shostak, K. *et al.* Codon-specific translation reprogramming promotes resistance to targeted therapy. *Nature* (2018).
471. Faião-Flores, F. *et al.* Targeting the hedgehog transcription factors GLI1 and GLI2 restores sensitivity to vemurafenib-resistant human melanoma cells. *Oncogene* **36**, 1849–1861 (2017).
472. Ramsdale, R. *et al.* The transcription cofactor c-JUN mediates phenotype switching and BRAF inhibitor resistance in melanoma. *Sci. Signal.* **8**, ra82 (2015).
473. Talebi, A. *et al.* Sustained SREBP-1-dependent lipogenesis as a key mediator of resistance to BRAF-targeted therapy. *Nat. Commun.* **9**, 1–11 (2018).
474. Zhang, G. *et al.* Targeting mitochondrial biogenesis to overcome drug resistance to MAPK inhibitors. *J. Clin. Invest.* **126**, 1834–1856 (2016).
475. Hsieh, J. J. *et al.* Renal cell carcinoma. *Nat. Rev. Dis. Prim.* **3**, 1–19 (2017).
476. Haas, N. B. & Nathanson, K. L. Hereditary Kidney Cancer Syndromes. *Adv. Chronic Kidney Dis.* **21**, 81–90 (2014).
477. Bianchi, M. *et al.* Distribution of metastatic sites in renal cell carcinoma: a population-based analysis. *Ann. Oncol.* **23**, 973–980 (2012).
478. McKay, R. R. *et al.* Impact of Bone and Liver Metastases on Patients with Renal Cell Carcinoma Treated with Targeted Therapy. *Eur. Urol.* **65**, 577–584 (2014).
479. Weichselbaum, R. R. & Hellman, S. Oligometastases revisited. *Nat. Rev. Clin. Oncol.* **8**, 378–382 (2011).
480. Escudier, B. *et al.* Renal cell carcinoma: ESMO Clinical Practice Guidelines for diagnosis, treatment and follow-up. *Ann. Oncol.* **30**, 706–720 (2019).
481. Haas, N. B. *et al.* Adjuvant sunitinib or sorafenib for high-risk, non-metastatic renal-cell carcinoma (ECOG-ACRIN E2805): A double-blind, placebo-controlled, randomised, phase 3 trial. *Lancet* **387**, 2008–2016 (2016).

482. Bex, A., Ljungberg, B., van Poppel, H. & Powles, T. The Role of Cytoreductive Nephrectomy: European Association of Urology Recommendations in 2016. *Eur. Urol.* **70**, 901–905 (2016).
483. Kovacs, G. *et al.* The Heidelberg classification of renal cell tumours. *J. Pathol.* **183**, 131–133 (1997).
484. Marconi, L. *et al.* Systematic Review and Meta-analysis of Diagnostic Accuracy of Percutaneous Renal Tumour Biopsy. *Eur. Urol.* **69**, 660–673 (2016).
485. De Peralta-Venturina, M. *et al.* Sarcomatoid differentiation in renal cell carcinoma: A study of 101 cases. *Am. J. Surg. Pathol.* **25**, 275–284 (2001).
486. Creighton, C. J. *et al.* Comprehensive molecular characterization of clear cell renal cell carcinoma. *Nature* **499**, 43–49 (2013).
487. Network, T. C. G. A. R. Comprehensive Molecular Characterization of Papillary Renal-Cell Carcinoma. *N. Engl. J. Med.* **374**, 135–145 (2016).
488. Davis, C. F. *et al.* The somatic genomic landscape of chromophobe renal cell carcinoma. *Cancer Cell* **26**, 319–330 (2014).
489. Ricketts, C. J. *et al.* The Cancer Genome Atlas Comprehensive Molecular Characterization of Renal Cell Carcinoma. *Cell Rep.* **23**, 313-326.e5 (2018).
490. Linehan, W. M. & Ricketts, C. J. The Cancer Genome Atlas of renal cell carcinoma: findings and clinical implications. *Nat. Rev. Urol.* **16**, 539–552 (2019).
491. Hakimi, A. A. *et al.* An Integrated Metabolic Atlas of Clear Cell Renal Cell Carcinoma. *Cancer Cell* **29**, 104–116 (2016).
492. Kapitsinou, P. P. & Haase, V. H. The VHL tumor suppressor and HIF: Insights from genetic studies in mice. *Cell Death Differ.* **15**, 650–659 (2008).
493. Herman, J. G. *et al.* Silencing of the VHL tumor-suppressor gene by DNA methylation in renal carcinoma. *Proc. Natl. Acad. Sci. U. S. A.* **91**, 9700–9704 (1994).
494. Tiedemann, R. L. *et al.* Dynamic reprogramming of DNA methylation in SETD2-deregulated renal cell carcinoma. *Oncotarget* **7**, 1927–1946 (2016).
495. Morris, M. R. *et al.* Identification of candidate tumour suppressor genes frequently methylated in renal cell carcinoma. *Oncogene* **29**, 2104–2117 (2010).
496. Brannon, A. R. *et al.* Molecular stratification of clear cell renal cell carcinoma by consensus clustering reveals distinct subtypes and survival patterns. *Genes and Cancer* **1**, 152–163 (2010).
497. Lameirinhas, A., Miranda-Gonçalves, V., Henrique, R. & Jerónimo, C. The complex interplay between metabolic reprogramming and epigenetic alterations in renal cell carcinoma. *Genes (Basel).* **10**, (2019).
498. Chen, F. *et al.* Multilevel Genomics-Based Taxonomy of Renal Cell Carcinoma. *Cell Rep.* **14**, 2476–2489 (2016).
499. Clark, D. J. *et al.* Integrated Proteogenomic Characterization of Clear Cell Renal Cell Carcinoma. *Cell* **179**, 964-983.e31 (2019).
500. Turajlic, S. *et al.* Deterministic Evolutionary Trajectories Influence Primary Tumor Growth: TRACERx Renal. *Cell* **173**, 595-610.e11 (2018).
501. Potente, M., Gerhardt, H. & Carmeliet, P. Basic and therapeutic aspects of angiogenesis. *Cell* **146**, 873–887 (2011).
502. Richards, F. M. *et al.* Mapping the Von Hippel-Lindau disease tumour suppressor gene: identification of germline deletions by pulsed field gel electrophoresis. *Hum. Mol. Genet.* **2**, 879–882 (1993).
503. Conti, A. *et al.* Progress of molecular targeted therapies for advanced renal cell

carcinoma. *Biomed Res. Int.* **2013**, (2013).
504. Ma, S. *et al.* The role of tumor microenvironment in resistance to anti-angiogenic therapy. *F1000Research* **7**, 326 (2018).
505. McDermott, D. F. *et al.* Randomized phase III trial of high-dose interleukin-2 versus subcutaneous interleukin-2 and interferon in patients with metastatic renal cell carcinoma. *J. Clin. Oncol. Off. J. Am. Soc. Clin. Oncol.* **23**, 133–141 (2005).
506. Escudier, B. *et al.* Sorafenib in Advanced Clear-Cell Renal-Cell Carcinoma. *N. Engl. J. Med.* **356**, 125–134 (2007).
507. Motzer, R. J. *et al.* Sunitinib versus Interferon Alfa in Metastatic Renal-Cell Carcinoma. *N. Engl. J. Med.* **356**, 115–124 (2007).
508. Motzer, R. J. *et al.* Pazopanib versus Sunitinib in Metastatic Renal-Cell Carcinoma. *N. Engl. J. Med.* **369**, 722–731 (2013).
509. Rini, B. I. *et al.* Comparative effectiveness of axitinib versus sorafenib in advanced renal cell carcinoma (AXIS): a randomised phase 3 trial. *Lancet (London, England)* **378**, 1931–1939 (2011).
510. Hutson, T. E. *et al.* Axitinib versus sorafenib as first-line therapy in patients with metastatic renal-cell carcinoma: a randomised open-label phase 3 trial. *Lancet. Oncol.* **14**, 1287–1294 (2013).
511. Escudier, B. *et al.* Phase III trial of bevacizumab plus interferon alfa-2a in patients with metastatic renal cell carcinoma (AVOREN): final analysis of overall survival. *J. Clin. Oncol. Off. J. Am. Soc. Clin. Oncol.* **28**, 2144–2150 (2010).
512. Santoni, M. & Massari, F. Chapter 25 - mTOR Pathway in Renal Cell Carcinoma. in (ed. Maiese, K. B. T.-M. to M. with mTOR) 417–428 (Academic Press, 2016). doi:https://doi.org/10.1016/B978-0-12-802733-2.00026-8.
513. Hudes, G. *et al.* Temsirolimus, Interferon Alfa, or Both for Advanced Renal-Cell Carcinoma. *N. Engl. J. Med.* **356**, 2271–2281 (2007).
514. Motzer, R. J. *et al.* Efficacy of everolimus in advanced renal cell carcinoma: a double-blind, randomised, placebo-controlled phase III trial. *Lancet* **372**, 449–456 (2008).
515. Atkins, M. B. & Tannir, N. M. Current and emerging therapies for first-line treatment of metastatic clear cell renal cell carcinoma. *Cancer Treat. Rev.* **70**, 127–137 (2018).
516. Motzer, R. J. *et al.* Lenvatinib, everolimus, and the combination in patients with metastatic renal cell carcinoma: a randomised, phase 2, open-label, multicentre trial. *Lancet. Oncol.* **16**, 1473–1482 (2015).
517. Choueiri, T. K. *et al.* Cabozantinib versus Everolimus in Advanced Renal-Cell Carcinoma. *N. Engl. J. Med.* **373**, 1814–1823 (2015).
518. Motzer, R. J. *et al.* Nivolumab versus Everolimus in Advanced Renal-Cell Carcinoma. *N. Engl. J. Med.* **373**, 1803–1813 (2015).
519. Motzer, R. J. *et al.* Nivolumab plus Ipilimumab versus Sunitinib in Advanced Renal-Cell Carcinoma. *N. Engl. J. Med.* **378**, 1277–1290 (2018).
520. Yang, D. C. & Chen, C. H. Potential New Therapeutic Approaches for Renal Cell Carcinoma. *Semin. Nephrol.* **40**, 86–97 (2020).
521. Rini, B. I. *et al.* Atezolizumab plus bevacizumab versus sunitinib in patients with previously untreated metastatic renal cell carcinoma (IMmotion151): a multicentre, open-label, phase 3, randomised controlled trial. *Lancet* **393**, 2404–2415 (2019).
522. Kotecha, R. R., Motzer, R. J. & Voss, M. H. Towards individualized therapy for metastatic renal cell carcinoma. *Nat. Rev. Clin. Oncol.* **16**, 621–633 (2019).
523. Porta, C. *et al.* The adjuvant treatment of kidney cancer: a multidisciplinary outlook.

Nat. Rev. Nephrol. **15**, 423–433 (2019).
524. Brooks, S. A. *et al.* ClearCode34: A prognostic risk predictor for localized clear cell renal cell carcinoma. *Eur. Urol.* **66**, 77–84 (2014).
525. Rini, B. *et al.* A 16-gene assay to predict recurrence after surgery in localised renal cell carcinoma: development and validation studies. *Lancet. Oncol.* **16**, 676–685 (2015).
526. Kapur, P. *et al.* Effects on survival of BAP1 and PBRM1 mutations in sporadic clear-cell renal-cell carcinoma: a retrospective analysis with independent validation. *Lancet. Oncol.* **14**, 159–167 (2013).
527. Motzer, R. J. *et al.* Molecular Subsets in Renal Cancer Determine Outcome to Checkpoint and Angiogenesis Blockade. *Cancer Cell* **38**, 803-817.e4 (2020).
528. Gupta, K., Miller, J. D., Li, J. Z., Russell, M. W. & Charbonneau, C. Epidemiologic and socioeconomic burden of metastatic renal cell carcinoma (mRCC): a literature review. *Cancer Treat. Rev.* **34**, 193–205 (2008).
529. Leibovich, B. C. *et al.* Prediction of progression after radical nephrectomy for patients with clear cell renal cell carcinoma: a stratification tool for prospective clinical trials. *Cancer* **97**, 1663–1671 (2003).
530. da Costa, W. H. *et al.* Impact of renal vein invasion and fat invasion in pT3a renal cell carcinoma. *BJU Int.* **109**, 544–548 (2012).
531. Zhang, B. Y. *et al.* A novel prognostic model for patients with sarcomatoid renal cell carcinoma. *BJU Int.* **115**, 405–411 (2015).
532. Gerlinger, M. *et al.* Intratumor Heterogeneity and Branched Evolution Revealed by Multiregion Sequencing. *N. Engl. J. Med.* **366**, 883–892 (2012).
533. Gerlinger, M. *et al.* Genomic architecture and evolution of clear cell renal cell carcinomas defined by multiregion sequencing. *Nat. Genet.* **46**, 225–233 (2014).
534. Wei, E. Y. & Hsieh, J. J. A river model to map convergent cancer evolution and guide therapy in RCC. *Nat. Rev. Urol.* **12**, 706–712 (2015).
535. Sankin, A. *et al.* The impact of genetic heterogeneity on biomarker development in kidney cancer assessed by multiregional sampling. *Cancer Med.* **3**, 1485–1492 (2014).
536. Robinson, D. R. *et al.* Integrative clinical genomics of metastatic cancer. *Nature* **548**, 297–303 (2017).
537. Turajlic, S. *et al.* Tracking Cancer Evolution Reveals Constrained Routes to Metastases: TRACERx Renal. *Cell* **173**, 581-594.e12 (2018).
538. Young, M. D. *et al.* Single-cell transcriptomes from human kidneys reveal the cellular identity of renal tumors. *Science.* **361**, 594–599 (2018).
539. Tirosh, I. *et al.* Dissecting the multicellular ecosystem of metastatic melanoma by single-cell RNA-seq. *Science.* **352**, 189–196 (2016).
540. Jerby-Arnon, L. *et al.* A Cancer Cell Program Promotes T Cell Exclusion and Resistance to Checkpoint Blockade. *Cell* **175**, 984-997.e24 (2018).
541. Hu, J. *et al.* Single-Cell Transcriptome Analysis Reveals Intratumoral Heterogeneity in ccRCC, which Results in Different Clinical Outcomes. *Mol. Ther.* **28**, 1658–1672 (2020).
542. Flippot, R., Beinse, G., Boilève, A., Vibert, J. & Malouf, G. G. Long non-coding RNAs in genitourinary malignancies: a whole new world. *Nature Reviews Urology* vol. 16 484–504 (2019).
543. Leucci, E., Coe, E. A., Marine, J. C. & Vance, K. W. The emerging role of long non-coding RNAs in cutaneous melanoma. *Pigment Cell Melanoma Res.* **29**, 619–626 (2016).
544. Disney, M. D., Dwyer, B. G. & Childs-Disney, J. L. Drugging the RNA world. *Cold Spring Harb. Perspect. Biol.* **10**, (2018).

545. Bennett, C. F. Therapeutic antisense oligonucleotides are coming of age. *Annu. Rev. Med.* **70**, 307–321 (2019).
546. Crooke, S. T., Witztum, J. L., Bennett, C. F. & Baker, B. F. RNA-Targeted Therapeutics. *Cell Metab.* **27**, 714–739 (2018).
547. Roberts, T. C., Langer, R. & Wood, M. J. A. Advances in oligonucleotide drug delivery. *Nat. Rev. Drug Discov.* **19**, 673–694 (2020).
548. Kim, J. *et al.* Patient-Customized Oligonucleotide Therapy for a Rare Genetic Disease. *N. Engl. J. Med.* **381**, 1644–1652 (2019).
549. Quemener, A. M. *et al.* The powerful world of antisense oligonucleotides: From bench to bedside. *Wiley Interdiscip. Rev. RNA* **11**, 1–22 (2020).
550. Koshkin, A. A. *et al.* LNA (Locked Nucleic Acids): Synthesis of the adenine, cytosine, guanine, 5-methylcytosine, thymine and uracil bicyclonucleoside monomers, oligomerisation, and unprecedented nucleic acid recognition. *Tetrahedron* **54**, 3607–3630 (1998).
551. Shen, W. *et al.* Chemical modification of PS-ASO therapeutics reduces cellular protein-binding and improves the therapeutic index. *Nat. Biotechnol.* **37**, 640–650 (2019).
552. Inoue, H. *et al.* Synthesis and hybridization studies on two complementary nona(2'-O-methyl)ribonucleotides. *Nucleic Acids Res.* **15**, 6131–6148 (1987).
553. Soifer, H. S. *et al.* Silencing of gene expression by gymnotic delivery of antisense oligonucleotides. *Methods Mol. Biol.* **815**, 333–346 (2012).
554. Crooke, S. T., Wang, S., Vickers, T. A., Shen, W. & Liang, X. H. Cellular uptake and trafficking of antisense oligonucleotides. *Nat. Biotechnol.* **35**, 230–237 (2017).
555. Prakash, T. P. *et al.* Targeted delivery of antisense oligonucleotides to hepatocytes using triantennary N-acetyl galactosamine improves potency 10-fold in mice. *Nucleic Acids Res.* **42**, 8796–8807 (2014).
556. Viney, N. J. *et al.* Antisense oligonucleotides targeting apolipoprotein(a) in people with raised lipoprotein(a): two randomised, double-blind, placebo-controlled, dose-ranging trials. *Lancet* **388**, 2239–2253 (2016).
557. Liang, X. H., Sun, H., Shen, W. & Crooke, S. T. Identification and characterization of intracellular proteins that bind oligonucleotides with phosphorothioate linkages. *Nucleic Acids Res.* **43**, 2927–2945 (2015).
558. Liang, X., Shen, W., Sun, H., Prakash, T. P. & Crooke, S. T. TCP1 complex proteins interact with phosphorothioate oligonucleotides and can co-localize in oligonucleotide-induced nuclear bodies in mammalian cells. *Nucleic Acids Res.* **42**, 7819–7832 (2014).
559. Lorenz, P., Misteli, T., Baker, B. F., Bennett, C. F. & Spector, D. L. Nucleocytoplasmic shuttling: a novel in vivo property of antisense phosphorothioate oligodeoxynucleotides. *Nucleic Acids Res.* **28**, 582–592 (2000).
560. Shen, W., Liang, X. & Crooke, S. T. Phosphorothioate oligonucleotides can displace NEAT1 RNA and form nuclear paraspeckle-like structures. *Nucleic Acids Res.* **42**, 8648–8662 (2014).
561. Lorenz, P., Baker, B. F., Bennett, C. F. & Spector, D. L. Phosphorothioate antisense oligonucleotides induce the formation of nuclear bodies. *Mol. Biol. Cell* **9**, 1007–1023 (1998).
562. Vickers, T. A. & Crooke, S. T. Development of a quantitative BRET affinity assay for nucleic acid-protein interactions. *PLoS One* **11**, 1–17 (2016).
563. Hagedorn, P. H. *et al.* Locked nucleic acid: modality, diversity, and drug discovery. *Drug Discov. Today* **23**, 101–114 (2018).

564. Geary, R. S. Antisense oligonucleotide pharmacokinetics and metabolism. *Expert Opin. Drug Metab. Toxicol.* **5**, 381–391 (2009).
565. Geary, R. S., Henry, S. P. & Grillone, L. R. Fomivirsen. *Clin. Pharmacokinet.* **41**, 255–260 (2002).
566. Rigo, F. *et al.* Pharmacology of a Central Nervous System Delivered 2'- O -Methoxyethyl–Modified Survival of Motor Neuron Splicing Oligonucleotide in Mice and Nonhuman Primates. *J. Pharmacol. Exp. Ther.* **350**, 46–55 (2014).
567. Finkel, R. S. *et al.* Nusinersen versus Sham Control in Infantile-Onset Spinal Muscular Atrophy. *N. Engl. J. Med.* **377**, 1723–1732 (2017).
568. Darras, B. T., Markowitz, J. A., Monani, U. R. & De Vivo, D. C. Spinal Muscular Atrophies. in *Neuromuscular Disorders of Infancy, Childhood, and Adolescence* 117–145 (Elsevier, 2015). doi:10.1016/B978-0-12-417044-5.00008-1.
569. Hua, Y. *et al.* Peripheral SMN restoration is essential for long-term rescue of a severe spinal muscular atrophy mouse model. *Nature* **478**, 123–126 (2011).
570. Groner, B., Lucks, P. & Borghouts, C. The function of Stat3 in tumor cells and their microenvironment. *Semin. Cell Dev. Biol.* **19**, 341–350 (2008).
571. Hong, D. *et al.* AZD9150, a next-generation antisense oligonucleotide inhibitor of STAT3 with early evidence of clinical activity in lymphoma and lung cancer. *Sci. Transl. Med.* **7**, (2015).
572. Reilley, M. J. *et al.* STAT3 antisense oligonucleotide AZD9150 in a subset of patients with heavily pretreated lymphoma: results of a phase 1b trial. *J. Immunother. cancer* **6**, 119 (2018).
573. Wang, X., Chen, M., Zhou, J. & Zhang, X. HSP27, 70 and 90, anti-apoptotic proteins, in clinical cancer therapy. *Int. J. Oncol.* **45**, 18–30 (2014).
574. Rosenberg, J. E. *et al.* Pivotal Trial of Enfortumab Vedotin in Urothelial Carcinoma After Platinum and Anti-Programmed Death 1/Programmed Death Ligand 1 Therapy. *J. Clin. Oncol.* **37**, 2592–2600 (2019).
575. Gilot, D. *et al.* A non-coding function of TYRP1 mRNA promotes melanoma growth. *Nat. Cell Biol.* **19**, 1348–1357 (2017).
576. Sarfi, M., Abbastabar, M. & Khalili, E. Long noncoding RNAs biomarker-based cancer assessment. *J. Cell. Physiol.* **234**, 16971–16986 (2019).
577. Renganathan, A. & Felley-Bosco, E. Long noncoding RNAs in cancer and therapeutic potential. *Adv. Exp. Med. Biol.* **1008**, 199–222 (2017).
578. Zaporozhchenko, I. A., Ponomaryova, A. A., Rykova, E. Y. & Laktionov, P. P. The potential of circulating cell-free RNA as a cancer biomarker: challenges and opportunities. *Expert Rev. Mol. Diagn.* **18**, 133–145 (2018).
579. Groskopf, J. *et al.* APTIMA PCA3 molecular urine test: Development of a method to aid in the diagnosis of prostate cancer. *Clin. Chem.* **52**, 1089–1095 (2006).
580. Bussemakers, M. J. *et al.* DD3: a new prostate-specific gene, highly overexpressed in prostate cancer. *Cancer Res.* **59**, 5975–9 (1999).
581. Lee, G. L., Dobi, A. & Srivastava, S. Diagnostic performance of the PCA3 urine test. *Nat. Rev. Urol.* **8**, 123–124 (2011).
582. Ploussard, G. & De La Taille, A. Urine biomarkers in prostate cancer. *Nat. Rev. Urol.* **7**, 101–109 (2010).
583. Ploussard, G. *et al.* The prostate cancer gene 3 (PCA3) urine test in men with previous negative biopsies: does free-to-total prostate-specific antigen ratio influence the performance of the PCA3 score in predicting positive biopsies? *BJU Int.* **106**, 1143–1147

(2010).
584. Fleischhacker, M. & Schmidt, B. Circulating nucleic acids (CNAs) and cancer--a survey. *Biochim. Biophys. Acta* **1775**, 181–232 (2007).
585. Zidan, H. E., Karam, R. A., El-Seifi, O. S. & Abd Elrahman, T. M. Circulating long non-coding RNA MALAT1 expression as molecular biomarker in Egyptian patients with breast cancer. *Cancer Genet.* **220**, 32–37 (2018).
586. Wang, F. *et al.* Development and prospective multicenter evaluation of the long noncoding RNA MALAT-1 as a diagnostic urinary biomarker for prostate cancer. *Oncotarget* **5**, 11091–11102 (2014).
587. De Rubis, G., Rajeev Krishnan, S. & Bebawy, M. Liquid Biopsies in Cancer Diagnosis, Monitoring, and Prognosis. *Trends Pharmacol. Sci.* **40**, 172–186 (2019).
588. Potrich, C. *et al.* OncomiR detection in circulating body fluids: A PDMS microdevice perspective. *Lab Chip* **14**, 4067–4075 (2014).
589. Wan, J. C. M. *et al.* Liquid biopsies come of age: Towards implementation of circulating tumour DNA. *Nat. Rev. Cancer* **17**, 223–238 (2017).
590. Gerami, P., Alsobrook, J. P., Palmer, T. J. & Robin, H. S. Development of a novel noninvasive adhesive patch test for the evaluation of pigmented lesions of the skin. *J. Am. Acad. Dermatol.* **71**, 237–244 (2014).
591. Gerami, P. *et al.* Development and validation of a noninvasive 2-gene molecular assay for cutaneous melanoma. *J. Am. Acad. Dermatol.* **76**, 114-120.e2 (2017).
592. Flippot, R. *et al.* Expression of long non-coding RNA MFI2-AS1 is a strong predictor of recurrence in sporadic localized clear-cell renal cell carcinoma. *Sci. Rep.* **7**, 1–9 (2017).

SECTION 3 - LINC00518 INTERACTION WITH THE GTPASE RAP2C PROMOTES OXIDATIVE PHOSPHORYLATION, MELANOMA CELL SURVIVAL AND RESISTANCE TO BRAF INHIBITION

Giovanni Gambi[1,2,3,4], Guillaume Davidson[1,2,3,4], Alessandro Cuomo[5], Tiziana Bonaldi[5], Sonia Cinque[6], Gabriel Malouf[1,2,3,4], Eleonora Leucci[6] and Irwin Davidson[1, 2, 3, 4, 7].

[1] Institut de Génétique et de Biologie Moléculaire et Cellulaire, Equipe Labélisée Ligue contre le Cancer. BP 163, 67404 Illkirch Cedex, C.U. Strasbourg, France

[2] Centre National de la Recherche Scientifique, UMR7104, 67404 Illkirch, France

[3] Institut National de la Santé et de la Recherche Médicale, U1258, 67404 Illkirch, France

[4] Université de Strasbourg, 67404 Illkirch, France

[5] Nuclear Proteomics to Study Gene Expression Regulation in Cancer Unit. Istituto Europeo di Oncologia. Via Adamello 16, 20139 Milano. Italy.

[6] Laboratory for RNA cancer biology. KU Leuven. ON I Herestraat 49, 3000 Leuven. Belgium.

[7] To whom correspondence should be addressed

Running Title : LINC00518 regulates oxidative phosphorylation

Key words : lncRNAs, melanoma, metabolism, GTPases, MAPK inhibition

ABSTRACT

The lineage-defining transcription factors MITF (Microphthalmia-associated transcription factor) and SOX10 promote melanoma cell proliferation and survival by regulating a repertoire of protein coding genes and the long intergenic non-coding (Linc)RNA SAMMSON. Here we show that MITF and SOX10 regulate the melanoma-expressed Linc00518 and Linc00520 whose expression is associated with disease progression in patients and that are essential for melanoma cell viability. Linc00518, Linc00520 and SAMMSON define a network of SOX10/MITF regulated LincRNAs that act cooperatively to promote melanoma cell survival. We show that Linc00518 interacts with the small GTPases of the RAP2 family, specifically RAP2C, promoting DRP1 phosphorylation and mitochondrial fusion to favour optimal oxidative phosphorylation required for melanoma cell proliferation and survival. We further show that Linc00518 and RAP2C are required for the metabolic switch from glycolysis to oxidative phosphorylation upon treatment with BRAF and MAP kinase inhibitors. Consequently, Linc00518 and RAP2C silencing cooperate with BRAF and MAP kinase inhibitors to induce melanoma cell apoptosis.

INTRODUCTION

Melanoma tumours can be highly heterogeneous, comprising cell populations with distinct properties and gene expression signatures (Konieczkowski et al. 2014; Müller et al. 2014; Tirosh et al. 2016; Tsoi et al. 2018; Ennen et al. 2017; Rambow et al. 2018; Rambow, Marine, and Goding 2019). Melanocytic type cells express the lineage-defining transcription factors MITF (Microphthalmia-associated transcription factor) and SOX10, neural crest-like cells express SOX10, but not MITF (Rambow et al. 2018; Laurette et al. 2020) while targeted

therapies can induce additional cells states such as the undifferentiated state expressing neither MITF nor SOX10 (Landsberg et al. 2012; Riesenberg et al. 2015; Jerby-Arnon et al. 2018; Rambow et al. 2018; Bai, Fisher, and Flaherty 2019). MITF and SOX10 bind together at cis-regulatory elements driving a gene expression program underlying many physiological features of melanocytes and melanocytic-type melanoma cells (Laurette et al. 2015; Seberg et al. 2017; Goding and Arnheiter 2019; Wouters et al. 2020). They promote proliferation and survival by regulating genes involved in DNA replication, DNA repair and mitosis as well as various aspects of cell metabolism (Giuliano et al. 2010; Strub et al. 2011; Shakhova et al. 2012; Cronin et al. 2013; Louphrasitthiphol et al. 2019). In addition, SOX10 regulates expression of the long intergenic non-coding (linc)RNA SAMMSON (Linc01212), essential for melanoma cell proliferation and survival (Leucci et al. 2016; Vendramin et al. 2018). The survival and proliferation halmark effects of SOX10 and/or MITF are therefore mediated by both protein coding genes and LincRNAs.

Through profiling of MITF and SOX10 genome localisation and RNA-seq following their knockdown, we identified Linc00518 and Linc00520 as novel SOX10 and MITF target genes highly expressed in melanoma and essential for melanoma cell proliferation and survival. These lincRNAs act cooperatively with each other and with SAMMSON defining a network of SOX10/MITF regulated lincRNAs that together promote melanoma cell survival and proliferation. We show that Linc00518 interacts with the small GTPases of the RAP2 family, specifically RAP2C, promoting DRP1 phosphorylation and mitochondrial fusion to favour optimal oxidative phosphorylation required for cell proliferation and survival and resistance to BRAF inhibitors.

RESULTS

MITF and SOX10-regulated LincRNAs in melanoma.

In addition to SAMMSON, ChIP-seq and RNA-seq in 501Mel cells identified Linc00518 (hereafter L518) and Linc00520 (L520) as MITF and/or SOX10 regulated genes. L518 lies close to the TFAP2A locus and its proximal promoter comprised a prominent SOX10 binding site (Fig. 1A). The L520 locus comprised multiple binding sites for MITF in the proximal promoter and upstream regions (Fig. 1A). At each locus, the MITF and/or SOX10 binding sites were associated with binding of BRG1 and high levels of H3K27ac. RNA-seq following siRNA-mediated MITF or SOX10 silencing in 501Mel cells showed that L518 was regulated by both MITF and SOX10, while L520 was regulated by MITF (Fig. 1B and (Laurette et al. 2015)). The proximal promoters of these primate-specific LincRNAs are formed by insertions of retroviral long terminal repeats (LTR), MLT1B ERVL-MaLR for L518 and THE1B ERVL-MaLR for L520, analogous to the LTR1 ERV1 of SAMMSON.

Mining of the public GTEX database showed that L518 expression was restricted to sun-exposed and non-exposed skin and testis (Fig. S1A). Mining of the Cancer Genome Atlas (TCGA) database showed L518 was strongly and specifically expressed in epidermal and uveal melanoma (Fig. S1B). Specific L518 expression in MITF-expressing melanocytes, but not keratinocytes, was confirmed by RNAscope on sections from normal skin (Fig. 1C). RNAscope further showed abundant expression of L518 in MITF-expressing cells of primary melanoma (Fig. 1C). Analyses of single cell (sc)RNA-seq (Tirosh et al. 2016) showed high L518 expression in melanoma cells, but not in infiltrating immune or stromal cells (Fig. 1D). L518 expression was up-regulated in melanoma compared to nevi (Badal et al. 2017; Kunz et al. 2018) (Fig.S1C) and its expression increased with Clark score (Fig.S1E) and with increased copy number, due

to its co-amplification with TFAP2A in around 6.5-8% of melanomas (Fig. S1F). High expression of L518 was associated with decreased survival of melanoma patients as previously described (Luan et al. 2019).

L520 showed low expression in several normal tissues with highest expression in oesophageal mucosa (Fig. S1A). L520 showed highest expression in cutaneous melanoma, but in contrast to L518 it was much more weakly expressed in uveal melanoma and was expressed at lower levels in several other tumour types (Fig. S1B). RNAscope showed L520 expression in normal melanocytes and in primary melanoma (Fig.1E), but unlike L518, L520 was not expressed in all melanomas in the Tirosh study (Tirosh et al., 2016) (Fig.1F), its increased expression in melanoma compared to nevi was seen only in the Badal (Badal et al., 2017) dataset (Fig.S1C) and its levels did not correlate with increased Clark score of melanoma lesions (Fig.S1E). Thus, its expression was more variable in melanoma than that of L518. Nevertheless, high L520 expression was associated with decreased survival of melanoma patients (Fig.S1D).

As described in the introduction, melanoma cells adopt multiple states with specific gene expression signatures. RT-qPCR on RNA from a collection of melanocytic and undifferentiated lines (Verfaillie et al. 2015) showed that L518 was expressed at variable levels in all tested lines irrespective of cell state and driver mutation (Fig. 2A). L520 was highly expressed in melanocytic lines, but at low levels in MM099 and MM047 and absent in Vemurafenib-resistant SK-MEL-25R and M229R or MM029, all of undifferentiated cell state (Fig. 2A-B). Differential expression was also reflected in the epigenetic profiles of the corresponding loci (Verfaillie et al., 2015): L518 was marked by H3K27ac in melanocytic and undifferentiated melanoma cells, whereas L520 was marked principally in melanocytic cells (Fig. S2A). Mining of scRNA-seq of a melanoma patient derived xenograft (PDX) (Rambow et

al., 2018) showed that L518 and SAMMSON were expressed in all described cell populations, whereas L520 was absent from neural crest-like and undifferentiated cells displaying minimal expression of MITF, the major activator of its expression in melanocytic cells (Fig. S2B).

L518 expression in undifferentiated cells suggested an alternative mode of regulation independent of MITF/SOX10. Examination of public ChIP-seq data from melanocytic and undifferentiated melanoma cells identified a number of potential enhancer elements (EN 1-6) in the TFAP2A/L518 locus based on ChIP-seq for various histone modifications and transcription factors (Laurette et al. 2015; Fontanals-Cirera et al. 2017; Seberg et al. 2017) (Fig. S2C). For example, a far upstream element (EN1) was marked by H3K27ac and H3K4me1 and potentially bound by TFAP2A and FOSL2, whereas the L518 promoter showed prominent SOX10 binding and H3K4me3. EN1 and EN5 harboured potential binding sites for TFAP2A that was expressed in all described cell types in PDX (Fig. S2B). SiRNA-mediated TFAP2A silencing diminished L518 expression in 501mel and MM047 lines, but had little effect on SAMMSON expression (Fig. S2D) Furthermore, L518 and TFAP2A expression were positively correlated in TCGA melanoma samples as well as collections of melanoma cell lines (Verfaillie et al., 2015; Tsoi et al., 2018) (Fig. S2E). Ubiquitous L518 expression in melanoma of different cell states may hence be explained by MITF/SOX10 regulation in melanocytic and neural crest-like cells and by TFAP2A in undifferentiated cells.

Together, the above data showed that L518 expression was highly restricted to melanocytes and melanoma, but was expressed in all types of melanoma cells. L520 on the other hand was principally regulated by MITF with more variable expression in melanomas due to its absence in neural crest-like and undifferentiated cells lacking MITF expression. Nevertheless, expression of both LincRNAs was associated with clinical features of melanoma highlighting their important roles in the disease.

LincRNAs are required for melanoma cell proliferation and survival.

To examine the effects of L518 and L520 silencing on melanoma cell physiology, we used 2 different locked nucleic acid oligonucleotides (LNA-GapmeRs) for each LincRNA to induce their degradation compared to a control non-targeting GapmeR (CTR).

Transfection of two L518-targeting GapmeRs (GAP#1 and GAP#2) strongly reduced its expression in each tested melanoma line (Fig. 2C). In both melanocytic and undifferentiated lines, reduced cell numbers were detected 72 hours after GapmeR transfection compared to control GapmeR (Fig. S2F), but no effect was seen in control HEK293T cells where it was not expressed. GapmeRs targeting L520 reduced its expression (Fig. 2D) and lead to diminished cell numbers in melanocytic cells, but had no effect in undifferentiated lines and in HEK293T cells where it was not expressed (Fig. S2G). The reduced cell numbers seen upon L518 and L250 silencing were the result of strongly reduced cell proliferation (Fig.2E) and increased apoptosis evidenced by the potent increase in cells with active Caspase 3 (Fig.2F) and in early and late apoptotic cells observed in flow cytometry using Annexin-V labelling (Fig. S2H). These results showed that L518 and L520 were essential for normal proliferation and survival of melanoma cells irrespective of the driver mutation, with L518 required in melanocytic and undifferentiated lines. The specificity was evidenced by lack of effect of L518 silencing in HEK293T cells and of L520 silencing in undifferentiated melanoma or HEK293T cells.

We addressed the role of L518 and L520 by an independent CRISPRi method using sgRNAs to direct a CRISPR/dCAS9-KAP1 fusion protein to the respective promoter regions. Melanoma cells were transfected with the vector encoding the CRISPRi fusion protein in the presence or absence of sgRNAs. Compared to the absence of sgRNAs, sgRNAs specific for the L518 and L520 promoters induced a dramatic reduction of their expression (Fig.S2I) associated with an increase in slow proliferating cells (Fig.S2J), in Annexin-V positive apoptotic cells

(Fig.S2K) and decreased colony forming capacity (Fig S2L). These results confirmed those of GapmeR-based silencing showing by an independent method that L518 and L520 were essential for melanoma cell proliferation and survival.

As L518 is located close to the TFAP2A gene, we examined whether L518 silencing affected TFAP2A expression or if it affected expression of MITF and SOX10. Immunoblots of 501Mel cell extracts where L518 was silenced showed mildly reduced MITF levels, but no changes in the expression of TFAP2A, SOX10 or BRG1 (Fig. S2M). L518 did not therefore regulate the nearby TFAP2A gene and the reduced cell proliferation and apoptosis cannot be explained by loss of MITF, SOX10 or BRG1 expression. Rather, L518 was required downstream of these transcription factors to mediate their proliferative and pro-survival effects.

We next assessed the effects of gain of L518 function. Databases predict several alternatively spliced L518 isoforms sharing a common last exon with 3 potential polyadenylation sites that we mapped by 3'RACE and are present in all isoforms (Fig. S3A). Exon-exon junctions were confirmed on 501mel RNA-seq data represented using Sashimi plots (Fig. S3A). Interrogation of public data sets indicated that isoforms 1, 3 and 5 were most abundantly expressed in human melanomas and in melanoma cell lines (Fig. S3B). We generated Lentiviral vectors directing Doxycycline (Dox)-inducible expression of isoforms 1 and 3, as well as the poorly expressed isoform 2, in 501Mel cells, with an inducible GFP-expressing vector as control. After infection and selection, flow cytometry analyses showed a large majority of cells displayed Dox-inducible GFP expression (Fig. S3C) and RT-qPCR detected a time-dependent increase of the L518 isoforms (Fig. S3D). In absence of Dox, all cell lines showed similar proliferation over 10 days of culture, while addition of Dox induced increase proliferation of cells overexpressing isoform 1 and 3 compared to the GFP control (Fig. S3E). Ectopic L518 expression also increased colony forming capacity (Fig.S3F) and growth as 3D

melanospheres (Fig. S3G). Increased L518 expression was confirmed to be stable in spheroids, even after 12 days of culture (Fig.S3H). Thus, while L518 silencing compromised melanoma cell proliferation and survival, its ectopic expression promoted growth under 2D and 3D conditions.

Cooperativity of Linc00518, Linc00520 and SAMMSON.

As L518, L520 and SAMMSON were all expressed in melanocytic type cells, we asked if they acted cooperatively with one another. We used suboptimal concentrations of GapmeRs for each LincRNA alone or in combination, using CTR GapmeR to ensure a constant amount of GapmeR in each condition. Compared to knockdown of each single LincRNA, each combination of LincRNA knockdowns led to a more potent reduction in proliferation of 501Mel and MM011 cells (Fig. 2G) and a synergistic increase in apoptotic activated Caspase 3-expressing cells (Fig. 2H). Similarly, combinatorial SAMMSON and L518 knockdown in undifferentiated MM047 cells also cooperatively induced slow proliferation and induced a potent increase in apoptotic activated Caspase 3-expressing cells (Fig. 2G-H). This synergistic effect was also evident by staining cells in 2D after 10 days of culture, by which time combinatorial knockdown eliminated essentially all cells (Fig.2H).

These data showed that L518, L520 and SAMMSON acted cooperatively to promote melanoma cell proliferation and survival. These LincRNAs are therefore critical mediators of the survival and proliferative hallmark functions of their SOX10, MITF and TFAP2A regulators.

Linc00518 interacts with the RAP2 GTPases.

As L518 was ubiquitously expressed in the various melanoma cell sub-types and was required for their proliferation and survival, we sought to better understand its molecular function. As shown above, RNAscope demonstrated that L518 was predominantly cytoplasmic in melanoma cells *in vivo* (Fig. 1C). Similarly, RNAscope on cultured melanoma cells also

revealed a predominantly cytoplasmic localization (Fig. 3A) that was confirmed by RT-qPCR on RNA from different cell compartments using XIST as a control for nuclear RNA and beta-actin mRNA for cytoplasmic RNA (Fig. S4A). Reconstitution of 3D cellular images showed L518 enrichment in the cytoplasm around the nuclear periphery (Figs. 1C and 3A).

To identify L518 interacting proteins, we performed pulldown experiments from cytoplasmic extracts of MM011 cells using a tiling array of complementary biotinylated oligonucleotides followed by mass-spectrometry. As a negative control, we used biotinylated oligonucleotides specific to the prostate cancer expressed LincRNA PCA3. RT-qPCR on the pulldown fractions showed that L518 was enriched using the corresponding tiling oligonucleotides, but not by the PCA3 control (Fig. 3B). After mass spectrometry, peptides for a small number of proteins were found uniquely in the L518 pulldown compared to the PCA3 one (Fig. S4B). These included several ribosomal proteins as well proteins associated with the endoplasmic reticulum, the Golgi and the mitochondria. To confirm their interactions with L518 we performed immunoprecipitation (IP) of RAP2, SURF4, SAR1B, and NDUFA6 with commercially available antibodies. However, only the antibody against RAP2 efficiently precipitated its target protein from cell extracts (Fig. 3C and S4C). RT-qPCR on the RAP2 and control IgG IP fractions showed a strong enrichment of L518, but not of SAMMSON, MALAT or NEAT1, specifically in the RAP2 IP (Fig. 3C and S4C). As additional controls, we performed IP of XRN2 that as previously reported (Vendramin et al., 2018) enriched SAMMSON, as well as NEAT1, but not L518 (Fig. S4C).

The RAP2 small GTPases are encoded by 3 paralogous genes RAP2A, RAP2B and RAP2C that show high amino acid identity, being distinguished by a short hypervariable C-terminal region (Fig. S4D). Consequently, the RAP2 antibody recognises all 3 paralogs. Analyses of scRNA-seq data of human melanoma indicated that all RAP2 paralogs were expressed in

tumour, stromal and immune cells (Fig. S4E), with RAP2A showing the lowest expression in melanoma cells (Fig. S4F). RAP2 paralogs were expressed in both MITF/SOX10 positive and negative populations, as assessed in a collection of melanoma cell lines (Fig. S4G) and in the scRNA-seq PDX data (Fig.S4H).

RT-qPCR with paralog-specific primers showed variable expression of each in 501Mel and MM047 cells (Fig. 3D). As the currently available antibodies do not distinguish the paralogs, we used siRNAs to selectively knockdown expression of each. Selective siRNA silencing of RAP2A and RAP2C was highly efficient, whereas that of RAP2B was less so (Fig.3E), but this paralog was almost absent from MM047 cells. Immunoblots of transfected cell extracts with the pan-RAP2 antibody indicated that siRAP2C induced the strongest decrease in overall RAP2 protein levels (Fig. 3E). Moreover, silencing of RAP2C, but not of RAP2A or B, led to an increase in slow proliferating cells (Fig. 3F) and induced apoptotic activated caspase 3-expressing cells (Fig. 3G), a phenotype analogous to L518 silencing. Thus, while all three paralogs were expressed at the mRNA level, RAP2C contributed most to the RAP2 protein pool in melanoma cells and more importantly was the biologically relevant form required for proliferation and survival.

To address whether the selective activity of RAP2C reflected its specific interaction with L518, we generated cell lines with Dox-inducible expression of FLAG-tagged RAP2A, B or C, each of which was efficiently expressed at the RNA level when compared to the endogenous levels seen in the control cells expressing Dox-inducible GFP (Fig. S4I). Nevertheless, at the protein level RAP2C accumulated to higher levels than RAP2A or B (Fig. S4I). RT-qPCR analyses of FLAG-IP of each recombinant protein or of the pan-RAP2 IP from the GFP-expressing cells showed that L518, but not SAMMSON, was enriched with all 3 RAP2 proteins in accordance with their variable expression levels (Fig. S4J). The specific activity of RAP2C could not

therefore be ascribed to a selective interaction with L518, but must reflect other aspects of its properties.

Linc00518 and RAP2C promote oxidative phosphorylation.

To further confirm L518-RAP2 interactions, we coupled RNAscope with immune-staining for RAP2. RAP2 showed strong localized cytoplasmic staining that overlapped well with the RNAscope signal for L518. Furthermore, RAP2 and L518 labelling strong coincided with the mitochondrial p32 protein indicating RAP2 and L518 association with mitochondria (Fig.4A and S5A). RAP2 and p32 co-localization was not limited to cultured cells, but also seen in sections from primary melanoma (Fig. S5B). In a complementary analysis, we performed RNA extraction from cytoplasmic and mitochondrial fractions of several melanoma cell lines and HEK293T cells and confirmed efficient separation using RT-qPCR against the 16S mitochondrial ribosomal RNA, which was present almost exclusively in the mitochondrial fraction. SAMMSON and L518 on the other hand were present in both the cytoplasmic and mitochondrial fractions (Fig. 4B). Immunoblots on protein extracts showed strong enrichment of p32 and HSP60 in the mitochondrial fraction where RAP2 was also enriched (Fig. 4C). These data show that L518 selectively co-precipitated with RAP2 and that RAP2 and L518 were both associated with the mitochondria.

We assessed the consequences of L518 knockdown on RAP2 localization. While RAP2 and p32 showed tight and almost unique co-localization in cells transfected with control GapmeR, L518 silencing resulted in a marked de-localization of RAP2 away from the p32 stained mitochondria into the surrounding cytoplasm (Fig. 4A). Similar results were obtained with standard immunofluorescence staining of RAP2 and p32 (Fig. 4D and S5C). We generated 501Mel and MM011 cells with a Dox-inducible control or L518-targeting shRNA that selectively reduced L518, but not SAMMSON expression in the both the cytoplasm and

mitochondria (Fig.4E). Similar to what was seen using GapmeR, L518 shRNA knockdown led to reduced RAP2-p32 co-localization by immunofluorescence (Fig.4F) and to reduced RAP2 levels in mitochondrial extracts assessed by immunoblot (Fig.4G). As an internal control, the GFP that was co-expressed with the shCTR or the sh518, did not co-localise with p32 or change after L518 knock down (Fig.4F). L518 was not essential for mitochondrial localization as a fraction of RAP2 protein remained associated with the mitochondria upon L518 knockdown and RAP2 also showed mitochondrial localization in HEK293T cells that did not express L518. Rather our observations suggested a dynamic RAP2 association with mitochondria that was promoted by L518.

We next investigated the effect of L518 and RAP2C silencing on mitochondrial activity by profiling oxidative phosphorylation (OXPHOS) using the Agilent Seahorse. Compared to control, L518 GapmeR silencing or siRAP2C silencing did not affect basal oxygen consumption rate (OCR), but led to potent decrease in maximal and reserve capacity in 501Mel cells. SAMMSON knockdown on the other hand potently reduced OCR under all conditions (Fig. 4H). Profiling OCR in 501Mel cells with Dox-inducible expression of L518 isoforms 1, 2 and 3 showed that overexpression of each isoform increased basal, maximal and reserve OCR (Fig. 4I). These data showed that both L518 and RAP2C were required for optimal OXPHOS in melanoma cells.

To link compromised OXPHOS to decreased cell growth and apoptosis, we asked if L518 knockdown or RAP2C silencing and the associated impaired mitochondrial function induced reactive oxygen species (ROS). We first performed flow cytometry analysis on control, L518 or RAP2C silenced cells labelled with Annexin-V, TOPRO and MitoTracker-red CMXRos and gated on Annexin-V/TOPRO-negative cells to focus on the non-apoptotic population. Compared to control, L518 or RAP2C silencing led to the appearance of higher proportions of CMXRos low

cells indicative of reduced mitochondrial polarization that was strongly induced using FCCP as a positive control (Fig.S5D).

We next performed flow cytometry analysis with Cell ROX labelling to investigate if mitochondrial depolarization led to increased ROS. We stained L518, RAP2C or control silenced cells with anti-Caspase 3 and Cell ROX to distinguish non-apoptotic cells from apoptotic cells and cells with increased ROS (Fig. S5E). Control GapmeR did not induce ROS (Q1) or apoptotic activated caspase 3-expressing cells (Q3). THBP (tert-Butyl hydroperoxide) on the other hand induced cells with ROS that was suppressed using the ROS scavenger NAC (N-acetyl-L-cysteine), whereas Staurosporine induced apoptosis, but not ROS. L518 or RAP2C silencing induced a large increase in apoptotic cells, but also cells with augmented ROS as well as apoptotic ROS-high cells (Q2). The strongly increased ROS following L581 or RAP2C silencing induced DNA damage observed by increased gamma-H2AX, not seen following RAP2A or RAP2B silencing (Fig. S5F), as well as increased TP53BP1 foci (Fig. S5G). L518 or RAP2C silencing also increased the population of G2M phase cells followed by defective mitosis with frequent bi-nucleate/multi-nucleate cells (Fig. S5H). These data supported the idea that L518 or RAP2C silencing impaired mitochondrial function leading to their depolarization and generating ROS that induced DNA damage, cell cycle block and finally triggering apoptosis.

Linc00518 is required for increased OXPHOS upon BRAF inhibition.

Mining public data sets of M229 melanoma cells treated with the BRAF inhibitor Vemurafenib (Vem) (Tsoi et al. 2018) showed that L518 expression was up-regulated 3 days after Vem exposure and then returned to basal level at later times. L520 and SAMMSON expression was on the other hand reduced during this acute phase, while TFAP2A, SOX10 and PAX3 were all up-regulated (Fig. S6A). We investigated L518 expression in Vem-treated M229, Sk-Mel-25, 501Mel and A375 cells by RT-qPCR confirming its up-regulation between 12-72

hours. TFAP2A, SOX10 and PAX3 were also up-regulated over the same period and correlated highly with L518 (Fig. 5A). Increased levels of TFAP2A protein, that we showed above was a major regulator of L518 expression, were further observed by immunoblot after Vem exposure (Fig. S6B).

To better understand L518 regulation by Vem, we analysed public ChIP-data sets for BRD4 and H3K27ac at the TFAP2A/L518 locus in A375 melanoma cells in presence or absence of Vem, THZ1, a CDK7 inhibitor, or the combination of both (Rusan et al. 2018). BRD4 binding and H3K27ac levels at the L518 promoter were increased by Vem, but not THZ1, that further abrogated the increased BRD4 occupancy with Vem alone. Vem also increased BRD4 and H3K27ac at the far upstream TFAP2A-bound EN1 element (Fig. S6C). In the corresponding RNA-seq experiments, L518 expression was potently induced by Vem, but not by THZ1, that in addition impaired Vem induction, whereas SAMMSON expression was only mildly affected. Vem also up-regulated SOX10 and TFAP2A expression that was again impaired by THZ1 (Fig. S6D). Vem-induced L518 expression was hence associated with epigenetic changes at the promoter and far upstream TFAP2A-binding EN1 implicated in L518 regulation as described above. Up-regulated TFAP2A binding at EN1 and of SOX10 at the promoter may therefore contribute to increased L518 expression in presence of Vem.

L518 expression was also up-regulated rapidly after treatment with the BRAF inhibitor Dabrafenib and the MEK inhibitor Trametinib that further induced TFAP2A expression (Fig. 5B and S6E). Examination of public datasets revealed acute induction of L518, TFAP2A, SOX10 and PAX3 by Encorafenib, but reduced SAMMSON and L520 expression (Fig. S6F). Similar observations were made using melanoma cells (Fig. S6G) and melanoma PDX treated in combination with Dabrafenib and Trametinib (Fig. S6H). In triple wild-type patients with no mutations in BRAF, NRAS of NF1, treatment with a Durvalumab-Trametinib immune

checkpoint-MAPK inhibitor combination also induced L518, SOX10 and PAX3 expression, but in this case SAMMSON was also up-regulated, whereas TFAP2A showed up-regulated expression in some patients, but reduction in others (Fig. S6I). Interestingly, this dataset suggested that L518 induction is not restricted to BRAF mutant melanoma, but characterises also triple wild-type cells after MEK1/2 inhibition. Together, these data indicated that L518 expression was rapidly induced upon inhibition of MAPK signalling either by inhibition of BRAF or MEK or both.

Inhibition of MAPK signalling in melanoma cells inhibits glycolysis inducing a metabolic switch to OXPHOS (Parmenter et al. 2014). Given the ability of L518 to stimulate OXPHOS, its rapidly increased expression upon Vem treatment suggested that L518 may play an important role in stimulating OXPHOS to maintain cell survival at this early stage, and hence that Vem-treated cells may display enhanced sensitive to L518 silencing. To investigate this idea, we profiled OXPHOS in DMSO/Vem-treated cells with or without L518 or RAP2C or TFAP2A silencing. Vem increased basal, reserve and maximal OCR compared to DMSO control. Increased OCR was strongly diminished in cells silenced for L518, RAP2C or TFAP2A showing the essential role of this axis in the adaptive metabolic switch (Fig. 5C). Consistently, we found increased L518 levels in mitochondria upon Vem treatment, while SAMMSON displayed a progressive reduction (Fig. S6J).

Vem treatment induced cell cycle arrest with a strong increase in the number of slow proliferating control cells after 3 and 6 days, that was not further increased by L518, RAP2C or TFAP2A silencing. On the other hand, their silencing induced slowed proliferation of control DMSO treated cells (Fig. 5D). In contrast, Vem did not appreciably induce apoptosis during this period. Importantly, Vem-treated cells displayed increased apoptosis compared to those treated with DMSO-treated after L518, RAP2C or TFAP2A silencing (Fig. 5E). The increased

apoptosis was particularly evident when comparing cells treated for 6 days with DMSO or Vem. L518 knock down was similarly induced in DMSO and Vem treated cells and its levels were also reduced by siTFAP2A, corroborating the role of this transcription factor in the Vem mediated L518 induction (Fig. S6K).

Similar to Vem, Dabrafenib and Trametinib treated cells were also more sensitive to L518 silencing (Fig. 5F). Thus, Vem and other inhibitors of BRAF and MAPK signalling cooperated with L518 silencing to induce melanoma cell apoptosis showing the critical role of the TFAP2A/LINC00518/RAP2C axis in the metabolic adaptation to drug treatment.

In further support of the above, we assessed OXPHOS in cells with Dox-inducible ectopic expression of GFP or L518 isoforms in presence of Vem. In GFP control cells, OCR levels were stimulated in presence of Vem and ectopic L518 expression further increased OCR, indicating that ectopic L518 expression potentiated the adaptive metabolic response (Fig. 5G). In line with this, Vem treated L518 inducible cells had higher L518 levels than in the presence of DMSO (Fig. 5H). Furthermore, inhibition of melanosphere formation by Vem treatment of control GFP-expressing cells was rescued in cells with ectopic L518 expression (Fig. S6L). Increased endogenous L518 expression as seen after BRAF inhibition or ectopic L518 expression therefore promoted survival of Vem-treated cells. The loss and gain of function experiments underscore the essential role of L518 in the adaptive response to BRAF and MAPK inhibition.

Linc00518 and RAP2C regulate DRP1 phosphorylation and mitochondrial fission

Activation of MAPK signalling during oncogenic transformation stimulates mitochondrial fission associated with high anaerobic glycolysis and reduced mitochondrial activity, whereas BRAF inhibition induces an increase in fused mitochondria associated with the metabolic switch to OXPHOS (Serasinghe et al. 2015; J. A. Kashatus et al. 2015; Ferraz et

al. 2020). In accordance with the observed diminished OXPHOS, L518 or RAP2C silencing increased mitochondrial fission leading to a switch from more elongated fused mitochondria seen in control cells to smaller and rounder mitochondria in the knockdown cells (Fig. 6A). As mentioned above, defective mitosis with bi- and multi-nucleate cells can be clearly seen following L518 and RAP2C silencing. Vem-treated cells displayed predominantly elongated mitochondria, but this effect was dampened when L518 or RAP2C were additionally silenced (Fig. 6B). Thus, L518 and RAP2C contributed to the adaptive increase of OXPHOS by promoting mitochondrial fusion.

The large GTPase DRP1 plays a key role in regulating mitochondrial fission. ERK2-mediated DRP1 S616 phosphorylation stimulates mitochondrial fragmentation (Serasinghe et al. 2015; J. A. Kashatus et al. 2015), whereas phosphorylation at S637 inhibits DRP1 function and mitochondrial fusion (Chang and Blackstone 2007; Cribbs and Strack 2007; W. Wang et al. 2012). Mitochondrial homeostasis is hence dynamically regulated by balance between these two events. Silencing of L518, RAP2C or TFAP2A all led to reduced DRP1 S637 phosphorylation both in presence and absence of Vem in agreement with the increased mitochondrial fragmentation observed upon their knockdown (Fig. 6C). Thus, even when the ERK2-S616 axis was blocked by BRAF inhibition, DRP1 activity was increased by reduced S637 phosphorylation via inhibition of the L518-RAP2C axis. As a consequence, mitochondrial fission and reduced OXPHOS took place under conditions where glycolysis was also blocked, leading to cell death.

We investigated whether there was an interaction between the large and small DRP1 and RAP2 GTPases. DRP1 was co-precipitated with RAP2 but not in control IgG IP showing an interaction of the two proteins (Fig. 6D). In accordance with this, L518 was enriched in both the RAP2 and DRP1 IP fractions, but not the corresponding control IgG IP (Fig.6E). The L518-

RAP2 complex therefore interacts with DRP1 to modulate S637 phosphorylation, mitochondrial fusion and cellular metabolic switch.

DISCUSSION

Malignant melanoma is the most aggressive skin cancer. Despite the development of targeted inhibitors and immune checkpoint therapies, a significant fraction of advanced stage patients are considered as 'non-responders' highlighting the need for additional therapeutic strategies (Schadendorf et al. 2015). LncRNAs are defined as RNA molecules longer than 200 nucleotides that do not contain known open reading frames but able to convey a wide array of functions in the nucleus and cytoplasm (Mattick 2018). Being increasingly appreciated as functionally involved in different biological processes (Ma et al. 2019), some lncRNAs were also shown to be expressed in a cancer-specific manner and to mediate pro-tumorigenic functions (Schmitt and Chang 2016). The possibility of inducing their degradation or sterically blocking their activity using GapmeR antisense oligonucleotides (ASOs) makes them attractive targets, as shown in preclinical models (Arun, Diermeier, and Spector 2018).

We previously contributed to characterize the melanoma specific SAMMSON lncRNA that promotes oncogenic anabolism by stimulating cytoplasmic and mitochondrial protein translation (Vendramin et al. 2018) and as shown here is essential for mitochondrial OXPHOS function. ASO-mediated SAMMSON targeting demonstrated preclinical efficacy in PDX models (Leucci et al. 2016). Further experiments will determine whether ASO-targeting of L518 will also prove efficient in PDX.

Similar to other screenings for potentially functional lncRNAs (Guttman et al. 2009; Sati et al. 2012), we analysed ChIP sequencing data of active histone marks (H3K27ac, H3K4me1, H3K4me3) and the MITF and SOX10 transcription factors to identify actively expressed

lncRNAs relevant for melanoma. We showed previously that MITF and SOX10 promote melanoma cell proliferation and survival by driving expression of genes involved in cell division, DNA repair and metabolism (Strub et al. 2011; Laurette et al. 2015). We identified a group of lncRNAs bound by MITF/SOX10 at their promoters or nearby enhancers and filtered for those whose expression levels were altered after their knock down, finally deciding to focus on the LINC00518 and LINC00520 genes.

LINC00518 is transcribed on chromosome 6p24.3 close to the TFAP2A locus and LINC00520 on chromosome 14q22.3. Both genes show high sequence conservation with Chimp, Gorilla, Gibbom and Rhesus, but conservation is reduced in other mammals already after the Mamorset. Their primate specificity may be explained by recent evolutionary transposon and retroviral element insertions that characterize LINC00518 and LINC00520 promoters (MLT1B ERVL-MaLR for the former and THE1B ERVL-MaLR for the latter). This mechanism has been associated to many lncRNAs (Kapusta et al. 2013) and characterises also SAMMSON (LTR1 ERV1). Interestingly, the SOX10 binding site at the LINC00518 promoter results from the juxtaposition of the MIRb SINE and the MLT1B LTR.

Similar to other targets (Laurette et al. 2015), MITF and SOX10 binding at LINC00518 and LINC00520 cis-regulatory elements is flanked by the enzymatic PBAF subunit BRG1 at surrounding nucleosomes. MITF or SOX10 knock down reduced BRG1 recruitment to LINC00518/LINC00520 promoters (data not shown), suggesting a transcriptional mechanism already described for other melanoma genes. After association with BRG1 in the nucleoplasm, MITF binds to its recognition motifs, along with SOX10 and other transcription factors at enhancers and recruits p300/CBP. The consequent histone acetylation and chromatin remodelling mediated by the PBAF complex promote nucleosome displacement/eviction and establishment of a transcriptionally favourable environment. MITF also localizes at promoters

where it cooperates with PBAF for nucleosome depletion to promote Pol II activity (Laurette et al. 2015). Accordingly, we found MITF at the promoters and nearby enhancers of the two lncRNAs, with LINC00518 uniquely characterized by SOX10 binding at the transcription start site (TSS). This is a very peculiar feature as out of 6000 SOX10 binding sites, only 80 are in proximal promoters and seem to mark genes with important functions in melanocytes and melanocytic melanoma cells (Laurette et al. 2015).

Interestingly, SAMMSON also has a SOX10 binding site at its promoter (Leucci et al. 2016) and this may explain the high melanoma predominance of these two lncRNAs. On on the other hand, LINC00520 seems to be weakly expressed in other tumours. However, in both cases we found very low expression in normal tissues, restricted to melanocytes and testis in the case of LINC00518. We further confirmed the higher expression of the lincRNAs in melanoma compared to normal skin by multiplex fluorescent FISH and their absence in stromal cells in tumours by scRNA-seq analysis (Tirosh et al. 2016). LINC00518 displayed higher expression than LINC00520 in cutaneous melanoma patients from TCGA, lower inter-tumoral heterogeneity and its expression discriminated primary melanomas from benign nevi from two different datasets (Badal et al. 2017; Kunz et al. 2018), while LINC00520 failed in one of them. These findings are in line with the demonstrated diagnostic power of LINC00518 expression, coupled with the one of the PRAME gene, in distinguishing malignant from benign melanocytic lesions (Gerami et al. 2017).

LINC00518 has also been previously indicated as a prognostic marker, positively correlating with worse survival of melanoma patients and is suggested to promote metastasis formation of xenografts in mice models (Luan et al. 2019). We expanded these findings showing a positive correlation between LINC00518 expression and Clark score of lesions and highlighted the high frequency of LINC00518 copy number gain (of one allele in 51% and of

both in 6.5% of TCGA SKCM patients). These amplifications, together with SOX10 mediated transcription, may explain the broader and higher expression of LINC00518 compared to LINC00520, which indeed is rarely amplified. Nevertheless, LINC00520 was also positively associated with poor survival of cutaneous melanoma patients.

Analyses of melanoma cell lines highlighted other differences between LINC00518 and LINC00520. While both of them were found to be more expressed in MITF/SOX10 positive cells, LINC00518 was present also in cells negative for these factors. Accordingly, LINC00518 but not LINC00520 locus was marked by H3K27ac in all cell lines of a panel of melanoma short term cultures (Verfaillie et al. 2015).

This prompted us to better understand its transcriptional regulation, exploiting additional publicly available ChIP seq datasets. We suggest the existence of a complex cis-regulatory landscape around the TFAP2A/LINC00518 locus with at least 6 potential active enhancer sequences marked by H3K27ac and H3K4me1 and bound by melanoma relevant transcription factors where in addition to SOX10 and MITF, we found binding sites for TFPA2A (Seberg et al. 2017), and the more generally expressed factors FOSL2 and TEAD4 (Fontanals-Cirera et al. 2017). We speculate these enhancers have a dominant effect on LINC00518 rather than TFAP2A, as treatment of melanoma cells with BET inhibitors reduced LINC00518 expression but not TFAP2A (analysis of RNAseq experiments from Fontanals-Cirera et al. 2017; data not shown). Further studies will be required to better define this cis-regulation and the existence of chromatin contacts between LINC00518 promoter and these enhancers.

AP-1 and TEAD transcription factors have been proposed as master regulators of the invasive program in undifferentiated melanoma cells (Verfaillie et al. 2015; Maurus et al. 2017; Ramsdale et al. 2015) and may explain LINC00518 expression in MITF/SOX10 negative cells, similarly to the SAMMSON dependency on SOX9 (unpublished communication by Leucci et

al.). However, LINC00518 does not positively correlate with these transcription factors, and its expression does not change after SOX9 knock down (data not shown). Rather than relying on undifferentiated-specific transcription factors, we believe that broad LINC00518 expression could rather be explained by the activity of a pan-melanoma expressed factor such as TFAP2A (Wouters et al. 2020). Indeed, LINC00518 and TFAP2A strongly correlated in cell lines and patient samples and TFAP2A knock down reduced LINC00518 expression in both MITF/SOX10 positive and negative cells. These data highlight a so far undescribed mechanism of transcriptional regulation, which may characterize also other coding and non-coding genes. Other transcription factors may also act in a "pan-melanoma" manner. This "universal" LINC00518 expression was evident in the melanoma states identified in-vivo from PDX scRNA-seq experiments (Rambow et al. 2018). Similar to SAMMSON, LINC00518 was detected in both melanocytic and undifferentiated populations, while LINC00520 only in the former; TFAP2A showed again a similar pattern to LINC00518.

Previous analyses of melanoma cell lines and patients samples highlighted the central role of TFAP2A (together with ALX1, DLX2, GAS7, LEF1, MITF, PAX3, SOX10) in the regulation of a gene signature which discriminates melanomas from other tumours and positively correlates with disease aggressiveness (Rambow et al. 2015). Cell lines characterized by this program show higher proliferative capacity, while patients have lesions with higher Breslow depth and shorter survival. Interestingly, LINC00518, designated as C6ORF218 in that paper, was proposed to be part of this signature, further highlighting its clinical prognostic value and the intimate relationship with TFAP2A. However, we showed that LINC00518 does not act as a cis-regulator of TFAP2A expression, so their positive correlation must rely on TFAP2A activity driving LINC00518 or to the fact that they can be co-amplified.

The different expression patterns of LINC00518 and LINC00520 were in accordance to the phenotypic changes that we noticed after their knock down by ASOs. Only LINC00518 silencing induced proliferation arrest and apoptosis in both melanocytic and undifferentiated cell lines. In SOX10/MITF positive cells, we further showed that apoptosis of melanocytic cells could be synergistically increased by combinatorial silencing of LINC00518, LINC00520 and SAMMSON; combining LINC00518 and SAMMSON silencing induced the same effect in undifferentiated cells. This suggests that these lncRNAs, despite being regulated by MITF/SOX10, probably mediate different downstream functions. Their co-targeting could represent an attractive therapeutic strategy and potentially, the LINC00518-SAMMSON ASOs combination would affect melanoma cells irrespective of phenotype or mutational status. This would give a new opportunity to therapy for refractory BRAF mutant melanomas (resistant to target- or immunotherapy) or NRAS/NF1 mutant or triple wild type patients, currently lacking effective treatments.

We decided to focus our efforts on the characterization of LINC00518 mechanism of action. According to other reports, we found the RNA to be predominantly cytoplasmic (Luan et al. 2019) but we could not confirm its suggested role as a competing endogenous RNA or evidence a general role in transcription (data not shown). We hypothesized its function could rely on a mechanism unrelated to transcription, possibly mediated by a protein interaction. The role of lncRNAs acting as scaffolds to bring together protein complexes has been widely described for nuclear chromatin remodelers (Tsai et al. 2010; K. C. Wang et al. 2011; McHugh et al. 2015; A. K. Jain et al. 2016), but it is increasingly emerging also for cytoplasmic cellular functions, such as signaling (B. Liu et al. 2015) and metabolism regulation (X. Liu et al. 2016; Vendramin et al. 2018). We thus performed LINC00518 pulldown in native conditions using biotinylated probes, coupled with shotgun mass spectrometry analysis of the enriched

proteins. Comparing the peptides obtained in three experiments using LINC00518 specific probes versus PCA3 used as negative controls, we obtained a list of proteins present only in the former. Among them we succeed in immunoprecipitating endogenous RAP2, confirming LINC00518 interaction by quantitative PCR.

RAP2 is a small GTPase proposed as an intermediate activation molecule in signalling cascades, such as the MAP4K4 (Machida et al. 2004) or the LATS1/2-YAP/TAZ (Meng et al. 2018). Knock down of LINC00518 did not affect these pathways (data not shown) excluding that the interaction with RAP2 was related to them. We noticed the FISH signals to be peculiarly perinuclear, so we hypothesized they reflected a specific subcellular localization. We tested if LINC00518 and RAP2 could be localized in the mitochondria (Papatriantafyllou 2012). Fractionation of these organelles from the remaining cytoplasm indicated presence of LINC00518 and RAP2, along with SAMMSON that displayed a similar distribution. At the protein level, we confirmed the enrichment of RAP2 with the mitochondrial HSP60 and p32 proteins with the latter showing co-localization with RAP2 also by immunofluorescence. Combining LINC00518 FISH with RAP2/p32 immunofluorescence further confirmed a common localization over the cytoplasmic area.

Since RAP2 was found in mitochondrial extracts also from the LINC00518 negative HEKT cells, we excluded that the lncRNA could be fully responsible for its mitochondrial targeting. We rather hypothesized a dynamic equilibrium of RAP2 localization where LINC00518 promotes mitochondrial association. Further experiments will be required to define if LINC00518 interacts directly with RAP2 or if other proteins are involved. We can also imagine a role for LINC00518 in bridging RAP2 to a mitochondrial protein that could be further activated by phosphorylation. We will thus seek to define the RAP2 interactome in melanoma cells by affinity purification coupled with mass spectrometry, in parallel with phospho-

proteomics following LINC00518 and /or RAP2 knock down. This combined approach should allow identification of RAP2 associated proteins and substrates of its GTPase activity in the mitochondria. In parallel, it would be interesting to map the domains of LINC00518 and RAP2 responsible for their interaction. Some studies demonstrated the feasibility of this approach using in vitro reconstituted segments of the lncRNA and recombinant protein candidates (B. Liu et al. 2015; Lin et al. 2016; Xing et al. 2017). This information would eventually allow targeting of the LINC00518/RAP2 axis using steric inhibitors instead of RNAseH1 dependent ASOs.

It also remains to be defined if LINC00518 specifically cooperates with one of the RAP2 paralogs (A/B/C). Expression analyses suggest a lower expression of RAP2A in melanoma cells in vitro and in vivo and accordingly its knock down does not affect them. RAP2B and C are more expressed but in a variable manner. We tested the effect of their silencing in two cell lines, one expressing both paralogs (501mel) and one expressing mostly RAP2C (MM047). In both cases, only RAP2C knock down induced a phenotype change similar to that of LINC00518, although RAP2B siRNA showed lower efficiency. Despite their high sequence homology, some studies suggested different localization of these two paralogs, with RAP2B more associated with the plasma membrane (Di et al. 2015) and RAP2C enriched in discrete cytoplasmic areas (Bruurs and Bos 2014) and in a perinuclear fashion (Guo et al. 2007). It is tempting to speculate that the differences in phenotype change reflect different subcellular localizations of RAP2 paralogs. Nevertheless, expression of tagged RAP2 proteins indicated that LINC00518 can potentially bind all of them, suggesting that the interaction domain resides in the conserved region.

Given LINC00518/RAP2 co-localization, we evaluated if their knock-down would impact mitochondrial function. We first noticed that unlike after SAMMSON knockdown, cells

were not experiencing a “mitochondrial catastrophe”, as evidenced by Agilent Seahorse analysis and p32 staining by immunofluorescence. We rather noticed a less dramatic but still relevant mitochondrial dysfunction phenotype, with the cells no longer capable of achieving their maximal OXPHOS capacity. In line with this, mitochondria were less depolarized and cells showed high levels of ROS, that we suppose are at least in part responsible for inducing DNA damage and ultimately cell cycle arrest and apoptosis.

A dominant view regarding cancer metabolism is that energy production is skewed towards glycolysis at the expense of OXPHOS. This misconception relies on Otto Warburg’s idea that cancer cells are characterized by damaged mitochondria (Weinhouse et al. 1956) and that they switch to aerobic glycolysis to avoid the detrimental effects of excessive ROS production (Jose, Bellance, and Rossignol 2011). Except tumours characterized by mutations in enzymes of the tricarboxylic acid (TCA) cycle or the electron transport chain (ETC) (Yang, Soga, and Pollard 2013), it is well accepted that mitochondrial metabolism is essential for tumorigenesis (Fogal et al. 2010) even in cells that display aerobic glycolysis. In melanoma for instance, both processes are globally upregulated compared to normal cells (Xiao, Dai, and Locasale 2019).

Another previous misconception is that mitochondria are static “bean” shaped powerhouses of the cell. Mitochondrial morphology ranges from an interconnected reticula to fragmented puncta and this process is dynamically regulated in response to energy demands, allowing tumours to adapt to stressful environments like starvation, hypoxia or drug treatments (Sabouny and Shutt 2020). These changes depend on the activities of proteins that promote fusion, such as mitofusin/MFN 1 and 2 and OPA1, or fission such as DRP1 and DYN2 (Chen and Chan 2017). Mitochondrial fragmentation begins with interaction with the endoplasmic reticulum (ER) and recruitment of DRP1 through association with a receptor on

the outer membrane such as MFF, MID49, MID51. Similar to dynamins, DRP1 oligomerizes around mitochondria and progressively constricts them. DYN2 is finally responsible for the complete scission (Chen and Chan 2017).

DRP1 activity is regulated by phosphorylation of Serine residues with opposing effects. Phosphorylation of S616 promotes activity whereas S637 phosphorylation reduces mitochondrial recruitment. S616 is targeted during early M phase by CDK1/cyclin B (downstream Aurora A) to promote a fragmentation process beneficial for equal distribution of mitochondria into daughter cells (Taguchi et al. 2007; D. F. Kashatus et al. 2011). This mechanism may be important to sustain efficient cycles of division by cancer cells and indeed S616 is also phosphorylated downstream the RAS oncogene by ERK1 and 2 (Serasinghe et al. 2015). On the other hand, other signalling molecules induce disassociation of DRP1 by acting on S637, notably GSK3beta (Loh et al. 2015), AKT/PIM1 (Din et al. 2013) and PKA (Cribbs and Strack 2007). Phosphorylation on this residue was shown also to reduce DRP1 GTPase activity (Chang and Blackstone 2007; Z. Wang et al. 2012), with the ultimate result of preventing excessive mitochondrial fragmentation and related apoptosis. Cancer cells are thus characterized by an intermediate state with a mix of fragmented and elongated mitochondria, whose equilibrium can change depending on the cellular status (Sabouny and Shutt 2020).

Given the importance of this equilibrium, we evaluated mitochondrial morphology after LINC00518 or RAP2C knock down by Mitotracker staining in living cells. While control cells displayed a mix of elongated and fragmented mitochondria with a perinuclear pattern, GapmeR/siRNA treated cells drastically shifted towards fragmentation. Since elongation protects from ROS release (Twig et al. 2008), this effect may be responsible for the increased oxidative stress that we saw after LINC00518/RAP2C knock down. Alternatively, it may also

directly participate in apoptosis due to release of cytochrome C (Cereghetti, Costa, and Scorrano 2010).

We hypothesized this effect could rely on altered DRP1 phosphorylation and indeed we noticed a reduction in phospho-S637 levels upon impairment of the LINC00518-RAP2-TFAP2A axis. These results suggest that mitochondria dynamics in melanoma cells depends on a balance between activation and inhibition of DRP1 association to mitochondria. While the former is promoted by ERK1/2, the latter may depend on the above described kinases, or even perhaps RAP2C itself. Preliminary results suggest an interaction between RAP2 and DRP1, that binds also to LINC00518. The formation of this ternary complex may represent a novel mechanism of regulation of mitochondrial fission. Alternatively, RAP2C may activate another kinase, similarly to the RALA GTPase, which via RALBP1 promotes CDK1 activity on S616 (D. F. Kashatus et al. 2011). An intriguing aspect is the unbalanced stoichiometry between the number of LINC00518 and RAP2/DRP1 molecules, with the latter present in large excess. We can speculate that the formation of the complex could be very dynamic and involving few events at a specific time point. Alternatively, there may exist other lncRNAs with similar structural motifs that could mediate the same function as LINC00518.

Mitochondrial activity is not relevant only for ATP production but also TCA cycle intermediates important to fuel macromolecule synthesis. Cancer cells exploit glutamine and its oxidation to produce oxaloacetate (for nucleotide biosynthesis) and citrate (for fatty acids) (Weinberg and Chandel 2015). The increased proliferation of LINC00518 overexpressing cells may thus rely not only on enhanced ATP production (a consequence of enhanced OXPHOS), but also on improved mitochondrial activity induced by increased fusion. We will evaluate if these cells experience increased DRP1 S637 phosphorylation and mitochondrial elongation.

The influence of LINC00518 on mitochondrial activity could be important also in vivo. It is known that the centres of many solid tumours are poorly perfused by blood vessels and suffer from glucose and oxygen restraints (R. K. Jain, Munn, and Fukumura 2002). Since ETC can function at oxygen levels as low as 0.5% (Rumsey et al. 1990), OXPHOS provides a more efficient way of producing ATP from limited amounts of nutrients compared to glycolysis. In addition, circulating cancer cells experience high oxidative stress that could be buffered by increased mitochondrial elongation (Tasdogan et al. 2020). This reinforces the need to evaluate the effect of LINC00518 overexpression in vivo with human xenografts on nude mice and isogenic murine melanoma cell line xenografts.

Mitochondrial dynamics are fundamental also to react to environmental changes, for instance changes in nutrient supply. Cells exposed to a rich nutrient space tend to keep mitochondria in a fragmented state, while starvation promotes elongation (Molina et al. 2009). This effect relies on increased levels of cAMP, which activates PKA and promote DRP1 phosphorylation on S637 (Gomes, Benedetto, and Scorrano 2011; J. Li et al. 2017). We hypothesized LINC00518 and RAP2C could participate in a similar mechanism and be relevant for metabolic stressful situations.

We decided to challenge melanoma cells with MAPK inhibitors, which are known to reduce glycolysis levels and stimulate OXPHOS to cope with reduced ATP production (Parmenter et al. 2014): ERK1/2 inhibition reduces activation of MYC and HIF1, dampening the expression of glycolytic genes. In parallel, DRP1 S616 phosphorylation is reduced and thus less associated with mitochondria. The result is an increase in elongation and OXPHOS that saves the cell from an ‘energy crisis’ (Serasinghe et al. 2015; 2018).

This response is part of an adaptive reaction relying on rapid transcriptional changes. ERK1/2 inhibition releases its suppressive activity on SOX10 (Han et al. 2018; Fufa et al. 2019)

and PAX3 (Smith et al. 2016) that positively act on MITF. Its increase promotes expression of anti-apoptotic genes (Haq, Yokoyama, et al. 2013) and PGC1alpha, a key regulator of mitochondrial biogenesis (Haq, Shoag, et al. 2013; Gopal et al. 2014). Given its regulation by MITF/SOX10 and its influence on mitochondrial activity, we postulated that LINC00518 may also act as a player in this adaptive response to MAPK inhibition.

We first evaluated if MAPK inhibition would modulate LINC00518 expression. We found that different molecules targeting BRAF (Vemurafenib, Dabrafenib) or MEK1/2 (Trametinib) had similar effects on LINC00518 induction in the first days of treatment, in line with the early response of SOX10 and PAX3. Indeed we confirmed both transcription factors to be induced in a similar manner in different cell lines and we additionally found a positive correlation of TFAP2A with LINC00518. LINC00518 induction should rely on SOX10 as well (Fufa et al. 2019). Remarkably, LINC00518 induction was evidenced also in vivo with comparable kinetics, as indicated by melanoma PDX treated with Dabrafenib and Trametinib (Rambow et al. 2018) and patients receiving anti-PDL1 plus Trametinib (GSE158403, unpublished data). The latter study involved triple WT patients, indicating that the effect of MAPK inhibition is not restricted to BRAF mutant cells. We will thus conduct further studies using NRAS mutant and WT cell lines treated with MEK inhibitors.

Unlike LINC00518, LINC00520 and SAMMSON were reduced in the same treatment phase. This is surprising given their transcriptional regulation by MITF/SOX10, especially in the case of SAMMSON that harbors a SOX10 binding site at its promoter. We reasoned this lncRNA may be subjected to additional regulatory constraints, limiting its anabolic effect in situations of energy stress. Protein translation is one of the most energy demanding cellular processes, so upon MAPK inhibition and the ensuing proliferation arrest, cells need to reduce its rate. SAMMSON would play a central role in this response, since it can coordinate cytoplasmic and

mitochondrial rRNAs biogenesis (Leucci et al. 2016). Once the cells regain control of energy production and eventually become resistant to MAPK inhibition, SAMMSON levels are restored. It is tempting to speculate that, since LINC00520 displays a similar expression pattern, it could also have an anabolic function like SAMMSON.

LINC00518 increase at total RNA level was accompanied by higher levels in mitochondrial extracts, which we hypothesized would result in changes in OXPHOS. Indeed we showed that unlike cells treated with Vemurafenib alone, those co-targeted with LINC00518 GapmeR were not able to induce the important increase in mitochondrial respiration. Accordingly, LINC00518 overexpression was able to further stimulate it in the presence of Vemurafenib. These effects were accompanied by induction of apoptosis in the former case and increased proliferation in the latter, suggesting an important role for LINC00518 dependent OXPHOS stimulation. In addition, we showed that co-targeting of Vemurafenib with siRNAs against LINC00518 transcriptional regulator (TFAP2A) or its effector partner (RAP2C) could also synergistically increase apoptosis, highlighting the existence of a whole new pathway involved in adaptation to MAPK inhibition.

Interestingly, we confirmed the role of LINC00518 and RAP2C in regulation of mitochondrial dynamics in this context, showing that their inhibition could suppress the Vemurafenib induced mitochondrial elongation. Again, we think this effect depends on the ability of LINC00518/RAP2C to modulate phosphorylation of DRP1 on S637 that was reduced in co-treated cells. All together, these results suggest a role for LINC00518 in regulating melanoma mitochondrial activity in basal conditions and upon metabolic stress. Further studies will be required to define the interplay between LINC00518, RAP2 and DRP1.

Our work has expanded the network of MITF/SOX10 regulated lncRNAs (Leucci et al. 2016; Coe et al. 2019) providing molecular characterisation of LINC00518 and LINC00520. It

may sound remarkable to find that like SAMMSON also LINC00518 seems involved in mitochondrial regulation. We think this may not be just by chance, but rather reflective of a broader level of cellular regulation involving many other lncRNAs. These and other examples (Sirey et al. 2019) should prompt the field to investigate the role of lncRNAs in regulating cancer cell metabolism.

We propose LINC00518 and LINC00520 as candidates for therapeutic targeting, as mono- or combination therapy with each other or SAMMSON. Although ASO delivery to treat oncologic patients is rather at its infancy (Quemener et al. 2020), future developments of this technology may unleash an unprecedented power to target cancer relevant genes like these lncRNAs. In this perspective, the fact that their cotargeting can act synergistically would constitute an interesting strategy to increse efficacy and lower toxicity. Co-inhibition of LINC00518 and SAMMSON may also allow targeting of all different melanoma subpopulations, possibly reducing the risk of minimal residual disease.

We also provided extensive characterisation of LINC00518 localisation and proposed a model for its mechanism of action. Given its 5' cap, polyadenylation sites and strong intron exclusion pattern, it is plausible to think that it gets post-transcriptionally modified and exported from the nucleus similarly to mRNAs. Less clear is to model its mitochondrial association, but given its perinuclear pattern it may not need to widely diffuse over the cytoplasm to find its partner. We can actually speculate a targeting towards ER associated mitochondria bound by DRP1, with LINC00518 promoting its S637 phosphorylation and dampening its activity to buffer fragmentation. Our results also suggest a novel role for RAP2 in mitochondrial regulation, which would be interesting to explore also outside the melanoma context.

The role of LINC00518 on mitochondrial activity seems to be therapeutically targetable. Similar to other strategies proposed in combination with MAPK inhibition (Zhang et al. 2016), LINC00518 targeting synergistically increased apoptosis, highlighting its relevance over the course of the adaptive response. It would be interesting to identify other coding or noncoding RNAs similarly involved in mitochondrial dynamics and important over therapy, in melanoma or other tumors. They would constitute a new family of targets more amenable and cancer specific compared to standard mitochondrial inhibitors, which have a low therapeutic index (Weinberg and Chandel 2015).

The analysis of LINC00518 regulation also provided new insights regarding melanoma cell transcriptional responses, highlighting the key role of TFAP2A in the expression of genes in a pan-phenotype manner and under stress response. The articulated cis-regulatory landscape at LINC00518 locus and its kinetics of induction upon MAPK inhibition may characterise other genes in a similar manner and they could be part of adaptive responses to environmental cues. This gene search could rely on the analysis of TFAP2A targets, which we showed to be relevant for metabolic reprogramming. In line with this finding, its expression is highest in the hypometabolic/SMC population amongst those identified in PDX scRNA-seq data (Rambow et al. 2018).

Finally, LINC00518 provides an example of an adaptive response mediated at the cytosolic level, but it is plausible to think that nuclear lncRNAs could be part of the transcriptional changes mediated by MAPK inhibition. In other contexts, they have demonstrated to mediate very rapid and specific cellular responses by proximity action, for instance by binding transcription factors that promote their synthesis to further boost or inhibit their activity (Hung et al. 2014; Saldaña-Meyer et al. 2014; X. L. Li et al. 2017; Schmitt et al. 2016). It would be interesting to evaluate if similar positive feedback loops also

characterise cells receiving MAPK or other signaling pathway inhibitors, with lncRNAs sustaining the activity of the factors that promote their synthesis.

MATERIALS AND METHODS

Cell culture and GapmeR transfections

Melanoma cell lines Sk-mel-25, Sk-mel-25R, Sk-mel-28 and 501mel were grown in RPMI 1640 medium supplemented with 10% Fetal Calf Serum (FCS) and gentamycin; IGR-37 and IGR-39 in RPMI 1640 medium supplemented with 15% FCS and gentamycin. MM011, MM117, MM047, MM099 were grown in HAM-F10 medium supplemented with 10% FCS, 5.2 mM glutamax, 25 mM Hepes and penicillin/streptomycin (7.5 ug/ml). M229, M229R, M249, M249R were grown in DMEM medium supplemented with glucose (4.5 g/l), 5% FCS and penicillin/streptomycin (7.5 ug/ml). A375 cells were grown in DMEM medium supplemented with glucose (4.5 g/l), 10% FCS and gentamycin. HEK293T cells were grown in DMEM medium supplemented with glucose (1g/l), 10% FCS and penicillin/streptomycin (7.5 ug/ml). To assess cell growth and viability cells were stained with Trypan Blue (Invitrogen). Vemurafenib (PLX4032), Trametinib (GSK1120212), Dabrafenib (GSK2118436) were purchased from Selleckchem.

For GapmeR and siRNA knockdown experiments cells were transfected using Lipofectamine RNAiMAX (Invitrogen) with 20 nM of GapmeR (Qiagen) or siRNA (Thermofisher) and harvested 48 or 72 hours as indicated. GapmeRs and siRNAs sequences are listed in Table 1. For combination GapmeR experiments cells were transfected with 15nM of L518 GAP#2 and/or L520 GAP#2 and/or 5nM SAMMSON Gapmer. For Vemurafenib/Trametinib+Dabrafenib-GapmeR co-treatment, cells were cultured for 3 days in presence or absence (DMSO only) of Vemurafenib (1uM), transfected with 15nM of control GapmeR, L518 GAP#2, siRAP2C or

siTFAP2A, then cultured for additional 3 days before harvesting, RNA and protein extraction, flow cytometry analysis or fixed and stained with crystal violet. Colony forming ability was assessed by plating 500 cells/9.6cm2, for 10 days and finally fixing in formalin and staining with 0.05% Crystal Violet solution (Sigma Aldrich).

Melanosphere formation assay

501mel cells were plated in 10cm petri dishes without any coating in KO DMEM medium supplemented with 25% KSR, AANE, 2.5mM Glutamax, 125ug/ml Penicillin/Streptomycin and 50mM Beta-mercaptoethanol. Every three days pictures of 10 different areas uniformly distributed across the petri were taken by light microscopy. Images were analysed by ImageJ to quantify the area occupied by melanospheres in each picture and the corresponding values used to calculate the mean and standard deviation for each sample.

Plasmid cloning and lentiviral transduction

GFP-RAP2B was a gift from Philip Stork (Addgene plasmid # 118321; http://n2t.net/addgene:118321 ; RRID:Addgene_118321), while pLJC2-RAP2A-3xFLAG was a gift from David Sabatini (Addgene plasmid # 87974 ; http://n2t.net/addgene:87974 ; RRID:Addgene_87974). L518 isoforms 1, 2, 3 and RAP2C cDNAs were synthesized by Genscript. L518 and RAP2 cDNAs were cloned into the pCW57-GFP-P2A-MCS vector (a gift from Adam Karpf; Addgene plasmid # 71783; http://n2t.net/addgene:71783; RRID: Addgene_71783). Lentiviral particles were produced after transfection of HEK293T cells with packaging plasmids, purified by ultracentrifugation and resuspended in PBS. After titration, melanoma cells were infected at MOI of 1 and selected by puromycin addition to the media (1ug/ml).

CRISPR-interference

501Mel cells were co-transfected using Fugene 6 (Promega) with a plasmid expressing dead Cas9 protein fused to the Kruppel-associated box (KRAB) domain-containing KAP1

(dCas9-KAP1) and the red fluorescent protein mScarlet (pX-dCas9-KRAB-Scarlet), together with a plasmid expressing GFP and three single guide RNAs targeting the transcription start sites of L518 or L520 (pcDNA3-sgRNA-GFP) or a control plasmid expressing GFP only (pCMV-GFP). Double Scarlet-GFP positive cells were sorted 24 hours after co-transfection, stained with Cell Trace Violet and kept in culture for additional 96 hours. Cells were harvested to prepare total RNA and stained with AnnexinV-APC (Biolegend). Cells were analysed on a LSRII Fortessa (BD Biosciences) and data were analysed with Flowjo software (Tree Star).

Analysis of oxygen consumption rate (OCR) in living cells

OCR was measured in an XF96 extracellular analyzer (Seahorse Bioscience). A total of 20000 transfected cells per well were seeded 48 hours prior the experiment. The cells were incubated at 37°C and the medium was changed to XF base medium supplemented with 1mM pyruvate, 2 mM glutamine and 10mM glucose for 1 hour before measurement. For OCR profiling, cells were treated following the Mitostress test kit instructions and sequentially exposed to 2 µM oligomycin, 1 µM carbonyl cyanide-4- (trifluorome- thoxy) phenylhydrazone (FCCP), and 0.5 µM rotenone and antimycin A. After measurement, cells were washed with PBS, fixed with 3% PFA, permeabilized with 0.2% triton. Nuclei were counterstained with Dapi (1:500) and number of cells per well determined by the IGBMC High Throughput Cell-based Screening Facility (HTSF, Strasbourg).

Proliferation and viability analyses by flow cytometry

To assess cell viability and proliferation after GapmeR or siRNA-mediated knockdown, cells were stained with Cell Trace Violet (Invitrogen) on the day of transfection harvested after 72 hours and stained with Annexin-V (Biolegend) and TOPRO-3 (Invitrogen) following manufacturer instructions. Where indicated, cells were stained with the active caspase 3 kit

(BD Biosciences) following manufacturer instructions. Cells were analysed on a LSRII Fortessa (BD Biosciences) and data were analysed with Flowjo software (Tree Star).

Cell cycle progression analysis by flow cytometry

Cells were transfected with GapmeRs or siRNA and after 72 hours stained using the Click-it Edu kit (Thermofischer) and TOPRO-3 following manufacturer instructions. Briefly, cells were cultured with 10uM Edu for 1 hour and 30 minutes, harvested by trypsinization, washed once in 1%BSA-PBS and fixed in 4%PFA for 15 minutes at room temperature. After a wash in 1%BSA-PBS cells were permeabilized with saponin-permeabilization buffer for 15 minutes and then stained with the Click-it reaction cocktail for 30 minutes. Finally, they were washed once in 1%BSA-PBS, resuspended in 500 ul of PBS with 10nM TOPRO-3 and left for 10 minutes at room temperature. Cells were analysed on a LSRII Fortessa (BD Biosciences) and data were analysed with Flowjo software (Tree Star).

Intracellular reactive oxygen species analysis by flow cytometry

Cells were transfected with GapmeRs or siRNAs for 48 hours and stained in adherent conditions with CellRox Deep Red (Thermofisher) at final concentration of 500nM following manufacturer instructions. After harvesting, cells were stained for active caspase 3 (BD bioscience) and analysed on a LSRII Fortessa (BD Biosciences). To induce ROS cells were treated with THBP (200uM) for 30 minutes; to inhibit ROS induction cells were treated with NAC (1uM) for 1 hour before THBP administration. To induce apoptosis cells were treated with Staurosporine (500nM) for 16 hours.

Mitotracker analysis by flow cytometry

Cells were transfected with GapmeRs or siRNAs for 48 hours, harvested and stained with Annexin V. After one wash in Annexin V binding buffer and PBS, cells were diluted in PBS+5% FCS and stained with Mitotracker CMXRos red (200nM) for 25 minutes at 37°C. After

one wash in PBS, cells were stained with TOPRO-3 for 10 minutes at room temperature. For FCCP treated samples, cells were incubated with 50uM FCCP for 30 minutes before Mitotracker staining. Samples were analysed on a LSRII Fortessa (BD Biosciences).

RNAscope

RNAs for L518, L520, MITF and SOX10 in sections of human melanomas or normal skin and cultured cells were detected with the RNAscope assay (Advanced Cell Diagnostics, ACD, Hayward, CA) according to the manufacturer's protocols. Briefly, patient sections were de-paraffinized, incubated with hydrogen peroxide at room temperature for 10 min, boiled with target retrieval reagent for 15 min, and then treated with protease plus reagent at 40°C for 30 min. The sections were hybridized with Hs-MITF probe (ACD, Cat. No. 310951), Hs-SOX10 probe (ACD, Cat. No. 484121), at 40°C for 2 h. Probes for Hs-L518 and Hs-L520 were custom designed by ACD. Hybridization signals were amplified and visualized with RNAscope Multiplex Fluorescent Reagent Kit v2 (ACD, Cat. No. 323100). For co-detection of RAP2 and p32 with L518, cells were fixed for 30 minutes with formaldehyde 3.7%, washed with PBS and incubated 10 minutes at room temperature with H2O2. After one wash in distilled water, primary antibodies diluted in co-detection diluent (1/100 for RAP2, 1/200 for p32) were added o/n at 4°C. Slides were washed in PBS+tween 0.1% (PBST), fixed in formaldehyde 3.7% for 30 minutes and washed again in PBST. Slides were treated with protease III and washed with PBS. L518 hybridization signals were amplified following the multiplex fluorescent kit. Finally, RAP2 and p32 signals were developed by secondary antibodies incubation (diluted 1/2000 in co-detection diluent) followed by Tyramide Signal Amplification (TSA plus kit, NEL760001KT, Perkin Elmer). Images were captured with a confocal (Leica DMI6000) microscope.

Immunofluorescence staining of fixed cells

Cells were grown on glass slides in 24-well plates, transfected with GapmeRs and fixed 72 hours after with 4% paraformaldheyde for 15 minutes. After two washes with PBS buffer they were permeabilized in PBS+triton X-100 0,1% for 5 minutes and blocked with PBS+10% FCS inactivated for 20 minutes. Primary antibodies were incubated overnight at 4°C and after three washes with PBS+Triton 0,1%, cells were stained for 1 hour at room temperature with AlexaFluor-488 conjugated secondary antibodies (Life technologies) diluted 1/500 in PBS+10% FCS. After three washes with PBS+Triton 0,1%, cells were stained with DAPI (final concentration 1 ug/ml) and mounted on microscopy slides. Anti-TP53BP1 (NB100-304), anti-RAP2 (SantaCruz, sc-515711) and anti-p32 (Bethyl, A302-863A) were diluted 1/200 in PBS+10% FCS; anti-gamma H2AX (Ser139, Abcam, ab11174) 1/400. Images were captured with a confocal (Leica DMI6000) microscope.

Mitotracker live imaging

Cells were cultured in 4 wells 35x10mm dishes (CellView, Greiner Bio-one), stained for 2 hours with Mitotracker Red CMXRos (125nM) and Hoechst 33342 (1ug/ml) and analysed with a confocal (Leica DMI6000) microscope in a temperature controlled (37°C) chamber.

RNA extraction and quantitative PCR

Total mRNA isolation was performed using Trizol and isopropanol precipitation. Isolation of cytosolic, nuclear soluble and chromatin associated RNA was performed as described in (Conrad and Ørom 2017). Briefly, cells were harvested and washed in PBS buffer, resuspended in 0.15% NP-40 lysis buffer and centrifuged on a 24% sucrose cushion (taking supernatant as the cytosolic fraction). Nuclei were resuspended in 1M Urea, 1% NP-40 lysis buffer and centrifuged to recover the nuclear soluble fraction in the supernatant. The chromatin pellet was finally resupended in 1ml of Trizol reagent (MRCgene), solubilized using a 21-gauge needle and isolated following manufacturer instructions. Cyosolic and nuclear

soluble fractions were cleared by centrifugation and RNA was isolated from 200 ul of each using 1ml of Trizol. Total and fractionated RNAs were treated with DNAseI following the TurboDnase free kit instructions (Thermofisher) and reversed transcribed using Superscript IV reverse transcriptase (Thermofisher) following manufacturer instructions. qRT-PCR was carried out with SYBR Green I (Roche) and monitored by a LightCycler 480 (Roche). Target genes expression was normalized using TBP, HBMS, GAPDH, ACTB, Rpl13a as reference genes. Actin and Xist were taken as RNA controls for cellular fractionation for cytosolic and nuclear soluble/chromatin associated fraction respectively. Primers for RT-qPCR were designed using Primer3 and are listed in Table 2.

Protein extraction and western blotting

Whole cell extracts were prepared by the standard freeze-thaw technique using LSDB 500 buffer (500 mM KCl, 25 mM Tris at pH 7.9, 10% glycerol (v/v), 0.05% NP-40 (v/v), 16mM DTT, and protease inhibitor cocktail). Cell lysates were subjected to SDS–polyacrylamide gel electrophoresis (SDS-PAGE) and proteins were transferred onto a nitrocellulose membrane. Membranes were incubated with primary antibodies in TBS+ 5% BSA + 0.01% Tween-20. Overnight at 4 °C. The membrane was then incubated with HRP-conjugated secondary antibody (Jackson ImmunoResearch) for 1h at room temperature, and visualized using the ECL detection system (GE Healthcare). Antibodies used are listed in Table 3.

Mitochondria fractionation

Mitochondria were isolated with the Mitochondria Isolation kit (Thermofisher) following manufacturer instructions. Briefly, harvested cells were washed and pelleted, resuspended in buffer A and incubated 2 minutes on ice. Buffer B was added for 5 minutes, vortexing every minute and diluted with buffer C (same volume of buffer A). Nuclei were pelleted 10 minutes at 700g and supernatant centrifuged for 15 minutes at 3000g. Purified

mitochondria were washed once in buffer C and used for RNA (Trizol-isopropanol precipitation) or protein (TBS+CHAPS 2%) extraction.

Linc00518 pull-down and liquid chromatography- tandem mass spectrometry (LC-MS/MS) analysis

MM011 cells were grown in 15cm petri dishes, harvested by trypsinization, washed, pelleted, re-suspended in lysis buffer (TrisHCl 20mM pH8, NaCl 200mM, MgCl2 2.5mM, Triton 0.05%, DEPC water) supplemented with fresh DTT (1mM), protease and phosphatase inhibitor cocktail (Thermofisher) and RNAsin (Thermofisher) and kept 20 minutes in ice. Membranes were pelleted 3000g for 3 minutes at 4°C and supernatant pre-cleared for 1 hour at 4°C with sepharose streptavidin coated beads. Aliquots were kept as RNA and protein inputs and the remaining lysate incubated 2 hours with streptavidin coated beads incubated with 400pmol anti-PCA3 or L518 specific DNA biotinylated oligonucleotides (sequences listed in Table 4). Beads were pelleted for 3 min at 3000g and washed 3 times with lysis buffer. After final wash beads were split in two for RNA and protein extraction. RNA was purified by Trizol and isopropanol precipitation, digested with DNAse, reverse transcribed and analysed by qPCR for L518 and TINCR expression. Proteins were eluted by boiling beads in Laemli sample buffer, boiled samples were run in NuPAGE® Novex 4-12% gradient gels. Three independent experiments were performed, and, in each case, the entire lane is excised in seven consecutive bands to be ben subjected to “in-gel” digestion protocol as previously described (Shevchenko et, al). Briefly, proteins were reduced in 10 mM DTT for 1 hour at 56º C and alkylated with 55 mM iodoacetamide for 45 minutes at room temperature. Enzymatic digestion was performed using 12.5 ng/µl trypsin overnight at 37ºC. Tryptic peptides were extracted from the gel with 3% trifluoroacetic acid (TFA) and 30% acetonitrile (ACN). The extracted peptides were concentrated onto homemade StageTips reversed phase microcolumns. Peptides were then

eluted in 40 µl buffer B (80% ACN, 0.1% formic acid (FA)). ACN was evaporated using a vacuum concentrator (Speed Vac, Eppendorf) and the volume of the eluates were adjusted to 5 µl with 1% TFA, to be then injected for peptide separation and analysis into a reversed-phase nano-flow liquid chromatographic (nRP-LC) column using an EASY-nLC 1200 (Thermo Fisher Scientific) coupled to an Q-Exactive HF instrument (Thermo Fisher Scientific) through a nano-electrospray ion source (EASY-Spray, Thermo Fisher Scientific). The nRP-LC system was operated in one column set-up with an EasySpray PEPMAP RSLC C18 (Thermo Fisher Scientific) kept at 45°C constant. Solvent A was 0.1% formic acid (FA) and solvent B was 0.1% FA in 80% ACN. Samples were loaded in aqueous 0.1% (FA) solution at constant pressure (980 Bar). Peptides were separated with a gradient of 3–30% solvent B over 69 min followed by a gradient of 30–60% for 5 min and 60–95% over 5 min at a flow rate of 300 nL/min. The Q-Exactive was operated in the data-dependent acquisition (DDA) mode and MS spectra (from m/z 375-1550) were analysed in the Orbitrap detector with resolution R=60,000 at m/z 200. The fifteen most intense peptide ions were isolated to a target value of 3e6 and fragmented by Higher Energy Collision Dissociation (HCD) with a normalized collision energy (NCE) setting of 28. The maximum allowed ion accumulation times was 80ms for MSMS. The dynamic exclusion time was set to 20s.

Post-acquisition MS data analysis for proteomics

Acquired raw data were analysed with the integrated suite of algorithms MaxQuant, version 1.6.1.1, using the Andromeda search engine. False discovery rate (FDR) for both peptides and protein identifications was set to a maximum of 0.01. Carbamidomethylation of Cysteine was set as a fixed modification. Uniprot Human sequence database was used for peptide identification (74470 Entries). LFQ intensity calculation was enabled requiring a minimum LFQ ratio count equal to two. The match between runs (MBRs) feature was selected

and a tolerance of 0.7 min was specified for the match time window option. The “protein groups” (.txt) output file from MaxQuant was processed by Perseus software for statistics. Briefly, no imputation for missing values was used, and the data were filtered, in order to have 3 valid values in at least one group. A t-student test was used to compare protein co-enriched in the L518- versus the PCA3- pull-down experiments and the threshold settings to select significant enriched proteins were S0=0 and FDR=0.05 (see MS_Supplementary_Table). Proteins identified uniquely in the L518 pulldown were listed in the corresponding spreadsheet in MS-Supplementary-Table.

Immunoprecipitation.

Cells were grown in 15cm petri dishes, harvested by scraping, resuspended in lysis buffer (20mM TrisHCl pH8, 200mM NaCl, 2.5mM MgCl2, 0.05%Triton, DEPC water) supplemented with DTT (1mM), protease/phosphatase inhibitor cocktail (Thermofisher) and RNAsin (Thermofisher) and kept on ice for 15 minutes, pipetting every 3 minutes. Membranes were pelleted 10 minutes at 10000g at 4°C and the supernatant precleared 1 hour at 4°C with protein G magnetic beads. Lysate was quantified by Bradford protein quantification assay (Biorad) and incubated overnight at 4°C with indicated antibodies. Protein G magnetic beads were added for 3 hours at 4°C to isolate RNA-protein complexes and washed 5 times in lysis buffer. After final wash beads were divided in two aliquots to perform RNA and protein extraction. RNA was purified by Trizol and isopropanol precipitation, digested with DNAse, reverse transcribed and analysed by qPCR for L518, SAMMSON, NEAT1, MALAT1 expression. Proteins were eluted by boiling beads in Laemli sample buffer and analysed by western blot with anti-RAP2, p32, XRN2, DRP1 antibodies.

Table 1

GapmeR/siRNA	Sequence
Negative A	AACACGTCTATACGC
L518#1	CCGACCTGAATTGCAA
L518#2	GTAGAGGCTAGAACTG
L520#1	TTTGATGAGTGAGTCG
L520#2	GAGTCGCTGAGAATTA
SAMMSON	GTGTGAACTTGGCT
siCTRL	TTAGTCGACATGTAAACCA
siRAP2A	TACTCTTAGCGGAAGTTTC
siRAP2B	TATATTAGCAAACTTTTCCC
siRAP2C	TACTGGACGACACAAGTTG
siTFAP2A	TGATCTGGGATGTTAATAC

Table 2

Primer name	Sequence
hbact_F	ACATCTGCTGGAAGGTGGAC
hbact_R	CCCAGCACAATGAAGATCAA
hGAPDH_F	ACAACTTTGGTATCGTGGAAGG
hGAPDH_R	GCCATCACGCCACAGTTTC
hRPL13a_F	TTGAGGACCTCTGTGTATTTGTCAA
hRPL13a_R	CCTGGAGGAGAAGAGGAAAGAGA
hHMBS_F	GGCAATGCGGCTGCAA
hHMBS_R	GGGTACCCACGCGAATCAC
hTBP_F	CGGCTGTTTAACTTCGCTTC
hTBP_R	CACACGCCAAGAAACAGTGA
hTFAP2A_F	ACCCGGGTATTAACATCCCA
hTFAP2A_R	GCATTGCTGTTGGACTTGGA
hLINC00518_F	ACCTAACCTGCGAATGCTGT

hLINC00518_R	GCCTAAACATTTGCTGCCCC
hLINC00520_F	CAATGCTTGGAAGGCGTGAT
hLINC00520_R	AAACGTATGGCCACCTCTGA
hNEAT1_F	GGAGAGGGTTGGTTAGAGAT
hNEAT1_R	CCTTCAACCTGCATTTCCTA
hMALAT1_F	GGATTCCAGGAAGGAGCGAG
hMALAT1_R	ATTGCCGACCTCACGGATTT
hSAMMSON_F	CCTCTAGATGTGTAAGGGTAGT
hSAMMSON_R	TTGAGTTGCATAGTTGAGGAA
hXIST_F	CCACCACACGTCAAGCTCTTC
hXIST_R	CAGGTGGGAAGGCTGACTTC
hRAP2A_F	AGATCATCCGCGTGAAGC
hRAP2A_R	CTTCGCTGGACGATACTTCTC
hRAP2B_F	AACAAAGCCTCGGTAGACGA
hRAP2B_R	CTCATCGCCGTTGGGCT
hRAP2C_F	ACCTCAATCATGGCCATACC
hRAP2C_R	CAAAGCAGCATCTGTGCAA
QT	CCAGTGAGCAGAGTGACGAGGACTCGAGCTCAAGCTTTTTTTTTTTTTTT
QO	CCAGTGAGCAGAGTGACG
QI	GAGGACTCGAGCTCAAGC

Table 3

Target	Lot	Host	Application	Dilution
TFAP2A (sc-12726)	D0218	Mouse	WB	1:1000
VINCULIN (V4505)	099M	Mouse	WB	1:2000
ACTIN (in house)		Mouse	WB	1:5000

C1QBP/p32 (A302-863)	1	Rabbit	WB IF	1:1000 1:200
HSP60 (ab46798)		Rabbit	WB	1:10000
RAP2 (sc-515711)	G2516	Mouse	WB IF IP	1:1000 1:200 1ug/1mg lysate
FLAG (F7425)	078M	Rabbit	IP	1ug/1mg lysate
FLAG (F1804)	SLCD3990	Mouse	WB	1:1000
XRN2 (A301-103)		Rabbit	WB IP	1:1000 1ug/1mg lysate
gamma H2A.X (phospho S139) (ab22551)	GR3358071-2	Mouse	WB IF	1:1000 1:400
53BP1 (NB100-303)	A2	Rabbit	IF	1:200
H3 (ab176843)	GR135176	Rabbit	WB	1:10000
Phospho DRP1 (S637) (4867)	4	Rabbit	WB	1:2000
DRP1 (14647)	3	Mouse	WB	1:2000
DRP1 (12957-1-AP)		Rabbit	IP	1ug/1mg lysate
Normal rabbit IgG (12-370)	3456023	Rabbit	IP	1ug/1mg lysate
Normal mouse IgG (sc-2025)	L0619	Mouse	IP	1ug/1mg lysate

Table 4

Oligo name	Sequence
L518-1	gtcactctcattgaggatga
L518-2	gcaaagaagacacacgtgct
L518-3	gagaagtagggaaacccagt

L518-4	aacttgaaatgggtggcagg
L518-5	caggttaggtacgcttaagt
L518-6	ctaagtcgtcactttggagg
L518-7	tgtagacagtagaggctaga
L518-8	ttttctgaaatccccaatcc
PCA3-1	gcacttgctatttcttctgt
PCA3-2	ctctgtttttctgatgccag
PCA3-3	tgtttgttgcatgtcttgtg
PCA3-4	attctttattgccaggagtg
PCA3-5	tatgcatattgtggttgtcc
PCA3-6	tgtctgaatcctctccaaac
PCA3-7	gctagcatccataataggag
PCA3-8	ttgcatgcatgtaccacaag

REFERENCES

Arun, Gayatri, Sarah D Diermeier, and David L Spector. 2018. "Therapeutic Targeting of Long Non-Coding RNAs in Cancer." *Trends in Molecular Medicine*. Elsevier Ltd. https://doi.org/10.1016/j.molmed.2018.01.001.

Badal, Brateil, Alexander Solovyov, Serena Di Cecilia, Joseph Minhow Chan, Li Wei Chang, Ramiz Iqbal, Iraz T. Aydin, et al. 2017. "Transcriptional Dissection of Melanoma Identifies a High-Risk Subtype Underlying TP53 Family Genes and Epigenome Deregulation." *JCI Insight* 2 (9). https://doi.org/10.1172/jci.insight.92102.

Bai, Xue, David E Fisher, and Keith T Flaherty. 2019. "Cell-State Dynamics and Therapeutic Resistance in Melanoma from the Perspective of MITF and IFNγ Pathways." *Nature Reviews Clinical Oncology*. Springer US. https://doi.org/10.1038/s41571-019-0204-6.

Bruurs, Lucas J.M., and Johannes L. Bos. 2014. "Mechanisms of Isoform Specific Rap2 Signaling during Enterocytic Brush Border Formation." *PLoS ONE* 9 (9): 1–9. https://doi.org/10.1371/journal.pone.0106687.

Cereghetti, G M, V Costa, and L Scorrano. 2010. "Inhibition of Drp1-Dependent Mitochondrial Fragmentation and Apoptosis by a Polypeptide Antagonist of Calcineurin." *Cell Death and Differentiation* 17 (11): 1785–94. https://doi.org/10.1038/cdd.2010.61.

Chang, Chuang Rung, and Craig Blackstone. 2007. "Cyclic AMP-Dependent Protein Kinase Phosphorylation of Drp1 Regulates Its GTPase Activity and Mitochondrial Morphology." *Journal of Biological Chemistry* 282 (30): 21583–87. https://doi.org/10.1074/jbc.C700083200.

Chen, Hsiuchen, and David C. Chan. 2017. "Mitochondrial Dynamics in Regulating the Unique

Phenotypes of Cancer and Stem Cells." *Cell Metabolism* 26 (1): 39–48. https://doi.org/10.1016/j.cmet.2017.05.016.

Coe, Elizabeth A., Jennifer Y. Tan, Michael Shapiro, Pakavarin Louphrasitthiphol, Andrew R. Bassett, Ana C. Marques, Colin R. Goding, and Keith W. Vance. 2019. "The MITF-SOX10 Regulated Long Non-Coding RNA DIRC3 Is a Melanoma Tumour Suppressor." *PLoS Genetics* 15 (12): 1–22. https://doi.org/10.1371/journal.pgen.1008501.

Conrad, Thomas, and Ulf Andersson Ørom. 2017. *Cellular Fractionation and Isolation of Chromatin-Associated RNA*. Edited by Ulf Andersson Ørom. *Enhancer RNAs: Methods and Protocols*. Vol. 1468. Methods in Molecular Biology. New York, NY: Springer New York. https://doi.org/10.1007/978-1-4939-4035-6.

Cribbs, J. Thomas, and Stefan Strack. 2007. "Reversible Phosphorylation of Drp1 by Cyclic AMP-Dependent Protein Kinase and Calcineurin Regulates Mitochondrial Fission and Cell Death." *EMBO Reports* 8 (10): 939–44. https://doi.org/10.1038/sj.embor.7401062.

Cronin, Julia C., Dawn E. Watkins-Chow, Art Incao, Joanne H. Hasskamp, Nicola Schonewolf, Lauren G. Aoude, Nicholas K. Hayward, et al. 2013. "SOX10 Ablation Arrests Cell Cycle, Induces Senescence, and Suppresses Melanomagenesis." *Cancer Research* 73 (18): 5709–18. https://doi.org/10.1158/0008-5472.CAN-12-4620.

Di, Jiehui, Hui Huang, Debao Qu, Juangjuan Tang, Wenjia Cao, Zheng Lu, Qian Cheng, et al. 2015. "Rap2B Promotes Proliferation, Migration, and Invasion of Human Breast Cancer through Calcium-Related ERK1/2 Signaling Pathway." *Scientific Reports* 5 (December 2014): 1–11. https://doi.org/10.1038/srep12363.

Din, Shabana, Matthew Mason, Mirko Völkers, Bevan Johnson, Christopher T. Cottage, Zeping Wang, Anya Y. Joyo, et al. 2013. "Pim-1 Preserves Mitochondrial Morphology by Inhibiting Dynamin-Related Protein 1 Translocation." *Proceedings of the National Academy of Sciences of the United States of America* 110 (15): 5969–74. https://doi.org/10.1073/pnas.1213294110.

Ennen, Marie, Céline Keime, Giovanni Gambi, Alice Kieny, Sebastien Coassolo, Christelle Thibault-Carpentier, Fanny Margerin-Schaller, et al. 2017. "MITF-High and MITF-Low Cells and a Novel Subpopulation Expressing Genes of Both Cell States Contribute to Intra- and Intertumoral Heterogeneity of Primary Melanoma." *Clinical Cancer Research* 23 (22): 7097–7107. https://doi.org/10.1158/1078-0432.CCR-17-0010.

Ferraz, Letícia Silva, Renata Torres da Costa, Cláudia Alves da Costa, César Augusto João Ribeiro, Denise Costa Arruda, Silvya Stuchi Maria-Engler, and Tiago Rodrigues. 2020. "Targeting Mitochondria in Melanoma: Interplay between MAPK Signaling Pathway and Mitochondrial Dynamics." *Biochemical Pharmacology* 178 (April). https://doi.org/10.1016/j.bcp.2020.114104.

Fogal, Valentina, Adam D. Richardson, Priya P. Karmali, Immo E. Scheffler, Jeffrey W. Smith, and Erkki Ruoslahti. 2010. "Mitochondrial P32 Protein Is a Critical Regulator of Tumor Metabolism via Maintenance of Oxidative Phosphorylation." *Molecular and Cellular Biology* 30 (6): 1303–18. https://doi.org/10.1128/mcb.01101-09.

Fontanals-Cirera, Barbara, Dan Hasson, Chiara Vardabasso, Raffaella Di Micco, Praveen Agrawal, Asif Chowdhury, Madeleine Gantz, et al. 2017. "Harnessing BET Inhibitor Sensitivity Reveals AMIGO2 as a Melanoma Survival Gene." *Molecular Cell* 68 (4): 731-744.e9. https://doi.org/10.1016/j.molcel.2017.11.004.

Fufa, Temesgen D., Laura L. Baxter, Julia C. Wedel, Derek E. Gildea, Stacie K. Loftus, and William J.

Pavan. 2019. “MEK Inhibition Remodels the Active Chromatin Landscape and Induces SOX10 Genomic Recruitment in BRAF(V600E) Mutant Melanoma Cells.” *Epigenetics and Chromatin* 12 (1): 1–18. https://doi.org/10.1186/s13072-019-0297-2.

Gerami, Pedram, Zuxu Yao, David Polsky, Burkhard Jansen, Klaus Busam, Jonhan Ho, Mary Martini, and Laura K. Ferris. 2017. “Development and Validation of a Noninvasive 2-Gene Molecular Assay for Cutaneous Melanoma.” *Journal of the American Academy of Dermatology* 76 (1): 114-120.e2. https://doi.org/10.1016/j.jaad.2016.07.038.

Giuliano, Sandy, Yann Cheli, Mickaël Ohanna, Caroline Bonet, Laurent Beuret, Karine Bille, Agnès Loubat, et al. 2010. “Microphthalmia-Associated Transcription Factor Controls the DNA Damage Response and a Lineage-Specific Senescence Program in Melanomas.” *Cancer Research* 70 (9): 3813–22. https://doi.org/10.1158/0008-5472.CAN-09-2913.

Goding, Colin R, and Heinz Arnheiter. 2019. “MITF — the First 25 Years.” *Genes and Development*, 1–25. https://doi.org/10.1101/gad.324657.119.ness.

Gomes, Ligia C., Giulietta Di Benedetto, and Luca Scorrano. 2011. “During Autophagy Mitochondria Elongate, Are Spared from Degradation and Sustain Cell Viability.” *Nature Cell Biology* 13 (5): 589–98. https://doi.org/10.1038/ncb2220.

Gopal, Y. N.Vashisht, Helen Rizos, Guo Chen, Wanleng Deng, Dennie T. Frederick, Zachary A. Cooper, Richard A. Scolyer, et al. 2014. “Inhibition of MTORC1/2 Overcomes Resistance to MAPK Pathway Inhibitors Mediated by PGC1α and Oxidative Phosphorylation in Melanoma.” *Cancer Research* 74 (23): 7037–47. https://doi.org/10.1158/0008-5472.CAN-14-1392.

Guo, Zekun, Jian Yuan, Wenwen Tang, Xinya Chen, Xiuting Gu, Kuntian Luo, Yingli Wang, Bo Wan, and Long Yu. 2007. “Cloning and Characterization of the Human Gene RAP2C, a Novel Member of Ras Family, Which Activates Transcriptional Activities of SRE.” *Molecular Biology Reports* 34 (3): 137–44. https://doi.org/10.1007/s11033-006-9023-9.

Guttman, Mitchell, Ido Amit, Manuel Garber, Courtney French, Michael F. Lin, David Feldser, Maite Huarte, et al. 2009. “Chromatin Signature Reveals over a Thousand Highly Conserved Large Non-Coding RNAs in Mammals.” *Nature* 458 (7235): 223–27. https://doi.org/10.1038/nature07672.

Han, Shujun, Yibo Ren, Wangxiao He, Huadong Liu, Zhe Zhi, Xinliang Zhu, Tielin Yang, et al. 2018. “ERK-Mediated Phosphorylation Regulates SOX10 Sumoylation and Targets Expression in Mutant BRAF Melanoma.” *Nature Communications* 9 (1): 1–14. https://doi.org/10.1038/s41467-017-02354-x.

Haq, Rizwan, Jonathan Shoag, Pedro Andreu-perez, Satoru Yokoyama, Hannah Edelman, Glenn C Rowe, Dennie T Frederick, et al. 2013. “Article Oncogenic BRAF Regulates Oxidative Metabolism via PGC1 a and MITF.” *Cancer Cell* 23 (3): 302–15. https://doi.org/10.1016/j.ccr.2013.02.003.

Haq, Rizwan, Satoru Yokoyama, Elena B. Hawryluk, Göran B. Jönsson, Dennie Tompers Frederick, Kevin McHenry, Dale Porter, et al. 2013. “BCL2A1 Is a Lineage-Specific Antiapoptotic Melanoma Oncogene That Confers Resistance to BRAF Inhibition.” *Proceedings of the National Academy of Sciences of the United States of America* 110 (11): 4321–26. https://doi.org/10.1073/pnas.1205575110.

Hung, Chiu Lien, Ling Yu Wang, Yen Ling Yu, Hong Wu Chen, Shiv Srivastava, Gyorgy Petrovics, and Hsing Jien Kung. 2014. “A Long Noncoding RNA Connects C-Myc to Tumor Metabolism.” *Proceedings of the National Academy of Sciences of the United States of America* 111 (52): 18697–702. https://doi.org/10.1073/pnas.1415669112.

Jain, Abhinav K., Yuanxin Xi, Ryan McCarthy, Kendra Allton, Kadir C. Akdemir, Lalit R. Patel, Bruce Aronow, et al. 2016. "LncPRESS1 Is a P53-Regulated LncRNA That Safeguards Pluripotency by Disrupting SIRT6-Mediated De-Acetylation of Histone H3K56." *Molecular Cell* 64 (5): 967–81. https://doi.org/10.1016/j.molcel.2016.10.039.

Jain, Rakesh K., Lance L. Munn, and Dai Fukumura. 2002. "Dissecting Tumour Pathophysiology Using Intravital Microscopy." *Nature Reviews Cancer* 2 (4): 266–76. https://doi.org/10.1038/nrc778.

Jerby-Arnon, Livnat, Parin Shah, Michael S. Cuoco, Christopher Rodman, Mei Ju Su, Johannes C. Melms, Rachel Leeson, et al. 2018. "A Cancer Cell Program Promotes T Cell Exclusion and Resistance to Checkpoint Blockade." *Cell* 175 (4): 984-997.e24. https://doi.org/10.1016/j.cell.2018.09.006.

Jose, Caroline, Nadège Bellance, and Rodrigue Rossignol. 2011. "Choosing between Glycolysis and Oxidative Phosphorylation: A Tumor's Dilemma?" *Biochimica et Biophysica Acta - Bioenergetics* 1807 (6): 552–61. https://doi.org/10.1016/j.bbabio.2010.10.012.

Kapusta, Aurélie, Zev Kronenberg, Vincent J. Lynch, Xiaoyu Zhuo, Lee Ann Ramsay, Guillaume Bourque, Mark Yandell, and Cédric Feschotte. 2013. "Transposable Elements Are Major Contributors to the Origin, Diversification, and Regulation of Vertebrate Long Noncoding RNAs." *PLoS Genetics* 9 (4). https://doi.org/10.1371/journal.pgen.1003470.

Kashatus, David F, Kian-Huat Lim, Donita C Brady, Nicole L K Pershing, Adrienne D Cox, and Christopher M Counter. 2011. "RALA and RALBP1 Regulate Mitochondrial Fission at Mitosis." *Nature Cell Biology* 13 (9): 1108–15. https://doi.org/10.1038/ncb2310.

Kashatus, Jennifer A., Aldo Nascimento, Lindsey J. Myers, Annie Sher, Frances L. Byrne, Kyle L. Hoehn, Christopher M. Counter, and David F. Kashatus. 2015. "Erk2 Phosphorylation of Drp1 Promotes Mitochondrial Fission and MAPK-Driven Tumor Growth." *Molecular Cell* 57 (3): 537–51. https://doi.org/10.1016/j.molcel.2015.01.002.

Konieczkowski, David J., Cory M. Johannessen, Omar Abudayyeh, Jong Wook Kim, Zachary A. Cooper, Adriano Piris, Dennie T. Frederick, et al. 2014. "A Melanoma Cell State Distinction Influences Sensitivity to MAPK Pathway Inhibitors." *Cancer Discovery* 4 (7): 816–27. https://doi.org/10.1158/2159-8290.CD-13-0424.

Kunz, Manfred, Henry Löffler-Wirth, Michael Dannemann, Edith Willscher, Gero Doose, Janet Kelso, Tina Kottek, et al. 2018. "RNA-Seq Analysis Identifies Different Transcriptomic Types and Developmental Trajectories of Primary Melanomas." *Oncogene* 37 (47): 6136–51. https://doi.org/10.1038/s41388-018-0385-y.

Landsberg, Jennifer, Judith Kohlmeyer, Marcel Renn, Tobias Bald, Meri Rogava, Mira Cron, Martina Fatho, et al. 2012. "Melanomas Resist T-Cell Therapy through Inflammation-Induced Reversible Dedifferentiation." *Nature* 490 (7420): 412–16. https://doi.org/10.1038/nature11538.

Laurette, Patrick, Sébastien Coassolo, Guillaume Davidson, Isabelle Michel, Giovanni Gambi, Wenjin Yao, Pierre Sohier, et al. 2020. "Chromatin Remodellers Brg1 and Bptf Are Required for Normal Gene Expression and Progression of Oncogenic Braf-Driven Mouse Melanoma." *Cell Death and Differentiation* 27 (1): 29–43. https://doi.org/10.1038/s41418-019-0333-6.

Laurette, Patrick, Thomas Strub, Dana Koludrovic, Celine Keime, Stephanie Le Gras, Hannah Seberg, Eric Van Otterloo, et al. 2015. "Transcription Factor MITF and Remodeller BRG1 Define Chromatin Organisation at Regulatory Elements in Melanoma Cells." *ELife* 2015 (4): 1–40. https://doi.org/10.7554/eLife.06857.

Leucci, Eleonora, Roberto Vendramin, Marco Spinazzi, Patrick Laurette, Mark Fiers, Jasper Wouters, Enrico Radaelli, et al. 2016. “Melanoma Addiction to the Long Non-Coding RNA SAMMSON.” *Nature* 531 (7595): 518–22. https://doi.org/10.1038/nature17161.

Li, J., Q. Huang, X. Long, X. Guo, X. Sun, X. Jin, Z. Li, et al. 2017. “Mitochondrial Elongation-Mediated Glucose Metabolism Reprogramming Is Essential for Tumour Cell Survival during Energy Stress.” *Oncogene* 36 (34): 4901–12. https://doi.org/10.1038/onc.2017.98.

Li, Xiao Ling, Murugan Subramanian, Matthew F. Jones, Ritu Chaudhary, Deepak K. Singh, Xinying Zong, Berkley Gryder, et al. 2017. “Long Noncoding RNA PURPL Suppresses Basal P53 Levels and Promotes Tumorigenicity in Colorectal Cancer.” *Cell Reports* 20 (10): 2408–23. https://doi.org/10.1016/j.celrep.2017.08.041.

Lin, Aifu, Chunlai Li, Zhen Xing, Qingsong Hu, Ke Liang, Leng Han, Cheng Wang, et al. 2016. “The LINK-A LncRNA Activates Normoxic HIF1α Signalling in Triple-Negative Breast Cancer.” *Nature Cell Biology* 18 (2): 213–24. https://doi.org/10.1038/ncb3295.

Liu, Bodu, Lijuan Sun, Qiang Liu, Chang Gong, Yandan Yao, Xiaobin Lv, Ling Lin, et al. 2015. “A Cytoplasmic NF-KB Interacting Long Noncoding RNA Blocks IκB Phosphorylation and Suppresses Breast Cancer Metastasis.” *Cancer Cell* 27 (3): 370–81. https://doi.org/10.1016/j.ccell.2015.02.004.

Liu, Xiaowen, Zhen Dong Xiao, Leng Han, Jiexin Zhang, Szu Wei Lee, Wenqi Wang, Hyemin Lee, et al. 2016. “LncRNA NBR2 Engages a Metabolic Checkpoint by Regulating AMPK under Energy Stress.” *Nature Cell Biology* 18 (4): 431–42. https://doi.org/10.1038/ncb3328.

Loh, Joon-Khim, Ching-Chih Lin, Ming-Chang Yang, Chia-Hua Chou, Wan-Shia Chen, Ming-Chang Hong, Chung-Lung Cho, et al. 2015. “GSKIP- and GSK3-Mediated Anchoring Strengthens CAMP/PKA/Drp1 Axis Signaling in the Regulation of Mitochondrial Elongation.” *Biochimica et Biophysica Acta (BBA) - Molecular Cell Research* 1853 (8): 1796–1807. https://doi.org/https://doi.org/10.1016/j.bbamcr.2015.04.013.

Louphrasitthiphol, Pakavarin, Ioanna Ledaki, Jagat Chauhan, Paola Falletta, Robert Siddaway, Francesca M. Buffa, David R. Mole, Tomoyoshi Soga, and Colin R. Goding. 2019. “MITF Controls the TCA Cycle to Modulate the Melanoma Hypoxia Response.” *Pigment Cell and Melanoma Research* 32 (6): 792–808. https://doi.org/10.1111/pcmr.12802.

Luan, Wenkang, Yuting Ding, Shaojun Ma, Hongru Ruan, Jinlong Wang, and Feng Lu. 2019. “Long Noncoding RNA LINC00518 Acts as a Competing Endogenous RNA to Promote the Metastasis of Malignant Melanoma via MiR-204-5p/AP1S2 Axis.” *Cell Death and Disease* 10 (11). https://doi.org/10.1038/s41419-019-2090-3.

Ma, Lina, Jiabao Cao, Lin Liu, Qiang Du, Zhao Li, Dong Zou, Vladimir B. Bajic, and Zhang Zhang. 2019. “Lncbook: A Curated Knowledgebase of Human Long Non-Coding Rnas.” *Nucleic Acids Research* 47 (D1): D128–34. https://doi.org/10.1093/nar/gky960.

Machida, Noriko, Masato Umikawa, Kimiko Takei, Nariko Sakima, Bat Erdene Myagmar, Kiyohito Taira, Hiroshi Uezato, Yoshihide Ogawa, and Ken Ichi Kariya. 2004. “Mitogen-Activated Protein Kinase Kinase Kinase Kinase 4 as a Putative Effector of Rap2 to Activate the c-Jun N-Terminal Kinase.” *Journal of Biological Chemistry* 279 (16): 15711–14. https://doi.org/10.1074/jbc.C300542200.

Mattick, John S. 2018. “The State of Long Non-Coding RNA Biology.” *Non-Coding RNA* 4 (3). https://doi.org/10.3390/ncrna4030017.

Maurus, K., A. Hufnagel, F. Geiger, S. Graf, C. Berking, A. Heinemann, A. Paschen, et al. 2017. “The AP-1 Transcription Factor FOSL1 Causes Melanocyte Reprogramming and Transformation.” *Oncogene* 36 (36): 5110–21. https://doi.org/10.1038/onc.2017.135.

McHugh, Colleen A., Chun Kan Chen, Amy Chow, Christine F. Surka, Christina Tran, Patrick McDonel, Amy Pandya-Jones, et al. 2015. “The Xist LncRNA Interacts Directly with SHARP to Silence Transcription through HDAC3.” *Nature* 521 (7551): 232–36. https://doi.org/10.1038/nature14443.

Meng, Zhipeng, Yunjiang Qiu, Kimberly C. Lin, Aditya Kumar, Jesse K. Placone, Cao Fang, Kuei Chun Wang, et al. 2018. “RAP2 Mediates Mechanoresponses of the Hippo Pathway.” *Nature* 560 (7720): 655–60. https://doi.org/10.1038/s41586-018-0444-0.

Molina, Anthony J A, Jakob D Wikstrom, Linsey Stiles, Guy Las, Hibo Mohamed, Alvaro Elorza, Gil Walzer, et al. 2009. “Mitochondrial Networking Protects Beta-Cells from Nutrient-Induced Apoptosis.” *Diabetes* 58 (10): 2303–15. https://doi.org/10.2337/db07-1781.

Müller, Judith, Oscar Krijgsman, Jennifer Tsoi, Lidia Robert, Willy Hugo, Chunying Song, Xiangju Kong, et al. 2014. “Low MITF/AXL Ratio Predicts Early Resistance to Multiple Targeted Drugs in Melanoma.” *Nature Communications* 5. https://doi.org/10.1038/ncomms6712.

Papatriantafyllou, Maria. 2012. “A Mitochondrial Flirtation with the Nucleus.” *Nature Reviews Molecular Cell Biology* 13 (8): 478–478. https://doi.org/10.1038/nrm3404.

Parmenter, Tiffany J, Margarete Kleinschmidt, Kathryn M Kinross, Simon T Bond, Jason Li, Mohan R Kaadige, Aparna Rao, Karen E Sheppard, Willy Hugo, and Gulietta M Pupo. 2014. “Response of BRAF -Mutant Melanoma to BRAF Inhibition Is Mediated by a Network of Transcriptional Regulators of Glycolysis,” *Cancer Discovery* 4. https://doi.org/10.1158/2159-8290.CD-13-0440.

Quemener, Anaïs M., Laura Bachelot, Anne Forestier, Emmanuelle Donnou-Fournet, David Gilot, and Marie Dominique Galibert. 2020. “The Powerful World of Antisense Oligonucleotides: From Bench to Bedside.” *Wiley Interdisciplinary Reviews: RNA* 11 (5): 1–22. https://doi.org/10.1002/wrna.1594.

Rambow, Florian, Bastien Job, Valérie Petit, Franck Gesbert, Véronique Delmas, Hannah Seberg, Guillaume Meurice, et al. 2015. “New Functional Signatures for Understanding Melanoma Biology from Tumor Cell Lineage-Specific Analysis.” *Cell Reports* 13 (4): 840–53. https://doi.org/10.1016/j.celrep.2015.09.037.

Rambow, Florian, Jean Christophe Marine, and Colin R Goding. 2019. “Melanoma Plasticity and Phenotypic Diversity: Therapeutic Barriers and Opportunities.” *Genes and Development*. https://doi.org/10.1101/gad.329771.119.

Rambow, Florian, Aljosja Rogiers, Oskar Marin-Bejar, Sara Aibar, Julia Femel, Michael Dewaele, Panagiotis Karras, et al. 2018. “Toward Minimal Residual Disease-Directed Therapy in Melanoma.” *Cell* 174 (4): 843-855.e19. https://doi.org/10.1016/j.cell.2018.06.025.

Ramsdale, Rachel, Robert N. Jorissen, Frederic Z. Li, Sheren Al-Obaidi, Teresa Ward, Karen E. Sheppard, Patricia E. Bukczynska, et al. 2015. “The Transcription Cofactor C-JUN Mediates Phenotype Switching and BRAF Inhibitor Resistance in Melanoma.” *Science Signaling* 8 (390): ra82. https://doi.org/10.1126/scisignal.aab1111.

Riesenberg, Stefanie, Angela Groetchen, Robert Siddaway, Tobias Bald, Julia Reinhardt, Denise Smorra, Judith Kohlmeyer, et al. 2015. “MITF and C-Jun Antagonism Interconnects Melanoma

Dedifferentiation with pro-Inflammatory Cytokine Responsiveness and Myeloid Cell Recruitment." *Nature Communications* 6. https://doi.org/10.1038/ncomms9755.

Rumsey, W L, C Schlosser, E M Nuutinen, M Robiolio, and D F Wilson. 1990. "Cellular Energetics and the Oxygen Dependence of Respiration in Cardiac Myocytes Isolated from Adult Rat." *The Journal of Biological Chemistry* 265 (26): 15392–402.

Rusan, Maria, Kapsok Li, Yvonne Li, Camilla L. Christensen, Brian J. Abraham, Nicholas Kwiatkowski, Kevin A. Buczkowski, et al. 2018. *Suppression of Adaptive Responses to Targeted Cancer Therapy by Transcriptional Repression*. *Cancer Discovery*. Vol. 8. https://doi.org/10.1158/2159-8290.CD-17-0461.

Sabouny, Rasha, and Timothy E. Shutt. 2020. "Reciprocal Regulation of Mitochondrial Fission and Fusion." *Trends in Biochemical Sciences* 45 (7): 564–77. https://doi.org/10.1016/j.tibs.2020.03.009.

Saldaña-Meyer, Ricardo, Edgar González-Buendía, Georgina Guerrero, Varun Narendra, Roberto Bonasio, Félix Recillas-Targa, and Danny Reinberg. 2014. "CTCF Regulates the Human P53 Gene through Direct Interaction with Its Natural Antisense Transcript, Wrap53." *Genes and Development* 28 (7): 723–34. https://doi.org/10.1101/gad.236869.113.

Sati, Satish, Sourav Ghosh, Vaibhav Jain, Vinod Scaria, and Shantanu Sengupta. 2012. "Genome-Wide Analysis Reveals Distinct Patterns of Epigenetic Features in Long Non-Coding RNA Loci." *Nucleic Acids Research* 40 (20): 10018–31. https://doi.org/10.1093/nar/gks776.

Schadendorf, Dirk, David E. Fisher, Claus Garbe, Jeffrey E. Gershenwald, Jean Jacques Grob, Allan Halpern, Meenhard Herlyn, et al. 2015. "Melanoma." *Nature Reviews Disease Primers* 1 (April): 1–20. https://doi.org/10.1038/nrdp.2015.3.

Schmitt, Adam M., and Howard Y. Chang. 2016. "Long Noncoding RNAs in Cancer Pathways." *Cancer Cell* 29 (4): 452–63. https://doi.org/10.1016/j.ccell.2016.03.010.

Schmitt, Adam M., Julia T. Garcia, Tiffany Hung, Ryan A. Flynn, Ying Shen, Kun Qu, Alexander Y. Payumo, et al. 2016. "An Inducible Long Noncoding RNA Amplifies DNA Damage Signaling." *Nature Genetics* 48 (11): 1370–76. https://doi.org/10.1038/ng.3673.

Seberg, Hannah E., Eric Van Otterloo, Stacie K. Loftus, Huan Liu, Greg Bonde, Ramakrishna Sompallae, Derek E. Gildea, et al. 2017. *TFAP2 Paralogs Regulate Melanocyte Differentiation in Parallel with MITF*. *PLoS Genetics*. Vol. 13. https://doi.org/10.1371/journal.pgen.1006636.

Serasinghe, Madhavika N., Jesse D. Gelles, Kent Li, Lauren Zhao, Franco Abbate, Marie Syku, Jarvier N. Mohammed, et al. 2018. "Dual Suppression of Inner and Outer Mitochondrial Membrane Functions Augments Apoptotic Responses to Oncogenic MAPK Inhibition." *Cell Death and Disease* 9 (2): 1–13. https://doi.org/10.1038/s41419-017-0044-1.

Serasinghe, Madhavika N., Shira Y. Wieder, Thibaud T. Renault, Rana Elkholi, James J. Asciolla, Jonathon L. Yao, Omar Jabado, et al. 2015. "Mitochondrial Division Is Requisite to RAS-Induced Transformation and Targeted by Oncogenic MAPK Pathway Inhibitors." *Molecular Cell* 57 (3): 521–36. https://doi.org/10.1016/j.molcel.2015.01.003.

Shakhova, Olga, Daniel Zingg, Simon M. Schaefer, Lisette Hari, Gianluca Civenni, Jacqueline Blunschi, Stãphanie Claudinot, et al. 2012. "Sox10 Promotes the Formation and Maintenance of Giant Congenital Naevi and Melanoma." *Nature Cell Biology* 14 (8): 882–89. https://doi.org/10.1038/ncb2535.

Sirey, Tamara M., Kenny Roberts, Wilfried Haerty, Oscar Bedoya-Reina, Sebastian Rogatti Granados, Jennifer Y. Tan, Nick Li, et al. 2019. “The Long Non-Coding Rna Cerox1 Is a Post Transcriptional Regulator of Mitochondrial Complex i Catalytic Activity.” *ELife* 8: 1–31. https://doi.org/10.7554/eLife.45051.

Smith, Michael P., Holly Brunton, Emily J. Rowling, Jennifer Ferguson, Imanol Arozarena, Zsofia Miskolczi, Jessica L. Lee, et al. 2016. “Inhibiting Drivers of Non-Mutational Drug Tolerance Is a Salvage Strategy for Targeted Melanoma Therapy.” *Cancer Cell* 29 (3): 270–84. https://doi.org/10.1016/j.ccell.2016.02.003.

Strub, T., S. Giuliano, T. Ye, C. Bonet, C. Keime, D. Kobi, S. Le Gras, et al. 2011. “Essential Role of Microphthalmia Transcription Factor for DNA Replication, Mitosis and Genomic Stability in Melanoma.” *Oncogene* 30 (20): 2319–32. https://doi.org/10.1038/onc.2010.612.

Taguchi, Naoko, Naotada Ishihara, Akihiro Jofuku, Toshihiko Oka, and Katsuyoshi Mihara. 2007. “Mitotic Phosphorylation of Dynamin-Related GTPase Drp1 Participates in Mitochondrial Fission.” *Journal of Biological Chemistry* 282 (15): 11521–29. https://doi.org/https://doi.org/10.1074/jbc.M607279200.

Tasdogan, Alpaslan, Brandon Faubert, Vijayashree Ramesh, Jessalyn M. Ubellacker, Bo Shen, Ashley Solmonson, Malea M. Murphy, et al. 2020. “Metabolic Heterogeneity Confers Differences in Melanoma Metastatic Potential.” *Nature* 577 (7788): 115–20. https://doi.org/10.1038/s41586-019-1847-2.

Tirosh, Itay, Benjamin Izar, Sanjay M. Prakadan, Marc H. Wadsworth, Daniel Treacy, John J. Trombetta, Asaf Rotem, et al. 2016. “Dissecting the Multicellular Ecosystem of Metastatic Melanoma by Single-Cell RNA-Seq.” *Science* 352 (6282): 189–96. https://doi.org/10.1126/science.aad0501.

Tsai, Miao-chih, Ohad Manor, Yue Wan, Nima Mosammaparast, Jordon K Wang, Fei Lan, Yang Shi, Eran Segal, and Howard Y Chang. 2010. “Long Noncoding RNA as Modular Scaffold of Histone Modification Complexes.” *Science* 329 (August): 689–93.

Tsoi, Jennifer, Lidia Robert, Kim Paraiso, Carlos Galvan, Katherine M. Sheu, Johnson Lay, Deborah J.L. Wong, et al. 2018. “Multi-Stage Differentiation Defines Melanoma Subtypes with Differential Vulnerability to Drug-Induced Iron-Dependent Oxidative Stress.” *Cancer Cell* 33 (5): 890-904.e5. https://doi.org/10.1016/j.ccell.2018.03.017.

Twig, Gilad, Alvaro Elorza, Anthony J.A. Molina, Hibo Mohamed, Jakob D. Wikstrom, Gil Walzer, Linsey Stiles, et al. 2008. “Fission and Selective Fusion Govern Mitochondrial Segregation and Elimination by Autophagy.” *EMBO Journal* 27 (2): 433–46. https://doi.org/10.1038/sj.emboj.7601963.

Vendramin, Roberto, Yvessa Verheyden, Hideaki Ishikawa, Lucas Goedert, Emilien Nicolas, Kritika Saraf, Alexandros Armaos, et al. 2018. “SAMMSON Fosters Cancer Cell Fitness by Concertedly Enhancing Mitochondrial and Cytosolic Translation.” *Nature Structural and Molecular Biology* 25 (11): 1035–46. https://doi.org/10.1038/s41594-018-0143-4.

Verfaillie, Annelien, Hana Imrichova, Zeynep Kalender Atak, Michael Dewaele, Florian Rambow, Gert Hulselmans, Valerie Christiaens, et al. 2015. “Decoding the Regulatory Landscape of Melanoma Reveals TEADS as Regulators of the Invasive Cell State.” *Nature Communications* 6: 1–16. https://doi.org/10.1038/ncomms7683.

Wang, Kevin C., Yul W. Yang, Bo Liu, Amartya Sanyal, Ryan Corces-Zimmerman, Yong Chen, Bryan R. Lajoie, et al. 2011. “A Long Noncoding RNA Maintains Active Chromatin to Coordinate Homeotic

Gene Expression." *Nature* 472 (7341): 120–26. https://doi.org/10.1038/nature09819.

Wang, Wenjian, Yin Wang, Jianyin Long, Jinrong Wang, Sandra B Haudek, Paul Overbeek, Benny H J Chang, Paul T Schumacker, and Farhad R Danesh. 2012. "Mitochondrial Fission Triggered by Hyperglycemia Is Mediated by ROCK1 Activation in Podocytes and Endothelial Cells." *Cell Metabolism* 15 (2): 186–200. https://doi.org/10.1016/j.cmet.2012.01.009.

Wang, Zhigao, Hui Jiang, She Chen, Fenghe Du, and Xiaodong Wang. 2012. "The Mitochondrial Phosphatase PGAM5 Functions at the Convergence Point of Multiple Necrotic Death Pathways." *Cell* 148 (1–2): 228–43. https://doi.org/10.1016/j.cell.2011.11.030.

Weinberg, Samuel E., and Navdeep S. Chandel. 2015. "Targeting Mitochondria Metabolism for Cancer Therapy." *Nature Chemical Biology* 11 (1): 9–15. https://doi.org/10.1038/nchembio.1712.

WEINHOUSE, S., O. WARBURG, D. BURK, and A. L. SCHADE. 1956. "On Respiratory Impairment in Cancer Cells." *Science* 124 (3215): 267–72. https://doi.org/10.1126/science.124.3215.267.

Wouters, Jasper, Zeynep Kalender-Atak, Liesbeth Minnoye, Katina I Spanier, Maxime De Waegeneer, Carmen Bravo González-Blas, David Mauduit, et al. 2020. "Robust Gene Expression Programs Underlie Recurrent Cell States and Phenotype Switching in Melanoma." *Nature Cell Biology* 22 (8): 986–98. https://doi.org/10.1038/s41556-020-0547-3.

Xiao, Zhengtao, Ziwei Dai, and Jason W Locasale. 2019. "Metabolic Landscape of the Tumor Microenvironment at Single Cell Resolution." *Nature Communications* 10 (1): 3763. https://doi.org/10.1038/s41467-019-11738-0.

Xing, Yu Hang, Run Wen Yao, Yang Zhang, Chun Jie Guo, Shan Jiang, Guang Xu, Rui Dong, Li Yang, and Ling Ling Chen. 2017. "SLERT Regulates DDX21 Rings Associated with Pol I Transcription." *Cell* 169 (4): 664-678.e16. https://doi.org/10.1016/j.cell.2017.04.011.

Yang, Ming, Tomoyoshi Soga, and Patrick J Pollard. 2013. "Oncometabolites: Linking Altered Metabolism with Cancer." *The Journal of Clinical Investigation* 123 (9): 3652–58. https://doi.org/10.1172/JCI67228.

Zhang, Gao, Dennie T. Frederick, Lawrence Wu, Zhi Wei, Clemens Krepler, Satish Srinivasan, Young Chan Chae, et al. 2016. "Targeting Mitochondrial Biogenesis to Overcome Drug Resistance to MAPK Inhibitors." *Journal of Clinical Investigation* 126 (5): 1834–56. https://doi.org/10.1172/JCI82661.

FIGURES

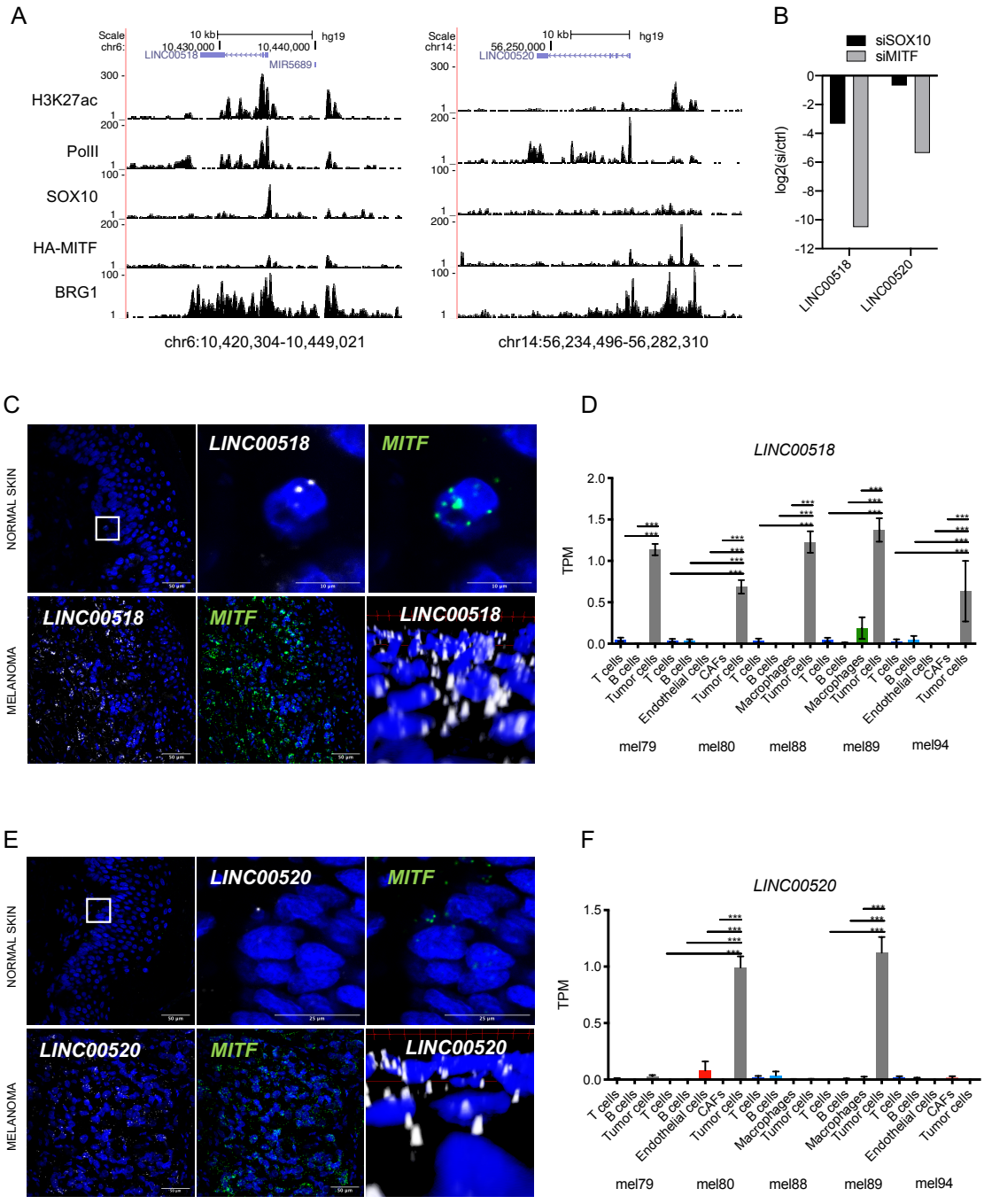

Figure 1. L518 and L520 are MITF/SOX10 regulated lncRNAs expressed in normal skin melanocytes and melanoma cells.

A. Chromatin immunoprecipitation followed by high throughput sequencing (ChIP-seq) data of 501mel cells were analysed to identify lincRNAs whose regulatory regions were bound by

MITF, SOX10, BRG1 and characterized by the active transcription marker H3K27ac. **B.** Regulation by SOX10 and MITF was confirmed by analysis of RNA sequencing and RT-qPCR data from 501mel cells following knock down of these factors. Data are expressed as log2 fold change of the siMITF or siSOX10 over the siCTRL. **C, E.** Normal skin and melanoma FFPE sections were analysed for L518 (C), L520 (E) and MITF expression using the multiplex fluorescent RNAscope protocol. DNA was stained using DAPI. Z-stack acquired images were processed to reconstruct the 3D signal density for L518 and DAPI. **D, F.** ScRNA-seq data (GSE72056) were analysed for L518 (D) and L520 (F) expression in melanoma and stromal cells (T and B cells, macrophages, endothelial cells, CAFs/cancer-associated fibroblasts). For each tumor, expression levels in the different cellular populations were compared by 1-way Anova (Kruskal-Wallis test).

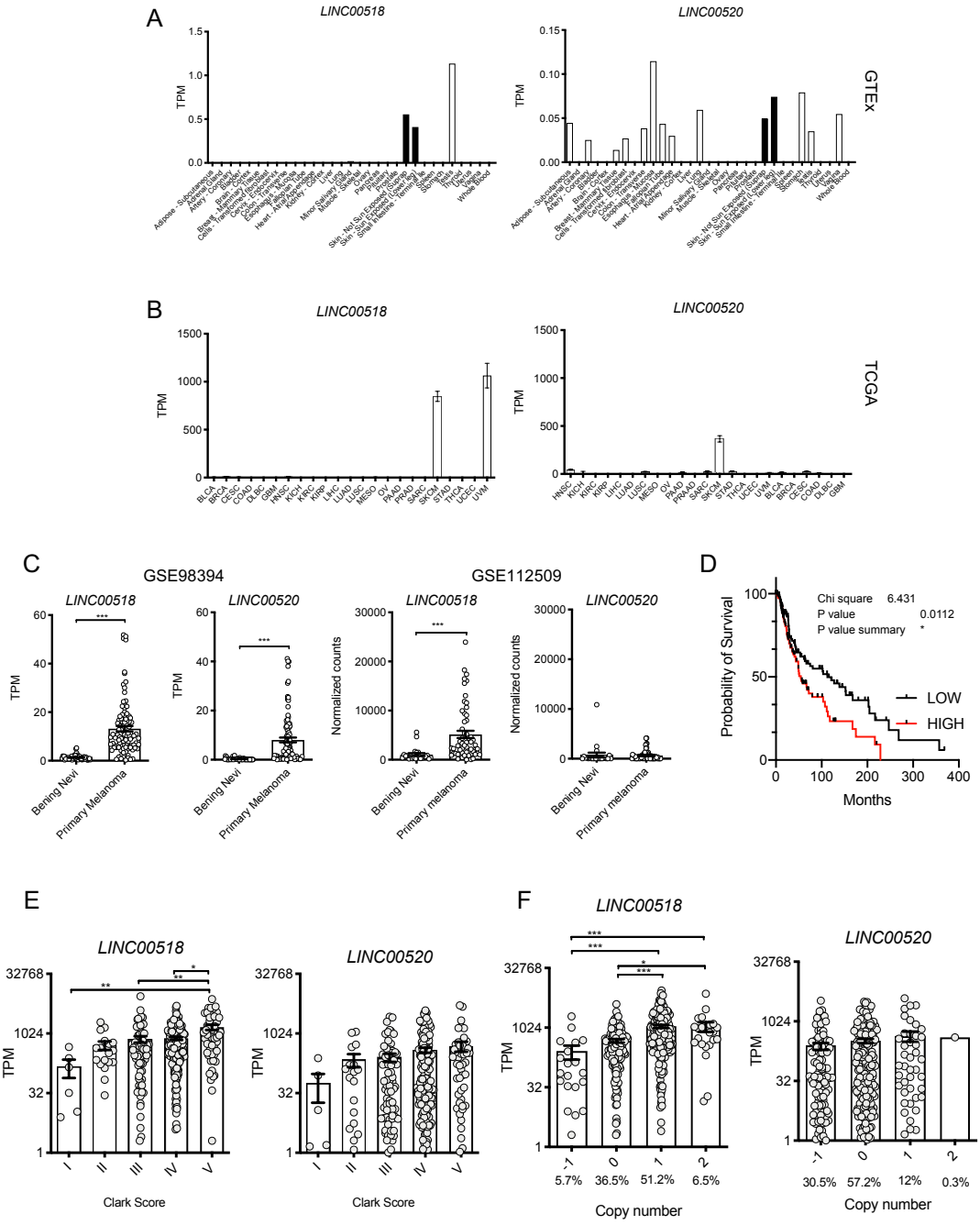

Figure S1. L518 and L520 are expressed in melanoma and associate with clinical features.

A, B. Genotype-Tissue Expression (GTEx) (A) and The Cancer Genome Atlas (TCGA) (B) databases were mined to assess L518 and L520 expression in normal and tumor tissues. **C.** L518 and L520 expression levels were evaluated in benign nevi and primary melanoma samples from two different RNA sequencing datasets (GSE98394, GSE112509) comparing the groups by unpaired t-test (Mann-Whitney test). **D.** Cutaneous melanoma (SKCM) patients from TCGA were divided into the 25% lowest and 25% highest L520-expressing quartiles and

survival probability was calculated for each. Survival curves were compared by Log Rank (Mantel-Cox) test. **E.** SKCM patients from were divided into 5 groups based on Clark score of the lesion at time of diagnosis. L518 and L520 expression levels were compared by 1-way Anova (Kruskal-Wallis test). **F.** SKCM patients from TCGA were divided into 4 quartiles based on allelic number of L518 and L520 (-1/deletion; 0/euploidy; 1/partial gain; 2/full gain). L518 and L520 expression levels have been compared by 1-way Anova (Kruskal-Wallis test).

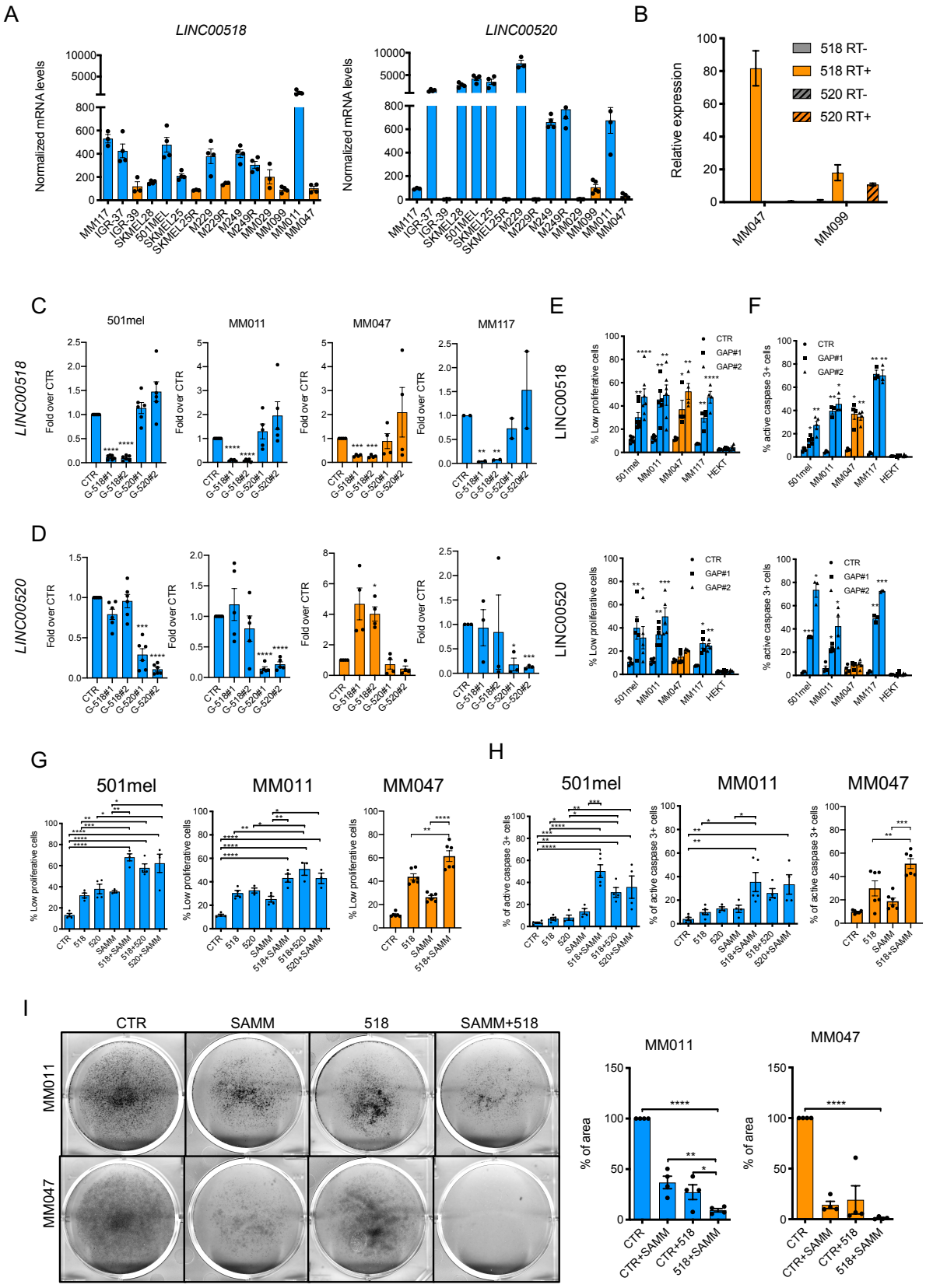

Figure 2. L518 is expressed by every melanoma subpopulation and affects their survival after single targeting or in combination with L520 or SAMMSON.

A. L518 and L520 RNA levels were determined in a panel of melanocytic (blue) and undifferentiated (orange) melanoma cell lines by RT-qPCR using specific primers and normalized on the geometric mean of 5 housekeeping genes. **B.** L518 expression in undifferentiated MM047 and MM099 cells was confirmed by qPCR analysis on RNA samples in the presence (RT+) or absence (RT-) of the Superscript IV reverse transcriptase enzyme. **C, D.** Melanoma cells were transfected with a negative control (CTR) or two different GapmeRs, GAP#1, GAP#2, targeting L518 or L520 and harvested after 48 hours. L518 (C) and L520 (D) expression was assessed by RT-qPCR and compared to the negative control by 1-way Anova (Dunnett's multiple comparison test). **E, F.** Melanoma cells transfected with L518 or L520 GapmeRs were incubated with the CellTrace Violet dye, cultured for 72 hours, stained with an anti-cleaved Caspase 3 antibody and analysed by flow cytometry. L518/L520 GapmeR transfected cells were compared to the CTR for percentages of single cells with high CellTrace Violet fluorescence levels (low proliferative cells) (E) or positive for Active Caspase 3 (F) by 1-way Anova (Dunnett's multiple comparison test). HEKT non-melanoma cells were used as a negative control. **G, H.** Melanoma cells transfected with suboptimal doses of L518/L520/SAMMSON GapmeRs as single agents or in pairwise combinations were incubated with the CellTrace Violet dye, cultured for 72 hours, stained with an anti-cleaved Caspase 3 antibody and analysed by flow cytometry. Percentages of low proliferative (G) and Active Caspase 3-positive cells (H) were compared between the groups by 1-way Anova. **I.** MM011 and MM047 cells were transfected as in G/H with CTR/L518/SAMMSON GapmeRs, cultured for 10 days and stained with Crystal violet. Percentages of area occupied by cells in each condition were compared by 1-way Anova.

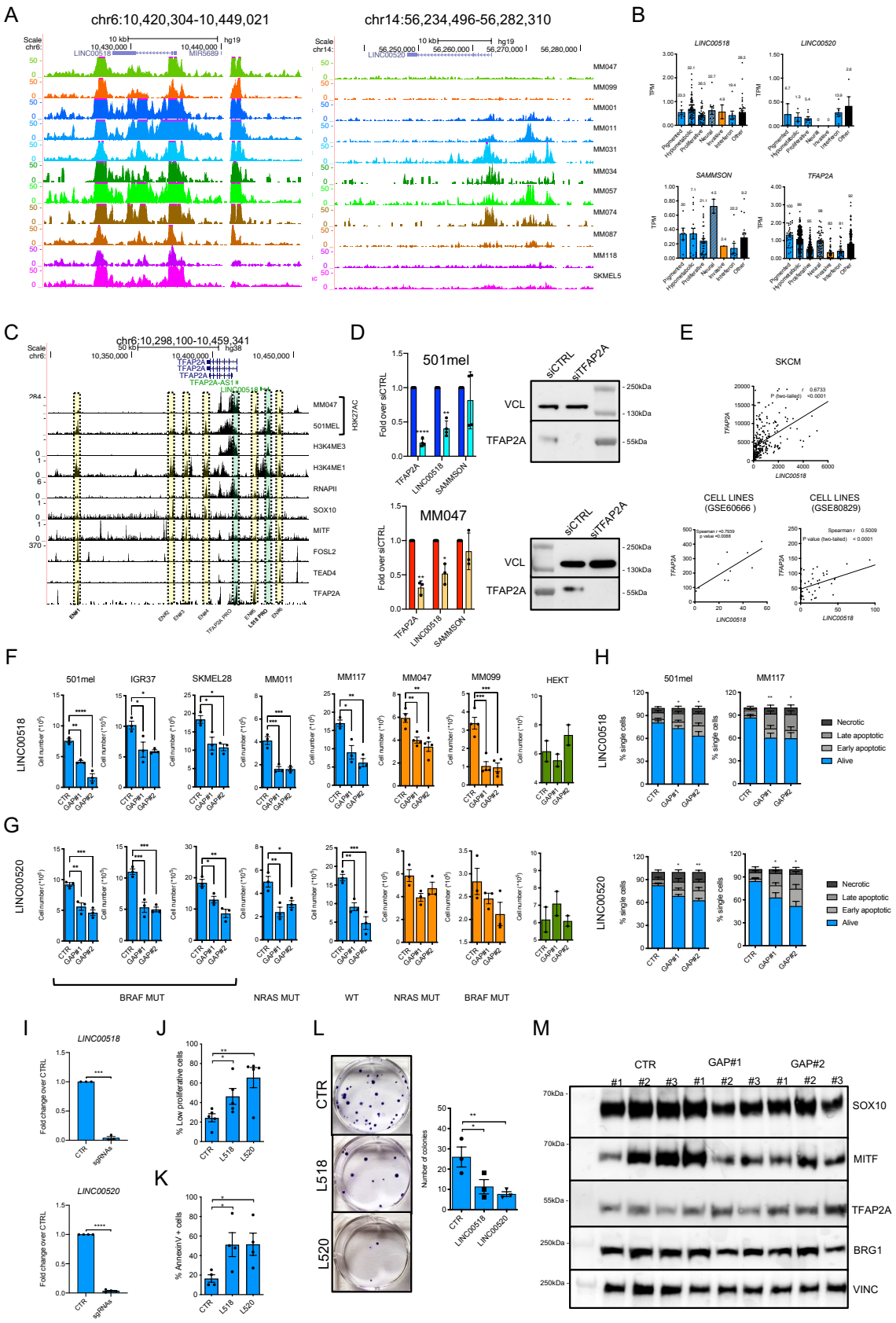

Figure S2. L518 is expressed in every melanoma subpopulation downstream TFAP2A and is required for cell viability.

A. H3K27ac over the L518 and L520 loci was evaluated using ChIP-seq data from a panel of melanoma short-term cultures (GSE60666). **B.** ScRNA-seq data from MEL001 PDX tumours (GSE116237) were analysed for L518, L520, SAMMSON and TFAP2A levels in the different melanoma subpopulations (melanocytic in blue; undifferentiated in orange). Only cells in which the different RNAs were captured were included in the analysis. Above each bar is indicated the % of cells analysed for each population. **C.** Regulatory regions (enhancers in yellow shadow, promoters in green) around TFAP2A/L518 locus were defined using ChIP-seq for H3K27ac, H3K4me1, H3K4me3 (GSE64137 and in-house data). At each element, binding of RNA Pol II (RNAPII) and transcription factors (SOX10, MITF, FOSL2, TEAD4, TFAP2A) was evaluated (GSE61965, GSE94488, GSE67555). **D.** 501mel and MM047 melanoma cells were transfected with a control siRNA (siCtrl) or siTFAP2A and harvested after 48 hours. Expression of L518, SAMMSON and TFAP2A was evaluated by RT-qPCR. SiCtrl and siTFAP2A samples were compared by paired t-test. From the same samples, total protein extracts were analysed by western blot for TFAP2A levels. VINCULIN was used as a loading control. **E.** Spearman correlation was calculated between L518 and TFAP2A RNA levels in samples obtained from the SKCM-TCGA dataset and two panels of melanoma cell lines (GSE60666 and GSE80829). **F, G.** Melanoma cells were transiently with a negative control or GapmeRs targeting L518 (F) or L520 (G). Cells were stained 72 hours post transfection with Trypan blue and Trypan-negative cells counted automatically using the Countess machine. L518 and L520 targeted cells were compared to the negative control by 1-way Anova (Dunnett's multiple comparison test). **H.** 501mel and MM117 melanoma cells were transfected with L518 and L520 targeting GapmeRs and after 72 hours stained with Annexin V and TOPRO-3 and analysed by flow cytometry. Single cells were defined as alive (AnnV-, TOPRO-3-), early apoptotic (AnnV+, TOPRO-3), late apoptotic (AnnV+, TOPRO-3+) and necrotic (AnnV-, TOPRO-3+). Percentages of alive cells in L518 and L520 targeted cells were compared to the negative control by 1-way Anova (Dunnett's multiple comparison test). **I.** 501mel cells were co-transfected with a plasmid expressing the dCas9-KAP1 protein together with mScarlet and a plasmid expressing GFP and single guide RNAs (sgRNAs) targeting L518 or L520 promoters. 24 hours post transfection, mScarlet/GFP double positive cells were sorted by flow cytometry, stained with the CellTrace Violet dye and kept in culture for a further 96 hours. An aliquot of cells was used for RNA extraction and RT-qPCR analysis of L518 and L520 expression. **J, K.** Cells transfected and sorted as in panel I were harvested, stained by Annexin V and analysed by flow cytometry.

Percentages of low proliferative (J) or AnnexinV positive (K) cells in the sgRNAs transfected samples were compared to the negative control by 1-way Anova (Dunnett's multiple comparison test). **L.** Cells transfected and sorted as in panel I were plated in 6 well plates at low cell number (500 c/well) and kept in culture for 10 days. Single colonies were fixed, stained with crystal violet and counted. Numbers of colonies were compared by 1-way Anova (Dunnett's multiple comparison test). **M.** 501mel cells were transfected with negative control (CTR) or L518 Gapmers and harvested 48 hours after. Total protein extracts were analysed by western blot for SOX10, MITF, TFAP2A, BRG1 levels. VINCULIN was used as a loading control.

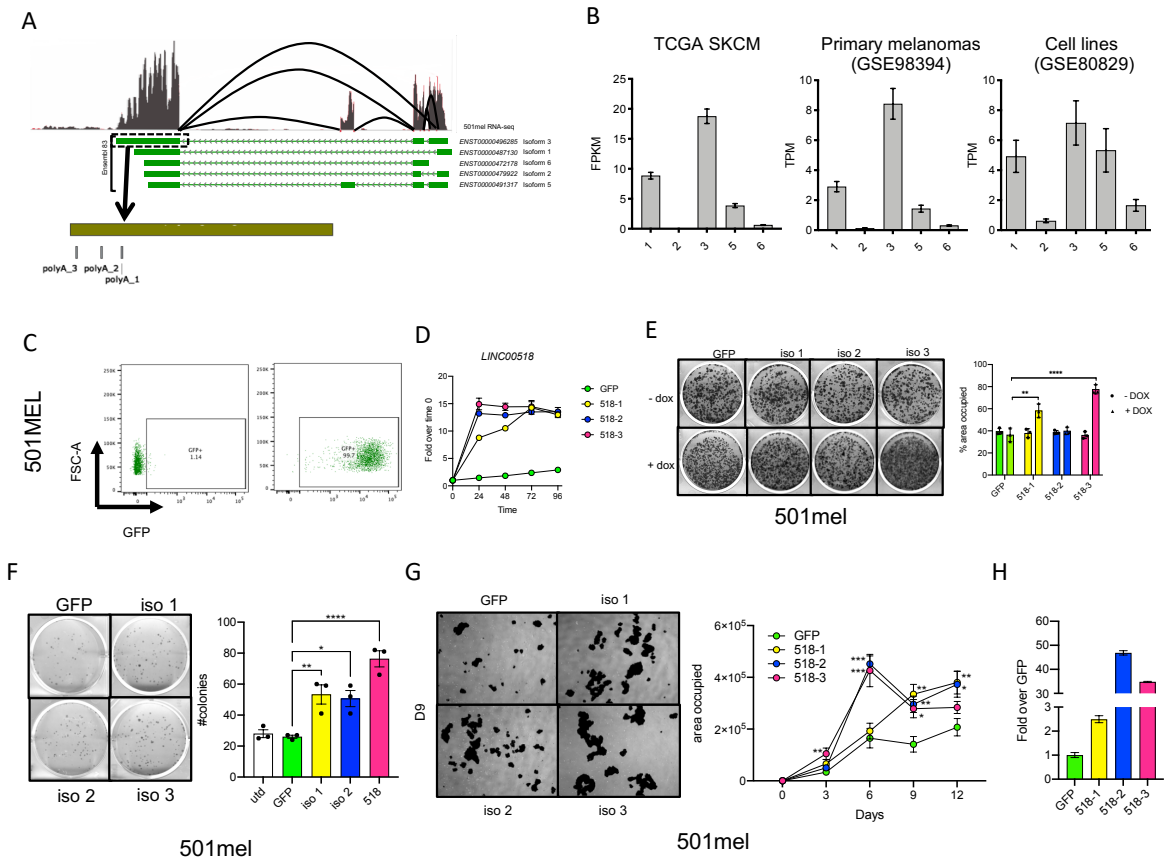

Figure S3. Ectopic L518 expression increases melanoma cell proliferation.

A. 501mel RNA-seq data were visualized on IGV to generate the Sashimi plot defining exon-exon junctions. Each isoform was defined on the basis of the Ensembl 83 annotations and numbered (1, 2, 3, 5, 6). 3'RACE on MM011 total RNA was performed to identify polyadenylation sites (polyA) at the last exon each isoform. **B.** Paired end RNA-seq data from melanoma patients (SKCM-TCGA; GSE98394) and cell lines (GSE80829) were analysed with the RSEM pipeline to define transcript quantification values for each L518 isoform. **C**. 501mel cells were infected with the pCW57 lentiviral vector modified to express GFP or L518 isoforms 1, 2

and 3 under a Tet-ON promoter. Cells were cultured for 48 hours with Dox and analysed by flow cytometry for GFP expression. **D**. 501mel cells modified as in C were cultured with Dox for 4 days, renewing Dox every 48 hours. Samples were collected every 24 hours and L518 expression was assessed by RT-qPCR. Each timepoint value was expressed as a fold change over the time 0 sample in absence of Dox. **E.** 501mel cells modified as in C were cultured in presence or absence of Dox for 10 days, renewing Dox every 48 hours. Cells were fixed and stained with crystal violet to quantify the percentage of area occupied by the cells. L518 isoform overexpressing cells in presence or absence of Dox were compared to the respective GFP control by 1-way Anova (Dunnett's multiple comparison test). **F**. 501mel cells modified as in C or untransduced were seeded at low density and cultured with Dox for 10 days, renewed every 48 hours. Single colonies were fixed, stained with crystal violet and counted. Numbers of colonies were compared by 1-way Anova (Dunnett's multiple comparison test). **G**. 501mel cells modified as in C were cultured in non-adherent conditions to induce melanosphere formation. Dox was added to the media every 2 days to sustain GFP or L518 isoform expression. Pictures of the petri dishes were taken every 3 days using a light microscope and analysed on ImageJ to calculate the area occupied by melanospheres. Experimental groups were compared by 1-way Anova (Dunnett's multiple comparison test). **H.** After 12 days of culture, melanospheres were harvested, RNA was extracted and retrotranscribed to analyse L518 expression by qPCR.

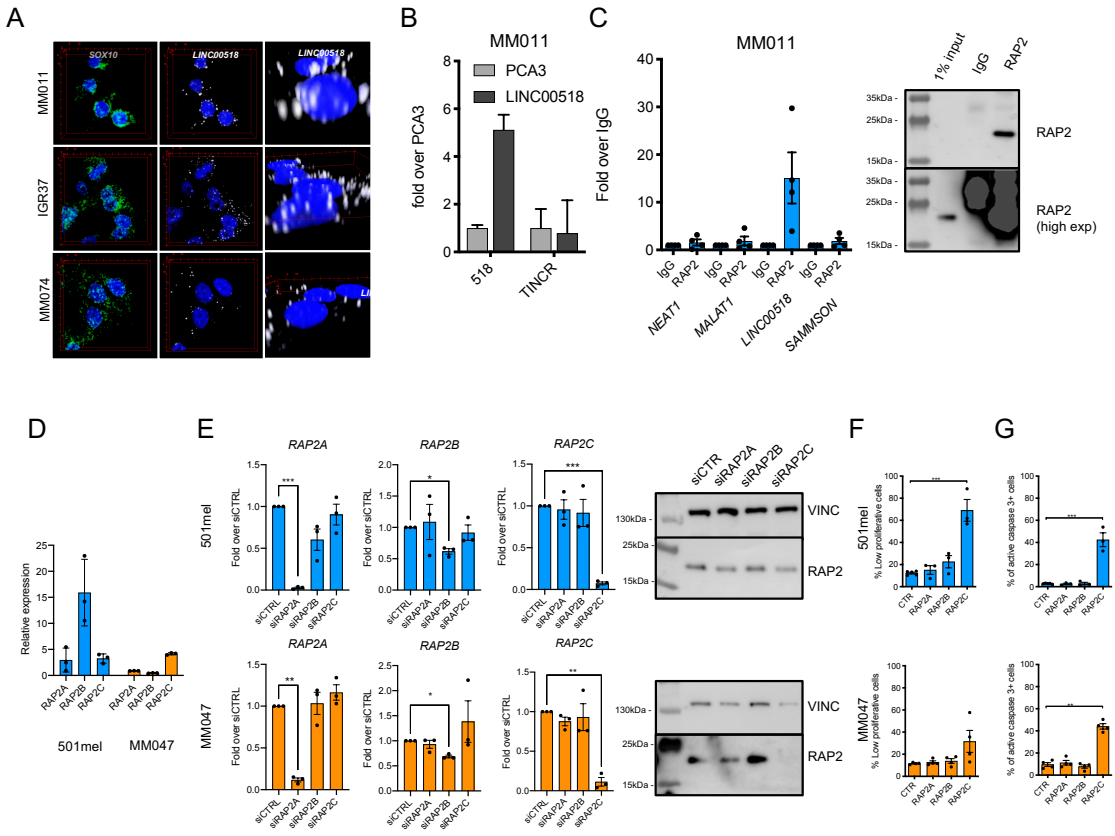

Figure 3. L518 interacts with the RAP2 GTPases and RAP2C is required for melanoma cell proliferation and survival.

A. SOX10 and L518 RNA molecules were detected in melanoma cells using specific DNA probes and the multiplex fluorescent RNAscope signal amplification protocol. DNA was stained with DAPI and Z-stack acquired images were processed to reconstruct the 3D signal density for L518 and DAPI. **B.** MM011 were lysed and cytoplasmic extracts were incubated with biotinylated DNA probes complementary to L518 or PCA3 RNAs. RNA-protein complexes were isolated using streptavidin Sepharose beads and divided in two aliquots to perform RNA and protein extraction. RNA was reverse transcribed and analysed by qPCR for L518 expression. TINCR was used as a negative control. Isolated proteins were analysed by mass spectrometry. **C.** MM011 cells were lysed and total extracts were incubated with normal IgG or an anti-RAP2 antibody. RNA-protein complexes were isolated using Protein G magnetic beads and divided in two aliquots to perform RNA and protein extraction. RNA was reverse transcribed and analysed by qPCR for L518, NEAT1, MALAT1 and SAMMSON expression. Results are expressed as fold change over the IgG control. Proteins were analysed by western blot using an anti-RAP2 antibody. A sample of the protein lysate before immunoprecipitation (1% input) was loaded

in parallel. The lower panel represents a long exposure of the membrane. **D.** Total RNA from 501mel (blue) and MM047 (orange) melanoma cells was reverse transcribed and analysed by qPCR for RAP2A, RAP2B and RAP2C expression normalized over housekeeping genes. **E.** 501mel (blue) and MM047 (orange) melanoma cells were transfected with a control siRNA (siCtrl) or siRAP2A, siRAP2B or siRAP2C. Cells were harvested 48 hours post transfection and total RNA and proteins extracts analysed by RT-qPCR for RAP2A/B/C levels and western blot using an anti-RAP2 antibody, respectively. VINCULIN was used as a loading control. siRAP2 transfected cells were compared to the siCtrl by 1-way Anova (Dunnett's multiple comparison test). **F, G.** 501mel (blue) and MM047 (orange) melanoma cells were transfected as in E and incubated with CellTrace Violet. 72 hours post transfection cells were harvested, stained with an anti-active caspase 3 antibody and analysed by flow cytometry. Percentages of low proliferative (F) and Active Caspase 3 positive cells (G) in the siRAP2A/B/C transfected groups were compared to the siCtrl by 1-way Anova (Dunnett's multiple comparison test).

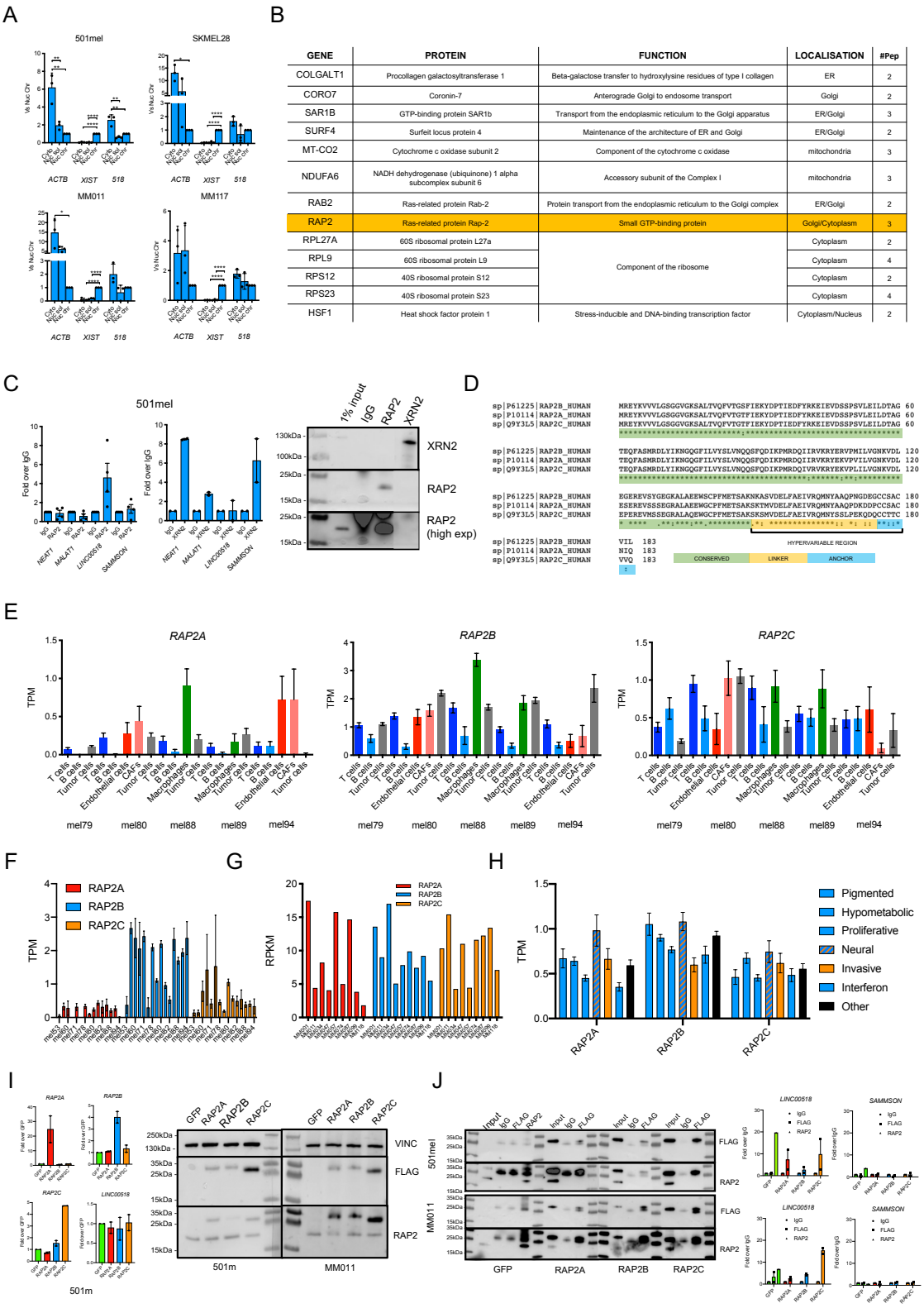

GENE	PROTEIN	FUNCTION	LOCALISATION	#Pep
COLGALT1	Procollagen galactosyltransferase 1	Beta-galactose transfer to hydroxylysine residues of type I collagen	ER	2
CORO7	Coronin-7	Anterograde Golgi to endosome transport	Golgi	2
SAR1B	GTP-binding protein SAR1b	Transport from the endoplasmic reticulum to the Golgi apparatus	ER/Golgi	3
SURF4	Surfeit locus protein 4	Maintenance of the architecture of ER and Golgi	ER/Golgi	2
MT-CO2	Cytochrome c oxidase subunit 2	Component of the cytochrome c oxidase	mitochondria	3
NDUFA6	NADH dehydrogenase (ubiquinone) 1 alpha subcomplex subunit 6	Accessory subunit of the Complex I	mitochondria	3
RAB2	Ras-related protein Rab-2	Protein transport from the endoplasmic reticulum to the Golgi complex	ER/Golgi	2
RAP2	Ras-related protein Rap-2	Small GTP-binding protein	Golgi/Cytoplasm	3
RPL27A	60S ribosomal protein L27a	Component of the ribosome	Cytoplasm	2
RPL9	60S ribosomal protein L9		Cytoplasm	4
RPS12	40S ribosomal protein S12		Cytoplasm	2
RPS23	40S ribosomal protein S23		Cytoplasm	4
HSF1	Heat shock factor protein 1	Stress-inducible and DNA-binding transcription factor	Cytoplasm/Nucleus	2

Figure S4. RAP2 paralog expression in melanoma cells.

A. Melanoma cells were lysed and separated into the cytoplasmic fraction (Cyto) and the nuclear fraction further divided into the nucleoplasm (Nuc sol) and the chromatin bound (Nuc

chr) fractions. ACTB, XIST and L518 expression was assessed by RT-qPCR RNA in each ACTB. Expression values from the cytoplasmic and nuclear soluble samples were expressed relative to the respective chromatin fraction and compared by 1-way Anova (Dunnett's multiple comparison test). **B.** L518 was isolated in 3 biological replicates from MM011 cells as described in Fig.3B and associated protein were analysed by mass spectrometry. Peptide data were analysed to identify proteins present only in the L518 pulldown and not in the negative PCA3 control. Identified proteins are listed in the table with the number of peptides in each pulldown experiment. **C.** 501mel were lysed and subjected to the same immunoprecipitation protocol as in Fig.3C using anti-RAP2 and XRN2 antibodies. L518, NEAT1, MALAT1 and SAMMSON expression was assessed by RT-qPCR. Results are expressed as fold change over the IgG control. Proteins were analysed by western blot using anti-RAP2 and XRN2 antibodies. A sample of the protein lysate before immunoprecipitation (1% input) was loaded in parallel. **D.** RAP2A, B and C protein sequences were aligned on ClustalW to define homology regions. **E.** RAP2A, B and C RNA levels were analysed in scRNA-seq data of melanoma tumors (GSE72056) to define expression in malignant and stromal cells (T and B cells, macrophages, endothelial cells, CAFs/cancer-associated fibroblasts). **F.** RAP2A, B and C RNA levels were analysed in melanoma cells from the scRNA-seq data of E. **G.** RAP2A, B and C RNA levels were analysed from RNA sequencing data of a panel of melanoma short term cultures (GSE60666). **H.** RAP2A, B and C RNA levels were analysed in scRNA-seq data from MEL001 PDX tumours (GSE116237). **I.** 501mel and MM011 cells were infected with the pCW57 lentiviral vector modified to express GFP or RAP2A, RAP2B or RAP2C under a Tet-ON promoter. After transduction and selection with puromycin, cells were cultured with Dox for 2 days and harvested to perform total RNA and protein extraction. RAP2A, RAP2B and RAP2C expression was assessed by RT-qPCR using specific primers. Values are expressed as fold change over the GFP sample. Protein extracts were analysed by western blot with anti-FLAG and anti-RAP2 antibodies. Vinculin was used as a loading control. **J.** 501mel and MM011 cells modified as in panel I were cultured with Dox for 2 days, lysed and total extracts immunoprecipitated with anti-FLAG or anti-RAP2 antibodies and divided in two aliquots to perform RNA and protein elution. Eluted proteins and the input were analysed by western blot with anti-FLAG and anti-RAP2 antibodies. L518 and SAMMSON expression was assessed by RT-qPCR. Values are expressed as fold change over the IgG control.

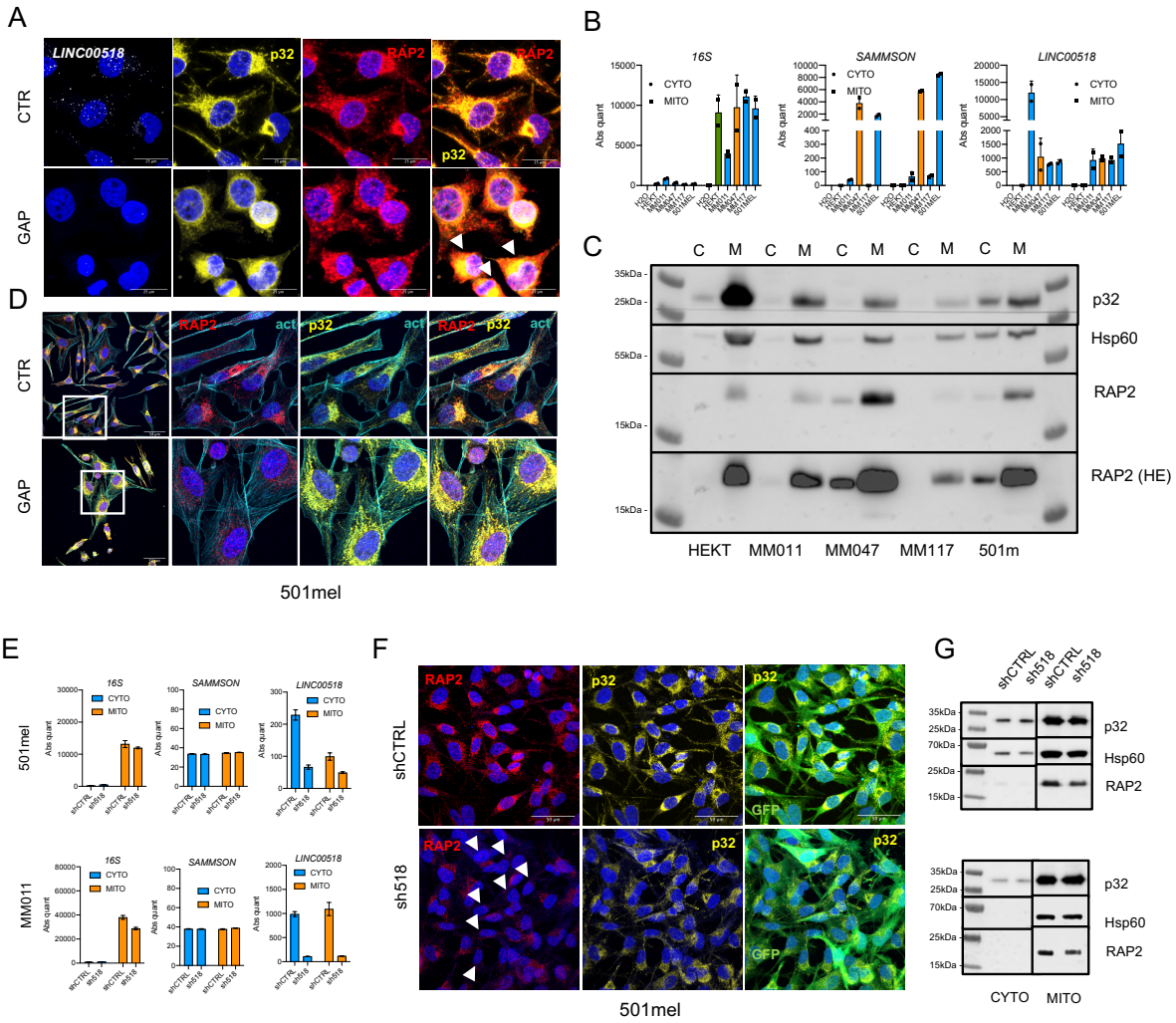
A
LINC00518
p32
RAP2
CTR
GAP
B
16S
SAMMSON
LINC00518
CYTO
MITO
Abs quant
C
C M C M C M C M C M
35kDa
25kDa
55kDa
15kDa
p32
Hsp60
RAP2
RAP2 (HE)
HEKT MM011 MM047 MM117 501m
D
act
501mel
E
501mel
MM011
F
shCTRL
sh518
GFP
501mel
G
shCTRL sh518 shCTRL sh518
CYTO MITO
H
oligo
FCCP
RotA
OCR (pmoles/min)
Time
GAP-CTR
GAP-518
SAMM
RAP2C
BASAL OCR
MAX OCR
RESERVE CAPACITY
siRAP2C
I
518-3
518-2
518-1
GFP
GFP-DMSO
518-1-DMSO
518-2-DMSO
518-3-DMSO

Figure 4. L518 and RAP2 localize to mitochondria and modulate oxidative phosphorylation. **A.** 501mel melanoma cells were transfected with a negative control (CTR) or a L518 (GAP) specific GapmeR. L518, RAP2 and p32 were detected using the RNAscope co-detection protocol DNA was stained with DAPI. Images were acquired by confocal microscopy. White arrows indicate cells with reduced RAP2-p32 co-localisation. **B.** HEKT and melanoma cells were lysed and total extracts and the mitochondrial and cytoplasmic fractions separated. 16S rRNA, SAMMSON and L518 expression was assessed in each fraction by RT-qPCR. **C.** Mitochondrial ad cytoplasmic fractions isolated as in B were analysed by western blot using an anti-RAP2 antibody. P32 and HSP60 were evaluated as mitochondrial markers. **D.** 501mel melanoma cells were transfected with a control (CTR) or L518 GapmeR (GAP) were co-stained with anti-RAP2 and anti-p32 antibodies. DNA was stained with DAPI and actin with Alexa488 conjugated phalloidin. Images were acquired by confocal microscopy. **E.** 501mel and MM011 melanoma cells were infected with the pLT3-GEPIR lentiviral vector modified to express a Scrambled (shCTRL) or a L518 specific (sh518) shRNA under a Tet-ON promoter. After Dox administration for 48 hours, 16S rRNA, SAMMSON and L518 expression was assessed in the cytoplasmic and mitochondrial fractions by RT-qPCR. **F.** 501mel melanoma modified as in E were cultured with doxycycline for 48 hours, fixed and analysed by immunofluorescence for RAP2, p32 and GFP expression by confocal microscopy. DNA was stained with DAPI. White arrows indicate cells with reduced RAP2-p32 co-localisation. **G.** Proteins from 501mel and MM011 were analysed by western blot using anti-p32, Hsp60 and RAP2 antibodies. **H.** 501mel cells were transfected with a GapmeR control (GAP-CTR), targeting L518 (GAP-518) or SAMMSON (GAP-SAMM) or with the siRAP2C. Cells were transferred to the Seahorse 96 well culture plate and underwent the Mitostress test 48 hours post transfection. Cells were treated with oligomycin, FCCP and RotenoneA/antimycin and oxygen consumption rate (OCR) was measured over time. OCR values were used to calculate the basal OCR, the maximal OCR (MRC) and the reserve capacity. Experimental groups were compared by 1-way Anova (Dunnett's multiple comparison test). **I.** 501mel cells were infected with the pCW57 lentiviral vector for Dox-inducible expression of GFP or L518 isoforms 1, 2 and 3. Cells were cultured in the Seahorse 96 cell culture plate and the Mitostress test was performed as in H. Experimental groups were compared by 1-way Anova (Dunnett's multiple comparison test).

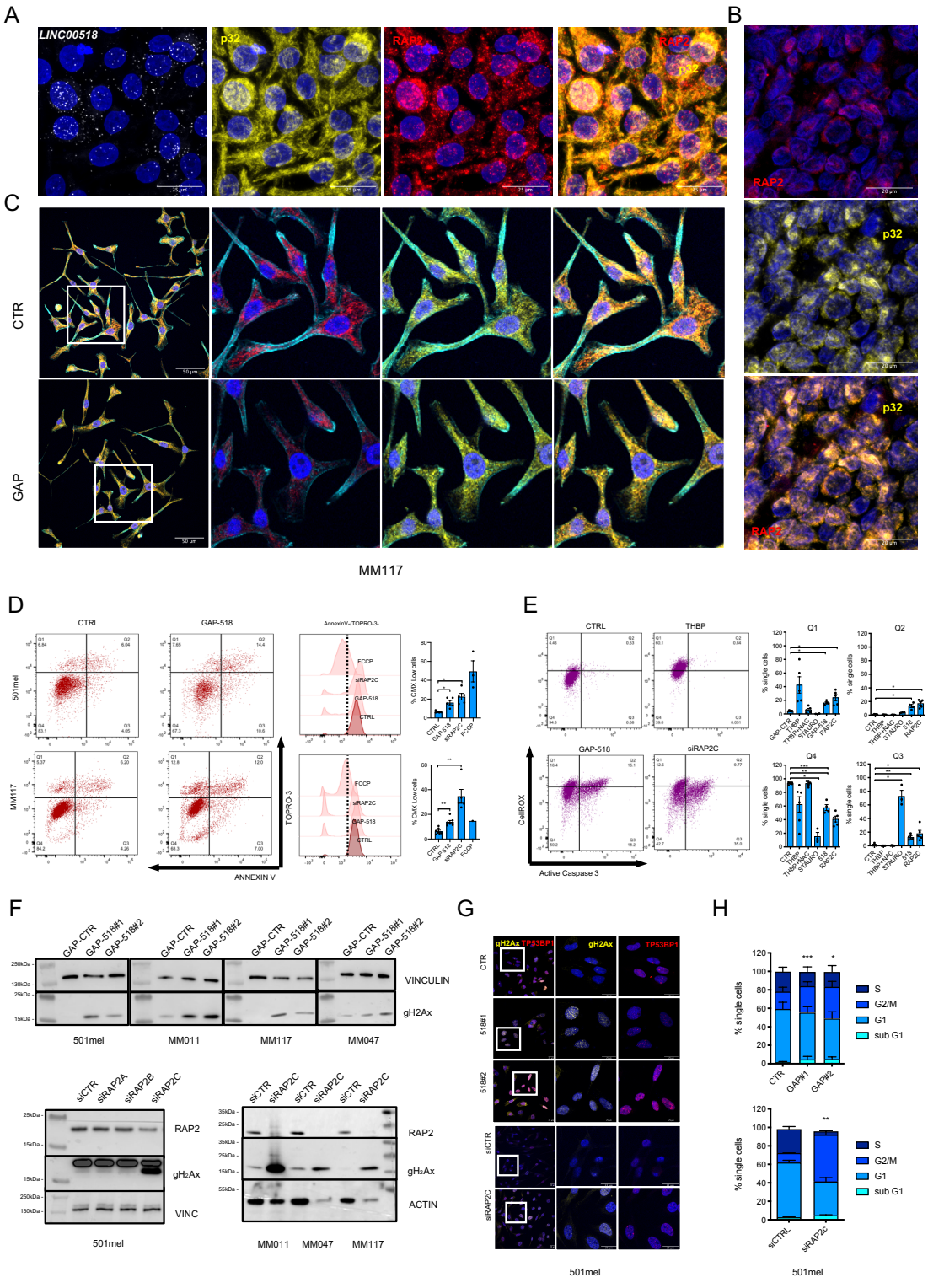

Figure S5. L518 and RAP2C knockdown induces mitochondrial dysfunction, release of reactive oxygen species (ROS), DNA damage and cell cycle block.

A. MM117 melanoma cells were analysed for L518, RAP2 and p32 using the RNAscope co-detection protocol as described in Fig.4A. **B.** A human melanoma FFPE section was stained for RAP2 and p32 proteins using specific antibodies and analysed by confocal microscopy. DNA

was stained with DAPI. **C.** MM117 melanoma cells were transfected with a control (CTR) or L518 GapmeR (GAP), cultured on chamber slides and co-stained with anti-RAP2 and anti-p32 antibodies. DNA was stained with DAPI and actin with Alexa488 conjugated phalloidin. Images were acquired by confocal microscopy. **D.** 501mel and MM117 melanoma cells were transfected with a control (CTRL) or L518 specific (GAP-518) GapmeR or siRAP2C. Cells were harvested after 48 hours and stained with AnnexinV, TOPRO-3, Mitotracker CMXROS and analysed by flow cytometry. Cells were gated on the AnnexinV/TOPRO-3 fluorescence values and AnnexinV-/TOPRO-3- cells were analysed for Mitotracker CMXROS, defining a population with low fluorescence values (CMX low). Cells were treated with FCCP 1uM for 30 minutes as a control for Mitotracker CMXROS reduction. Percentages of CMX Low cells were compared by 1-way Anova (Dunnett's multiple comparison test). **E.** 501mel cells were transfected with a control (CTRL) or L518 specific (GAP-518) GapmeR or siRAP2C, harvested after 48 hours and stained with CellROX and an anti-active caspase 3 antibody and analysed by flow cytometry. Cells were also treated with the ROS inducer THBP, in the presence or absence of N-acetylcysteine (NAC), and with the apoptosis inducer Staurosporine. Cells were gated on the active Caspase-3 and CellROX fluorescent values into 4 populations (Caspase3-/CellROX+ as Q1; Caspase3+/CellROX+ as Q2; Caspase3+/CellROX- as Q3; Caspase3-/CellROX- as Q4). Percentages of single cells for each population were compared among the experimental groups by 1-way Anova. **F.** Melanoma cells were transfected with a control (CTRL) or L518 specific GapmeRs or a siRNA control (siCtrl) or those targeting RAP2A (siRAP2A), RAP2B (siRAP2B), RAP2C (siRAP2C). 72 hours post transfection cells were harvested, lysed and analysed by western blot with anti-gammaH2Ax and anti-RAP2 antibodies. Vinculin and Actin were used as loading controls. **G.** 501mel cells were transfected with a control (CTRL) or L518 specific GapmeRs or a siRNA control (siCtrl) or targeting RAP2C (siRAP2C). 72 hours post transfection cells were fixed, stained with anti-gH2Ax and anti-TP53BP1 antibodies and analysed by confocal microscopy. DNA was stained with DAPI. **H.** 501mel cells were transfected as in G. 72 hours post transfection, cells were incubated 90 min with 5-ethynyl-2'-deoxyuridine (Edu), harvested, fixed and Edu was conjugated with the Alexa 488 fluorophore by a Click-it reaction. Cells were stained with TOPRO-3 and analysed by flow cytometry. Single cells were divided into 4 populations based on Edu/TOPRO-3 fluorescence (sub G1, G1, S, G2/M) and percentages of cells in the G2/M phase were compared among the experimental conditions by 1-way Anova. (Dunnett's multiple comparison test) or paired t-test.

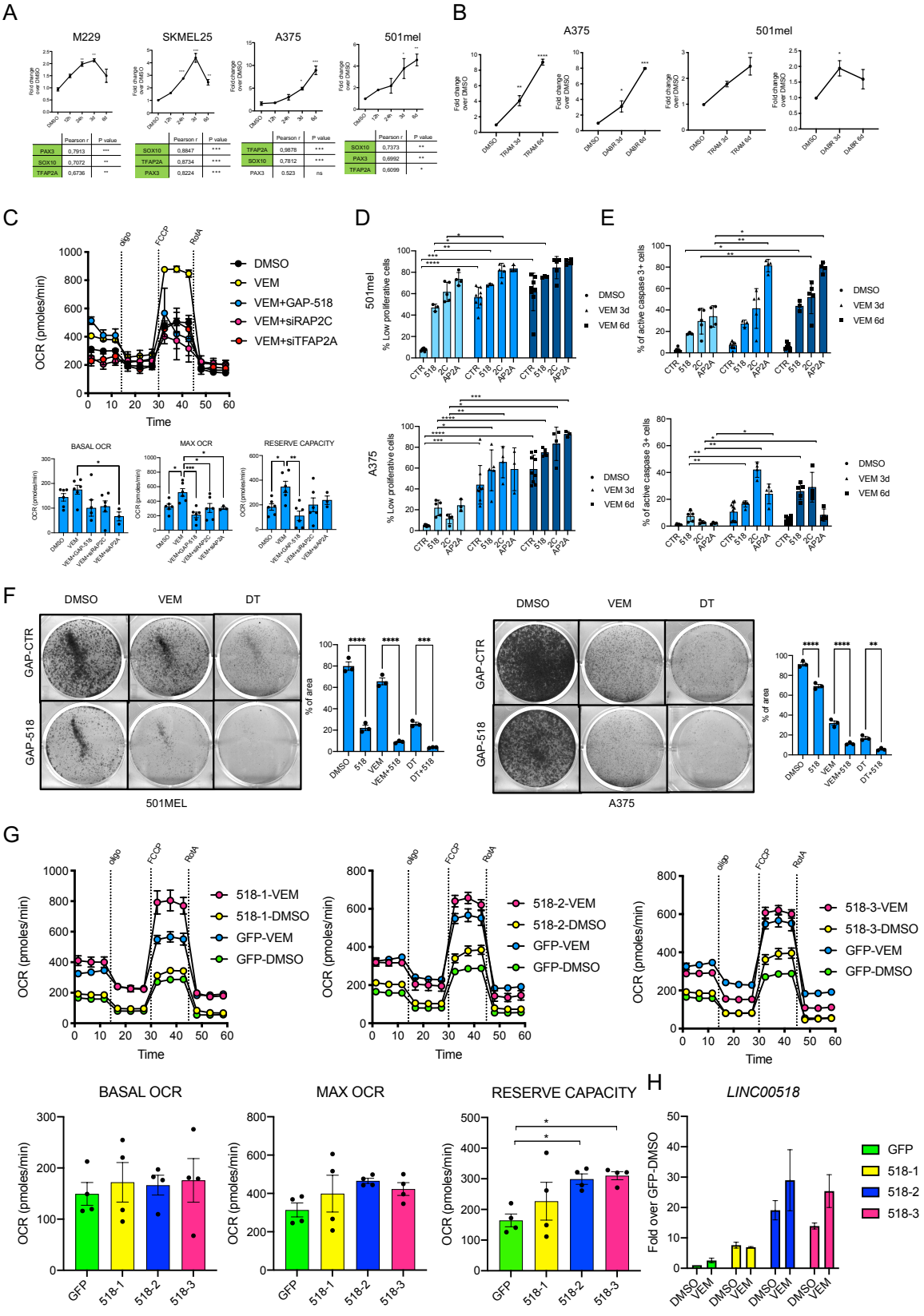

Figure 5. L518 and RAP2C are required for the metabolic switch upon BRAF inhibition by Vemurafenib.

A. BRAF mutant melanoma cell were grown for 6 days in the presence of Vemurafenib (1uM), added fresh every three days and L518, SOX10, TFAP2A, PAX3 expression was analysed by RT-qPCR. Data were expressed as fold change over the DMSO treated cells and compared by 1-way Anova (Dunnett's multiple comparison test). Spearman correlation was calculated in a pairwise manner between L518 and TFAP2A, SOX10 and PAX3 fold changes over the DMSO sample. **B.** 501mel and A375 cells were grown for 6 days in the presence of Trametinib (2nM for A375, 100nM for 501mel) or Dabrafenib (10nM for A375, 100nM for 501mel), added fresh every three days. L518 expression as analysed by RT-qPCR and expressed as fold change over the DMSO treated cells and compared by 1-way Anova (Dunnett's multiple comparison test). **C.** 501mel cells were grown for 3 days in the presence of DMSO or Vemurafenib (1uM), transfected with a negative control or a L518 specific GapmeR, siRAP2C or siTFAP2A, grown for a further 3 days in the presence of DMSO or Vemurafenib and subjected to the Mitostress test as in Fig.4H. OCR values were used to calculate the basal OCR, the maximal OCR (MRC) and the reserve capacity. Experimental groups were compared by 1-way Anova (Dunnett's multiple comparison test). **D, E.** 501mel and A375 were treated as above, harvested and analysed by flow cytometry for CellTrace Violet (D) and active caspase 3 (E) as previously described in the paper. Experimental groups were compared by 1-way Anova. **F.** BRAF mutant melanoma cells were grown for 3 days in the presence of DMSO, Vemurafenib (VEM) or Dabrafenib+Trametinib (DT) at the concentrations used in panels A and B, transfected with a negative control or a L518 specific GapmeR grown for a further 3 days in the presence of DMSO or the inhibitors, fixed and stained with crystal violet. Percentages of area of area occupied by cells were compared by 1-way Anova. **G.** 501mel modified as in Fig.4I were grown in the presence of Dox, DMSO or Vemurafenib (1uM) for 6 days and subjected to the Mitostress test. OCR values were used to calculate the basal OCR, the maximal OCR (MRC) and the reserve capacity. Experimental groups were compared by 1-way Anova (Dunnett's multiple comparison test). **H.** 501mel cells treated as in G were harvested and L518 expression analysed by RT-qPCR.

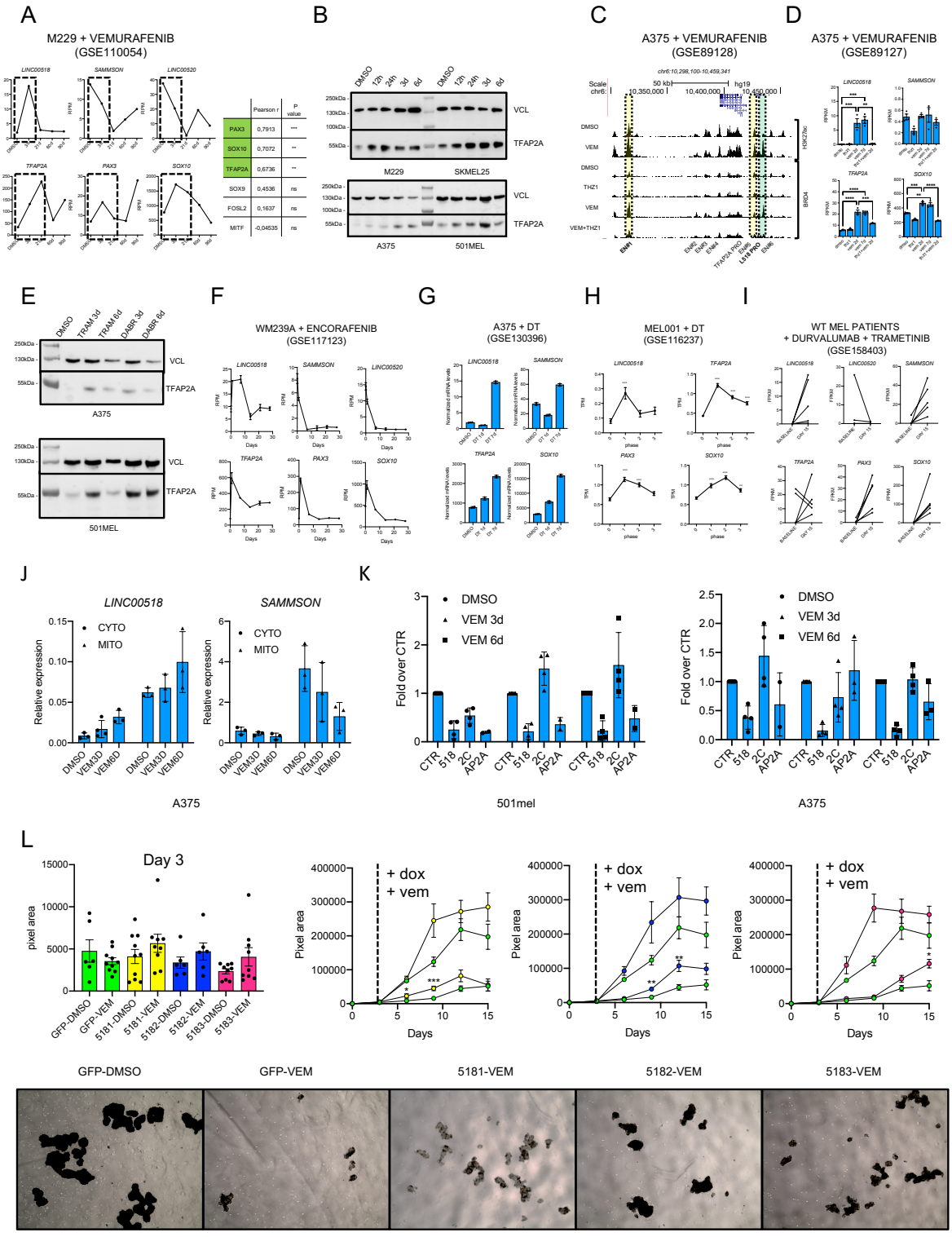

Figure S6. MAPK pathway inhibition increases L518 expression downstream of TFAP2A.

A. RNA sequencing data from M229 cells treated with Vemurafenib (GSE110054) were analysed for L518, SAMMSON, L520, TFAP2A, SOX10, MITF, PAX3, SOX9 and FOSL2 expression. Spearman correlation was calculated in a pairwise manner between L518 and TFAP2A, SOX10, PAX3, MITF, SOX9 and FOSL2 fold changes over the DMSO control. **B.** BRAF mutant melanoma

cells treated as described in Fig.5 panel A and analysed by western blot with an anti-TFAP2A antibody. Vinculin was used as a loading control. **C.** ChIP-seq data from A375 cells treated with Vemurafenib and THZ1 (GSE89128) were analysed to define changes in H3K27ac and BRD4 signals at the TFAP2A/L518 locus in the different experimental conditions. Cis-regulatory regions were defined as in Fig.S2C. **D.** RNA sequencing data from A375 cells treated with Vemurafenib and THZ1 (GSE89127) were analysed for L518, SAMMSON, TFAP2A and SOX10 expression. Experimental groups were compared by 1-way Anova. **E.** A375 and 501mel cells treated as in Fig.5B were analysed by western blot with an anti-TFAP2A antibody. Vinculin was used as a loading control. **F.** RNA sequencing data from WM239A cells treated with Encorafenib (GSE117123) were analysed for L518, SAMMSON, L520 TFAP2A, PAX3 and SOX10 expression. **G.** RNA sequencing data from A375 cells treated with Dabrafenib and Trametinib (GSE130396) were analysed for L518, SAMMSON, TFAP2A and SOX10 expression. **H.** ScRNAseq data from MEL001 PDX treated with Dabrafenib and Trametinib (GSE116237) were analysed for L518, TFAP2A, PAX3 and SOX10 expression. Expression levels at different treatment phases were compared by 1-way Anova. **I.** RNA sequencing data from triple wild-type melanoma patients treated with anti-PDL1 (Durvalumab) and Trametinib (GSE158403) were analysed for L518, SAMMSON, L520 TFAP2A, PAX3 and SOX10 expression. **J.** A375 were treated with DMSO or Vemurafenib (1uM) for 3 or 6 days, harvested and lysed to isolate mitochondria. L518 and SAMMSON expression was analysed by RT-qPCR. **K.** 501mel and A375 treated as in Fig.5D were harvested and L518 expression assessed by RT-qPCR. **L.** 501mel cells modified as in Fig.4I were grown in non-adherent conditions the presence of Dox and Vemurafenib (1uM) for 12 days (Dox and Vemurafenib were renewed every two days). During the first 3 days of culture cells were left untreated to allow initial melanosphere formation in a similar manner across experimental groups. Culture dishes were photographed using a light microscope and images were quantified with ImageJ for area occupied by melanospheres. Experimental groups were compared by 1-way Anova.

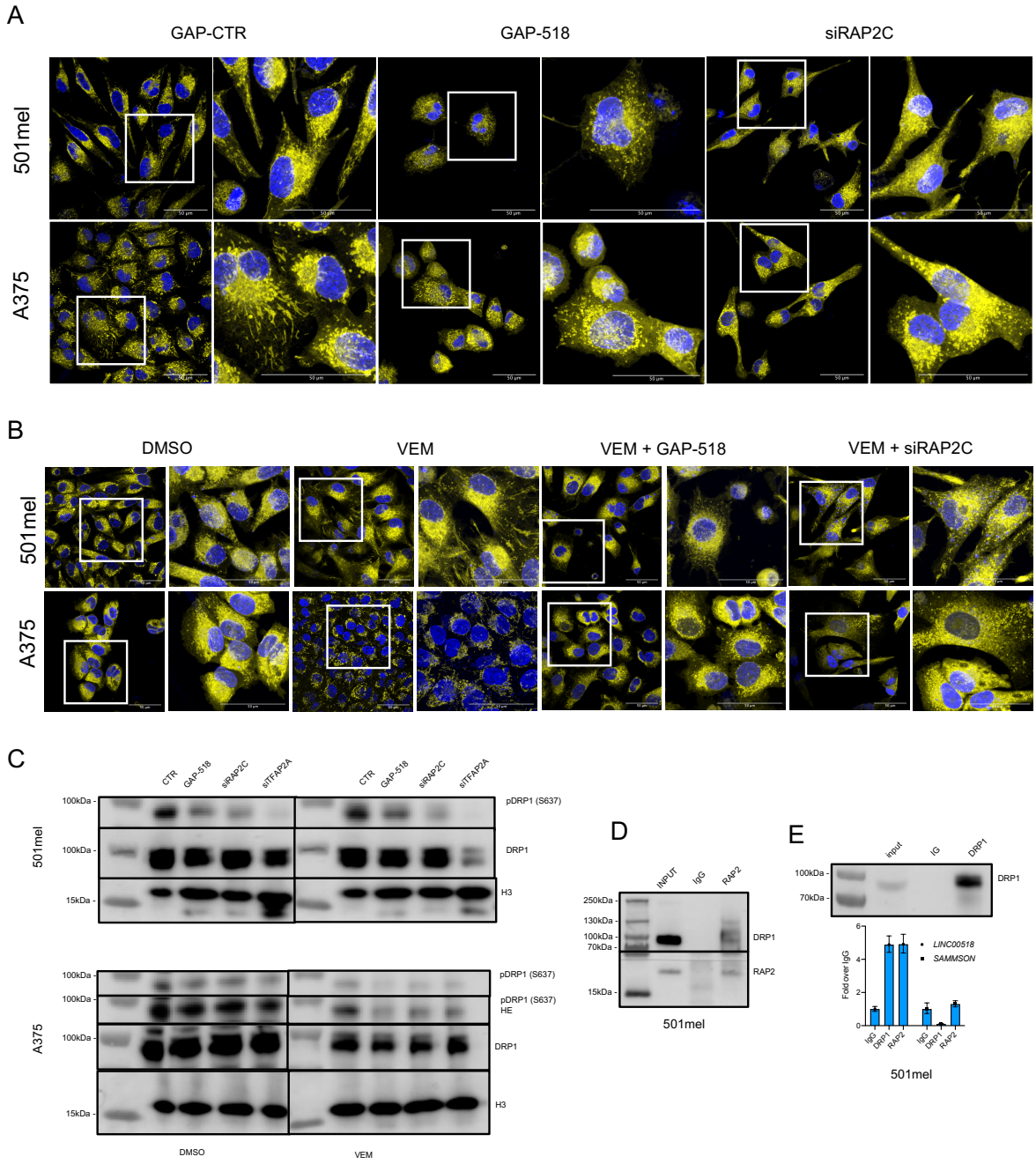

Figure 6. L518 and RAP2 interact with DRP1 regulating its phosphorylation on serine 637 and mitochondrial fusion.

A. 501mel and A375 cells were transfected with a negative control or L518 specific GapmeR or siRAP2C, cultured on microscope slides and incubated two hours with Mitotracker CMXROS Red and Hoescht to stain mitochondria and DNA, respectively. Cells were analysed by confocal microscopy without fixation keeping the temperature of the chamber at 37°C. **B.** 501mel and A375 cells were treated with DMSO or Vemurafenib (1uM) for three days, transfected with L518 GapmeR or siRAP2C, cultured for a further 3 days with DMSO or Vemurafenib and

analysed by confocal microscopy as in A. **C.** 501mel and A375 cells treated as above were analysed by western blot with anti-phospho DRP1 (S637) and total-DRP1 antibodies. H3 was evaluated as a loading control. **D.** 501mel were lysed and total extracts were immunoprecipitated with normal IgG or anti-RAP2 antibody and the IP analysed by western blot using anti-DRP1 and anti-RAP2 antibodies. A sample of the protein lysate before immunoprecipitation (1% input) was loaded in parallel. **E.** 501mel were lysed and total extracts immunoprecipitated as above and divided in two aliquots to perform RNA and protein extraction. L518 and SAMMSON expression as analysed by RT-qPCR and values were expressed as fold change over the IgG control. Proteins were analysed by western blot using an anti-DRP1 antibody. A sample of the protein lysate before immunoprecipitation (1% input) was loaded in parallel.

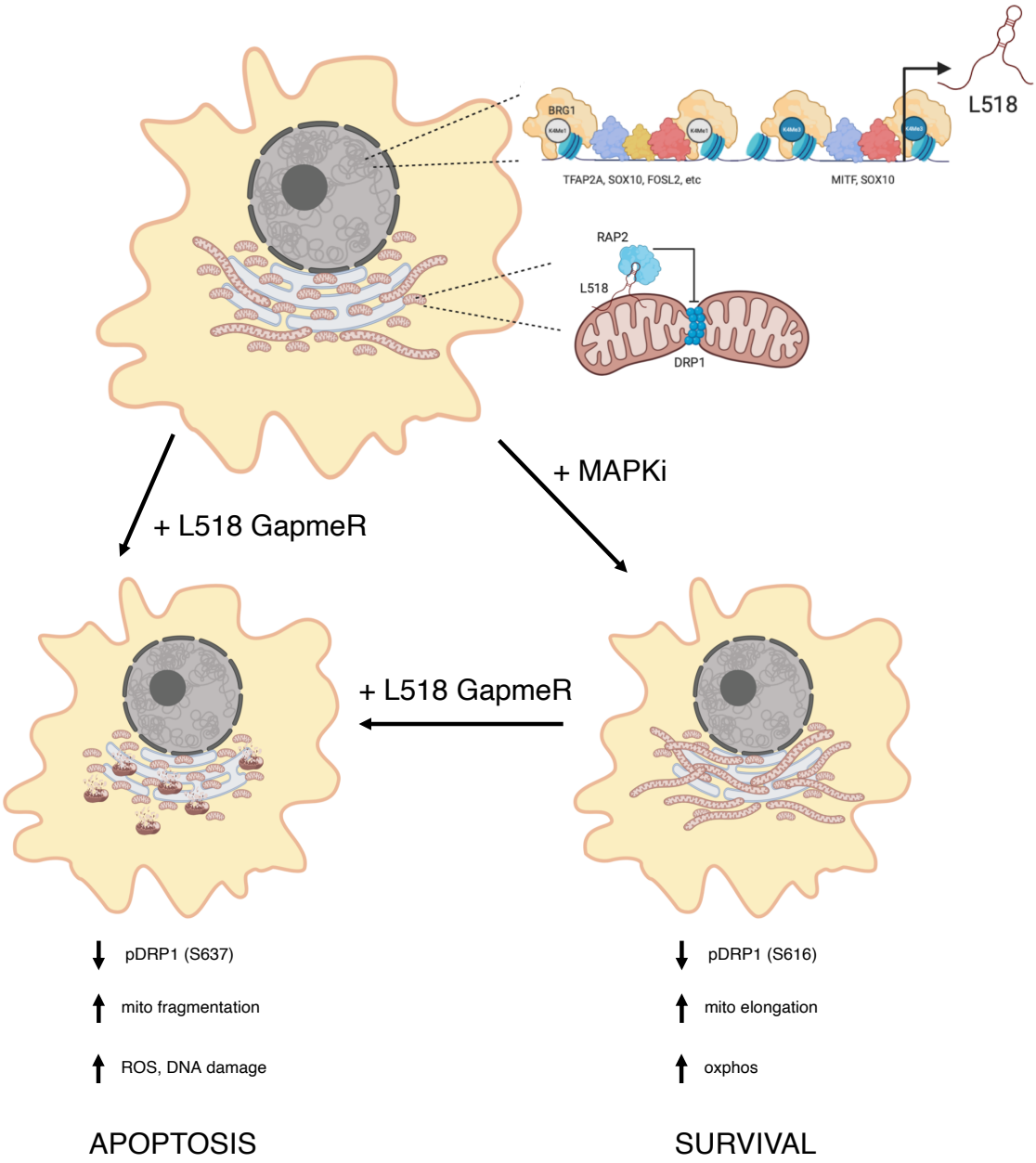

FIGURE 7. Proposed mechanism of action of L518

L518 is transcribed in a MITF/SOX10/BRG1/TFAP2A dependent manner and it expressed in both melanocytic and undifferentiated melanoma cells. In the cytoplasm, it associates with the RAP2 GTPases at the mitochondrial level and together they regulate DRP1 serine 637 phosphorylation. This activity ensures a steady state level of elongated mitochondria and adequate oxidative phosphorylation. L518 degradation by LNA GapmeRs increases mitochondrial fragmentation, release of ROS and results in apoptosis induction. Upon MAPK inhibition, cells adapt to glycolysis reduction by stimulating mitochondrial activity. Concomitant L518 degradation by GapmeRs prevents mitochondrial elongation and oxidative phosphorylation increase, thus inducing cells apoptosis.

SECTION 4 - MFI2-AS1 IS A NUCLEAR SPECKLE ASSOCIATED LNCRNA REGULATING GENE EXPRESSION, PROLIFERATION AND SURVIVAL OF MELANOMA AND RENAL CANCER CELLS.

Giovanni Gambi[1,2,3,4], Guillaume Davidson[1,2,3,4], Véronique Debien[1,2,3,4], Gabriel Malouf[1,2,3,4,5] and Irwin Davidson[1,2,3,4,5]#.

[1] Institut de Génétique et de Biologie Moléculaire et Cellulaire, Equipe Labélisée Ligue contre le Cancer. BP 163, 67404 Illkirch Cedex, C.U. Strasbourg, France

[2] Centre National de la Recherche Scientifique, UMR7104, 67404 Illkirch, France

[3] Institut National de la Santé et de la Recherche Médicale, U1258, 67404 Illkirch, France

[4] Université de Strasbourg, 67404 Illkirch, France

[5] To whom correspondence should be addressed

Running Title : MFI2AS1 regulates a proliferative gene expression program

Key words : lncRNA, melanoma, ccRCC, proliferation, MYC, chromatin

ABSTRACT

Clear cell renal carcinomas (ccRCC) can be stratified on the basis of expression of long non-coding (lnc)RNAs. Of more than 1934 ccRCC-expressed lncRNAs, MFI2-AS1 is the most potent predictor of ccRCC recurrence, with a strong positive correlation between its expression, tumour relapse, metastatic dissemination and poor patient outcome. Here we show that MFI2-AS1 localizes to the nucleus of ccRCC and melanoma cells in culture and in primary tumours where it is associated with a subset of nuclear speckles. Oligonucleotide-mediated MFI2-AS1 pulldown from melanoma cells coupled with high throughput sequencing shows enriched binding to active promoters of highly expressed genes. Comparison with public ChIA-PET data revealed that MFI2-AS1 was enriched at RNA polymerase II-mediated long-range promoter-promoter interactions. Anti-sense oligonucleotide-mediated MFI2-AS1 knockdown in ccRCC and melanoma cells induced slowed proliferation as well as deregulated expression of genes involved in proliferation, cell cycle and DNA repair. As a consequence, its knockdown induced a DNA damage response and apoptosis. These results show that MFI2-AS1 is essential in melanoma and ccRCC cells and we propose that its acts by regulating high-order chromatin structures at 'transcription factories' localized at the periphery of nuclear speckles to promote an oncogenic and proliferative gene expression program of high clinical significance for ccRCC.

INTRODUCTION

Clear cell RCC (ccRCC), designated after the predominance of clear cell histology in metastatic disease (83–88%), is the most common subtype of renal cell carcinoma accounting for the majority of deaths from kidney cancer (Hsieh et al. 2017). Localized RCC can be treated

with partial or radical nephrectomy, ablation or active surveillance. Despite nephrectomy with curative intent, ~30% of patients with localized ccRCC eventually develop metastases that require systemic therapies and are associated with high mortality (Porta et al. 2019). Targeted therapies have been developed, but treatment response is varied and most patients eventually progress (Fallah et al. 2019). Immunotherapies show promise, but predicting response is difficult and still a large fraction of patients becomes refractory to therapy (Escudier et al. 2019). Our previous studies showed that expression of long non-coding RNA (lncRNA) can be used to stratify ccRCC (Malouf et al. 2015). In an effort to identify new biomarkers for disease recurrence prediction, we analysed the transcriptomes of 351 localized ccRCCs from The Cancer Genome Atlas validated lncRNA-based recurrence classification in an independent cohort of 167 localized ccRCCs (Flippot et al. 2017). Through this pipeline, we identified lncRNA MFI2-AS1 as best candidate to predict disease progression with its expression tightly associated with shorter disease-free survival. Compared to normal samples, MFI2-AS1 was upregulated in tumor tissue, and higher expression was associated with metastatic dissemination. This result was also validated in an independent cohort by quantitative PCR analysis using TaqMan probes (Flippot et al. 2017). MFI2-AS1 is also highly expressed in melanoma. Given the importance of MFI2-AS1 in the clinical behavior of ccRCC, we aimed to characterize its molecular function in both ccRCC and melanoma cells.

We show MFI2-AS1 to be predominantly nuclear and bound to chromatin in melanoma and ccRCC cells in vitro and in vivo, forming foci that overlap with the nuclear speckle marker SC35. Pulldown of MFI2-AS1 associated chromatin in formaldehyde fixed cells coupled to high-throughput sequencing showed its specific genomic binding profile, with an enrichment at promoters of housekeeping genes. Accordingly, MFI2-AS1 knock-down by locked nucleic acid GapmeRs in melanoma and ccRCC cell lines impacts on the expression of genes promoting cell

division, survival and DNA repair. This ultimately leads to DNA damage accumulation, cell cycle block and apoptosis. Overexpression of MFI2-AS1 in the non-expressing HEKT renal cells increases MYC expression, proliferation and colony forming capacity, corroborating an oncogenic function of the lncRNA. ccRCC patients are also characterized by a positive correlation between MFI2-AS1 levels and the expression of MYC and cell cycle genes. The prognostic value of MFI2-AS1 in ccRCC may thus reflect its ability to promote expression of genes associated with cell proliferation.

RESULTS

Nuclear localization of MFI2-AS1.

The LncRNA MFI2-AS1 is located at the 3' end of the MFI2 melanotransferrin gene. MFI2-AS1 is transcribed antisense to MFI2 and databases predict the existence of several alternatively spliced isoforms (Fig. 1A). To assess which isoforms were expressed in melanoma and RCC, we analysed TCGA RNA-seq data from the corresponding tumours. Isoform 1 was essentially not expressed while expression of isoform 3 and 4 was rather low. Isoforms 2 and 5 were in contrast the most abundantly expressed with in general higher expression in melanoma compared to RCC. Similar results were observed upon analyses of data of the Cancer Cell Line Encyclopaedia (CCLE) (Fig. 1B). Using isoform-specific primers, we assessed isoform 2 and 5 expression in a collection of melanoma and RCC cell lines. Isoform 2 was expressed in almost all tested melanocytic and dedifferentiated melanoma cell lines with its expression being more abundant than isoform 5. In RCC lines, isoform 2 expression was generally lower and more variable from line to line with highest expression in RCC4 and A498 cells. Isoform 5 was strongly expressed in un-transformed TERT-immortalized primary renal epithelium RPTEC cells and in UOK-109 cells and to lower levels in UOK-112, both translocation

RCC lines, and A498 cells (Fig.1C). Thus, paradoxically while MFI2-AS1 is a major predictor for RCC progression *in vivo*, its expression was low and variable in cultured cell lines and was higher expressed in in melanoma lines than in RCC lines despite the fact that it is not a biomarker in melanoma.

We examined MFI2-AS1 expression in tumours *in situ* and cell lines using RNAscope. In sections from RCC, we observed MFI2-AS1 expression as discrete nuclear foci in the nucleus of the PAX8 expressing tumour cells. Similarly, MFI2-AS1 was also detected as discrete nuclear foci in MITF-expressing melanoma cells (Fig. 1D). Analogous observations were made in melanoma and RCC cell lines and 3D reconstruction of the confocal images confirmed that a majority of the signal was found localized in discrete nuclear foci (Fig. 1E). To confirm this, we analysed isoform 2 and isoform 5 expression by RT-qPCR in RNA from cytoplasmic and nuclear fractions using ACTB mRNA and 45S pre-rRNA as controls for efficient cytoplasmic and nuclear RNA separation. In both melanoma and RCC lines, isoform 2 was strongly enriched in the nucleus, whereas isoform 5 was present in both fractions (Fig. 1F). Nevertheless, as isoform 2 expression was much higher than isoform 5, the RT-qPCR and RNAscope approaches both pointed to MFI2-AS1 as a predominantly nuclear localized RNA in melanoma and RCC.

MFI2-AS1 is enriched at promoters of actively transcribed genes.

As MFI2-AS1 is a chromatin bound RNA, we asked if it bound to specific genomic regions. To address this, we performed MFI2-AS1 pulldown from formaldehyde fixed 501Mel cell chromatin using complementary biotinylated oligonucleotides, in parallel with the pulldown of NEAT1, a well characterized paraspeckle component as a positive control and of the prostate cancer lncRNA PCA3 as a negative control. MFI2-AS1 isoforms 2 and 5 were specifically enriched after pulldown with the complementary oligonucleotides, but not by the NEAT1 or PCA3 oligonucleotides, while NEAT1 was also specifically enriched only with its

complementary oligonucleotides (Fig. 2A). The isolated DNA in each case was analysed by high throughput sequencing. More than 19582 bound sites were detected after MFI2-AS1 pulldown, 25253 by NEAT1 and 14007 by PCA3 that showed a lower overall peak score than MFI2-AS1 or NEAT1 and served as control for non-specific peaks (Fig. 2B). Comparison of peak distribution indicated a much higher enrichment of MFI2-AS1 at the transcriptional start sites (TSS) than NEAT1 (Fig. 2C). Read density cluster maps centred on the MFI2-AS1 peaks showed virtually no overlap with NEAT1 or with a non-specific PCA3 peaks, indicating a specific genomic occupation (Fig. 2D). Further comparison with H3K27ac, H3K4me1 and H3K4me3 ChIP-seq data of 501mel cells, indicated that a large sub-fraction of MFI2-AS1 peaks were located at H3K27ac and H3K4me3 marked active promoters (C2 and C3) with a small set located at H3K27ac-marked enhancers (C1) (Fig. 2E). Peaks in C2 and C3 showed the highest peak score and were located close to the TSS of highly expressed genes (Fig. 2F). The genes in these clusters were enriched in several functions including cell cycle, transcription regulation and DNA repair (Fig. 2G). MFI2-AS1 was therefore specifically enriched at promoters of highly expressed genes involved in multiple cellular housekeeping functions.

Consistent with this idea, MF12-AS1 occupied promoters were more frequently TATA-less than TATA-containing (Fig. 2H). Motif discovery analysis performed using the MEME and ISMARA tools, indicated the presence of binding motifs for GABPA, SP1, ZFX and YY1 at MFI2-AS1 peaks (Fig. 2I). The majority of peaks containing these transcription factor binding sites were associated with the clusters 2 and 3 (Fig. 2J). Consistently we found an overlap between MFI2-AS1 ChIRP signal and the ChIP-seq of GABPA, ZNF143 and YY1 from Hela cells, but also E2F1 and MYC from MCF7 and K562 (Fig. 2K). These findings are in line with binding of MFI2-AS1 at promoters of housekeeping genes, which indeed were actively expressed and marked

by H3K4me3 also in non-melanoma or ccRCC cell lines, with typical examples of binding at the CDC20 and RAD51 promoters (Fig. 2L).

Genes with housekeeping functions have been shown to be engaged in multi-gene complexes organized by promoter-promoter interactions involving RNA polymerase II (Pol II) (Li et al.2012) and CTCF (Tang et al.2015) and characterized by higher stability (as assessed by the PET count). This 3D genome architecture is thought to reflect the existence of transcription factories organized at the periphery of nuclear speckles (Quinodoz et al. 2018). Among the Pol II and CTCF mediated chromatin interactions identified by ChIA-PET in K562 cells (Li et al.2012; Tang et al.2015), we filtered those that presented MFI2-AS1 ChIRP peaks at both anchors. The mean PET count of the MFI2-AS1 positive Pol II-mediated interactions was significantly higher than the global interaction means. However, there was no difference in the mean PET count for the CTCF-mediated interactions (Fig. 2M). These results suggest that MFI2-AS1 binding to promoters is non-random and enriched for those engaged in stable Pol II-mediated interactions, possibly those occurring at the periphery of nuclear speckles.

MFI2-AS1 localizes to nuclear speckles.

The discrete nuclear foci outside nucleoli regions seen by RNAscope (Fig. 1E) and the results of the pulldown experiment suggested MFI2-AS1 may localize to nuclear speckles. We therefore coupled RNAscope for MFI2-AS1 with immunostaining for the nuclear speckle marker SC35. Staining with SC35 labelled multiple nuclear foci distinct from the nucleolus labelled with fibrillarin (FBL) in 501Mel, MM117 and 786-O RCC cells. Overlay of the RNAscope signal indicated that MFI2-AS1 localized to a subset of these nuclear speckles (Fig. S1). The RNAscope signal was abrogated after transfection with a locked nucleic acid GapmeR to specifically knockdown MFI2-AS1 compared to the control non-targeting GapmeR. However,

MFI2-AS1 silencing did not noticeably affect the SC35 staining. These data showed that MFI2-AS1 was associated with a subset of nuclear speckles in both melanoma and RCC cells.

MFI2-AS1 is required for cell viability and regulates cell cycle genes.

Given MFI2-AS1 binding to genes involved in proliferation, cell cycle and DNA repair, we next examined the effects of MFI2-AS1 silencing on these processes and the expression of their gene signatures. We used 2 independent GapmeRs to silence MFI2-AS1 expression and a non-targeting GapmeR as control. We transfected the GapmeRs in a collection of melanoma and RCC lines and assessed their effect on expression of isoforms 2 and 5. In all cell lines, GapmeRs 1 and 2 efficiently targeted isoform 2 expression while targeting of isoform 5 was more variable with GapmeR 1, but efficient with GapmeR 2 (Fig. 3A). Importantly, in these experiments we verified that MFI2-AS1 silencing did not affect MFI2 expression (Fig. 3B) and that the subsequent effects were due to loss of MFI2-AS1 and not MFI2. Targeting of MFI2-AS1 with either GapmeR led to a strong increase in the proportion of slow proliferating cells in all of the tested melanoma and RCC lines, but not in HEK293T cells where it was not expressed (Fig. 3C). Slow proliferation was the consequence of increased proportion of cells blocked in the G2M phase of the cell cycle (Fig. 3D). Moreover, both GapmeRs induced a potent increase in apoptotic activated caspase 3-expressing melanoma and RCC cells, but not in HEK293T (Fig. 3E). These data showed that MFI2-AS1 is essential for melanoma and RCC cell proliferation and viability.

To assess the effects on gene expression, we performed RNA-seq after transfection of 501Mel and RCC4 cells with Gapmer 2 and control GapmeR, which confirmed no change of MFI2 expression (Fig. S2A). 1638 genes were up-regulated and 407 down regulated after MFI2-AS1 silencing in 501mel cells (defined as log2 Fold-change > 1 and adjusted p-value < 0.05) (Fig. S2B). RCC4 cells displayed globally more subtle changes (35 genes up- and 28 genes

downregulated with the above criteria) (Fig. S2B). Nevertheless, in both cell types, GSEA analyses, that consider all expression changes, indicated that MFI2-AS1 knockdown led to reduced expression of cell cycle genes designated by ontology terms such as E2F targets, MYC targets and in agreement with the G2M phase block, mitotic spindle and G2M checkpoint. In contrast, the P53 pathway genes were up-regulated (Fig. S2C). A closer examination confirmed that a large number of the cell cycle and mitosis signature genes identified by Gene Ontology analysis of MFI2-AS1 binding regions (Fig. 2G) were down-regulated, with only a small number up-regulated (Fig. S2D). Similarly, genes involved in transcription (Fig. S2E), in particular those regulating cell cycle such as MYC or members of the E2F family, were also down-regulated both at the mRNA (Fig. S2F) and protein (Fig. S2G) levels, although the extent of their diminished expression may not fully account for the potent effects on expression of their target genes. This suggested that MFI2-AS1 cooperated with these factors to regulate their target genes rather than acting only as an upstream regulator of these master regulators themselves.

We also noted that DNA repair genes were enriched amongst those down-regulated (Fig. S2H-I). Lowered expression of RAD51 for example was also seen by immunoblot (Fig. S2J). As a consequence of their lowered expression, we observed an activation of the DNA damage response with strong increase in phosphorylated gamma H2AX, ATM and CHK2 (Fig. S2J).

Together these data showed that MFI2-AS1 promoted expression of the cell cycle and DNA repair gene expression programs as well as the expression of several their master regulators. MFI2-AS1 silencing impacted these programs leading to a G2M phase block in the cell cycle and activation of the DNA damage response likely responsible for inducing apoptosis and compromised cell viability.

To further investigate the role of MFI2-AS1 in cell proliferation, we generated 501Mel, 786-O and HEK293T cell lines with Doxycycline (Dox)-inducible expression of MFI2-AS1 isoforms 2 or 5 using corresponding GFP-expressing lines as control. After puromycin selection, Dox induced high and homogenous GFP expression in the vast majority of the selected cell populations (Fig. S3A). Isoform 2 expression was strongly increased after 48 hours in each cell type, whereas isoform 5 accumulated to lower levels in HEK293T and 501 Mel and higher in 786-O cells. MFI2 expression was not increased in any of the lines (Fig. S3B). RNAscope revealed that a large proportion of the ectopic MFI2-AS1 localized in the cytoplasm. Nevertheless, in 501Mel and 786-O cells, an increase in the number of nuclear foci was observed, and in HEK293T cells that did not express endogenous MFI2-AS1, de novo nuclear foci were observed (Fig. S3C).

In HEK293T cells gain of MFI2-AS1 function promoted cell proliferation (Fig. 4A) and increased colony forming ability (Fig. 4B). In contrast, overexpression in 501Mel and 786-O cells led to reduced cell proliferation (Fig. 4C and E) and colony forming activity (Fig. 4D and F). In these experiments, it should be noted that Dox reduced colony forming ability of the GFP cells, hence the specific effect of Dox on the colony forming ability of MFI2-AS1 overexpressing 501Mel cells was marginal. In contrast, the specific effect on 786-O cells was much stronger. Interestingly, ectopic MFI2-AS1 activated MYC expression in HEK293T cells, but rather reduced its expression in the other lines (Fig. S3B). These data show that gain of function in HEK293T cells promoted proliferation, whereas overexpression in cells with endogenous expression had a negative effect, suggesting these lines already expressed optimal amounts.

In line with a positive relationship between MFI2-AS1 and MYC in renal carcinoma cells, we found that MFI2-AS1 mRNA levels positively correlated with MYC mRNA and protein levels

in ccRCC patients from TCGA, but not in normal kidney samples (Fig. S3D). Accordingly, ccRCC patients expressing high levels of MFI2-AS1 are characterized by increased mRNA expression of cell cycle genes (Fig. S3E) and increased protein levels of MYC, CDK1, and cyclins (Fig. S3F). These data suggest MFI2-AS1 may promote expression of MYC and cell cycle genes also in vivo.

DISCUSSION

The majority of renal carcinomas presents a clear cell histology (ccRCC), loss of VHL and increased HIF-1A activity (Chappell, Payne, and Kimryn Rathmell 2019). The resulting high tumoral vascularization prompted the development of anti-angiogenic drugs to treat advanced disease, leading to an improvement in patients' outcome (Fallah et al. 2019). Immune checkpoint inhibitors (Nivolumab, Ipilimumab) have also been introduced as first line therapy. Unfortunately, both regimens still leave a significant fraction or patients as non-responders (Atkins and Tannir 2018). In addition, despite the fact that 70% of patients manifest localized disease and can be cured by local resection, 30-35% of them develop distant metastases after surgery (Gupta et al. 2008). It is thus necessary to find new therapeutic targets for metastatic disease and biomarkers to predict recurrence.

LncRNAs have been shown to mediate different biological processes in normal and cancer cells (Ma et al. 2019). Some of them display pro-tumorigenic functions also in genitourinary malignancies (Flippot et al. 2019) and constitute candidates for targeting by antisense oligonucleotides (ASOs). Some represent also potential biomarkers, given their cancer specific expression, their prognostic value and a sufficient presence in body fluids (Qian, Shi, and Luo 2020). Nevertheless, so far only PCA3 demonstrated the features required for an approved test for prostate cancer detection (Ploussard and De La Taille 2010). The field

of non-invasive diagnosis using circulating nucleic acids still suffers from lack of standardization and methods to perform analyses on a routinely clinical basis.

We previously searched for lncRNAs associated with aggressive ccRCC disease and risk of recurrence by analysing RNA-seq data from patients of the TCGA KIRC dataset and an independent cohort of matched tumour-normal samples. Among 5 candidates we focused on the antisense lncRNA MFI2-AS1 given its low expression in normal tissues and the consistent correlation with all survival endpoints considered (Flippot et al. 2017). Its expression level (assessed by quantitative PCR/qPCR) in an independent group of 167 primary biopsies allowed stratification of patients with higher risk of recurrence and worse overall survival. This approach demonstrates the feasibility of discriminating ccRCC patients based on lncRNA expression analysis of primary biopsies, allowing for more personalized clinical management.

Given its association with clinical features of the disease, we decided to study MFI2-AS1 more in detail, characterising its expression, subcellular localisation and proposing a mechanism of action. MFI2-AS1 is expressed in an antisense fashion at the 3' end of the MFI2 gene encoding Melanotransferrin. This protein has sequence homology with the transferrin receptor, but does not seem to regulate iron uptake or metabolism (Suryo Rahmanto, Dunn, and Richardson 2007). MFI2 owes its name to its high expression in melanoma samples (Rose et al. 1986) and accordingly MFI2-AS1 is also expressed in these tumours. We thus decided to study the lncRNA in ccRCC and melanoma.

MFI2-AS1 is alternatively spliced as 5 isoforms, two of which we found to be more expressed in ccRCC and melanoma patients and cell lines RNA-seq data. This pattern was also reproduced in RT-qPCR analyses of our panel of cell lines. These two transcripts differ in their intracellular localisations, with isoform 2 being chromatin bound and isoform 5 being cytoplasmic. The latter may be responsible for some of the effects associated with MFI2-AS1

in other tumour types (Liu, Liu, and Bo 2019; C. Li et al. 2019; Yu et al. 2020; Wei et al. 2020) in which the lncRNA was proposed to act as a cytoplasmic competing endogenous RNA (ceRNA). These studies however did not provide information regarding the sequence targeted by RNA interference experiments or the one used for overexpression.

RNAscope FISH experiments on ccRCC and melanoma patients and cell lines indicated a predominantly nuclear staining. In addition, the TaqMan probes used for the analysis of the 167 ccRCC biopsies were specific for isoform 2 (Flippot et al. 2017). It is therefore nuclear isoform 2 that is predominantly detected in the tumour sections and associated with aggressive disease.

To better understand its function, we performed MFI2-AS1 pulldown from crosslinked cells using biotinylated oligonucleotides and sequenced the associated chromatin. In parallel we performed the pulldown of NEAT1 as a positive control and PCA3 as a negative one. The chromatin binding profile of MFI2-AS1 was globally different to those of the other two lncRNAs. The distinguishing feature was a positive correlation between peak score, expression levels of nearby genes and their H3K4me3-marked promoters. MFI2-AS1 seemed to enrich at the TSS and gene ontology analyses of bound genes indicated, amongst others, enrichment for regulation of transcription, cell division and DNA repair, all fundamental cellular processes that constitute hallmarks of cancer (Hanahan and Weinberg 2011). Accordingly, amongst sequences enriched at MFI2-AS1 peaks we found the binding motifs for GABPA, SP1, YY1, ZNF143, ZFX, E2F1 and MYC, all transcription factors regulating housekeeping genes and with cell proliferation and oncogenic functions in different cancer types (Bieda et al. 2006; Michaud et al. 2013; Rhie et al. 2018). These genes were characterized by similar levels of H3K4me3 in melanoma and Hela cells.

This specific genome binding profile was actually difficult to reconcile with MFI2-AS1 expression levels. Although FISH probes may not fully detect all the RNA molecules, we observed MFI2-AS1 at only a few nuclear foci, whereas thousands of binding sites were observed in the pulldown. To reconcile these observations, we propose that MFI2-AS1 may not directly interact independently with all these sites, but rather be component of a subcellular structure implicated in organizing the higher order structure of different chromatin regions, each one containing multiple genes.

The existence of high order chromatin structures has been suggested in the last years by Hi-C techniques and studies of Pol II and CTCF by ChIA-PET, a method that couples immunoprecipitation comparable to standard ChIP with a proximity ligation reaction linking together nearby DNA sequences (G. Li et al. 2010). In this manner it is possible to evaluate not only the profile of a chromatin binding protein, but also the associated higher order DNA-DNA interactions. Pol II ChIA-PET experiments highlighted that genes could be clustered into three groups: those regulated only at their promoter level, those whose promoters interacted with an enhancer (single-gene model) and those engaged in multi-gene complexes with many promoters connected between each other. Housekeeping genes tend to be organized in multi-gene complexes, with increased levels of active marks (H3K27ac, H3K4me3), binding of Pol II and transcription factors (YY1, MYC, E2F4) (G. Li et al. 2012). CTCF ChIA-PET experiments showed that the majority of RNA Pol II associated chromatin loops are found in CTCF-mediated chromatin contact domains (CCDs), with anchor regions enriched for TSSs of actively transcribed genes, active histone marks and Pol II occupancy (Tang et al. 2015). These high order structures can be functionally considered as transcription factories, in which chromatin is folded to allow concentration of the transcription machinery and increased expression of the involved genes (Sutherland and Bickmore 2009).

Transcription is coupled with the maturation of the nascent RNAs and indeed these high order structures were found to be associated at the periphery of the nuclear speckles (Quinodoz et al. 2018; Chen and Belmont 2019). These nuclear bodies result from a phase separation reaction from the rest of the nucleoplasm due to interactions amongst their protein components, characterized by intrinsically disordered domains (Galganski, Urbanek, and Krzyzosiak 2017). These proteins (such as the SR factors) are involved in splicing regulation and the proposed function of nuclear speckles is to promote this process in a co-transcriptional manner (Girard et al. 2012). MALAT1 is a lncRNA found in nuclear speckles which promotes splicing of multi-exonic transcripts (Engreitz et al. 2014). However, unlike NEAT1 for paraspeckles, it does not constitute an integral component of these nuclear bodies (Nakagawa et al. 2012).

Given MFI2-AS1 enrichment at promoters of highly transcribed genes, we thought it could constitute a structural component of transcription factories, possibly localized at the periphery of nuclear speckles. Its co-detection with the SC35 marker corroborated this hypothesis, while staining for Fibrillarin indicated exclusion from the nucleoli. This would explain why we could pulldown thousands of loci, an effect probably resulting from indirect crosslinking events induced by formaldehyde.

Although this overlap could be the result of transcription and splicing at its own locus, we hypothesized a more general role for MFI2-AS1 in regulation of the genes where it is bound at their promoters. RNA-seq after MFI2-AS1 knock down in melanoma cells showed an overall stronger up- rather than down-regulation of gene expression. Nevertheless, GSEA analysis highlighted a reduction in the E2F and MYC-regulated gene signatures that were also enriched in the MFI2-AS1 pulldown. Accordingly, also ontologies related to cell division such as G2M checkpoint and mitotic spindle, as well as regulation of transcription and DNA repair were

affected, suggesting an influence of MFI2-AS1 on the expression of its pulldown targets. MFI2-AS1 knockdown in RCC4 led to more subtle changes, with fewer deregulated genes and at lesser effect on their expression. However, global analysis confirmed reduced scores for the same gene signatures and the upregulation of P53 targets.

These transcriptomic findings were mirrored by changes in the levels of key proteins. We confirmed the reduction in E2F1, BPTF, MYC and homology directed DNA repair factors RAD51, BRCA1, with concomitant increase in the DNA damage response, G2M cell cycle arrest and apoptosis. These effects were not seen in the MFI2-AS1 negative HEKT cells, excluding toxic effects of the GapmeRs. These loss of function studies suggest a role for MFI2-AS1 in the regulation of a gene expression program driving proliferation and survival of melanoma and ccRCC cells.

We also assessed the effects of gain of MFI2-AS1 function by ectopic Dox-inducible expression of isoforms 2 in HEKT cells and in parallel with 501mel and 786-O cells where it is already present. Ectopic MFI2-AS1 expression did not affect MFI2 expression in agreement with the results obtained upon loss of function, suggesting it may not have a cis-activity. Ectopic expression in HEKT cells up-regulated MYC levels and associated with higher proliferation rate and colony forming capacity in vitro. In contrast, MYC expression was not increased in 501mel and 786-O cells, that in addition showed diminished proliferation and colony forming capacity. These observations suggest that overexpression may not be beneficial for cellular fitness. We actually observed a phenotype change in these cells, becoming more flattened and elongated at light microscopy evaluation. They may have acquired a more invasive but slow cycling phenotype, or undergo senescence. Future experiments will be performed to test these hypotheses.

It is also important to note that ectopic MFI2-AS1 expression led to formation of de novo nuclear foci in HEKT cells an increase in nuclear foci in 501Mel and 786-O cells, but also a strong accumulation of the exogenous RNA in the cytoplasm in particular in the melanoma and RCC cells. It is therefore possible that this overexpression actually induced a stress for the cells rather than boosting MFI2-AS1 function. If MFI2-AS1 interacts with nuclear proteins, the high expression in the cytoplasm may even titrate these proteins away from the nucleus. We will verify that the FISH signals in the HEKT overexpressing cells are also in close proximity with nuclear speckles. RNA-seq and ChiRP experiments will determine if the genomic binding profile of MFI2-AS1 and the transcriptomic changes occurring in HEKT cells are in accordance with what we observed with the endogenous RNA in melanoma and RCC cells. Using this heterologous cell system, may reveal if MFI2-AS1 is directly involved in the observed gene expression and physiology changes.

Analyses of TCGA KIRC samples indicate how MFI2-AS1 expression correlates with that of MYC and cell cycle genes in these patients, possibly explaining the increased risk of recurrence. To test if MFI2-AS1 can increase tumour aggressiveness in vivo, we will overexpress it in murine renal carcinoma Renca cells and evaluate changes in xenograft growth or metastasis formation. These experiments should help to determine if MFI2-AS1 is a therapeutic target for ccRCC.

An intriguingly point relates to the prognostic value of MFI2-AS1 in ccRCC but not in melanoma, despite the fact that MFI2-AS1 expression is higher in melanoma than in RCC cells in vitro and the more severe effect on gene expression upon its knockdown. We wonder if differences between these tumour types underlie a stronger dependency of ccRCC on MFI2-AS1 expression. Alternatively, it is possible that the lower expression at least of isoform 2 in ccRCC patients facilitates patient stratification. Patients with lowest expression may not

accumulate sufficient number of copies and thus not benefit at all by its pro-tumorigenic effects. Once a certain threshold is reached, MFI2-AS1 may become advantageous for cancer cells in the absence of further positive correlation with its expression. In line with this, we did not observe an advantage when it was overexpressed in already positive cells.

Beside ccRCC and melanoma, other tumour types express MFI2-AS1, such as glioblastomas and lower grade gliomas. We found MFI2-AS1 to be expressed in all TCGA tumour types, more uniformly than MFI2 and at higher levels compared to matched normal tissues (data not shown). Accordingly, MFI2-AS1 is listed among the epigenetically activated (EA) lncRNAs characterized by promoter hypomethylation and higher expression levels in cancer compared to normal tissues (Wang et al. 2018). A similar pan-cancer expression pattern characterizes the SNHG12 and MINCR lncRNAs, both of which are known MYC targets. Preliminary mining of public datasets suggest that MFI2-AS1 may also be regulated by MYC and sensitive to BET inhibitors in different cancer cell lines (data not shown), suggesting that similar to other lncRNAs (Hart et al. 2014; Hung et al. 2014; Doose et al. 2015) it could be involved in a MYC-related positive feedback loop that sustains tumorigenesis.

Similar to MYC or BET inhibition, MFI2-AS1 seems also to reduce the expression of genes involved in homology directed DNA repair and knock down cells displayed a DNA damage response. This effect could be therapeutically combined with PARP inhibition that is known to be synthetically lethal with RAD51 or BRCA1 deficiency, genetic (such as in ovarian cancer)(Ashworth and Lord 2018) or induced by BET inhibition (Yang et al. 2017). MFI2-AS1 targeting could represent a strategy to sensitize cells to PARP inhibitors with eventually a better therapeutic index compared to BETi. Combined with the hypothesis of its pan-cancer expression, this strategy could be attractive for different tumour types.

Our data provide new insights regarding MFI2-AS1 expression, localization and activity. Unlike previous studies, we suggest this lncRNAs to act at nuclear level by regulating expression of genes with key functions for cancer cells. This proliferative role may explain the link with disease aggressiveness and recurrence in ccRCC patients, but several questions remain to be answered, most importantly MFI2-AS1 mechanism of action.

We showed MFI2-AS1 co-localizes at a subset of SC35-labeled nuclear speckles, but we do not know if this implicates MFI2-AS1 as a component of nuclear speckles like MALAT1 or its involvement in transcription factories at the periphery of these nuclear bodies. In the first case MFI2-AS1 knock down may affect their structure or splicing efficiency: preliminary results did not allow us to conclude if nuclear speckle structure was compromised and we did not explore if deregulation of splicing takes place. It would be interesting to perform super-resolution microscopy analyses of MFI2-AS1 localization together with nuclear speckle proteins, similarly to what has been done with NEAT1 and MALAT1 (Yamazaki et al. 2018; Liao and Regev 2020). In parallel, we will explore eventual MFI2-AS1-protein interactions by coupling its pulldown with mass spectrometry analysis to identify potential interacting proteins.

Regarding its binding to the genome, we will repeat the ChiRP experiments on additional melanoma, ccRCC or other tumour-derived cell lines to evaluate if the binding profile is consistent. The same experiment on the HEKT with inducible expression would further indicate if exogenous MFI2-AS1 promotes the same activity as the endogenous one.

We are tempted to speculate on a role for MFI2-AS1 in high order chromatin organization that may relate to CTCF or other proteins involved in looping. CTCF dimerization has been shown to depend on RNA binding and from the existing CTCF CLIP-seq experiment we could detect MFI2-AS1 among its partners, despite its very low expression (Saldaña-Meyer

et al. 2014). It would be interesting to evaluate if this interaction is functional by repeating the CTCF RNA-immunoprecipitation in melanoma and RCC cells.

Some lncRNAs have already been shown to regulate 3D chromosomal organization, such as XIST and FIRRE (Engreitz, Ollikainen, and Guttman 2016). From their transcription locus they establish functional contacts with proximal chromatin regions in cis and trans. MFI2-AS1 may also act by proximity from its transcription locus and somehow regulate other genomic regions, possibly by interacting with a protein(s) involved in transcription factories. Combining MFI2-AS1 binding profile with chromosome topology data may help to answer this question. Alternatively, we could exploit new technologies exploring RNA-chromatin (Bonetti et al. 2020) and RNA-RNA interactions (Quinodoz et al. 2018) to demonstrate MFI2-AS1 proximity to the loci it interacts with and the related nascent transcripts. Despite being very challenging to prove, this model would explain how such a low abundant RNA could impact on cancer cell physiology.

In line with this hypothesis we noticed MFI2-AS1 was enriched at stable RNA Pol II mediated interactions and at multi-gene complexes of members of the same gene family, such as the 58 HIST1H genes on chromosome 6: MFI2-AS1 seemed more densely located at the clusters 1, 2 and 3 and devoid in the intervening loop regions. Moreover, MFI2-AS1 knockdown induced a global reduction of genes present in the clusters and an increase of those in the loops (Fig.5A). This outcome may rely on a global re-organization of the region, with promoters of the clusters losing their contacts and and reduced transcription, while the genes in the loops are re-expressed as they are no longer constrained in a suppressive environment (Fig. 5B). This effect may also explain the increased expression of many genes after MFI2-AS1 knock down, despite the absence of its binding with these epigenetically repressed regions. If true, this model would unveil a so far uncharacterized function of a

lncRNA, with the ability to regulate a comprehensive tumorigenic gene expression program through regulating higher order chromatin structure.

MATERIALS AND METHODS

Cell culture and GapmeR transfections

Melanoma 501mel cells were grown in RPMI 1640 medium supplemented with 10% Fetal Calf Serum (FCS) and gentamicine; MM011, MM117, MM047 were grown in HAM-F10 medium supplemented with 10% FCS, 5.2 mM glutamax, 25 mM Hepes and penicillin/streptomycin (7.5 ug/ml). ccRCC cell line 786-O was grown in RPMI medium supplemented with 10mM Hepes, 10%FCS, glucose (2.5g/L), 1mM sodium pyruvate and gentamicine. RCC4 and HEK293T cells were grown in DMEM medium supplemented with glucose (1g/l), 10% FCS and penicillin/streptomycin (7.5 ug/ml). To assess cell growth and viability cells were stained with Trypan Blue (Invitrogen). For GapmeR experiments cells were transfected using Lipofectamine RNAiMAX (Invitrogen) according to manufacturer instructions with 20 nM of GapmeR (Qiagen) and harvested 48 or 72 hours after to perform RNA, protein extraction or flow cytometry analysis. GapmeRs sequences are listed in Table 1. Colony forming ability was assessed by plating 500 501Mel, or 1000 HEKT or 786-O cells per 9.6 cm2 dish, keeping them in culture for 10 days and finally fixing in formalin and staining the colonies with 0.05% Crystal Violet solution (Sigma Aldrich).

Plasmid cloning and lentiviral transduction

MFI2-AS1 isoform 2 cDNA was synthesized by Genscript and cloned into the pUC57 vector. cDNA was then cloned into the pCW57-GFP-P2A-MCS vector, which was a gift from Adam Karpf (Addgene plasmid # 71783; http://n2t.net/addgene:71783; RRID: Addgene_71783). Lentiviral particles were produced after transfection of HEK293T cells with

packaging plasmids, purified by ultracentrifugation and re-suspended in PBS. After titration, cells were infected at MOI of 1 and selected by puromycin addition to the media (1ug/ml).

Proliferation and viability analyses by flow cytometry

To assess cell viability and proliferation after GapmeR mediated knock down, cells were stained with Cell Trace Violet (Invitrogen) on the day of transfection. They were harvested after 72 hours and stained using the active caspase 3 kit (BD Biosciences) following manufacturer instructions. Cells were analysed on a LSRII Fortessa (BD Biosciences) and data were analysed with Flowjo software (Tree Star).

Cell cycle progression analysis by flow cytometry

Cells were transfected with GapmeRs and after 72 hours stained using the Click-it Edu kit (Thermofischer) and TOPRO-3 following manufacturer instructions. Briefly, cells were cultured with 10uM Edu for 1 hour and 30 minutes, harvested by trypsinization, washed once in 1%BSA-PBS and fixed in 4%PFA for 15 minutes at room temperature. After a wash in 1%BSA-PBS cells were permeabilized with saponin-permeabilization buffer for 15 minutes and then stained with the Click-it reaction cocktail for 30 minutes. Finally, they were washed once in 1%BSA-PBS, re-suspended in 500 ul of PBS with 10nM TOPRO-3 and left for 10 minutes at room temperature. Cells were analysed on a LSRII Fortessa (BD Biosciences) and data were analysed with Flowjo software (Tree Star).

RNAscope

RNAs for *MFI2-AS1*, *MITF* and *PAX8* in sections of human melanomas or normal skin and cultured cells were detected with the RNAscope assay (Advanced Cell Diagnostics, ACD, Hayward, CA) according to the manufacturer's protocols. Briefly, patient sections were de-paraffinized, incubated with hydrogen peroxide at room temperature for 10 min, boiled with target retrieval reagent for 15 min, and then treated with protease plus reagent at 40°C for 30

min. The sections were hybridized with Hs-*MITF* probe (ACD, Cat. No. 310951), Hs-*PAX8* probe (ACD, Cat. No. 402361-C2), Hs-*MELTF-AS1* (ACD, Cat.No. 570031) at 40°C for 2 h. Hybridization signals were amplified and visualized with RNAscope Multiplex Fluorescent Reagent Kit v2 (ACD, Cat. No. 323100). For co-detection of SC35 and FBN1 with *MFI2-AS1*, cells were fixed for 30 minutes with formaldehyde 3.7%, washed with PBS and incubated 10 minutes at room temperature with H2O2. After one wash in distilled water, primary antibodies diluted in co-detection diluent (1/200 for SC35, 1/100 for FBN1) were added o/n at 4°C. Slides were washed in PBS+tween 0.1% (PBST), fixed in formaldehyde 3.7% for 30 minutes and washed again in PBST. Slides were treated with protease III and washed with PBS. MFI2-AS1 hybridization signals were amplified following the multiplex fluorescent kit. Finally, SC35 and FBN1 signals were developed by secondary antibodies incubation (diluted 1/2000 in co-detection diluent) followed by Tyramide Signal Amplification (TSA plus kit, NEL760001KT, Perkin Elmer). Images were captured with a confocal (Leica DMI6000) microscope.

RNA extraction, quantitative PCR and RNA sequencing analysis

Total mRNA isolation was performed using Trizol and isopropanol precipitation. Isolation of cytosolic, nuclear soluble and chromatin associated RNA was performed as described in Conrad and Orom paper (*Enhancer RNAs: Methods and protocols*, 2017). Briefly, cells were harvested and washed in PBS buffer, re-suspended in 0.15% NP-40 lysis buffer and centrifuged on a 24% sucrose cushion (taking supernatant as the cytosolic fraction). Nuclei were re-suspended in 1M Urea, 1% NP-40 lysis buffer and centrifuged to recover the nuclear soluble fraction in the supernatant. The chromatin pellet was finally re-supended in 1ml of Trizol reagent (MRCgene), solubilized using a 21-gauge needle and isolated following manufacturer instructions. Cytosolic and nuclear soluble fractions were cleared by centrifugation and RNA was isolated from 200ul of each using 1ml of Trizol. Total and

fractionated RNA were treated with DNAseI following the TurboDnase free kit instructions (Thermofisher) and reverse transcribed using Superscript IV reverse transcriptase (Thermofisher) following manufacturer instructions. qRT-PCR was carried out with SYBR Green I (Roche) and monitored by a LightCycler 480 (Roche). Target genes expression was normalized using *TBP*, *HBMS, ACTB, GAPDH* and *Rpl13a* as reference genes. *ACTB* and 45S pre-rRNA were taken as RNA controls for cellular fractionation for cytosolic and nuclear soluble/chromatin-associated fractions respectively. Primers for RT-qPCR were designed using Primer3 and are listed in Table 2. RNA-seq was performed essentially as previously described (Laurette et al., Cell Death Diff, 2019). Gene ontology analyses were performed with the Gene Set Enrichment Analysis software GSEA v3.0 using the hallmark gene sets of the Molecular Signatures Database v6.2 and the functional annotation clustering function of DAVID.

Protein extraction and western blotting

Whole cell extracts were prepared by the standard freeze-thaw technique using LSDB 500 buffer (500 mM KCl, 25 mM Tris at pH 7.9, 10% glycerol (v/v), 0.05% NP-40 (v/v), 16mM DTT, and protease inhibitor cocktail). Cell lysates were subjected to SDS–polyacrylamide gel electrophoresis (SDS-PAGE) and proteins were transferred onto a nitrocellulose membrane. Membranes were incubated with primary antibodies in TBS+ 5% BSA + 0.01% Tween-20. Overnight at 4 °C. The membrane was then incubated with HRP-conjugated secondary antibody (Jackson ImmunoResearch) for 1h at room temperature, and visualized using the ECL detection system (GE Healthcare). Antibodies used are listed in table Table 3.

MFI2-AS1 pulldown using biotinylated probes followed by high throughput sequencing

501mel cells were grown in 15cm petri dishes and harvested by trypsinization. Cells were counted and fixed in 3.7% formaldehyde for 30 minutes at room temperature.

Formaldehyde was quenched with 2M glycine for 5 minutes and cells pelleted 5' at 800g. After two washes with cold PBS, cells were aliquoted in tubes (100mg/tube). Each aliquot was re-suspended in 500ul of lysis buffer (50 mM Tris–Cl pH 7.0, 10 mM EDTA, 1 % SDS) supplemented with fresh 1mM PMSF, protease/phosphatase inhibitors cocktail (Thermofisher) and RNAsin (Thermofisher). After 10' on ice, lysates were transferred to Covaris tubes and sonicated in a Covaris sonicator to obtain small DNA fragments (100-50bp in length). After sonication, lysates were centrifuged 20' at 12000g and transferred to a new tube to proceed for preclearing using C1 streptavidin magnetic beads (30ul/ml of lysate) for 30' at 37°C. After bead removal, lysate was diluted with 2 times the volume of hybridization buffer (750 mM NaCl, 1% SDS, 50 mM Tris–Cl pH 7.0, 1 mM EDTA, 15% formamide) supplemented with fresh 1mM PMSF, protease/phosphatase inhibitors cocktail (Thermofisher) and RNAsin (Thermofisher). Anti-PCA3/MFI2-AS1/NEAT1 DNA biotinylated probes were added to the lysate (100pmol/100mg of cells) and incubated 16 hours at 37°C. Probes sequences are listed in Table 4. To recover RNA-chromatin complexes, C1 streptavidin magnetic beads were added to each sample and incubated 30' at 37°C. Beads were then washed 4 times with wash buffer (2× SSC, 0.5 % SDS) and after final wash divided in two aliquots for RNA and DNA elution. RNA was extracted with Trizol and isopropanol precipitation, DNAse digested, reverse transcribed and analysed by qPCR for MFI2-AS1 isoforms 2 and 5 and NEAT1 expression. For DNA extraction beads were re-suspended twice in DNA elution buffer (50 mM NaHCO3, 1% SDS) supplemented with RNAseA (final 100ug/ml) and RNAseH (0.1 U/ul) and incubated 30' at 37°C. DNA was then purified by phenol-chloroform extraction protocol, precipitated in ethanol and sodium acetate, re-suspended in water and sequenced on Illumina Hiseq 4000 sequencer as Single-Read 50 base reads following Illumina's instructions. Sequenced reads were mapped to the Homo sapiens genome assembly hg19 using Bowtie with the following arguments: -m 1 --

strata --best -y -S -l 40 -p 2. After sequencing, peak detection was performed using the MACS software. Global clustering analysis and quantitative comparisons were performed using seq-MINER ([Ye et al., 2011] http://bips.u-strasbg.fr/seqminer/) and R (http://www.r-project.org/). De novo motif discovery was performed using the MEME suite (https://academic.oup.com/nar/article/37/suppl_2/W202/1135092) and ISMARA tool (Balwierz et al., Genome Research, 2014).

Table 1

GapmeR/siRNA	Sequence
Negative A	AACACGTCTATACGC
MFI2-AS1#1	CTTTGGGTCACTGTAT
MFI2-AS1#2	TTCTGGAAAGAGCGCA

Table 2

Primer name	Sequence
hACTB_F	ACATCTGCTGGAAGGTGGAC
hACTB_R	CCCAGCACAATGAAGATCAA
hGAPDH_F	ACAACTTTGGTATCGTGGAAGG
hGAPDH_R	GCCATCACGCCACAGTTTC
hRPL13a_F	TTGAGGACCTCTGTGTATTTGTCAA
hRPL13a_R	CCTGGAGGAGAAGAGGAAAGAGA
hHMBS_F	GGCAATGCGGCTGCAA
hHMBS_R	GGGTACCCACGCGAATCAC
hTBP_F	CGGCTGTTTAACTTCGCTTC
hTBP_R	CACACGCCAAGAAACAGTGA
h45S_F	TCGCTGCGATCTATTGAAAG
h45S_R	AGGAAGACGAACGGAAGGA
hMFI2_F	GGCTGACGCCATCACTCT

hMFI2_R	CCACGGCGTAATAGGAGGTA
hMFI2-AS1 (iso2)_F	CTGGAAGAGGCGTTCAGAAG
hMFI2-AS1 (iso2)_F	TGGTTGCAGAACACAAGTCC
hMFI2-AS1 (iso5)_F	GAGACGACATCCCTTCCAGC
hMFI2-AS1 (iso5)_F	GGTTGCAGAACACAAGTCCC

Table 3

Target	Lot	Host	Application	Dilution
VINCULIN (V4505)	099M	Mouse	WB	1:2000
gamma H2A.X (phospho S139) (ab22551)	GR3358071-2	Mouse	WB	1:1000
BPTF (A300-973A)		Rabbit	WB	1:1000
E2F1 (3742)		Rabbit	WB	1:1000
MYC (SC-764)	J2215	Rabbit	WB	1:1000
RAD51 (ab213)	GR3281461-2	Mouse	WB	1:1000
BRCA1 (sc-6954)	H2919	Mouse	WB	1:1000
Phospho ATM (Ser1981) (5883)	6	Rabbit	WB	1:1000
Phospho CHK2 (Thr68) (2197)	12	Rabbit	WB	1:1000
SC35 (ab11826)	GR3248373-3	Mouse	IF	1:200
Fibrillarin (ab4566)	GR3266127-5	Mouse	IF	1:200

Table 4

Oligo name	Sequence
MFI2-AS1-1	gtgtgaacgctcaaaacggc
MFI2-AS1-2	tgtcaagcttatgacttcca
MFI2-AS1-3	aagtccctctcgaaattgtt

MFI2-AS1-4	ccacagaacggtcattctag
MFI2-AS1-5	ctggaaagagcgcatacccg
MFI2-AS1-6	cagacggacctgggtaatga
MFI2-AS1-7	atattctgtgactggttgca
MFI2-AS1-8	ttctggaaagagcgcatacc
MFI2-AS1-9	ggtgggtcagtgaagacacg
MFI2-AS1-10	ctcatactacttctggtctt
MFI2-AS1-11	ggaaagagcgcatacccg
MFI2-AS1-12	ttcgcagcagtccaggtg
MFI2-AS1-13	ctggtgctattcagaccc
MFI2-AS1-14	agcaccgcagtgcttctg
MFI2-AS1-15	ccaatcagttgtcaagct
MFI2-AS1-16	ccagctcacctgatattc
PCA3-1	gcacttgctatttcttctgt
PCA3-2	ctctgtttttctgatgccag
PCA3-3	tgtttgttgcatgtcttgtg
PCA3-4	attctttattgccaggagtg
PCA3-5	tatgcatattgtggttgtcc
PCA3-6	tgtctgaatcctctccaaac
PCA3-7	gctagcatccataataggag
PCA3-8	ttgcatgcatgtaccacaag
PCA3-9	ggactagctcttcacttatt
PCA3-10	cctcagatggtaaagtcagc
PCA3-11	cctgtgtgtgtggatattta
PCA3-12	tcattttctaatgtccttcc
PCA3-13	aggacttagtcatctttgca
PCA3-14	tgcctgacatgttcaaggaa
PCA3-15	caaacgtgccccataaacat
PCA3-16	gggatttgcactgcatgaat

REFERENCES

Ashworth, Alan, and Christopher J. Lord. 2018. "Synthetic Lethal Therapies for Cancer: What's next after PARP Inhibitors?" *Nature Reviews Clinical Oncology* 15 (9): 564–76. https://doi.org/10.1038/s41571-018-0055-6.

Atkins, Michael B., and Nizar M. Tannir. 2018. "Current and Emerging Therapies for First-Line Treatment of Metastatic Clear Cell Renal Cell Carcinoma." *Cancer Treatment Reviews* 70 (July): 127–37. https://doi.org/10.1016/j.ctrv.2018.07.009.

Bieda, Mark, Xiaoqin Xu, Michael A. Singer, Roland Green, and Peggy J. Farnham. 2006. "Unbiased Location Analysis of E2F1-Binding Sites Suggests a Widespread Role for E2F1 in the Human Genome." *Genome Research* 16 (5): 595–605. https://doi.org/10.1101/gr.4887606.

Bonetti, Alessandro, Federico Agostini, Ana Maria Suzuki, Kosuke Hashimoto, Giovanni Pascarella, Juliette Gimenez, Leonie Roos, et al. 2020. "RADICL-Seq Identifies General and Cell Type–Specific Principles of Genome-Wide RNA-Chromatin Interactions." *Nature Communications* 11 (1): 1–14. https://doi.org/10.1038/s41467-020-14337-6.

Chappell, John C, Laura Beth Payne, and W. Kimryn Rathmell. 2019. "Hypoxia, Angiogenesis, and Metabolism in the Hereditary Kidney Cancers." *Journal of Clinical Investigation*. https://doi.org/10.1172/JCI120855.

Chen, Fengju, Yiqun Zhang, Yasin Şenbabaoğlu, Giovanni Ciriello, Lixing Yang, Ed Reznik, Brian Shuch, et al. 2016. "Multilevel Genomics-Based Taxonomy of Renal Cell Carcinoma." *Cell Reports* 14 (10): 2476–89. https://doi.org/10.1016/j.celrep.2016.02.024.

Chen, Yu, and Andrew S. Belmont. 2019. "Genome Organization around Nuclear Speckles." *Current Opinion in Genetics and Development* 55: 91–99. https://doi.org/10.1016/j.gde.2019.06.008.

Doose, Gero, Andrea Haake, Stephan H. Bernhart, Cristina López, Sujitha Duggimpudi, Franziska Wojciech, Anke K. Bergmann, et al. 2015. "MINCR Is a MYC-Induced LncRNA Able to Modulate MYC's Transcriptional Network in Burkitt Lymphoma Cells." *Proceedings of the National Academy of Sciences of the United States of America* 112 (38): E5261–70. https://doi.org/10.1073/pnas.1505753112.

Engreitz, Jesse M., Klara Sirokman, Patrick McDonel, Alexander A. Shishkin, Christine Surka, Pamela Russell, Sharon R. Grossman, Amy Y. Chow, Mitchell Guttman, and Eric S. Lander. 2014. "RNA-RNA Interactions Enable Specific Targeting of Noncoding RNAs to Nascent Pre-MRNAs and Chromatin Sites." *Cell* 159 (1): 188–99. https://doi.org/10.1016/j.cell.2014.08.018.

Engreitz, Jesse M, Noah Ollikainen, and Mitchell Guttman. 2016. "Long Non-Coding RNAs: Spatial Amplifiers That Control Nuclear Structure and Gene Expression." *Nature Reviews Molecular Cell Biology*. Nature Publishing Group. https://doi.org/10.1038/nrm.2016.126.

Escudier, B., C. Porta, M. Schmidinger, N. Rioux-Leclercq, A. Bex, V. Khoo, V. Grünwald, S. Gillessen, and A. Horwich. 2019. "Renal Cell Carcinoma: ESMO Clinical Practice Guidelines for Diagnosis, Treatment and Follow-Up." *Annals of Oncology* 30 (5): 706–20. https://doi.org/10.1093/annonc/mdz056.

Fallah, Asghar, Ali Sadeghinia, Houman Kahroba, Amin Samadi, Hamid Reza Heidari, Behzad Bradaran, Sirous Zeinali, and Ommoleila Molavi. 2019. "Therapeutic Targeting of Angiogenesis Molecular Pathways in Angiogenesis-Dependent Diseases." *Biomedicine and Pharmacotherapy* 110 (December 2018): 775–85. https://doi.org/10.1016/j.biopha.2018.12.022.

Flippot, Ronan, Guillaume Beinse, Alice Boilève, Julien Vibert, and Gabriel G. Malouf. 2019. “Long Non-Coding RNAs in Genitourinary Malignancies: A Whole New World.” *Nature Reviews Urology*. https://doi.org/10.1038/s41585-019-0195-1.

Flippot, Ronan, Roger Mouawad, Jean Philippe Spano, Morgan Rouprêt, Eva Compérat, Marc Olivier Bitker, Jérôme Parra, et al. 2017. “Expression of Long Non-Coding RNA MFI2-AS1 Is a Strong Predictor of Recurrence in Sporadic Localized Clear-Cell Renal Cell Carcinoma.” *Scientific Reports* 7 (1): 1–9. https://doi.org/10.1038/s41598-017-08363-6.

Galganski, Lukasz, Martyna O. Urbanek, and Wlodzimierz J. Krzyzosiak. 2017. “Nuclear Speckles: Molecular Organization, Biological Function and Role in Disease.” *Nucleic Acids Research* 45 (18): 10350–68. https://doi.org/10.1093/nar/gkx759.

Girard, Cyrille, Cindy L. Will, Jianhe Peng, Evgeny M. Makarov, Berthold Kastner, Ira Lemm, Henning Urlaub, Klaus Hartmuth, and Reinhard Luhrmann. 2012. “Post-Transcriptional Spliceosomes Are Retained in Nuclear Speckles until Splicing Completion.” *Nature Communications* 3. https://doi.org/10.1038/ncomms1998.

Gupta, Kiran, Jeffrey D Miller, Jim Z Li, Mason W Russell, and Claudie Charbonneau. 2008. “Epidemiologic and Socioeconomic Burden of Metastatic Renal Cell Carcinoma (MRCC): A Literature Review.” *Cancer Treatment Reviews* 34 (3): 193–205. https://doi.org/10.1016/j.ctrv.2007.12.001.

Hanahan, Douglas, and Robert A. Weinberg. 2011. “Hallmarks of Cancer: The next Generation.” *Cell* 144 (5): 646–74. https://doi.org/10.1016/j.cell.2011.02.013.

Hart, Jonathan R, Thomas C Roberts, Marc S Weinberg, Kevin V Morris, and Peter K Vogt. 2014. “MYC Regulates the Non-Coding Transcriptome.” *Oncotarget* 5 (24): 12543–54. https://doi.org/10.18632/oncotarget.3033.

Hsieh, James J., Mark P. Purdue, Sabina Signoretti, Charles Swanton, Laurence Albiges, Manuela Schmidinger, Daniel Y. Heng, James Larkin, and Vincenzo Ficarra. 2017. “Renal Cell Carcinoma.” *Nature Reviews Disease Primers* 3: 1–19. https://doi.org/10.1038/nrdp.2017.9.

Hung, Chiu Lien, Ling Yu Wang, Yen Ling Yu, Hong Wu Chen, Shiv Srivastava, Gyorgy Petrovics, and Hsing Jien Kung. 2014. “A Long Noncoding RNA Connects C-Myc to Tumor Metabolism.” *Proceedings of the National Academy of Sciences of the United States of America* 111 (52): 18697–702. https://doi.org/10.1073/pnas.1415669112.

Li, Chenglong, Fengbo Tan, Qian Pei, Zhongyi Zhou, Yuan Zhou, Lunqiang Zhang, Dan Wang, and Haiping Pei. 2019. “Non-Coding RNA MFI2-AS1 Promotes Colorectal Cancer Cell Proliferation, Migration and Invasion through MiR-574-5p/MYCBP Axis.” *Cell Proliferation* 52 (4). https://doi.org/10.1111/cpr.12632.

Li, Guoliang, Melissa J. Fullwood, Han Xu, Fabianus Hendriyan Mulawadi, Stoyan Velkov, Vinsensius Vega, Pramila Nuwantha Ariyaratne, et al. 2010. “ChIA-PET Tool for Comprehensive Chromatin Interaction Analysis with Paired-End Tag Sequencing.” *Genome Biology* 11 (2): 1–13. https://doi.org/10.1186/gb-2010-11-2-r22.

Li, Guoliang, Xiaoan Ruan, Raymond K. Auerbach, Kuljeet Singh Sandhu, Meizhen Zheng, Ping Wang, Huay Mei Poh, et al. 2012. “Extensive Promoter-Centered Chromatin Interactions Provide a Topological Basis for Transcription Regulation.” *Cell* 148 (1–2): 84–98. https://doi.org/10.1016/j.cell.2011.12.014.

Liao, Susan E, and Oded Regev. 2020. “Splicing at the Phase-Separated Nuclear Speckle Interface: A Model.” *Nucleic Acids Research*, December, 1–10. https://doi.org/10.1093/nar/gkaa1209.

Liu, K., J. Liu, and Q. F. Bo. 2019. “MFI2-AS1 Regulates the Aggressive Phenotypes in Glioma by Modulating MMP14 via a Positive Feedback Loop.” *European Review for Medical and Pharmacological Sciences* 23 (13): 5884–95. https://doi.org/10.26355/eurrev_201907_18333.

Ma, Lina, Jiabao Cao, Lin Liu, Qiang Du, Zhao Li, Dong Zou, Vladimir B. Bajic, and Zhang Zhang. 2019. “Lncbook: A Curated Knowledgebase of Human Long Non-Coding Rnas.” *Nucleic Acids Research* 47 (D1): D128–34. https://doi.org/10.1093/nar/gky960.

Malouf, Gabriel G., Jianping Zhang, Ying Yuan, Eva Compérat, Morgan Rouprêt, Olivier Cussenot, Yunxin Chen, et al. 2015. “Characterization of Long Non-Coding RNA Transcriptome in Clear-Cell Renal Cell Carcinoma by next-Generation Deep Sequencing.” *Molecular Oncology* 9 (1): 32–43. https://doi.org/10.1016/j.molonc.2014.07.007.

Michaud, Joëlle, Viviane Praz, Nicole James Faresse, Courtney K. JnBaptiste, Shweta Tyagi, Frédéric Schütz, and Winship Herr. 2013. “HCFC1 Is a Common Component of Active Human CpG-Island Promoters and Coincides with ZNF143, THAP11, YY1, and GABP Transcription Factor Occupancy.” *Genome Research* 23 (6): 907–16. https://doi.org/10.1101/gr.150078.112.

Nakagawa, Shinichi, Joanna Y. Ip, Go Shioi, Vidisha Tripathi, Xinying Zong, Tetsuro Hirose, and Kannanganattu V. Prasanth. 2012. “Malat1 Is Not an Essential Component of Nuclear Speckles in Mice.” *Rna* 18 (8): 1487–99. https://doi.org/10.1261/rna.033217.112.

Ploussard, Guillaume, and Alexandre De La Taille. 2010. “Urine Biomarkers in Prostate Cancer.” *Nature Reviews Urology* 7 (2): 101–9. https://doi.org/10.1038/nrurol.2009.261.

Porta, Camillo, Laura Cosmai, Bradley C. Leibovich, Thomas Powles, Maurizio Gallieni, and Axel Bex. 2019. “The Adjuvant Treatment of Kidney Cancer: A Multidisciplinary Outlook.” *Nature Reviews Nephrology* 15 (7): 423–33. https://doi.org/10.1038/s41581-019-0131-x.

Qian, Yuchen, Lei Shi, and Zhong Luo. 2020. “Long Non-Coding RNAs in Cancer: Implications for Diagnosis, Prognosis, and Therapy.” *Frontiers in Medicine* 7 (November): 1–8. https://doi.org/10.3389/fmed.2020.612393.

Quinodoz, Sofia A., Noah Ollikainen, Barbara Tabak, Ali Palla, Jan Marten Schmidt, Elizabeth Detmar, Mason M. Lai, et al. 2018. “Higher-Order Inter-Chromosomal Hubs Shape 3D Genome Organization in the Nucleus.” *Cell* 174 (3): 744-757.e24. https://doi.org/10.1016/j.cell.2018.05.024.

Rhie, Suhn Kyong, Lijun Yao, Zhifei Luo, Heather Witt, Shannon Schreiner, Yu Guo, Andrew A. Perez, and Peggy J. Farnham. 2018. “ZFX Acts as a Transcriptional Activator in Multiple Types of Human Tumors by Binding Downstream from Transcription Start Sites at the Majority of CpG Island Promoters.” *Genome Research* 28 (3): 310–20. https://doi.org/10.1101/gr.228809.117.

Rose, T M, G D Plowman, D B Teplow, W J Dreyer, K E Hellström, and J P Brown. 1986. “Primary Structure of the Human Melanoma-Associated Antigen P97 (Melanotransferrin) Deduced from the MRNA Sequence.” *Proceedings of the National Academy of Sciences* 83 (5): 1261 LP – 1265. https://doi.org/10.1073/pnas.83.5.1261.

Saldaña-Meyer, Ricardo, Edgar González-Buendía, Georgina Guerrero, Varun Narendra, Roberto Bonasio, Félix Recillas-Targa, and Danny Reinberg. 2014. “CTCF Regulates the Human P53 Gene through Direct Interaction with Its Natural Antisense Transcript, Wrap53.” *Genes and*

Development 28 (7): 723–34. https://doi.org/10.1101/gad.236869.113.

Suryo Rahmanto, Y., L. L. Dunn, and D. R. Richardson. 2007. "The Melanoma Tumor Antigen, Melanotransferrin (P97): A 25-Year Hallmark - From Iron Metabolism to Tumorigenesis." *Oncogene* 26 (42): 6113–24. https://doi.org/10.1038/sj.onc.1210442.

Sutherland, Heidi, and Wendy A. Bickmore. 2009. "Transcription Factories: Gene Expression in Unions?" *Nature Reviews Genetics* 10 (7): 457–66. https://doi.org/10.1038/nrg2592.

Tang, Zhonghui, Oscar Junhong Luo, Xingwang Li, Meizhen Zheng, Jacqueline Jufen Zhu, Przemyslaw Szalaj, Pawel Trzaskoma, et al. 2015. "CTCF-Mediated Human 3D Genome Architecture Reveals Chromatin Topology for Transcription." *Cell* 163 (7): 1611–27. https://doi.org/10.1016/j.cell.2015.11.024.

Wang, Zehua, Bo Yang, Min Zhang, Weiwei Guo, Zhiyuan Wu, Yue Wang, Lin Jia, et al. 2018. "LncRNA Epigenetic Landscape Analysis Identifies EPIC1 as an Oncogenic LncRNA That Interacts with MYC and Promotes Cell-Cycle Progression in Cancer." *Cancer Cell* 33 (4): 706-720.e9. https://doi.org/10.1016/j.ccell.2018.03.006.

Wei, Yongpeng, Zhuo Wang, Yi Zong, Dewu Deng, Peiqin Chen, and Junhua Lu. 2020. "LncRNA MFI2-AS1 Promotes HCC Progression and Metastasis by Acting as a Competing Endogenous RNA of MiR-134 to Upregulate FOXM1 Expression." *Biomedicine and Pharmacotherapy* 125 (December 2019): 109890. https://doi.org/10.1016/j.biopha.2020.109890.

Yamazaki, Tomohiro, Sylvie Souquere, Takeshi Chujo, Simon Kobelke, Yee Seng Chong, Archa H. Fox, Charles S. Bond, Shinichi Nakagawa, Gerard Pierron, and Tetsuro Hirose. 2018. "Functional Domains of NEAT1 Architectural LncRNA Induce Paraspeckle Assembly through Phase Separation." *Molecular Cell* 70 (6): 1038-1053.e7. https://doi.org/10.1016/j.molcel.2018.05.019.

Yang, Lu, Youyou Zhang, Weiwei Shan, Zhongyi Hu, Jiao Yuan, Jingjiang Pi, Yueying Wang, et al. 2017. "Repression of BET Activity Sensitizes Homologous Recombination-Proficient Cancers to PARP Inhibition." *Science Translational Medicine* 9 (400). https://doi.org/10.1126/scitranslmed.aal1645.

Yu, Tianyu, Lingling Tong, Yu Ao, Genmao Zhang, Yunpeng Liu, and Hejia Zhang. 2020. "Upregulation of Triap1 by the Lncrna Mfi2-As1/Mir-125a-5p Axis Promotes Thyroid Cancer Tumorigenesis." *OncoTargets and Therapy* 13: 6967–74. https://doi.org/10.2147/OTT.S236476.

FIGURES

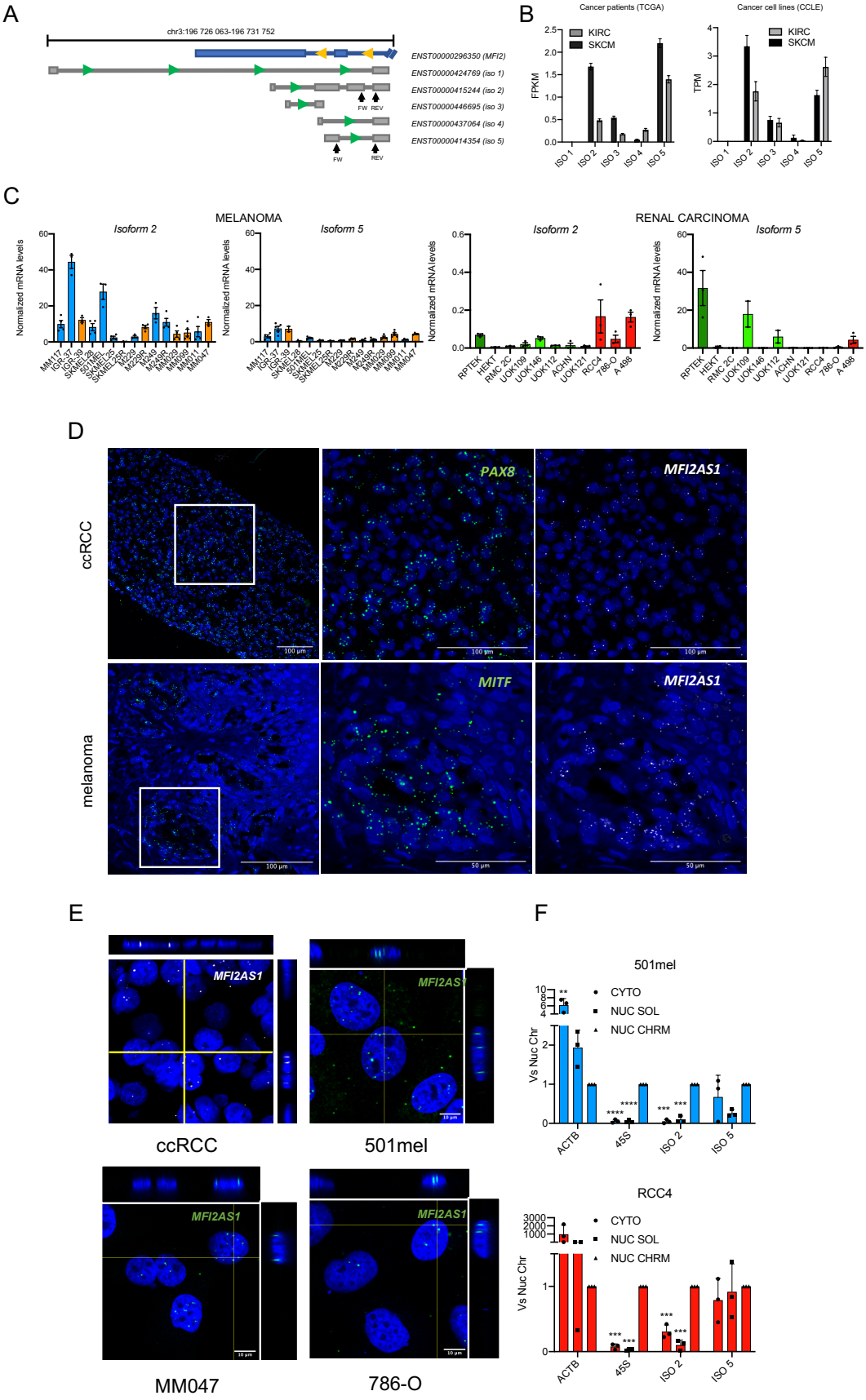
A
chr3:196 726 063-196 731 752
ENST00000296350 (MFI2)
ENST00000424769 (iso 1)
ENST00000415244 (iso 2)
ENST00000446695 (iso 3)
ENST00000437064 (iso 4)
ENST00000414354 (iso 5)
FW
REV
B
Cancer patients (TCGA)
Cancer cell lines (CCLE)
KIRC
SKCM
FPKM
TPM
ISO 1
ISO 2
ISO 3
ISO 4
ISO 5
C
MELANOMA
RENAL CARCINOMA
Isoform 2
Isoform 5
Normalized mRNA levels
D
ccRCC
melanoma
PAX8
MFI2AS1
MITF
E
ccRCC
501mel
MM047
786-O
F
501mel
RCC4
CYTO
NUC SOL
NUC CHRM
Vs Nuc Chr
ACTB
45S
ISO 2
ISO 5

Figure 1 - MFI2-AS1 is a predominantly nuclear lncRNA in melanoma and ccRCC.

A. Graphic representation of the MFI2-AS1 locus showing exons and introns of each isoform, defined using the Ensembl 83 annotations. **B.** RNA sequencing data from melanoma (SKCM) and ccRCC (KIRC) patients (TCGA) and cell lines (CCLE) were analysed for MFI2-AS1 transcript quantification. **C.** MFI2-AS1 isoform 2 and 5 levels were determined in a panel of melanocytic (blue) and undifferentiated (orange) melanoma cell lines and clear cell (red) and not-clear cell (light green) renal carcinoma cell lines by quantitative PCR (qPCR) using specific primers. Data were normalized over the geometric mean of 5 housekeeping genes. **D.** MFI2-AS1, PAX8 and MITF RNA molecules were detected in melanoma and ccRCC patient FFPE sections using complementary DNA probes and the multiplex fluorescent RNAscope signal amplification protocol. DNA was stained with DAPI. **E.** MFI2-AS1 RNA molecules were detected in melanoma and ccRCC cells using complementary DNA probes and the multiplex fluorescent RNAscope signal amplification protocol. DNA was stained with DAPI. Z-stack acquired images were processed to obtain XZ and YZ orthogonal views at the yellow lines indicated. **F.** 501mel and RCC4 cells were lysed and the cytoplasmic (Cyto) and nuclear fractions separated. The latter was further separated into the nucleoplasm (Nuc sol) and the chromatin bound (Nuc chr) fractions. RNA was extracted from each and analysed by qPCR for *ACTB*, 45S-rRNA and MFI2-AS1 expression. Data obtained from the cytoplasmic and nuclear soluble fractions were expressed relative to the chromatin fraction and compared by 1-way Anova (Dunnett's multiple comparison test).

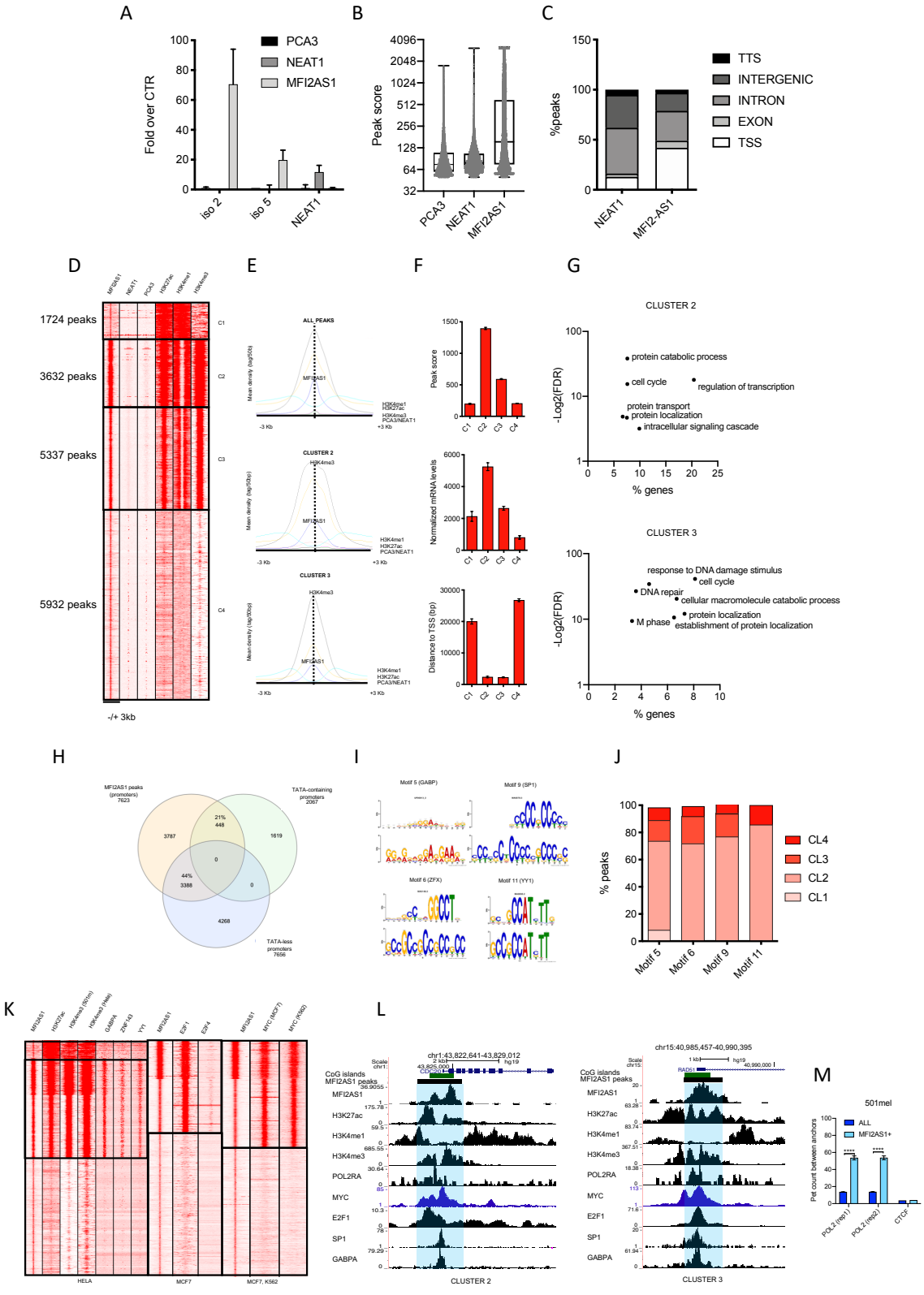

Figure 2 – MFI2-AS1 binds to promoters of housekeeping genes.

A. 501mel cells were formaldehyde crosslinked, lysed, sonicated and chromatin extracts were incubated with biotinylated DNA probes complementary to MFI2-AS1, NEAT1 or PCA3. RNA-

chromatin complexes were isolated using streptavidin magnetic beads and divided in two aliquots to perform RNA and DNA extraction. RNA was analysed by qPCR for MFI2-AS1 isoform 2 and 5 and NEAT1 expression. DNA was de-crosslinked and sequenced. **B.** Distributions of the scores of the ChIRP peaks of each pulldown identified using MACS. **C.** Genomic localization of ChIRP peaks for NEAT1 and MFI2-AS1 expressed as % of the total number of peaks. **D.** ChIRP data were analysed using Seq-Miner and compared between each other and Chip-seq data of histone marks (H3K27ac, H3K4me1, H3K4me3) obtained from the same cell line (501mel) around Ensembl 76 gene transcription start sites (-/+ 3kb of TSSs). Alignment of ChIRP and Chip-seq experiments allowed definition of 4 clusters of genes. **E.** ChIRP and Chip-seq profiles of each cluster defined in D. **F.** Genes associated with MFI2-AS1 binding in each cluster were analysed to define the corresponding peak score in the MFI2-AS1 ChIRP, the distance to the closest TSS and the expression level in 501mel cells. **G.** Gene lists constituting Cluster 2 and 3 were analysed using The Database for Annotation, Visualization and Integrated Discovery (DAVID) v6.8 tool to define significantly enriched gene ontologies (GO) for biological functions. GOs were ordered based on the percentage of genes characterizing the GO being present in the clusters and the FDR transformed by -log2. **H.** MFI2-AS1 bound promoters were compared to the lists of TATA-less and TATA-containing promoters obtained from the Eukaryotic Promoter Database (EPD). Percentages express the ratio of MFI2-AS1 bound promoters positive for each category over the total number. **I.** MFI2-AS1 binding sequences were analysed by MEME and ISMARA to identify significantly enriched transcription factors binding motifs. **J.** MFI2-AS1 positive peaks for each motif were analysed to define their association to the clusters identified in Fig.2D. **K.** MFI2-AS1 ChIRP data were aligned by Seq-Miner to Chip-seq data of transcription factors GABPA, ZNF143, YY1, E2F1 and MYC identified from the analysis in panel I. **L.** MFI2-AS1 ChIRP and Chip-seq data of histone marks and transcription factors were visualized using the UCSC genome browser at the promoters of two representative genes coming from clusters 2 and 3 defined in Fig.2D. **M** Pol II and CTCF K562 cells ChIA-PET interactions data from GSE33664 and GSE72816 were compared to MFI2-AS1 ChIRP data from 501mel cells. MFI2-AS1 positive interactions were defined when an MFI2-AS1 ChIRP peak was present at both anchors of a Pol II- or CTCF interaction. The Pet count between the anchors of all Pol II or CTCF interactions was compared to those of MFI2-AS1 associated interactions ones by Upaired t-test.

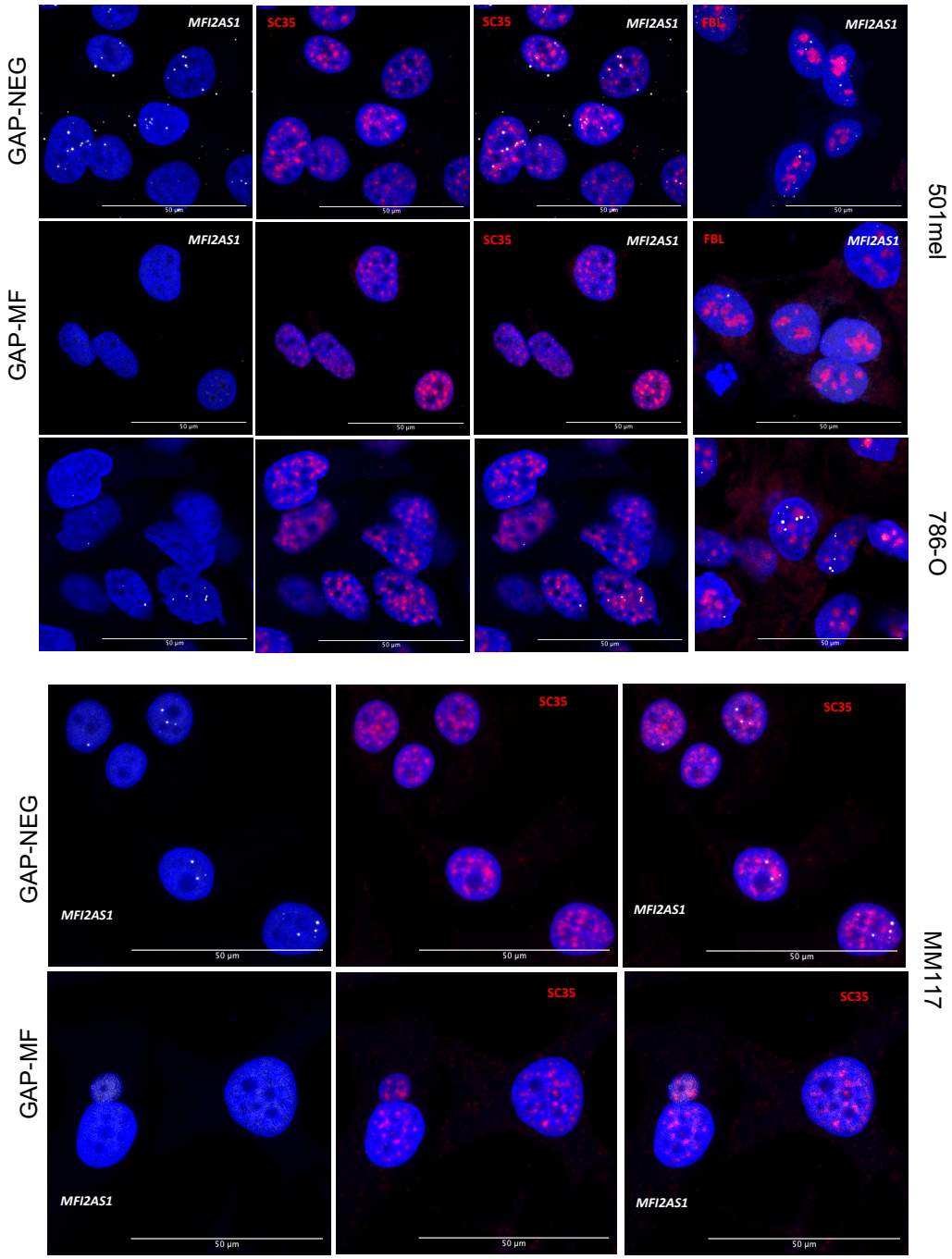
GAP-NEG
GAP-MF
501mel
786-O
MM117
MFI2AS1
SC35
FBL
50 µm

Figure S1 – MFI2-AS1 localizes to a subset of nuclear speckles.

501mel, MM117 melanoma cells and 786-O ccRCC cells were transfected with a negative control or MFI2-AS1 specific GapmeR, transferred to microscopy chamber slides and fixed with formalin 48 hours post-transfection. MFI2-AS1 RNA molecules were detected by RNAscope concomitantly with antibody staining for SC35 and fibrillarin (FBL) proteins. DNA was stained with DAPI.

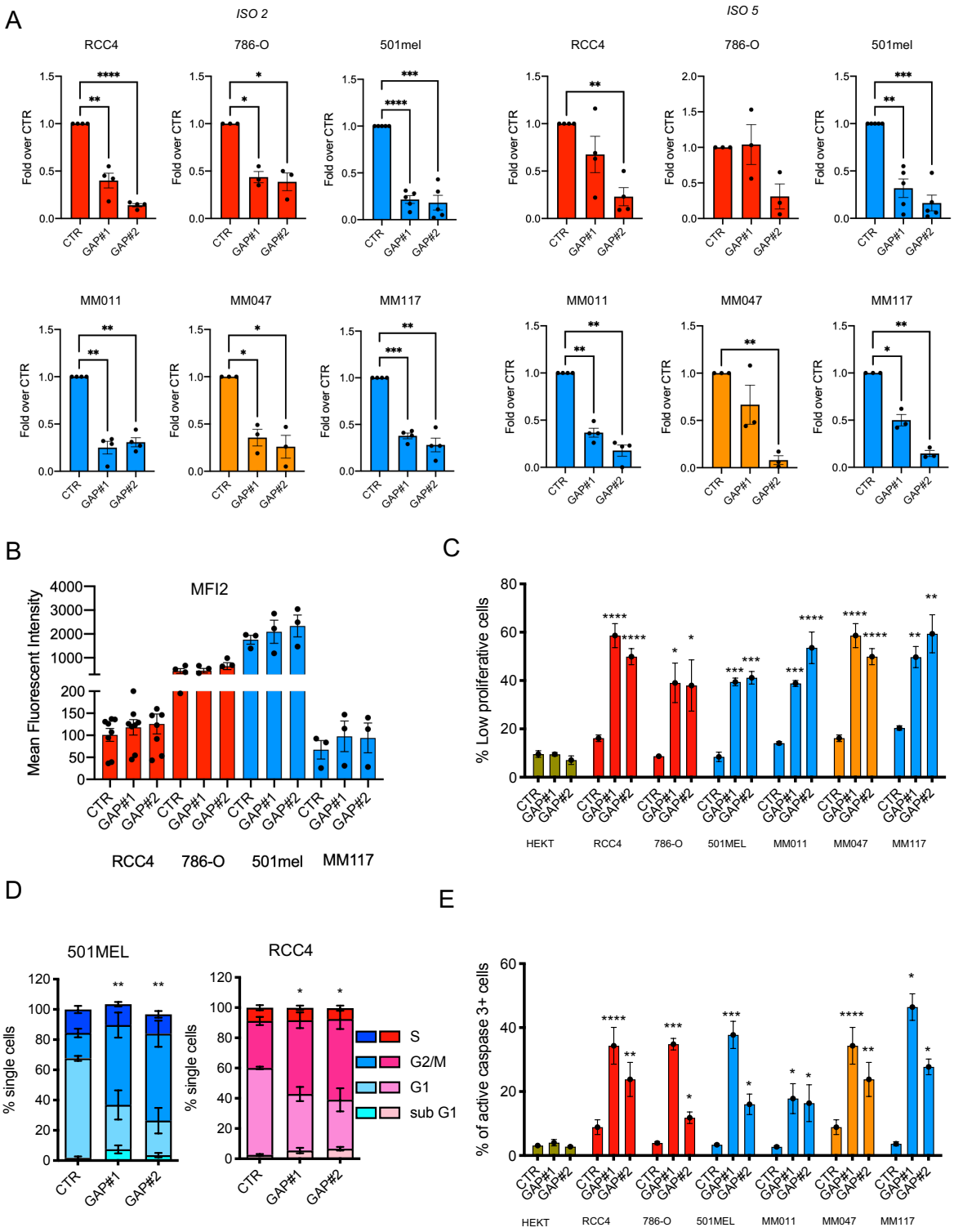

Figure 3 – MFI2-AS1 knock down affects proliferation and survival of melanoma and ccRCC cells.

A. ccRCC (red) and melanoma (blue/melanocytic; orange/undifferentiated) cell lines were transfected with a negative control GapmeR or two MFI2-AS1 specific GapmeRs and after 48

hours analysed by RT-qPCR for MFI2-AS1 isoform 2 and 5 expression. MFI2-AS1 GapmeR transfected cells were compared to the negative control by 1-way Anova (Dunnett's multiple comparison test). **B.** ccRCC and melanoma cell lines were transfected as in panel A, harvested after 72 hours, stained with an anti-MFI2 antibody and analysed by flow cytometry. **C.** ccRCC and melanoma cell lines were transfected as in panel A, stained with Cell Trace Violet, harvested after 72 hours and analysed by flow cytometry. Percentages of low proliferative cells in the MFI2-AS1 GapmeR groups were compared to the negative control by 1-way Anova. (Dunnett's multiple comparison test). HEKT cells were used as a MFI2-AS1 non-expressing control. **D.** 501mel and RCC4 cells were transfected as in panel A and after 72 hours incubated 90 minutes with Edu to allow its incorporation in newly synthesized DNA. Cells were then harvested, fixed and Edu was conjugated with the Alexa 488 fluorophore after a Click-it reaction. Cells were stained with TOPRO-3 and analysed by flow cytometry. Cells were divided into 4 populations based on Edu/TOPRO-3 fluorescence (sub G1, G1, S, G2/M) Percentages of cells in the G2/M phase were compared among the experimental conditions by 1-way Anova. (Dunnett's multiple comparison test). **E.** ccRCC and melanoma cell lines were transfected as in panel A, stained with an anti-active caspase 3 antibody and analysed by flow cytometry. Percentages of single cells positive for Active Caspase 3 were compared to the negative control by 1-way Anova (Dunnett's multiple comparison test). HEKT cells were used as a MFI2-AS1 non-expressing control.

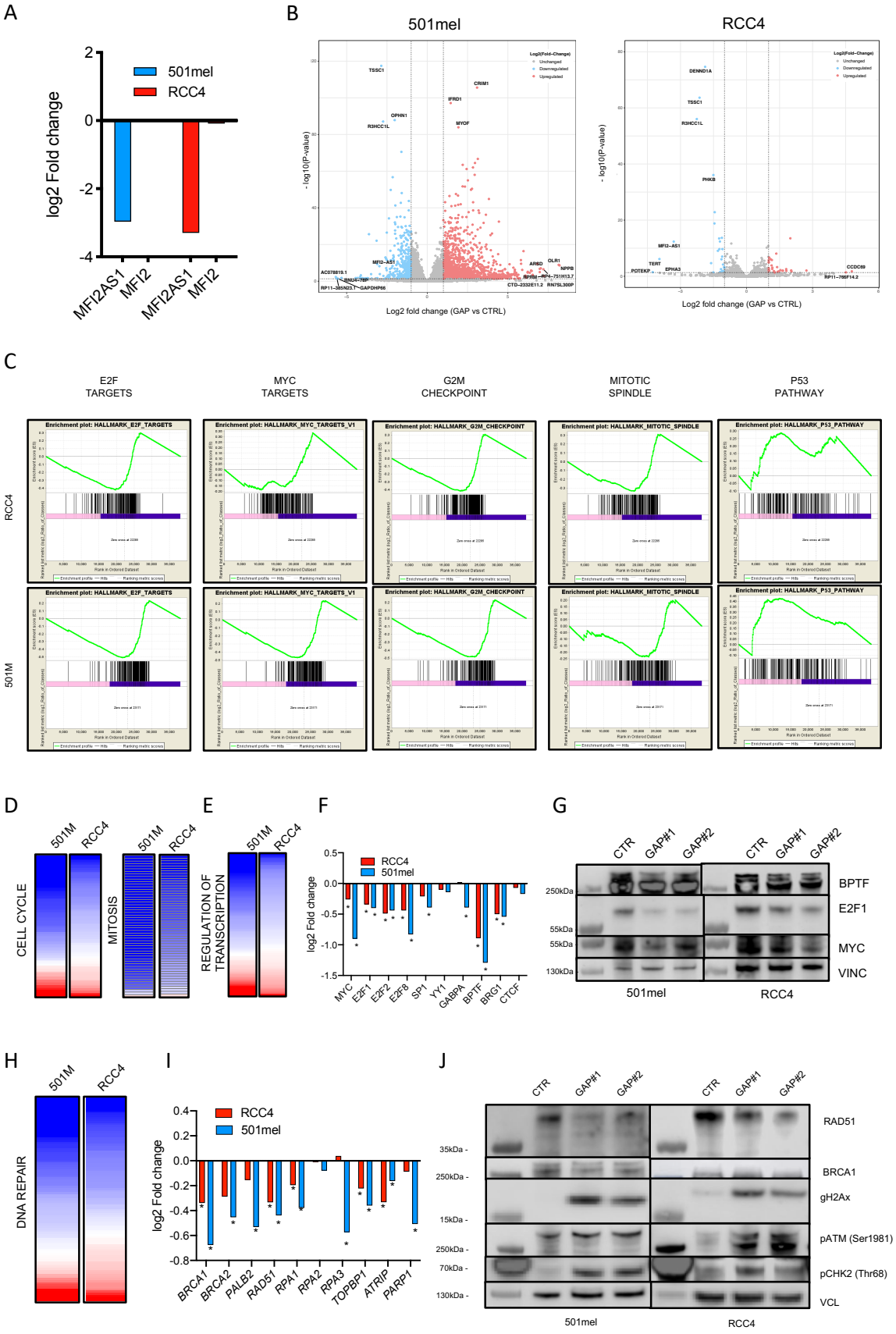

Figure S2 – MFI2-AS1 regulates expression of genes involved in cell cycle and DNA repair.

A. 501mel and RCC4 cells were transfected with a negative control or MFI2-AS1 specific GampeR 2, harvested and total RNA extracted and sequenced. Log2 fold changes of MFI2-AS1 and MFI2 from 501mel and RCC4 are indicated. **B.** Volcano plots of deregulated genes as defined by log2 Fold-change > 1 and adjusted p-value < 0.05 in 501mel and RCC4 cells. **C.** RNA-seq of 501mel and RCC4 cells treated as described in Fig. S2A were analysed by Gene Set Enrichment Analysis (GSEA). **D.** Analyses of 501mel and RCC4 RNA-seq data. Genes from the "Cell cycle" (GO:0007049) and "mitosis" (GO:0000278) gene ontologies were extracted and represented in the heatmap using Morpheus (https://software.broadinstitute.org/morpheus/; -0.5/0.5 log2 fold change)**. E.** Log2 fold changes from the "Regulation of Transcription" gene ontology (GO:0006355) were represented as described in panel D. **F.** Log2 fold changes of selected transcription factors constituting the GO "Regulation of transcription". Stars indicate significant changes. **G.** 501mel and RCC4 cells were transfected as in Fig.3A and after 72 hours were analysed by western blot with anti-BPTF, E2F1 and MYC antibodies. Vinculin was used as a loading control. **H.** Log2 fold changes of genes of the "DNA repair" GO:0006281 gene set were represented in a heatmap as described in panel D. **I.** Log2 fold changes of selected genes involved in homologous recombination from the "DNA repair" ontology gene set. **J.** Total protein extracts were analysed by western blot with anti-RAD51, BRCA1, E2F1 and MYC antibodies. Vinculin was used as a loading control.

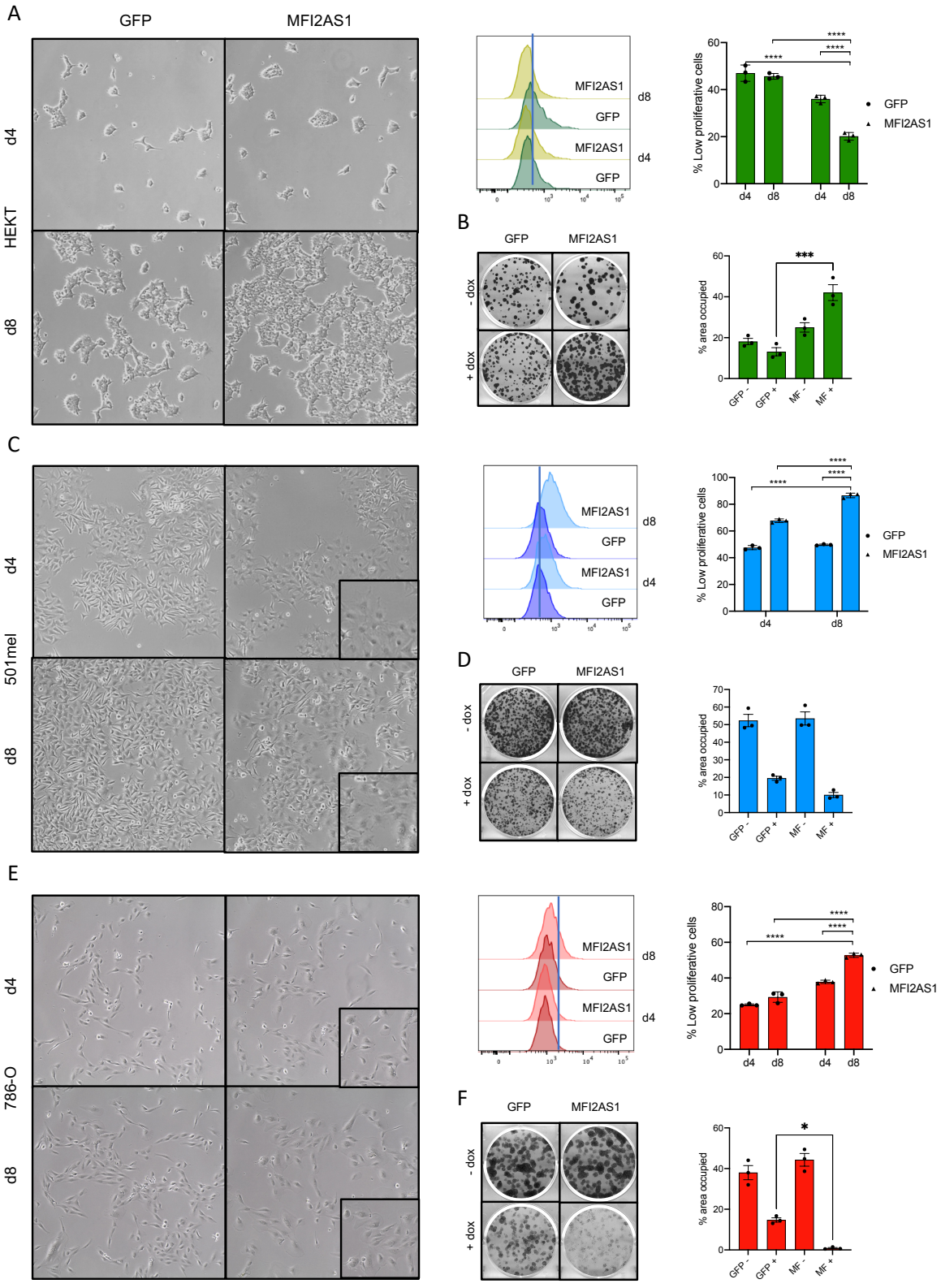

Figure 4 – Ectopic MFI2-AS1 modulates proliferation of HEKT, 501MEL AND 786-O cells.

A, C and **E.** HEKT, 501mel and 786-O cells were infected with the pCW57 lentiviral vector to allow Dox-inducible expression of GFP or MFI2-AS1 isoform 2. After transduction cells were

selected by puromycin, cultured with or without Dox for 4 days, stained with Cell Trace violet and cultured for another 4 days in the presence of Dox. After 8 days in total, GFP and ectopic MFI2-AS1 expressing cells were compared. Cells were photographed by light microscope, harvested and analysed for CellTrace Violet fluorescence by flow cytometry (A/C/E). Percentages of low proliferative cells were compared between experimental groups by 1-way Anova. **B, D** and **F.** HEKT (B), 501mel (D) and 786-O (F) cells modified as in panels A/C/E were seeded at low cellular densities and cultured for 10 days in the presence or absence of Dox. Cells were fixed, stained with crystal violet and percentage of wells area occupied was quantified with ImageJ. Percentages of areas were compared between experimental groups by 1-way Anova.

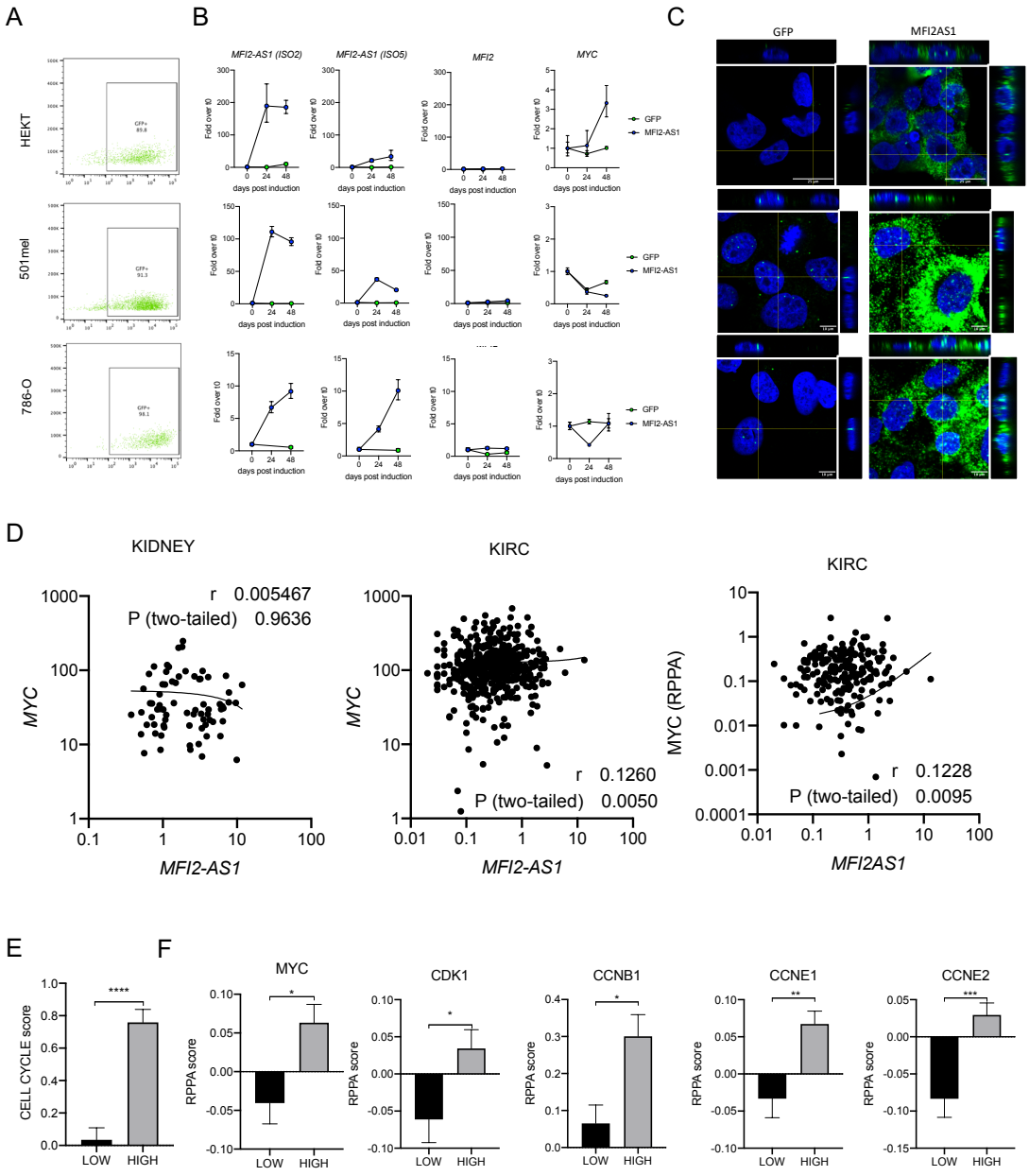

Figure S3 – MFI2-AS1 levels correlate with higher MYC and cell cycle gene expression in ccRCC patients.

A. HEKT, 501mel and 786-O cells were infected with the pCW57 lentiviral vector allowing Dox-inducible expression of GFP or MFI2-AS1 isoforms 2 or 5. After transduction cells were selected by puromycin, cultured for 48 hours with Dox and analysed by flow cytometry for GFP expression. **B.** HEKT, 501mel and 786-O cells were harvested before Dox (t0) and after 24 and 48 hours of Dox treatment. MFI2-AS1 isoform 2 and 5, MFI2 and MYC expression was analysed by RT-qPCR. **C.** HEKT, 501mel and 786-O cells were cultured 48 hours with Dox, fixed

and MFI2-AS1 RNA molecules were detected by RNAscope multiplex fluorescent kit. DNA was stained with DAPI. Z-stack acquired images were processed to obtain XZ and YZ orthogonal views at the yellow lines. **D.** RNA-seq and RPPE data of normal kidney (KIDNEY) and ccRCC (KIRC) from TCGA were analysed for MYC and MFI2-AS1 isoform 2 expression. Spearman correlation was calculated in a pairwise manner between MFI2-AS1 isoform 2 RNA levels and MYC RNA and protein levels. **E,F.** KIRC TCGA patients were divided into the 25% lowest and 25% highest MFI2-AS1 isoform 2 expressing quartiles and analysed for the mRNA cell cycle score defined in (F. Chen et al. 2016) and RPPA values for MYC, CDK1, CCNB1, CCNE1 and CCNE2. MFI2-AS1 high and low groups were compared by unpaired t-test.

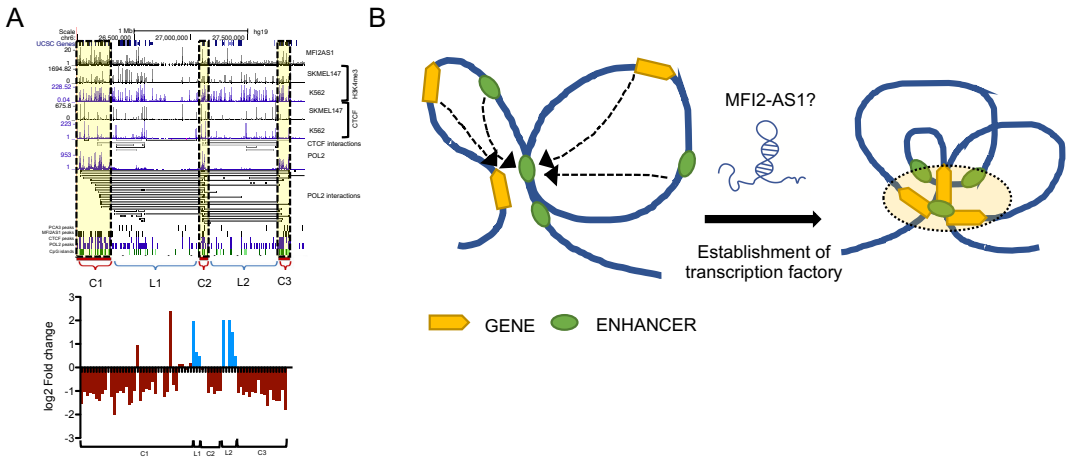

Figure 5 – Proposed mechanism of action of MFI2-AS1.

A. MFI2-AS1 ChIRP data were uploaded on the UCSC Genome Browser together with ChIP-seq data of H3K4me3 and CTCF from leukemia K562 cells and melanoma SKmel147 cells and CTCF and RNA Pol2 ChIA-PET data from K562. The three HIST1 genes clusters were highlighted in yellow shadow. Expression changes of the genes contained in the clusters and loops were evaluated in RNAseq data of 501mel cells knockdown for MFI2AS1. **B.** MFI2AS1 may play a role in the stabilisation of multi-gene complexes of housekeeping genes.

SECTION 5 – GENERAL CONCLUSIONS

LncRNAs are fascinating molecules that convey a wide variety of functions by interactions with other nucleic acids or proteins. The discovery of large numbers of lncRNAs in higher organisms generated great enthusiasm as they provided a means to resolve the discrepancy between increasing multicellular organism complexity without a similar increase in the number of coding genes. Nevertheless, care should be taken in defining what is functional and what results from neutral selection.

Some lncRNAs arose early during evolution and fulfill similar processes in different organisms. They are normally expressed in a ubiquitous manner across cell types and at moderate levels. Others are evolutionarily "younger" and frequently originated after transposon or retroviral insertions in a restricted set of species. This class is involved in regulation of more specific processes during development or in response to environmental cues and are often expressed in a spatial or temporal restricted manner, sometimes at low levels. They may have been selected due to their intrinsic functional capacity once their transcription was acquired. Indeed, a model for how functional lncRNAs can arise rapidly without strong evolutionary selection has been recently proposed (Palazzo and Koonin 2020) and is relevant for the lncRNAs studied here, that like Linc00518 and SAMMSON make specific protein interactions to mediate their functions. Carcinogenesis can be ascribed as one of these biological processes requiring molecules to rapidly adapt to situations of stress. Not surprisingly, several cancer-specific lncRNAs have emerged and the functions of others have been hijacked. As exemplified here, they regulate oncogenic processes and help cancer cells to react to external insults.

The unique regulatory mechanisms governing these LncRNAs confer a highly tumour-specific expression and absence in normal tissues, making them attractive candidates for ASO mediated therapy. To date around 20 RNA-targeting drugs have been FDA approved for a variety of pathologies, the large majority of which target coding mRNAs (Crooke et al. 2018). Nevertheless, companies such as Ionis Pharmaceuticals and others are heavily investing in ASOs to target LncRNAs to exploit their unique highly tissue or tumour-specific expression compared to widely expressed mRNAs.

Another intriguing feature underlying lncRNA function is energy 'economics'. As lncRNAs do not have to be translated into proteins to exert a function, they require less energy commitment by the cell and due to their unstable nature, they can be turned over rapidly to adapt to the environment. This constitutes an advantage and allows cells to save a lot of energy. A clear example is X chromosome inactivation with Xist acting on the surrounding chromatin. Importing a protein from the cytosol would require much more energy to identify specifically only one of the two X chromosomes to initiate and spread silencing all over it. It is plausible that other similar processes exist.

Another field of study boosted by lncRNA research concerns phase separation. The discovery that RNAs can regulate the oligomerization of proteins with intrinsically disordered domains helped to explain formation of nuclear bodies. This concept may be further expanded in the future, with the appreciation of smaller or more dynamically regulated nuclear compartments whose local concentrations of RNA and proteins is relevant to regulate biological processes. It is tempting to speculate that these structures could exist not only in the nucleus but also in the cytoplasm.

Another provocative idea relates to lncRNA partners, so far mostly nucleic acids or proteins. What if other macromolecules such as lipids or carbohydrates could be directly or indirectly

bound by lncRNAs and sequestered in discrete domains? This could constitute an additional level of buffering for metabolic intermediates and allow lncRNAs to influence the activity of enzyme pathways.

Despite being exotic, these hypotheses underlie the need to increase experimental efforts to characterize lncRNA interactors. This still represents a challenging task due to the discrepancy between proteomic sensitivity and the medium/low abundance of most lncRNAs. Identification of partners should also be more frequently accompanied by evaluation of the stoichiometric ratio between the lncRNA and the protein, their localization and the definition of the structural features of their interactions, for example, protein and RNA domains, post-transcriptional modification of lncRNA and post-translational protein modifications. Indeed, often what is lacking in published studies and also in ours is a demonstration and characterization of a direct interaction between the recombinant protein and in vitro synthesized lncRNA.

A more integrated definition of these parameters may provide a completely new way to predict lncRNAs function and open the possibility to develop sterically blocking agents using small molecules. This could expand the scope of lncRNA inhibition, that currently relies mostly on ASO-mediated degradation. ASOs have turned out to be very useful research tools, but very difficult to administer systemically for therapeutic purposes. Nevertheless, ongoing research is devoted into improving their pharmaco-utility, making lncRNA based therapeutics more than a vague possibility for the future.

REFERENCES

Crooke, Stanley T., Joseph L. Witztum, C. Frank Bennett, and Brenda F. Baker. 2018. "RNA-Targeted Therapeutics." *Cell Metabolism* 27 (4): 714–39. https://doi.org/10.1016/j.cmet.2018.03.004.

Palazzo, Alexander F., and Eugene V. Koonin. 2020. "Functional Long Non-Coding RNAs Evolve from Junk Transcripts." *Cell* 183 (5): 1151–61. https://doi.org/10.1016/j.cell.2020.09.047.

ANNEXES

Giovanni GAMBI

Targeting lncRNAs in human cancer: insights into melanoma and clear cell renal cell carcinoma

Résumé

Le cancer est un problème de santé mondial majeur. Les patients atteints d'une maladie avancée sont souvent caractérisés par un pronostic défavorable et réfractaires aux traitements disponibles. Nous avons cherché à caractériser les ARN longs non codants (ARNlnc) en tant que cibles thérapeutiques potentielles pour le mélanome et le carcinome rénal à cellules claires (CCRcc). Nous avons démontré leur expression spécifique à la tumeur, leur pertinence dans la prolifération et la survie des cellules cancéreuses et leur ciblage en utilisant des oligonucléotides antisens comme agents singles, en combinaison ou administrés avec une thérapie ciblée. Nous avons fourni des informations mécanistes pour deux d'entre eux et leurs partenaires, en proposant deux nouveaux modes d'action. LINC00518 interagit avec la GTPase RAP2 et, ensemble, ils influencent la phosphorylation du DRP1, l'élongation des mitochondries et la phosphorylation oxydative. Cette activité soutient la santé des mitochondries à l'état stable et permet de s'adapter au stress énergétique. MFI2AS1 se lie aux promoteurs des gènes de ménage dans les mélanomes et les cellules ccRCC, soutenant un programme d'expression génétique prolifératif. Nous suggérons qu'il agit en régulant les structures de chromatine d'ordre élevé à la périphérie des speckles nucléaires.

Mot clés : ARNlnc, cancer, mélanome, ccRCC, métabolisme, mitochondries, chromatine, prolifération

Résumé en anglais

Cancer is a major worldwide health issue. Patients with advanced disease are often characterized by unfavourable prognosis and refractory to available treatments. We sought to characterise long non-coding RNAs (lncRNAs) as potential therapeutic targets for melanoma and clear cell renal cell carcinoma (ccRCC). We demonstrated their tumour specific expression, their relevance in cancer cells proliferation and survival and their targetability using antisense oligonucleotides as single agents, in combination or administered with targeted therapy. We provided mechanistic information for two of them and their binding partners, proposing two novel modes of action. LINC00518 interacts with the RAP2 GTPase and together they influence DRP1 phosphorylation, mitochondria elongation and oxidative phosphorylation. This activity sustains mitochondrial health at steady state and allows to adapt to energy stress. MFI2AS1 binds to promoters of housekeeping genes in melanoma and ccRCC cells, supporting a proliferative gene expression program. We suggest it acts by regulating high-order chromatin structures at the periphery of nuclear speckles.

Keywords: lncRNAs, cancer, melanoma, ccRCC, metabolism, mitochondria, chromatin, proliferation